UNIVERSITA' DEGLI STUDI DI PARMA

Dottorato di ricerca in Ecologia

Ciclo XXIV

An integrated modelling approach to investigate the dynamics of *Planktothrix rubescens* blooming in a medium-sized pre-alpine lake (North Italy)

Coordinatore:

Chiar.mo Prof. Paolo Menozzi

Tutor:

Prof. Pierluigi Viaroli

Dr. Gianni Tartari

Dr. Diego Copetti

Dr. Franco Salerno

Dottoranda: Elisa Carraro

A mia mamma, Clara

Lo studio riportato in questa tesi è parte delle ricerche finanziate dalla fondazione CARIPLO e dal Parco Regionale della Valle del Lambro nell'ambito del progetto PIRoGA 'Progetto Integrato lago/bacino per il Recupero della qualità ecologica e la Gestione idrologica delle Acque del Lago di Pusiano', svolte presso l'Istituto di Ricerca sulle Acque del Consiglio Nazionale delle Ricerche (IRSA CNR).

ABSTRACT

In a medium-sized pre-alpine lake (Lake Pusiano, North Italy) the cyanobacterium *Planktothrix rubescens* has strongly dominated the phytoplankton assemblage since 2000 despite improvements in water quality, similarly to what happened in many pre-alpine lakes. The ecological success of the ubiquitous harmful species has been ascribed to largely depend on its eco-physiological traits, lakes re-oligotrophication (and increasing N:P ratios) as well as climate oscillations. Whatever the viewpoint, it has been the dominating algal species over the last two decades but the scientific community is debating about the crucial factors determining the dynamics. A great difficulty is certainly the comprehension of the effects due to human pressures at different scales. Also the natural changes and the interactions within the ecosystem may cause a high uncertainty. The present research focused on the necessity to solve some of the most paradoxical features about *P.rubescens* large success. Is the global warming favouring a cold stenotherm species? Is a general lakes restoration the causal factor of a simultaneous widespread blooming in Europe? Are the species physiological traits sufficient to explain an ecological success?

An intensive field campaign was conducted to evaluate distributions of phytoplankton taxa, as well as *P. rubescens*, using spectrally-resolved fluorescence measurements and cell enumeration. These provided a high spatially and temporally resolved database, suitable to calibrate and validate a coupled three-dimensional hydrodynamic and ecological model for lakes ecosystem. The simulations revealed the fundamental role of physiological features. They led to characteristic vertical patterns of distribution, notably a deep chlorophyll maximum, and a visible influence of lake hydrodynamic processes, particularly during high-discharge inflows in summer stratification. The simulations were used to examine growth-limiting factors that help to explain its increased prevalence during a re-oligotrophication phase.

A long-term series (1960-2010), assessed over measured data, was reconstructed for some ecological indicators. A natural external phosphorus load was simulated by a hydrological and nutrients transport model (SWAT), after it was calibrated on a natural sub-basin. Data by a paleolimnological survey were used to initialize the lake ecological

model to reproduce the past conditions. A specific statistical technique (Spectral Singular Analysis) was used to isolate the trend of air temperature daily series, avoiding the periodic climatic fluctuations. Four different scenarios were simulated to characterize different levels of local and global pressure on lake ecology, combining each alternative driver into the lake model. The integrated lake-basin tool was also proposed as a dynamic tool to simulate the biogeochemical cycle in an alternative pristine ecological state. The output for phosphorus reference conditions was compared to the results by the most traditional methods (previously assessed for subalpine lakes).

After decades of lake eutrophication, the simulated temperatures warming did not enhance *P. rubescens* blooming. Conversely, a positive relation was found when the pressure from the catchment (e.g. phosphorus pollution) was switched off by the simulation, as emerged by the Mann-Kendall statistics on daily model output. In other words, the global warming may have different effects on *P. rubescens* dynamics, depending on the trophic evolution of a lake. The simulation of a pristine condition projected the lake into an oligo-mesotrophy, as the results of equilibrium between the external phosphorus loading and the trasformations across the internal exchanging pools. The simulation of lake transparency and productivity depicted a good ecological state, but the hypolimnetic waters remained anoxic during the thermal stratification, as confirmed by the paleolimnological survey (to pre-industrial age). *P. rubescens* persisted in that conditions, but its growth resulted strongly limited by low phosphorus concentration, resulting in a low productivity.

Table of contents

List of abbreviations

The following table describes the significance of various abbreviations and acronyms used throughout the thesis. Abbreviation for biogeochemical variables and models selected parameters are given in Table 4 and 10,11,14 respectively.

Abbreviation	Meaning
μ_g, μ_{max}	growth rate, maximum growth rate
1D-3D	mono-, three-dimensional
ABSerr	Absolute error
Alk	Alkalinity
APAT	Agenzia per la Protezione dell'Ambiente e per i servizi Tecnici
Aph-f-a	Aphanizomenon flos-aquae
ARPA	Agenzia Regionale per la Protezione dell'Ambiente
Ast-f	Asterionella formosa
C	Carbon
CAEDYM	Computational Aquatic Ecosystem Dynamics Model
Cal	Calibrated
CD	chlorophyll derivatives
CDF	Cumulative Distribution Function
Chl-a	Chlorophyll-a
Cond	Conductivity
Cry-er	Cryptomonas erosa
Crypto	Cryptophyta
Cry-rostr	Cryptomonas rostratiformis
Cry-sp	Cryptomonas (other) species
CSOs	Combined Sewage Overflows
CTD	Conductivity, Temperature, Depth (probe)
CUR	Current
CWT	Continuous Wavelet Transform
d.w.	dry weight
DCMs	Deep Chlorophyll Maximum species
Diat	Diatoms
Dm-MC-LR	Dimethyl-Microcystin-LR
Dm-MC-RR	Dimethyl-Microcystin-RR
DRP	Dissolved Reactive Phosphorus
DYRESM	DYnamic REServoir Simulation Model
ELCOM	Estuary, Lake and Coastal Ocean Model
E_{NS}	Nash–Sutcliffe index
ENSO	El Niño Southern Oscillation
eof1	empirical orthogonal functions (1st order)
FP	FluoroProbe
GCMs	Global Climate Models
GIS	Geographical Information System
GPS	Global Pressure Simulation
GWS	Global Wavelet Spectrum
H-A	High Alkalinity
HPLC-DAD	High-Performance Liquid Chromatography with Diode-Array Detection
HRUs	Hydrologic Response Units

IP	(Algal) Internal Phosphorus
IRSA-CNR	Istituto di Ricerca sulle Acque - Consiglio Nazionale delle Ricerche
LIMNO	Limnological Database
LM-A	Low and Moderate alkalinity
LOI	Loss Of Ignition
LPS	Local Pressure simulation
MB	Mean Bias
MEI	Morfo
N	Morphoedaphic Index
NAO	North Atlantic Oscillation
obs	observed
OECD	Organisation for Economic Co-operation and Development
OLS	Ordinary Least Squares
P	Phosphorus
PAR	Photosynthetically Active Radiation
PBIAS	Percent BIAS
PCA	Principal Component Analysis
PIRoGA	Progetto Integrato lago/bacino per il Recupero della qualità ecologica e la Gestione idrologica delle Acque del Lago di Pusiano
P-rub	Planktothrix rubescens
Q-Q	Quantile-Quantile
R^2	correlation coefficient
R^2_{CV}	cross-validated correlation coefficient
RCMs	Regional Climate Models
RELerr	Relative error
RES	Regional Earth System
RMSE	Root Mean Square Error
Sal	Salinity
SCS	Soil Conservation Service
SD	Secchi Disk
sd	Standard Deviation
S-DSC	Statistical Downscaling
Si	Silica
sim	simulated
SSA	Singular Spectrum Analysis
ST	Station
SWAT	Soil and Water Assessment Tool
TC	total carotenoids
TP Chloro	Chlorophyll inferred model for Total Phosphorus
TP EXP coeff	Total Phosphorus by export coefficients
TSI	Trophic State Index
TSS	Total Suspended Solids
TURB	Turbidity
UND	Undisturbed
Val	Validated
WFD	Water Framework Directive (2000/60/EC)
WTC	Wavelet coherence
XWT	Cross wavelet transform

List of figures

Figure 9 a Dominant species of the phytoplankton assemblage as mean biovolume ($mm^3\ m^{-3}$) along water column by monthly identification. Mean total biovolume by all species is also reported as black dots. Log-regressions between biovolume ($mm^3\ m^{-3}$) and chlorophyll concentration (µg Chl-a L^{-1}) determined fluorometrically at every depth and date for : **b** total biovolume and chlorophyll concentration; **c** P-rub fingerprint; **d** Cyanobacteria spectral group; **e** Diatoms spectral group; **f** Cryptophyta spectral group.

Figure 10. Scatterplots with smoothed densities by simulated (on Y axes) and field (on X axes) data; E_{NS} value (NS), Mean Bias (MB) and Root Mean Square Error (RMSE) are also reported as indices of model fit for **a** temperatures (° C), **b** dissolved oxygen (mg L^{-1}), **c** silica (mg L^{-1}), **d** orthophosphate (mg L^{-1}), **e** ammonium (mg L^{-1}), **f** nitrate (mg L^{-1}), **g** Diat (µg Chl-a L^{-1}), **h** Crypto (µg Chl-a L^{-1}) and **i** P-rub (µg Chl-a L^{-1}). See in the text for more information.

Figure 11 On each subplot: RMSE (black line, referred to the main Y axes) and MB (grey line, referred to the secondary Y axes) at ST6 station computed by simulated and field for each sampling date (above); field (black lines) versus model (contour plot in scale of gray) profiles at ST6 station (below) as **a** function of depth (as meters on Y axes) and time (sampling date on X axes) for a temperatures in °C, **b** dissolved oxygen in mg DO L^{-1}, **c** silica mg Si-SiO_4 L^{-1}, **d** orthophosphate mg P-PO_4 L^{-1}, **e** ammonium mg N-NH_4 L^{-1}, **f** nitrate mg N-NO_3 L^{-1}, **g** Diat, µg Chl-a L^{-1} **h** Crypto µg Chl-a L^{-1} and **i** P-rub µg Chl-a L^{-1}. The missing values among the RMSE and MB of Diat and P-rub depended on the absence of measured profiles.

Figure 12. Spatial model performance description through RMSE computed by simulated and measured data residuals at each monitoring station for **a** temperatures, **b** dissolved oxygen, **c** Diat, **d** Crypto and **e** P-rub. For each variable RMSE is relative to the full scale. Light gray expresses a lower error.

Figure 13. Simulation output at the depth of 2 meters (left) and of 8 meters (right) at ST6 station for the limitation terms to phytoplankton growth. For each algal group the time evolution (322 days from 23 Feb. 2010 to 12 Jan. 2011, expressed as day of year). Each window of 30 days in the sub-plots corresponds to the area in the polygons (above each sub-plot) representing determinant periods for the phytoplankton phenology: (from left to right) late-winter from 53 to 80 day of year, early-spring from 85 to 120 day of year, mid-summer from 200 to 230 day of year, late-autumn from 300 to 330 day of year. The algal growth is determined by the influence of temperature f(T), orthophosphate f(P), dissolved inorganic nitrogen f(N), silica f(Si), light f(L), respiration (R) and grazing (G) for: **a** Diat, **b** Crypto and **c** P-rub.

Figure 14 Representation of spatial horizontal patterns before, during and after a flood event as mean values of salinity (Sal) and P-rub maximum Chl-a concentrations on surface plots. X and Y are spatial axes (m); thin arrows represent velocity and direction of the water currents in lake and the thick arrow on the lake center represents velocity and direction of the wind.

Figure 15. Panel (a) : Lake Pusiano with the catchment area, the reference and secondary meteorological stations and the closest PROTHEUS node. Panel (b): the method outline illustrating data flux to build the hydrological and meteorological forcing for the integrated modelling purpose.

Figure 16. Panel a: natural (simulated by SWAT) and anthropogenic (estimated out of the model) annual P-load to Lake Pusiano. Panel b: mean annual atmospheric real temperature associated to the trend computed with SSA and annual series after a detrending computation on the real temperature.

Figure 17. Measured (black line or circles) and simulated (grey solid line) daily values for the lake levels (a), the winter values for temperature (b), TP (c), TN (d) and the early spring values for total Chl-a (e). The error bars on simulated monthly mean values represent the daily maximum and minimum.

Figure 18. Scenarios comparisons: (a) simulated mean annual temperatures, representing the lake heat content; (b) simulated total phosphorus (TP) and (c) total nitrogen (TN) concentration at winter overturn; (d) simulated Chl-a concentration at early spring. CUR=Current scenario, GPS=Global Pressure Scenario; LPS=Local Pressure Scenario; UND=Undisturbed scenario.

Figure 19. Continuous Wavelet Transform (CWT) spectrum of periodic frequencies of the simulated *P. rubescens* (as µg Chl-a L^{-1}) daily time series (from 1960 to 2010) for each scenarios (CUR=Current scenario, GPS=Global Pressure Scenario; LPS=Local Pressure Scenario; UND=Undisturbed scenario). (a) Daily simulated series of the Chl-a data, (b) continuous wavelet power spectrum showing the periodicity (the black curve indicates the region without edge effects; solid lines are significant ($p < 0.05$) coherent time–frequency regions) and (c) the wavelet power for each period is normalized by the Global Wavelet Spectrum (GWS) and depicts the periods that explain a high proportion of the temporal variance of the series (y-axis) and the recurrence strength of the periods (x-axis). The continuous wavelet spectrum illustrates how the strength of the periodicities changed over time; colours indicate differing degrees of variance (dark red indicates high intensity; dark blue indicates low intensity).

Figure 20. *On the main sub-plots*: Mann–Kendall statistic for simulated *P. rubescens* (as µg Chl-a L^{-1}) monthly time series (from 1960 to 2010) for each scenarios (CUR=Current scenario, GPS=Global Pressure Scenario; LPS=Local Pressure Scenario; UND=Undisturbed scenario). *On the left:* the Sen slope values are associated to the colours-bar. *On the right*: the significance of annual trends (splitted for each month) *p-value=0.05;** p-value =0.01; *** p-value =0.005. *Above*: mean monthly simulated series for simulated *P. rubescens* (as µg Chl-a L^{-1}). *Below*: MKS test with forward-trend (black line) and backward-trend (grey line). Horizontal lines represent critical values [-2;2] corresponding to the 95% confidence interval. The intersection of the test statistic for the forward and the backward lines is identified as the change point in the series.

Figure 21. a) Map showing the location of the selected lakes used for MEI, Export Coefficient model and chlorophyll inferred TP model (Guilizzoni et al., 2011); b) Map of Lake Pusiano watershed for land use, meteorological and water quality monitoring stations. The sub-basin of reference (Gajum) used to calibrate the natural P-loading is marked (red line).

Figure 22. PCA Biplot for 35 selected lakes considering the TP, alkalinity, calcium and pH measured values. The red line includes the High Alkalinity (H-A) and the blue line includes the Low-Medium Alkalinity (LM-A) group.

Figure 23. Analysis of the correlation coefficient, the significance and the associated error for the traditional models used to predict the phosphorus (as mean TP concentration) reference condition for subalpine lakes. Morpho-Edaphic model using as predictor a) alkalinity (TP MEI alk) and b) conductivity (TP MEI cond); c) Export coefficient model (TP EXP coeff) d) Chlorophyll inferred TP model (TP Chloro) tested over 15 subalpine selected lakes from Guilizzoni et al. (2011) dataset. For each correlation, the coefficient (r) is significant at p-value<0.001 '***'; p-value <0.01 '**'; p-value<0.05 '*'; p-value <0.1 '.' (2-tailed). Confidence level is at 95%.

Figure 24. a) Regression analysis between the turbidity and the corresponding hourly TP concentration, measured at the outlet of Gajum sub-basin ('***'p-value<0.001).

Figure 25. Process-based and dynamic lake-basin modelling (1998-2010) results, as annual aggregated values. a) Cumulated annual rainfall (measured data) and TP external loading (SWAT simulation); b) TP lake concentrations at winter overturn estimated with the Vollenweider's model and simulated by DYCD (REFERENCE-Sim).

Figure 26. Phosphorus reference conditions for Lake Pusiano as evaluated by traditional methods and the process-based and dynamic lake-basin approach. The error bars represents the RMSE associated at each predictive model. The trophic classification was based only on phosphorus concentration (OECD, 1982).

Figure 27. Daily time series of transparency (SD), TP, TChl-a and *P. rubescens* Chl-a as simulated in the pristine (REFERENCE-sim) and current (CURRENT-sim) scenarios.

Figure 28. Monthly evolution (as monthly mean over the 1998-2010 period) of a) dissolved oxygen (DO) and b) orthophosphate ($P\text{-}PO_4$) at lake bottom (25 m depth) as simulated in the pristine (REFERENCE-sim) and current (CURRENT-sim) scenarios. The difference between scenarios (as REFERENCE-sim – CURRENT-sim) is also shown.

Figure 29. a) The Trophic State Index (Carlson, 1977) modified (TSI*), adapted to Italian lakes and ranked by trophic thresholds (De Bernardi et al., 1985), aggregated in mean annual values. Bar errors indicates the sd over all the daily data for each year. b) The TP at lake winter overturn, as mean monthly value in February for each year. Bar

errors indicates the sd over the daily data of February for each year. The trophic thresholds refer to OECD (1982).

Figure 1A. Lake Pusiano seasonal evolution of nutrients (as linear interpolation of monthly values measured at the maximum depth ST6 during 2010) for: a) ammonium (mg $N\text{-}NH_4$ L^{-1}); b) nitrate (mg $N\text{-}NO_3$ L^{-1}); c) silica (mg $Si\text{-}SiO_2$ L^{-1}); d) orthophosphate (µg $P\text{-}PO_4$ L^{-1}); e) total nitrogen (mg N L^{-1}); f) total phosphorus (µg P L^{-1}). It was used to initialize the nutrient levels in CAEDYM model and to assess them along the simulations.

Figure 2A. Lake Pusiano seasonal evolution of carbon, as monthly concentrations of Dissolved Organic Carbon (DOC) and Particulate Organic Carbon (POC) measured at the maximum depth (ST6) during the water sampling in 2010 for: epilimnion, metalimnion and hypolimnion. POC content was determined only for lake circulation (23rd February) and maximum stratification (2nd September). It was used to initialize the carbon level in CAEDYM model and to assess it along the simulation.

Figure 3A. Lake Pusiano monthly evolution of phytoplankton, as the biovolume (mm^3/m^3) of the main taxonomic groups in the water column, by cell enumeration microscopy of the samples taken at the maximum depth (ST6).

Figure 4A. Lake Pusiano monthly evolution of phytoplankton, as the biovolume (mm^3/m^3) of the main spectral groups in the water column, evaluated by cell enumeration of the samples taken at the maximum depth (ST6). It was used to calibrate the spectral groups of the FluoroProbe for four the dominant taxonomic groups.

Figure 5A. Lake Pusiano monthly evolution of phytoplankton, as the biovolume (mm^3/m^3) of the key-species in the water column, by cell enumeration of the samples taken at the maximum depth (ST6). It was used to determine the key-species and parameterize the three algae groups in the CAEDYM model.

Figure 6A. Lake Pusiano total annual biomass of phytoplankton, as percentage of the species by cell enumeration of the samples taken at the maximum depth (ST6).

Figure 7A. The linear regression of both the total endocellular microcystins and the Chl-*a* concentrations with the biovolume of *P. rubescens* measured in Lake Pusiano at different depths in 2010. It was used to determine the fingerprint of the specific spectral response for *P. rubescens.*

Figure 8A. Percentages of the three main zooplanktonic groups by the annual (2010) survey in Lake Pusiano. It was used to initialize the zooplankton model (CAEDYM).

Figure 9A. Linear regressions between measured values (by CTD or fluorimetric probe) and the relative analytic determinations for pH, conductivity and total chlorophyll-a.

(***) is for p-value < 0.005 and (**) for p-value < 0.01. It was used to calibrate both the probes profiling all the lake stations and to get a three-dimensional description of variability along the time and the space axes.

Figure 10A. Surface (the section cut is at 2 meters depth) and vertical (the section cut is on SW-NE axis: ST16c; ST13; ST10; ST6; ST2; refer to the map in Figure 2) profiles of temperature, dissolved oxygen, pH and turbidity, measured by the CTD probe on the 23rd February for each station and depth of the lake and used to initialize the three-dimensional model (ELCD).

Figure 11A. Surface (the section cut is at 2 meters depth) and vertical (the section cut is on SW-NE axis: ST16c; ST13; ST10; ST6; ST2; refer to the map in Figure 2) profiles of the chlorophyll-a concentration measured by the FluoroProbe on the 23rd February for each station and depth of the lake and used to initialize the three-dimensional model (ELCD). The spectral response (or signal) is associated to the total concentration (as sum of all), *P. rubescens*, Diatoms and Cryptophytae.

Figure 12A. Vertical (section cut is on SW-NE axis: ST16c; ST13; ST10; ST6; ST2; refer to the map in Figure 2) profiles of salinity measured on each sampling date and used to check the river entrance plume and the lake patterns during the simulation of the three-dimensional model (ELCD).

Figure 13A. Three-dimensional interpolations (Matlab® software) of all the measured profiles, here only to show *P. rubescens* spatial and temporal evolution during the seasonal growth, from the metalimnetic niche formation at the end of the summer, through the bloom in autumn up to the cells deterioration in late winter. This was used to check and calibrate the *P. rubescens* behaviour during high-frequency simulation of the three-dimensional model (ELCD).

Figure 14A. Lake Pusiano map showing the two transept for the sediment sampling, the maximum depth station (II) and the middle-depth (Lambro River closest) station (I). Sediment transepts were characterized at the beginning and at the maximum of the thermal stratification (30th March and 7th September, respectively). Furthermore sediment cores were taken on 28th September in the I and II stations to determine the phosphorus content by Psenner Fractionation.

Figure 15A. Results for the sediment transepts characterization by water content (as % of wet weight), dry sediment weight (as %), organic matter (Loss On Ignition, as % of dry weight), calcium carbonate (as % of dry weight) and carbonate (as % of dry weight). This was used to calibrate the sediment parameters in the CAEDYM model.

Figure 16A. Phosphorus fractionation (Psenner et al. 1984, modified by Hupfer et al., 2004) of Lake Pusiano sediment. This was used to calibrate the sediment P-content and release rate in the CAEDYM model.

Figure 17A. The wind rose was plotted with the wind speed and direction hourly data collected at the lake meteoreological station (Geretta, refer to map in Figure 2). This was used as metereological input for the simulation with the three-dimensional model (ELCD).

Figure 18A. The wind speed (on the left) and direction (on the right) hourly data are shown as histograms of distribution classes (frequency), aggregated for the morning and the afternoon events.

Figure 19A. All the other meteoreological hourly series: a) temperature: b) global solar radiation; c) percentage of humidity; d) rainfall; e) percentage of cloud cover. This was used to force the metereology of the three-dimensional model (ELCD).

Figure 20A. Lake Pusiano Hypsographic curve of the lake volume by the depth, used to compute the weight averages of such a variables.

Figure 21A. A visualization of the internal wave activity by the interpolation of the lake temperature measured every 15 minutes by the thermistors chain at each meters of depth from 30th April to 20th September 2010. The wind speed plot is also shown to compare the intensity peaks to the microcirculation patterns occurring in the lake. White in the plot is for lost data. This was compared to the internal wave activity simulated by the three-dimensional model (ELCD).

Figure 22A. Lambro River high-frequency (15 minutes) measured temperature (blue dot) by the multiparametric probe sensor that was fixed near the lake entrance, compared to the same series computed by the measured air temperature (red line). This was used both to force the hydrology of the 3D model (ELCD) and to reconstruct the river water temperature for the long term series.

Figure 23A. Lambro River high-frequency (15 minutes) measurements for dissolved oxygen (DO), as % of saturation (blue dot) by the multiparametric probe sensor that was fixed near the lake entrance, compared the measured rainfall (black lines and rings). This was used as input of river water quality forcing the 3D model (ELCD).

Figure 24A. High-frequency (15 minutes) measured discharge of the three main tributaries to Lake Pusiano, used to prepare the hydrological forcing for the 3D model (ELCD).

Figure 25A. Continuous Wavelet Transform (CWT) spectrum for Lambro River temperature, measured at high frequency (15 minutes) in 2010. The sub-plot above shows the average centered and normalized by the standard deviation series. The wavelet power for each period is normalized by the Global Wavelet Spectrum (dimensionless, on the right) and highlights the dominant recurrent cycles. Here the daily and the half-daily are the dominant cycles, but some patterns were found also for 2,4,8 days in June. The power of the wavelet spectrum decreased considerably in autumn and winter ow-

ing to a low temperature excursion and resulting in low resolution in that period. The cone of influence (black curve) indicates the region without edge effects. The power values are coded from dark blue for low power to dark red for high power, as shown in the bar of classes below (refer to Materials and Methods for further information). This was performed to find a synchronicity between lake and river ocillations.

Figure 26A. Continuous Wavelet Transform (CWT) spectrum for Lambro River turbidity, measured at high frequency (15 minutes) in 2010. The sub-plot above shows the average centered and normalized by the standard deviation series. The wavelet power for each period is normalized by the Global Wavelet Spectrum (dimensionless, on the right) and highlights the dominant recurrent cycles. Here the dominant recurrent patterns are between 4 and 16 days, but some pulses were found also at hourly scale during rainfall. The power of the wavelet spectrum increase in autumn and winter owing to higher rainfall and runoff from the catchment. The cone of influence (black curve) indicates the region without edge effects. The power values are coded from dark blue for low power to dark red for high power, as shown in the bar of classes below (refer to Materials and Methods for further information). This was performed to find the period of pulses due to the catcment runoff during the rainfall.

Figure 27A. Continuous Wavelet Transform (CWT) spectrum for Lambro River conductivity, measured at high frequency (15 minutes) in 2010. The sub-plot above shows the average centered and normalized by the standard deviation series. The wavelet power for each period is normalized by the Global Wavelet Spectrum (dimensionless, on the right) and highlights the dominant recurrent cycles. Here the dominant period is between 1 and 4 days, thus meaning a daily periodic chage in the river water composition. The power of the wavelet spectrum decrease in autumn and winter owing to higher rainfall and water diluition. The cone of influence (black curve) indicates the region without edge effects. The power values are coded from dark blue for low power to dark red for high power, as shown in the bar of classes below (refer to Materials and Methods for further information). This was performed to find the periodicity of Lambro River chemical variation.

Figure 28A. Continuous Wavelet Transform (CWT) spectrum for Lambro River dissolved oxygen, measured at high frequency (15 minutes) in 2010. The sub-plot above shows the average centered and normalized by the standard deviation series. The wavelet power for each period is normalized by the Global Wavelet Spectrum (dimensionless, on the right) and highlights the dominant recurrent cycles. Here the daily and the half-daily are the dominant cycles, thus resulting linked to the temperature patterns. The power of the wavelet spectrum decreased considerably in autumn and winter owing to higher discharges and low variability thus resulting in low resolution in that period. The cone of influence (black curve) indicates the region without edge effects. The power values are coded from dark blue for low power to dark red for high power, as shown in

the bar of classes below (refer to Materials and Methods for further information). This was performed to characterize the river water quality.

Figure 29A. Cross Wavelet Transform (XWT, above) and Wavelet Coherence (WTC, below) spectra for rainfall and Lambro River discharge comparison. The Global Wavelet Spectrum (dimensionless, on the right) of both the variables were compared to analyze their covariance. The river discharge strongly responded to high rainfall events, with a time lag of few hours (the corrivation time of Pusiano watershed is 4-6 hours) only at high frequency (1-8 days). This was helpful to isolate the events during the multiregression analysis used to build the catchment loading.

Figure 30A. Cross Wavelet Transform (XWT, above) and Wavelet Coherence (WTC, below) spectra for turbidity and Lambro River discharge comparison. The Global Wavelet Spectrum (dimensionless, on the right) of both the variables were compared to analyze their covariance. A covariance was hard to detect; apparently a tendency to form a common pattern is identified around a period of recurrence of 1, 2, 4 and 16 days probably owing to a strong change of turbidity depending on the rainfall span and the river discharge. This supported the outcome by the 3D simulation (ELCD): during an important rainfall event the river enters to the lake with higher concentrations of substances at the beginning and with a more diluite water after 1-2 or more days.

Figure 31A. Map of Pusiano watershed with the rivers monitoring points.

Figure 32A. Characterization of different sub-basins by annual average and variability (via standard deviation) of phosphorus species during the field campaign in 2010, used to calibrate and validate the SWAT model for natural P-load (Gajum sub-basin).

Figure 33A. Percentage of organic matter (% LOI d.w.), carbon (% CO_3 d.w.), total sedimentary chlorophyll derivatives (as unit CD g LOI^{-1}), sedimentary total carotenoids (as mg TC g LOI^{-1}) and 430 nm : 410 nm pigments ratio detected in the core cut sections. The estimated chlorophyll water concentrations was used to initialize the unidimensional model for long term simulations (DYCD).

Figure 34A. Percentage (% d.w.) of total carbon (C_{tot}), inorganic carbon (C_{inorg}), organic carbon (C_{org}), total nitrogen (N) and sulphur (S) and the C_{org} : N ratio. The estimated nitrogen and carbon water concentrations were used to initialize the unidimensional model for long term simulations (DYCD).

Figure 35A. Distribution of pigment concentrations in Lake Pusiano sediment dated core and the relative association to algal groups. This information was used to characterize the algal community in the unidimensional model for long term simulations (DYCD) and for the assessment of phosphorus reference conditions by inferential models.

Figure 36A. Increasing trend over the annual averages of daily air temperature since 1960 to 2010, collected at the metereological stations within Pusiano catchment area. The slope (0.015° C yr^{-1}) confirmed those found for Italian lakes (Ambrosetti and Barbanti, 1999).

Figure 37A. Air temperature daily series was processed by the Singular Spectrum Anlysis (Ghil and Vautard, 1991) to detect the best running average (thick lines are for 3 to 25 years span). The closest to the linear trend (15, 20 and 25 years span) were compared to choose the slope for the best detrended series (i.e. the 20 years span), which the onset was the closest to the original series (refer to Chapter 3 for a further explanation).

Figure 38A. Water temperature measured in Lake Pusiano during the winter overturn (end of January) since 1972.

Figure 39A. Total phosphorus (TP), nitrogen (TN) and silica (Si-SiO_2) detected in Lake Pusiano during the winter overturn (end of January) since 1972.

Figure 40A. Phosphorus and nitrogen ratio evolution, as TN:TP mass ratio, computed by the winter overturn series since 1984 to 2010.

Figure 41A. Mean annual biomass (mm^3 m^{-3}) of the main phytoplankton groups in Lake Pusiano by monthly surveyes from 2002 to 2010.

Figure 42A. Seasonal evolution of *P. rubescens* biomass (mm^3 m^{-3}) by cell enumeration in water samples taken at different depths from 2002 to 2010, in Lake Pusiano. The series was used to assess the last 9 years of the long term simultions with the 1D model (DYCD).

Figure 43A. Seasonal evolution of: *above*) thermal profile measured by CTD probe at the maximum depth station (ST6, refer to the map in Figure 2) from 2002 to 2010, in Lake Pusiano; *below)* thermal stability computed by temperature and salinity profiles to get the Brunt-Väisälä frequency, or buoyancy frequency (Mortimer, 1974) at the maximum depth station (ST6, refer to the map in Figure 2) from 2002 to 2010, in Lake Pusiano. The series was used to assess the last 9 years of the long term simultions with the 1D model (DYCD).

Figure 44A. Increasing trend over the monthly temperature series, measured by the CTD probe at Lake Pusiano bottom (22-25 meters depth) from 2002 to 2010.

Figure 45A. Seasonal evolution of *P. rubescens* compared to the remaining biomass (as % of total), by cell enumeration in water samples taken at different depths in Lake Pusiano and the cumulated monthly rainfall measured from 2002 to 2010 in Pusiano catchment. This elaboration was used to parameterized the two algal groups (*P. rubescens* and a general competitor G2) in long term simultions with the 1D model (DYCD).

List of tables

Table 14. The Vollenweider model

Table A1. Statistical indexes for the hydrochemical analysis in water samples of Lake Pusiano taken during 2010.

Table A2. The microcystin concentration detected at different depth in Lake Pusiano, during crucial peak of chlorophyll in 2010. The Dimethyl-Microcystin-RR (Dm-MC-RR) and Dimethyl-Microcystin-LR (Dm-MC-LR) are the main kind of endocellular microcystin revealed in laboratory by the HPLC-DAD.

Table A3. List of zooplanktonic taxa detected in Lake Pusiano during the four seasonal surveys (30th March, 16th June, 10th September, 14th December 2010). It was used to parameterize the dominant herbivore species in the CAEDYM model.

Table 4A. Statistics of the nitrogen species detected by the water samples collected at each station to characterize the nutrients transport in the Pusiano catchment during 2010. This was used to prepare the nutrients input to the 3D model (ELCD).

Table 5A. Statistics of the phosphorus species and the total suspended solids (TSS) detected by the water samples collected at each station to characterize the nutrients transport in the Pusiano catchment during 2010. This was used to prepare the nutrients input to the 3D model (ELCD).

Table 6A. Pearson correlation matrix for all the variables measured in Lake Pusiano during the limnological campaigns from 1972 to 2005 (performed to assess the experimental plan of the last campaigns in 2010). Correlation coefficients are significant at the 0.05 level (2-tailed).

Acknowledgments

The author wish to thank Franceso Spada, Alessandro Perotto and all the EPSON Meteo Centre (http://www.meteo.it/) for the computational support, the Centre for Water Research (http://www.cwr.uwa.edu.au/) for kindly supplying the hydrodynamic-ecological model DYRESM/ELCOM-CAEDYM, Andrea Lami and Giuseppe Morabito (CNR-ISE) for the precious paleolimnological analysis and the support of a second Fluroprobe, Sandro Calmanti (ENEA) for kindly providing meteorological RES PROTEUS data forcing. Special thanks to Severino Giudici and Vittorio Mattiolo for the fundamental and friendly support during the field activities, without which the present study would not have placed. The author is infinitely grateful to Sarah Groves for kindly and helpfully reviewing the present work.

Preface

The main body of this thesis comprises three Chapters (Chapters 2–4) which have been prepared in a paper format owing to submission for publication in peer reviewed scientific journals. I was responsible for the field work program, sampling and data analysis, and for writing this thesis. Laboratory activities and watershed modelling were under the direct responsibility of Dr. Copetti and Dr. Salerno. Except when referenced, the material in this thesis was produced by the author's own ideas and work undertaken under the supervision of Dr. Gianni Tartari (Water Research Institute, Italy). Prof. David Hamilton (University of Waikato, New Zealand) has contributed as co–author of the published paper constituting Chapter 2 (below) with discussions and revisions to the manuscript prior to submission. Prof. Pierluigi Viaroli (University of Parma, Italy) has supervised the thesis project and the scientific statement. Dr. Sarah Groves (University of NSW, Australia) has supervised and reviewed the final draft.

Referees: Prof. Roland Psenner (University of Innsbruck, Austria); Prof. Andrea Capodaglio (University of Pavia, Italy)

Chapter 2 has been published as: Carraro E., Guyennon N., Hamilton D.P, Viviano G., Manfredi E., Valsecchi L., Salerno F., Tartari G. and Copetti D. 2012. Coupling high-resolution measurements to a three-dimensional lake model to assess the spatial and temporal dynamics of the cyanobacterium *Planktothrix rubescens* in a medium-sized lake. Hydrobiologia 698: 77–95 ($IF_{5\text{-years}}$=1.997)

Chapter 3 has been published as: Carraro E., Guyennon N., Viviano G., Manfredi E., Valsecchi L., Salerno F., Tartari G. and Copetti D. Impact of Global and Local Pressures on the Ecology of a Medium-Sized Pre-Alpine Lake. In: Models of the Ecological Hierarchy: From Molecules to the Ecosphere. Elsevier B.V., pp. 259–274.

Chapter 4 is to be submitted to Environmental Science & Technology (IF_{2011}=5.228).

The title is "Total phosphorus reference conditions for subalpine lakes: a comparison between traditional methods and a new process-based and dynamic lake-basin ap-

proach". List of authors: Salerno F., Viviano G., Carraro E., Manfredi E., Lami A., Guyennon N., Copetti D. and Tartari G.

In the **Appendix** the reader can find more data (raw or processed) series, mostly used to implement and assess the models or analyse the trends.

Publications out of the thesis work:

- Nizzoli D., Carraro E., Nigro V. and Viaroli P, 2010. Effect of organic enrichment and thermal regime on denitrification and dissimilatory nitrate reduction to ammonium (DNRA) in hypolimnetic sediments of two lowland lakes. Water Research, 44: 2715-24. ($IF_{5\text{-years}}$=4.966)
- Copetti D., Valsecchi L., Ghislanzoni L., Pozzoni F., Carraro E., Guyennon N., Tartari G. and Guzzella L. An intense *Planktothrix rubescens* bloom in a South Italy multiple-uses reservoir and its impact on the agricultural irrigation network. Submitted to Environmental Toxicology ($IF_{5\text{-years}}$= 2.164)

1 Introduction

1.1 General overview

The present work is a part of a more general project called PIRoGA (*Integrated Lake/Watershed Project for Lake Pusiano ecological recovery and hydrological management*). The final goal of the project is to understand the dynamic linkage between a medium-sized pre-alpine lake (Lake Pusiano) and its watershed by field data analysis and numerical models. The project lasted three years (2009-2011) and resulted in a scientific support to the lake restoration and to the management plans, addressing one of the key objectives of the Water Framework Directive (further – WFD; Directive 2000/60/EC), i.e. the achievement of a minimum of good ecological quality in natural lakes. In general, the state of good quality aimed by the WFD should be close to a 'reference state', to be defined as 'pre-disturbance' condition for each ecosystem (Bennion et al., 2005). When the WFD was included in the national Italian law (Dlgs. 152/2006 and following), river basin specific planning has been needed to integrate the management of all the water bodies into a unique basin scale approach. The WFD requires that all European lakes > 50 ha should be in ''high'' or ''good'' ecological conditions within 2015, as identified with integrated bioindicators (fish, macroinvertebrates, macrophytes, phytobenthos and phytoplankton). The ecological status of lakes and rivers is defined on the basis of the degree of deviation from type specific minimally impaired reference conditions (EU - IntercalibrationTechnical Report, 2006).

The achievement of a good ecological state for a lake can be a complex set of issues, in particular:

- how to define undisturbed or minimally impaired systems, rare or absent today, due to widespread eutrophication;
- how to manage incidental disequilibria when the conditions are improving (e.g. the appearance of certain types of algal blooms despite the improvement of the trophic conditions).

The Directive 2008/105/EC established the Environment Quality Standards (EQS) and amended the WFD assessing priority substances, pollutants and water policy. Ecological conditions have been assessed in the national laws on the basis of the population of

phytoplankton, fishes and benthic organisms but EU is still working to intercalibrate common standard procedures for monitoring and defining reference conditions.

There is worldwide evidence that the spatial and temporal incidence of harmful algal blooms is increasing (Huisman et al., 2005) posing potential risks to human health and ecosystem quality. Algal blooms in freshwater are predominantly cyanobacteria, some of which produce dangerous cyanotoxins (Carmichael, 2001). Scientist have identified a host of causative factors spanning many ecological levels: bottom-up factors, such as nutrients in contrast to global warming (Brookes & Carey, 2011); physiological features opposite to a decrease in top-down predators on the community level (Reynolds, 2006); thermal stability (Paerl and Huisman, 2008) and the altered structure and function of a whole water ecosystem (Scheffer et al., 1997). At present, the standards for the surface water quality are not sufficient enough to protect the public health against possible cyanobacteria and their toxic negative influence. Therefore, the definition of good ecological conditions may result in variations amongst the EU Member States (Lileikytė and Belous, 2011) often because of the lack of adequate information about the blooming dynamics. Moreover, the massive occurrence of cyanobacteria makes the proposed WFD ecological classes difficult to define, being the phytoplankton one of the four key biological quality elements to be used in the ecological classification of lakes in Europe (Søndergaard et al., 2011). The WFD imposes a planning process that consists of identification of the system with an impact-effect analysis supported by monitoring programs for water physico-chemistry and ecology. This process requires the integration, synthesis, analysis and communication of large amounts of information and knowledge on geophysical, biological, social and economic aspects in order to assist in the decision making process.

In recent years, freshwater ecologists have increasingly ascribed some biological responses to physical processes (Wetzel, 2001). Determining the ecological consequences of a physical structure change in lakes, caused by different forces acting on spatial or temporal scales, is a challenge for controlling ecosystem productivity. Bloom events have been related to hydrological processes, like overflow events, which inject rich nutrient water into lakes and enhance lakes productivity (Bargu et al., 2011). Since many limnological processes occur during periods of 1 hour to less than 1 week, high fre-

quency monitoring data have been increasingly hard to collect and track the ecosystem changes at small time scales (Pomati et al. 2011). The attempt of these monitoring programs is to demonstrate how high frequency and in situ measurements, tailored to short-time forecasting and warning system for phytoplankton blooms (including cyanobacteria), could be the base of monitoring designs to support the WFD objectives (Le Vu et al. 2011).

A range of modeling approaches is available to support a systematic or integrated view of aquatic ecosystems as summarized in Jørgensen (2010). Yet recently Trolle et al. (2012) demonstrated the importance to push ahead in the development of aquatic ecosystem models. The existence of a new community-based framework is supporting an enhanced union between some of the traditional ecologists and model developers. Lake models have been increasingly used for testing hypotheses in research. Many different approaches and levels of complexity have been and are used to achieve different goals, as overviewed in Reichert and Mieleitner (2008). Since few studies have high time resolution in phytoplankton measurements, the increasing use of models coupled with an adequate initial set of measurements has allowed the reproduction of spatial heterogeneity at high time resolution without a great effort in monitoring.

Some of the most common drawbacks of deterministic models deal with an extensive data input requirement (Robson et al., 2008), difficult calibration and process interpretation and high run times (Mooij et al., 2010). The parsimony principle of system identification states that a model should not be more complicated than necessary for the description of the data (Omlin et al., 2001a). Thus it is important to properly tailor the modeling purpose to the aims of the study before implementing any model.

1.2 Motivation

The toxic cyanobacterium *Planktothrix rubescens* has strongly dominated the phytoplankton community in the medium-sized pre-alpine Lake Pusiano (North Italy) since the early 2000s. The use of an integrated modelling tool, with a functional representation of key processes, enabled the linkage of small-scale and large-scale representations (Zhao et al. 2008). The need for process-focused models becomes particularly evident when considering the varying responses to environmental conditions of different taxonomic and functional groups of phytoplankton. The modelling purpose was to capture

the competitive potential of different phytoplankton species or groups and therefore the seasonal sequences and shifts in community composition, including responses to major environmental alterations such as eutrophication and climate change.

1.3 State of the Art

1.3.1 Lake ecosystems between global and local changes

Recent global changes, alterations in catchment nutrients input and an increasing translocation of species appear to have induced changes in phytoplankton assemblages. The rate of establishment of invasive or harmful species, such as cyanobacteria, has increased (Paerl and Huisman, 2008; Salmaso, 2010; Zhang et al., 2011). In particular, global warming has different impacts on the ecology of lacustrine environments. The progressive increase of water column stability leads to lakes meromixis, an expansion of the anoxic/hypoxic layer in productive environments (Verburg et al., 2003) and an increase of the nutrients release from sediments (Jeppesen et al., 2009). In general the global warming is expected to enhance many biogeochemical processes, exacerbating the eutrophication (Schindler, 2001) and altering the foodwebs (Schindler, 2001). Alterations of the phytoplankton phenology have been observed in relation to the increase of waters temperature producing extensions of the growing season and allowing, an earlier spring or later autumn bloom (Thackeray et al., 2008). Loss of regularity in the spring-autumn pattern, may result in irregular pulses of biomass and changes in the phytoplankton assemblages (Winder and Cloern, 2010).

The ecological lake dynamics are also strongly influenced by local impacts due to human modifications in the catchment. A mitigation of external loading pressure often leads to a general improvement of the lakes water quality, even though high rates of internal recycling of nutrients between the sediments and the overlying water column could lessen or delay the benefits of management actions at the catchment level (Søndergaard et al., 2003; Jeppesen et al., 2005). The increasing incidence of blooms was immediately correlated with the nutrients enrichment, suggesting a powerful causal link with the increased phosphorus availability (Gorham et al., 1974). Indeed reductions in nutrient concentrations before the growth season are still considered to be an important strategy to decrease the risk of cyanobacterial blooms, even under a scenario of warming temperatures (Brookes and Carey, 2011). There are evidences in some deep alpine

lakes, that the most important modifications to the pristine oligotrophic conditions were marked by occurrence of the *Planktothrix* species (Salmaso, 2005) Nevertheless, blooms of *P. rubescens* have been increasingly observed in lakes that have undergone recent re-oligotrophication, especially in lakes in pre-alpine European regions (Ernst et al., 2009). In many Swiss and Austrian lakes it has emerged as a 'keystone species' (often contributing > 50% of total phytoplankton biomass) and forms the characteristic deep chlorophyll maximum (DCM).

1.3.2 *Planktothrix rubescens*: an efficient ecosystem engineer?

Many planktonic cyanobacteria can aggregate at the water surface and form dense blooms and scums, with potential for production of potent toxins, including hepatotoxic microcystins (Carmichael, 2001). Gas-filled vesicles provide buoyancy and variable levels of photosynthetic carbohydrate reserves; this property can assist in buoyancy regulation in thermally stratified environments, to optimize nutrient and light acquisition and create greater propensity for bloom formation (Walsby et al., 1997). In thermally-stratified lakes blooms may persist through the stratified period until the surface mixed layer begins to deepen preceding winter overturn (Huisman et al., 2005). In their review Carey et al. (2012) examine how several cyanobacterial eco-physiological traits, specifically: the ability to grow in warmer temperatures; buoyancy; high affinity for, and ability to store, phosphorus; nitrogen-fixation; akinete production; and efficient light harvesting, vary amongst cyanobacteria genera and may enable them to dominate in future climate scenarios. Such blooms are certainly not new: from being well dispersed through the water column, they are 'telescoped' to the surface when the wind drops, concentrating along lee shores and giving a greatly exaggerated impression of abundance (Reynolds, 1971). Some species of cyanobacteria can also form dense metalimnetic populations in oligotrophic lakes as other species compete less effectively at reduced irradiance levels and they are strongly nutrient-limited in the surface mixed layer (Dokulil and Teubner, 2000). Metalimnetic populations are also known to form dense surface blooms and scums when they become 'overbuoyant' at critical stages in the seasonal stratification cycle (Walsby and Booker, 1980).

The behaviour of DCMs species has been stated as 'paradoxical' because the epilimnion should be more attractive for autotrophic organisms (Davis et al., 2003). *P. rubescens*,

blooming and spreading wide in the last two decades, the so-called 'burgundy-blood' algae (Walsby et al., 2006) has been observed in lakes of different sizes (Guiry and Guiry, 2011) but largely studied only in deep, stratifying and eutrophic lakes. Luxury storage of internal phosphorus may increase its competitiveness during re-oligotrophication when phosphate can be strongly depleted from the water column (Feuillade, 1994). In general the ecological success of *Planktothrix* species depends largely on gas vesicles, which provide cells with sufficient buoyancy to enable them to optimise resource capture at selected depths in thermally stratified lakes (Bürgi and Stadelmann, 2002; Walsby and Schanz, 2002; Walsby et al., 2006). *P. rubescens* can survive during complete water column mixing as it has a high light-capture efficiency; warm winters may also lead to larger inocula of this species for the subsequent summer growth cycle (Reynolds, 2006). Hamilton et al. (2010) provide evidence that oligotrophic lakes are more likely to support DCMs as a result of a euphotic depth that extends at least as far as the depth range of the metalimnion but *Planktothrix* spp. are also known to alter gas vesicle strength as a response to lake morphometry, depth, hydrology and circulation patterns (D'Alelio, 2011). Plunging river inflows that insert into the metalimnion can additionally provide nutrients necessary to sustain or stimulate DCMs (Wurtsbaugh et al. 2001) whilst recurrent internal waves have been demonstrated to enhance metalimnetic cyanobacterial populations by vertical excursions of the metalimnion and exposure to strong gradients of light and nutrients (Pannard et al., 2011). After decades of data collecting and analysing in Lake Mondsee (Austria) Dokulil and Teubner (2012) provided evidence for the impacts of climate warming and other environmental constraints on *P. rubescens* population and concluded that it only benefits from climate warming (ascribed to the Winter North Atlantic Oscillation) early in the year, during late spring overturn and early summer. Longer periods of summer stratification did not favour biovolume development. In the deep subalpine Lake Garda (North Italy), *P. rubescens* benefitted from the long-term increase in phosphorus concentrations and the year-to-year fluctuations in surface phosphorus availability, controlled by the East Atlantic pattern and lake mixing processes (Salmaso and Cerasino, 2012).

Padisák et al. (2010) states that of the coexisting species in an algal community, only few maintain the matter–energy processing ecosystem functions. Selection of these dominants is probably driven by mesoclimatic cycles, coupled with human-induced

forcing. The arising of a dominant species is often the result of 'an ecological memory' interacting with the environment changes. The results by the mentioned paper show that interspecific interactions and such particular autoecological features of the dominants, together with their effects on the whole ecosystem, may act as the major organizing force. Some phytoplankton species, like *P. rubescens*, are efficient 'ecosystem engineers' with cascading effects of both a top-down and bottom-up nature.

1.3.3 An eco-physiological model for *P. rubescens*

A number of different modelling techniques have been adopted to predict the timing, spatial distribution and magnitude of cyanobacterial blooms, and to derive knowledge about their dynamics. None of these models is perfect and, so long as there is argument about how blooms come about, there will not be a definitive model.

What kind of approach has to be chosen in modelling phytoplankton dynamics is an open question. The debate arises by whether outdated paradigms, modern molecular knowledge or enhanced measuring equipment have to be comprised into the equations for phytoplankton physiology. Much of the debate has also centered on empirical versus mechanistic models, a discussion that has been ongoing for decades (Jørgensen, 2010).The first ones have definitely success in balancing simplicity and realism but the use of complex deterministic models to reproduce aspects of the dynamics of aquatic systems may assist with capturing the spatial and/or heterogeneity within systems. Good process-based models of phytoplankton may differentiate some features of cyanobacteria from those of other phytoplankton, especially those leading to blooms (Robson and Hamilton 2004), such as buoyancy regulation, nitrogen storage capacity, the capability to catch the light of different wavelengths and to balance between energy capture, nutrient uptake, nutrient assimilation, cellular composition and cellular metabolism. Different cyanobacterial taxa also vary in their relative capacity and efficiency in relation to these processes and the current suite of mechanistic models is severely challenged when presented with predicting the dominance of particular cyanobacterial taxa, due to limitations in the level of model process description and differentiation amongst the different taxa.Also most such models have extensive data input requirements and the calibration and interpretation processes are made difficult by the requirement of intense spatial da-

ta, with often extended computer run times compared to simpler models (Grayson et al., 2002; Robson et al., 2008; Mooij et al., 2010).

Mieleitner and Reichert (2008) tried to reduce this complexity by combining empirical observations of phytoplankton temporal variations with biological knowledge that enabled definitions of functional groups for particular lakes. Several complex models claim to simulate cyanobacteria species or populations with some accuracy (e.g., Serra et al., 2007; Gal et al., 2009; Elliot, 2010) but most efforts to include spatial distributions and dynamics of different species have been focused on surface bloom-forming populations (Ibelings et al., 2003; Missaghi and Hondzo, 2010; Vilhena et al., 2010). Cuypers et al. (2011) used a simple physical model of cell transport to examine horizontal and vertical distributions of metalimnetic populations of *P. rubescens*, focusing on the role of seiches due to wind forcing during summer stratification. They found, however, that there were mismatches between simulated and observed data and attributed these to nonlinear effects on the biomass due to governing physical processes. An interesting attempt to simplify a complex model was developed by Mellard et al. (2011) to explore how the phytoplankton forming DCMs respond through growth and movement, to opposing resource gradients (i.e. of light and nutrients) and different mixing conditions. Variations in population density in the vertical dimension were determined by externally imposed heterogeneity in the form of resource gradients and mixing interact and by internally generated heterogeneity in the form of competition and movement.

According to Reynolds et al. (2002), *P. rubescens* can be classified within the solitary filamentous cyanobacteria group which prefers stratified waters. Being a cold-water stenotherm species and strongly limited by high irradiance (Bright and Walsby, 2000), it is usually located in the metalimnetic layers in summer at moderate temperatures (Dokulil and Teubner, 2000). In Lake Zürich, during summer stratification, Walsby and Schanz (2002) reported the peak of maximum production at depths between 10.5 and 13.5 m which corresponds to a water temperature range from 11 to 14 °C. *P. rubescens* is able to regulate its position, seeking water layers characterized by a Z_{eu}/Z_m (euphotic zone/mixed zone) ratio of around 0.7 - 1.2 at which the light intensity is around 1-5 % of the surface incident radiation (Dokulil and Toubner, 2000). Laboratory studies conducted by Walsby and Booker (1980) have shown that the *P. rubescens'* growth is saturated (in a 12h:12h light:dark cycle) at irradiances exceeding 20 µmol m^{-2} s^{-1} which rep-

resents one of the lowest thresholds for freshwater phytoplankton. A stable metalimnion, with a density gradient of at least of 0.05 kg m^{-1} (Bürgi and Stadelmann, 2002), allows *P. rubescens* to maintain a summer metalimnetic niche ready to insert into the surface layer at the onset of autumn (Walsby et al., 2006). As suggested by Scheffer et al. (1997) filamentous cyanobacteria are superior competitors at low light levels as they have evolved to exploit phosphorus resources at higher turbidity conditions, setting up a positive feedback mechanism. Numerical studies (Omlin et al., 2001; Scheffer, et al., 1997) suggest that *P. rubescens* is characterized by low maximum growth and respiration rate. Bright and Walsby (2001) measured this cyanobacterium has a maximum growth rate of 0.4 d^{-1} when cultured in continuous light and only 0.12 to 0.19 d^{-1} on a light-dark cycle. Cyanobacteria cannot be classified as a group with high growth affinity for phosphorus (Dokulil and Teubner, 2000), because their half saturation constant for phosphorus uptake is generally higher than those known for the other algae, such as green algae and diatoms, suggesting that they should be poor competitors in conditions of strong phosphorus limitation. However in several numerical studies (e.g. Scheffer, et al. 1997; Omlin et al., 2001; Rigosi et al., 2011) the ecological behaviour of filamentous cyanobacteria was successfully simulated by a low half saturation constant for phosphorus (0.003, 0.0019 and 0.002 mg P L^{-1} respectively). It has also be proved that the *P. rubescens* nutrients uptake is improved through vertical buoyancy regulation (Walsby et al., 2006) adjusting their position to maximize the utilization of light from the surface and nutrient from the chemiolimnion, thus avoiding the limitations of the phosphorous poor epilimnetic surface layer. Therefore the occupation of the metalimnetic niche can be modelled as a strategy to compete during the summer nutrients depletion in the epilimnion.

Owing to their small size the velocity of *P. rubescens* filaments movement ranges between 0.1-0.86 m d^{-1} (Wasby et al., 2001) which is somewhat less than the vertical velocity associated with basin scale internal wave seiching (Cuypers et al., 2011). This results in a major impact of hydrodynamics on the distribution of *P. rubescens* proliferating in the metalimnic layer of a deep lake which could influence the growth of this species by a direct impact on light availability.

In their theoretical study Scheffer et al. (1997) approached the problem of the filamentous cyanobacteria dominance in shallow lakes by simplifying the system in only two

stable states. The first characterized by the dominance of the filamentous cyanobacteria and the second by all the other phytoplankton species. In this simplified model they considered the stability of the system as a function of two principal parameters: phosphorus concentration and light availability. Analysing field data from 55 Dutch shallow lakes (3 m mean depth) they found that for total phosphorus concentrations below a certain value P1 (oligotrophy) only the non-cyanobacteria stable state was found, whereas for values higher than a certain value P2 (iper-eutrophy) only the cyanobacterial association might exist. Inside this range both stable states were found to exist and the system was characterized by hysteresis, that allowed for a switch one into the other. Furtermore, they found that the fate of the system was determined by the initial conditions: initial shady conditions brought about a filamentous cyanobacteria system whereas clear water produced a green algae system. In the first situation the system is characterized by a sort of 'auto-catalytic' process, incremented by the shady positive feedback. The shift from one to the other state was usually found to be 'catastrophic' and can be driven by changes in the hydraulic regimes. For example, an increase of the water renewal time to a value of greater than 18% of the lake volume per day caused filamentous cyanobacteria to disappear.

Ultimately, the key question is whether the ecological success of *P. rubescens* (when it occurs) is related to a performing physiology (Carey et al., 2012) or rather to the ability, in such conditions, to change the environment (Padisák et al., 2010).

1.4 Study area

A more complete description of time series for Lake Pusiano is given in the Appendix.

Lake Pusiano (45°48'20'' N, 9°16'33'' E) is a medium-sized lake (surface area 5 km^2) located in North of Italy. It is a typical warm monomictic lake with maximum depth 25 m and residence time ca. 1 year, overturning between January and February at which time temperature is ca. 5° C. The watershed area is about 95 km^2 (mean slope = 39%, maximum altitude = 1,453 m a.s.l, median altitude = 683 m a.s.l.) which produces a rapid hydrological response (typically ca. 4 h) in the Lambro River (mean discharge is 1.4 $m^3\ s^{-1}$). Two other minor rivers, Gallarana and Emissario del Segrino, enter the lake on the west side. The total mean inflow into the lake, calculated for the last 10 years, (including rainfall) is 2.6 $m^3\ s^{-1}$. The outflow is a complex system of two channels, mainly regulated by Canale Diotti located on the south-west side. Natural lands cover about the 82% of the catchment area while only 1% is devoted to agriculture. Urbanized areas (17%) are principally distributed along the river and lake shores.

The temperature time series, measured in the lake at winter overturn, has increased in the last 40 years (ca. 0.015 °C y^{-1}), in line with other studies on European alpine lakes (Ambrosetti & Barbanti, 1999; Livingstone, 2003). The lake is phosphorus-limited (Legnani et al., 2005). Total phosphorus (TP) concentrations increased until the mid 1980s (0.2 mg P L^{-1} at 1984 winter overturn) and progressively decreased toward the mesotrophic limit (0.04 mg P L^{-1}) by winter 2011, after the construction of a wastewater treatment plant in 1985. Total nitrogen concentrations have remained relatively constant (about 1.5 mg N L^{-1} at overturn) mainly due to substantial contributions of wet and dry atmospheric deposition to the nitrogen load (Balestrini et al., 2000).

Phosphorus loading to the lake has been described in Vuillermoz et al. (2006), who summarized several studies carried out in the Lake Pusiano watershed between 1972 and 2005. The main contribution to the lake comes from the Lambro River, which shows great variability, ranging from 20 to 7 t P y^{-1} in 2000-2003, due mostly to the inter-annual rainfall variability (Salerno & Tartari, 2009).

Currently, the main source of phosphorus pollution originates by the point sources, consisting in a network of combined sewage overflows (CSOs), which release polluted water into the rivers during rainfall events (Figure 1).

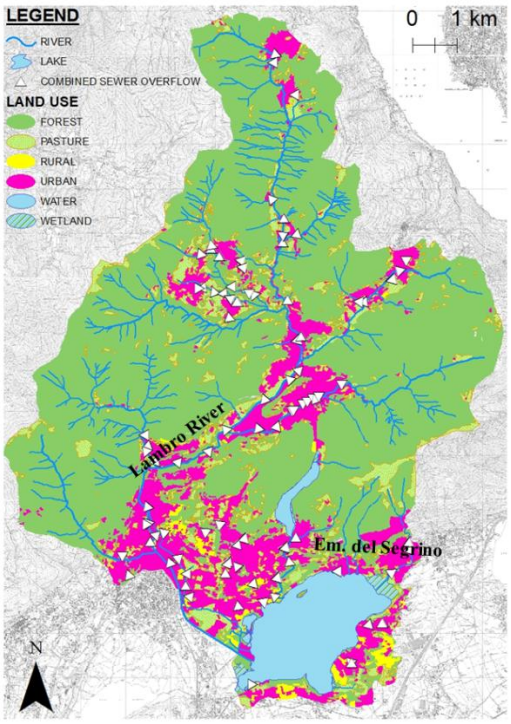

Figure 1. Pusiano lake and catchment are overlapped to the Soil Use. The main two tributaries in length and discharge are Lambro River and Emissario del Segrino.

The cyanobacterium *P. rubescens* became the dominant species in the phytoplankton assemblage in Lake Pusiano from 2001, blooming in the autumn, despite reduced nutrient concentrations, as simultaneously observed in many subalpine lakes (D'Alelio et al., 2011). However, after an intense flood event in November 2002 it completely disappeared for all of 2003 and a greater diversity was observed in the phytoplankton community in this year (Legnani et al., 2005).

1.5 Research statement

The ecological success of the ubiquitous harmful *P.rubescens* has been ascribed to largely depend on gas vesicles, which provide the cells with buoyancy (e.g. Walsby et al., 2006), genetic/phenotypic selection of adaptive traits (e.g. D'Alelio et al., 2011), lakes re-oligotrophication (Ernst et al., 2009), long-lasting nutrients enrichment interacting with the interannual variations in the thermal regime (e.g. Salmaso, 2010) or conversely a contrasting equilibrium between the timing of the onset and the duration of

stratification (Dokulil and Teubner, 2012) due to climate change. The increasing N:P (inorganic species) ratios, together with low consumption by predators, favour this non-N2-fixing cyanobacterium, thus lake mixing represents the main mechanism of seasonal population control (Posch et al., 2012; Salmaso and Cerasino, 2012). Whatever the viewpoint, *P. rubescens* has been the dominating algal species over the last two decades, becoming an efficient 'ecosystem engineer' (Padisák et al., 2010) but no attempts have been tried to isolate any determining factors with the aim to predict blooms. The major difficulty is certainly to differentiate the effects due to the human disturbance acting at different scales. Also the natural changes and the interactions within the ecosystem may cause high uncertainty. Global climate change has driven the phytoplankton shift (Winder and Cloern, 2010) as well as the local pollution favoured the conditions for the establishment of harmful species (Brookes & Carey, 2011; Salmaso and Cerasino, 2012).

The present research focused on the necessity to solve some of the most paradoxical features about *P.rubescens* large success. Is the global warming favouring a cold stenotherm species? Is a general lakes restoration the causal factor of a simultaneous widespread blooming in Europe? Are the species physiological traits sufficient to explain an ecological success?

1.6 Materials and methods

Further analysis and plots of measurements to implement models are outlined in the Appendix

1.6.1 Field and laboratory methods

During the 2010 monitoring monthly program, water samples were collected for chemical and biological analysis at the deepest point in Lake Pusiano (ST6, Figure 2) by a Van Dorn bottle at eight different depths (0.5, 2.5, 5, 7.5, 10, 15, 20, 24 m). Dissolved inorganic nitrogen species (NH_4-N, NO_3-N), total dissolved nitrogen (TDN) and total nitrogen (TN), phosphorus (PO_4-P), total dissolved phosphorus (TDP) and total phosphorus (TP), silica (SiO_2-Si) and other hydrochemical parameters such as sulphate, chloride, carbonate, calcium, magnesium, sodium and potassium were determined according to methods of APHA (1992).

Phytoplankton cell counts were conducted on Lugol-preserved water samples from ST6 at discrete depths within the lake epilimnion, metalimnion and hypolimnion. Identification to species level was carried out for each sample with an inverted microscope (Leica) after sedimentation and the biovolume was estimated for each species by geometrical approximations (Legnani et al., 2005).

The zooplankton survey was conducted seasonally using a 74 µm plankton net (horizontal tow) sampling at four different depths (0.5, 5, 10, 15, 23.5 m). Samples were pooled and preserved in 5% formalin and poured inside Imhoff sedimentation cones of 1000 cm^3 volume. Organisms were then counted and identified under an Utermöhl inverted microscope to calculate densities on dilute representative subsamples of 1 cm^3 volume, recording for each taxon the developmental stages (nauplii, copepodites or juveniles, and adults).

From February 2010 vertical profiles of conductivity (at 20 °C), pH, temperature, turbidity, redox, photosynthetically active radiation (PAR), dissolved oxygen, percentage of oxygen saturation and chlorophyll-a were obtained on multiple stations in the lake (Figure 2), using a multiparameter probe (Idronaut Ocean 7 Plus). Simultaneously vertical profiles of chlorophyll-a concentration were taken with a spectrofluorometric probe (BBE FluoroProbe, Moldaenke). The FluoroProbe (FP) differentiates up to four 'spectral groups' of phytoplankton *in vivo* and *in situ*. The original device is provided with spectral 'fingerprints' for Bacillariophyceae and Dinophyceae both recognized as Diatoms ('Diat'), Cyanobacteria ('Cyano'), Chlorophyceae ('Chlor') and Cryptophyceae ('Crypto'). The phylogenetic composition is determined from fluorescence stimulated by accessory pigments of the light-harvesting complex, and thus on the form which a characteristic phylum fingerprint is detected (Leboulanger et al., 2002). For a detailed description of FP, see Beutler et al. (2002). A dedicated software (FP 2.2.6, BBE-Moldaenke) was then used to calculate the relative amount of each algal class, expressed in terms of the equivalent amount of chlorophyll-a (as µg Chl-a L^{-1}). The FP algae fingerprints can be calibrated for a specific signal. A strain of *P. rubescens* was isolated from Lake Pusiano at known chlorophyll concentration (between 50 and 100 µg Chl-a L^{-1}) and used to calibrate a specific fingerprint, after an offset determination for a filtered water sample (0.45 µm cellulose-acetate filter). Indeed this species has a higher phycoerythrin content and its fluorescence signal (dominated by red emission) is closer

to the factory-calibrated Cryptophyceae signal than the Cyanobacteria one (rich in phycocyanin). The instrument reliability had been previously assessed by total chlorophyll analytical measurements.

The discharge of the main outflow from the lake was derived from hourly flow measurements while other minor tributaries and the outflow discharges were obtained daily from a hydrological model which was calibrated on Lake Pusiano watershed (Salerno & Tartari, 2009) and validated by lake measured levels and hydrological balance in 2010. Temperature, conductivity (and derived salinity), dissolved oxygen and turbidity were measured hourly in Lambro River with a fixed multiparameter probe (TROLL 9500, In-Situ Inc.); water quality variables (total nitrogen and total phosphorus) were determined by high-frequency monitoring with an automatic water sampler (WATSAM portable and refrigerated type, ISOIL Ind.) which included periods of both high and low discharge. Monthly sampling and laboratory determinations were carried out for the water quality of other two tributaries.

Meteorological data of wind velocity and direction, solar radiation, air temperature, rainfall, relative humidity were recorded hourly at a meteorological station close to the lake (Figure 2).

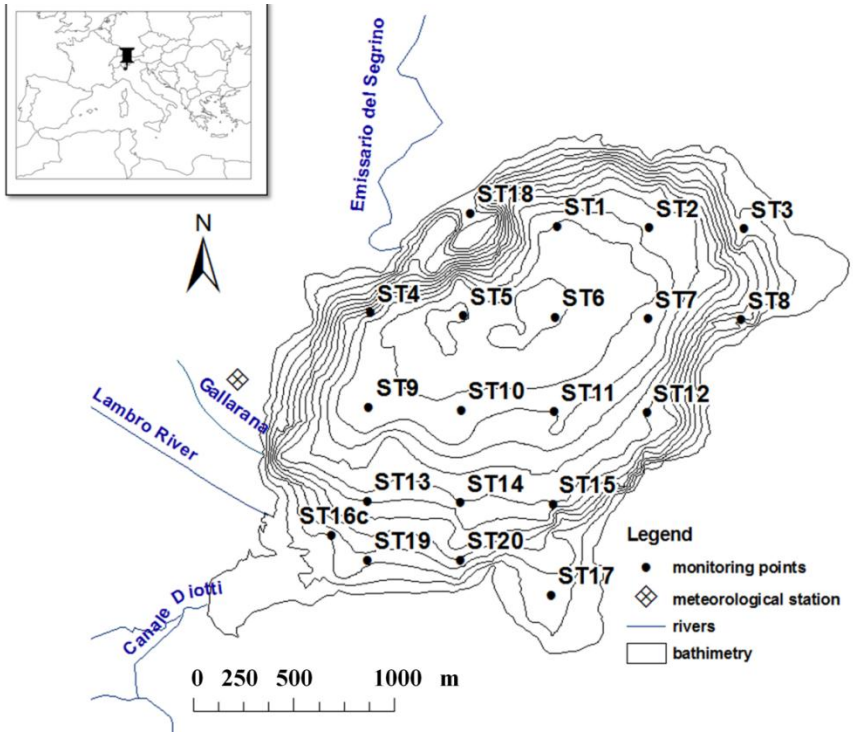

Figure 2. Location and bathymetry of Lake Pusiano. The outermost contour line refers to the surface level (0 m) and other contours are at 2 m depths. In the map the tributaries that have been characterized for nutrients input, the outflow, the meteorological and the sampling stations are also indicated.

A long term time series of physical and chemical lake measures (temperature, transparency, pH, oxygen, phosphorus, nitrogen, silica and principal ions) during winter overturn was reconstructed from 1984 to 2011. The time series was completed by data from six limnological campaigns were carried out (Gerletti and Marchetti 1977; Chiaudani and Premazzi 1992; Legnani et al., 2005; Vuillermoz et al., 2006; Carraro et al., 2012) performed between 1973 and 2010.

Sediment cores of about 80 cm were collected on several stations, from the river entry to the lake center, during the experimental campaign in spring 2010 for paleolimnological investigations (Lami, personal communication). The cores were cut at 1 cm layers and dated by radiometric techniques until the pre-industrial period (1730 AC). The sedimentation rate was determined using the CRS model for the ^{210}Pb profiles (Appleby, 2001). The geochemical analysis (Lami et al., 2000), i.e. water content, organic matter, carbonates, carbon, nitrogen, sulphur (C, N, S), algal pigments, fossil diatom and metals (Hg, Cr), were carried out on core layers to reconstruct the time series (1730-2010). A method inferring past TP lake concentrations was performed by spectrophotometrically-measured sedimentary pigments, mainly the total carotenoids, and a significant statistical correlation (Gulizzoni et al., 2011).

1.6.2 Statistical analysis

ABSerr and RELerr have been described in Salerno and Tartari (2009) for SWAT hydrological performance. The first shows on average each daily simulation deviating, in absolute terms, from the observed value: when ABSerr = 0 the two series perfectly coincide. The second one evaluates how much, in a given interval, the model under- or over-estimates the discharge (thus when RELerr = 0 the two series do not necessarily coincide, meaning that the positive and negative errors offset each other). The Nash–Sutcliffe index (E_{NS}) is a normalized index, used for hydrological, river water quality and ecological models, to evaluate the quantitative agreement between simulated and

observed data, comparing the relative magnitude of residual variances (Nash and Sutcliffe, 1970). It is called 'modelling efficiency index' indicating the 1:1 line as reference for an optimal fit and ranges from $-\infty$ to 1 with E_{NS}=1 being the optimal value. Values between 0.0 and 1.0 are generally viewed as acceptable levels of performance, whereas values < 0 indicate that the mean observed value is a better predictor than the simulated value, or an unacceptable performance. The Mean Bias (MB) was adopted for the ecological model and measures the average tendency of the simulated data to be larger or smaller than their observed counterparts. The optimal value of MB is 0.0, with low-magnitude values indicating accurate model simulation. Positive values indicate model underestimation and negative values indicate model overestimation (Gupta et al., 1999). The Root Mean Squared Error (RMSE) is one of the commonly used error index statistics. It represents the square root of the Mean Squared Error (MSE) and quantifies the model performance of each variable (e.g. Trolle et al., 2008). Also the correlation (R^2) coefficient was used for each simulation. The ABSerr, RELerr, RMSE and MB have the units of the variable tested, thus expressing the internal error. Ordinary least squares (OLS) regression analysis was used to test the correlation (R^2) between the biovolume and the chlorophyll concentration determined for each phytoplankton group. Criterion for entry and acceptance was p-value < 0.05. Both dependent and independent axes were log-transformed to meet the statistical requirements for normal distribution; then the residuals of the regressions were tested for homoscedasticity (Howarth & Earle, 1979).

Environmental data are typically non-stationary and nonhomogeneous, and processing of such data by means of conventional techniques such as classical spectral analysis or correlation approaches can lead to problems in the interpretation of the results obtained (Larson, 2007). Wavelet analysis (WA) is advantageous when dealing with time series that change their periodic behavior (i.e., are not stationary) as this method quantifies the temporal evolution of time series with different rhythmic components (Daubechies 1992). It performs a time-scale decomposition of the signal by estimating its spectral characteristics as a function of time (Torrence & Compo 1998). The WA was used to extract both the periodic components of variability in the series of high frequency data measured by the probes in Lambro River and the recurrence strength of (seasonal or yearly) cycles in multi-years simulated scenarios. Time series were analyzed using the

continuous wavelet transform (CWT); for time series with unknown frequencies, the Morlet function often gives the clearest picture (Grinsted et al., 2004). The frequency or the time range over which it fluctuates is set by a scale parameter. In general, wavelet scale is related to the conventional Fourier period of oscillations. For analyses of the river high-frequency series (the range is 8 months), a start scale of 1 hour (15 minutes is the sampling interval) was specified and the spacing between the discrete scales was chosen as 1/12 (12 suboctaves per octave). The number of octaves was set to 2.5, resulting in 30 scales ranging from 1 h to 64 days. For analyses of Chl-a series by long-term (the range is 50 years) simulated data, a start scale of 2 days (1 day is the model output) thus the scales ranged from 2 days to 10 years. It is often desirable to examine two time series together to determine how they are linked. This can be accomplished computing the Cross Wavelet Transform (XWT) from two CWTs, which will expose their common power and relative phase in time-frequency space. Furthermore a measure of Wavelet Coherence (WTC) between two CWTs is defined as a significant coherence, even though the common power is low (see Grinsted et al., 2004, for all the mathematical details). In this study both a XWT and WTC were used to investigate phases covariance among the rainfall, river discharge, conductivity, temperature and turbidity measured during 2010 at high frequency time scal. Preliminary results were drawn to analyse the time lag in arising river levels after high rainfall, the oscillations of conductivity depending by the water temperature and the discharge, as well as the dependace of turbidity on the discharge. All measured data were average centered and normalized by the standard deviation in order to allow the CWT, XWT and WTC analysis even in case of missing data within the series. The analysis was carried out using a free Matlab-software package (WTC-R15), provided by the Proudman Oceanographic Laboratory of the Natural Environment Research Council (NERC-UK) and available at the URL: http://www.pol.ac.uk/home/research/waveletcoherence/download.html (see the Appendix for the results).

The investigation of long time series is of particular importance when meteorology and climatology are studied together with limnology. For example, in studying trends, variations, etc., the occurrence of recurrent events is often the subject of investigation. In such studies, it is of interest to determine as accurately as possible the beginnings, ends and variations of such events. These results can be used for the detection of climate

changes and as basic information for the climate impact research on lake ecosystems. Problems arise when the processes to be investigated are quasi-periodic, i.e. those periodically varying by recurrent events with different length of period (Olberg & Rakoczi 1984). One well-known application often used in solving such problems is the estimation of the beginning of a trend using the sequential version of the Mann-Kendall non parametric test, coming under the class of rank tests. It is robust to outliers and can be used to detect linear or nonlinear monotonic trends. The sequential version of the test, suggested by Sneyers (1990) and hereinafter called the Mann-Kendall-Sneyers (MKS) test, was used here to detect the changing points that occured in the temporal behaviour of the simulated series, especially these points at which the trend changes its direction from upward to downward or vice versa, as it happens within lake temperatures, productivity, *P. rubescens* as chlorophyll concentrations etc. all variables strictly related to seasonal and long term events (rainfall, air temperatures, irradiance etc). The slopes of the trends were calculated by least square linear fitting and tested by the seasonal Mann-Kendall test (period = 12 months).

1.6.3 The integrated lake-basin modelling tool

The catchment model

Hydrological and nutrients transport models can be distinguished by different approaches, i.e. lumped or distributed and physical or stochastic processes, often linked to water quality models. The choice of a suitable model depends on the availability of data and the aims to be achieved. The Soil and Water Assessment Tool (SWAT, Srinivasan and Arnold, 1994) was chosen as a deterministic model encompassing the spatial heterogeneity due to weather, soil, topography, and vegetation variability through the support of a Geographical Information System (GIS) interface (Neitsch et al., 2005). Model input and output are organized into Hydrologic Response Units (HRUs) or areas of homogeneous land use, management and soil characteristics while the hydrological modelling is based on the water balance equation, including surface runoff, precipitation, evapotranspiration, infiltration and subsurface runoff. The implementation of SWAT model for the Pusiano basin required the creation of a proper soil map that covered the entire catchment area. The taxonomic system for soils, the geological, pedological, hydrological and climatic factors have been described in the previous model application to

Pusiano basin, as well as the sensitivity analysis and the description of all the hydrological equations for the water balance (Salerno and Tartari, 2009).

In this study SWAT was used to simulate discharge and phosphorus loads form the main tributary with a daily time step. Through the use of deterministic equations and considering the spatial variability of the simulated processes, SWAT allows to study the generation and the dynamics of the water flows and the consequent transport of nutrients within the watershed. The soil profile is represented by up to 10 layers, a shallow and a deep aquifer. When the field capacity in one layer is exceeded the water is routed to the lower soil layer. When the deepest layer is saturated, a lateral flow occurs. Surface runoff is computed by the SCS (Soil Conservation Service) curve number method and is therefore a non-linear function of precipitations and retention coefficients. Once all hydrological processes are simulated for a homogeneous sub-basin, the resulting flows are considered to contribute directly to the main channel. SWAT does not include the water balance of a given lake located in the watershed, so this has to be computed out of the proper modeling exercise.

Nutrient loadings to the channel depends on the concentrations in the upper soil layer and the runoff volumes. SWAT simulates six different pools of nutrients in the soil (Figure 3). Three pools are inorganic forms of P (mineral) while the other three are organic forms. Simulated TP loads are given by the sum of mineral-P + organic-P forms (Neitsch et al., 2005).

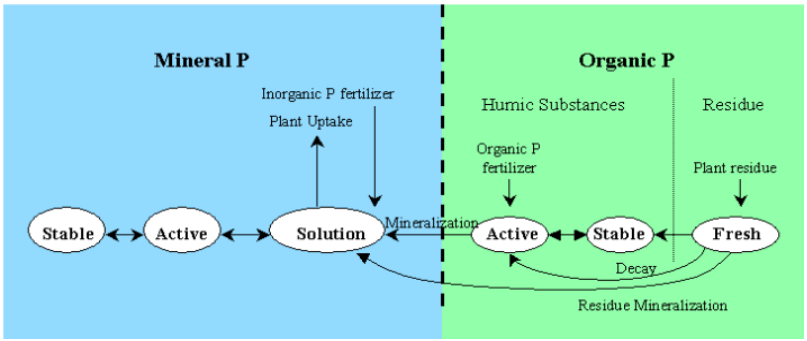

Figure 3. Phosphorus dynamics in SWAT

The methodology developed to build the climatic forcing (schematized in Figure 4) was based on the analysis of the available time series of rainfall and temperature daily data,

collected from the meteorological stations within the catchment, in order to obtained the longest series as possible. Data were processed through criteria of homogeneity, significance and continuity, a critical step to develop good process-based simulations. The climatic forcing was completed using the Regional Earth System (RES) PROTHEUS hind cast simulation (Artale et al., 2010), forced by the ERA40 (1958–1999) reanalysis (Simmons and Gibson, 2000), thus obtaining the longest climate reference for the available local historical series. A statistical downscaling (S-DSC) was performed to correct the RES output for local bias (mainly due to the raw approximation of land use and topography in RES). Finally, referring to the wavelet theory (see Appendix for the results), the coherence between the simulated and the real data collected in the stations was proved to reinforce the strength of the generated climatic forcing.

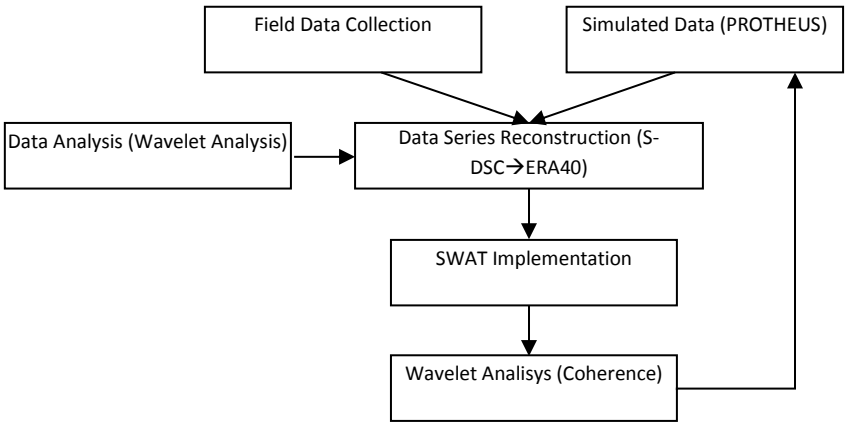

Figure 4. Scheme of climatic and hydrological forcing integration process.

The discharges of some sections of the Lambro River have been monitored in the previous study (Salerno and Tartari, 2009) obtaining the calibration of the curve of stream velocity. In SWAT only manual calibration approach is possible and requires the user to compare measured and simulated values, and then to use expert judgment to determine which variables to adjust, how much to adjust them, and ultimately assess when reasonable results have been obtained. Among nearly 20 different statistical tests that can be used for evaluating SWAT stream flow or river water quality output during a manual calibration process, Ens and R^2 coefficients are the most recommended for comparing monthly or weekly aggregated output to observed data (Gassman et al., 2007); they

have been compared with ABSerr and RELerr indexes and used to verify daily output with high frequency measured data (Table 1).

Lambrone (stream gauge)	**Ens**	**RELerr**	**ABSerr**	**RMSE**	**R^2**
Cal (01/01/2001 - 30/04/2004)	0,64	-0,08	0,4	2,2	0,67
Val (01/01/2010 – 31/01/2011)	0,47	0,01	0,5	2,7	0,67
Lambrone (probe)	**Ens**	**ER**	**EA**	**RMSE**	**R2**
Cal (22/02/2004 - 14/06/2004)	0,44	0	0,32	4	0,52
Val (29/04/2010 – 14/01/2011)	0,56	0,13	0,5	3	0,60

Table 1. Calibration (Cal) and validation (Val) of SWAT discharges simulation. The statistical indexes (see the previous paragraph) shows the model performance at daily time scale.

In 2010 a validation was performed using discharge data collected for all the tributaries of Lake Pusiano, thus determining the direct drainage basin and the whole daily inflow to the lake. The lake volume change (dV/dt) was derived by the daily measurements of lake levels and compared to the simulated lake volume change (Eq. 1), resulting by the water balance between the simulated inflow discharges (I_{sim}) by SWAT, the measured rainfall (R) and outflow discharges (O) and the estimation of the other loss (L_{est}) terms (i.e., evaporation and the groundwater contribution).

$$\frac{dV_{der}}{dt} = I_{SIM} + R - L_{est} - O \qquad \text{Equation 1}$$

SWAT model contains many equations accounting the phosphorus transport processes in the from the soil to the rivers. The main parameters were trained by data from high frequency (sub-hourly) system of a multiparameter probe coupled to an automatic water sampler for a monitoring in continuous. The turbidity was evaluated as a good predictor due to the presence of suspended solids and thereby of phosphorus that is associated at

the particulate form (Grayson et al., 1996; Stubblefield et al., 2007). SWAT was calibrated and validated with data for phosphorus (dissolved and particulate species) sampled at the outlet of a selected sub-basin fully covered by naturally growing deciduous forests, called 'Gajum' (Table 2).

Gajum sub-basin	**Ens**	**R^2**
Calibration (Jan 2004 – May 2004 weekly sampling)	1	0,99
Validation (Nov 2011 monitoring in continuous)	1	0,98

Table 2. Calibration (Cal) and validation (Val) of SWAT simulation for phosphorus concentrations measured at the outlet of a natural sub-basin (Gajum). The statistical indexes (see the previous paragraph) shows the model performance at daily time scale.

A turbidity probe, previously calibrated in laboratory with a reference formazin suspension (APAT e IRSA-CNR, 2003), was settled in the outlet of Gajum sub-basin. The turbidity-phosphorus regression model (Figure 5) was assessed through hourly monitored data, also during precipitation events, at different intensity. The regression model allowed to pass from long term available data to the corresponding values of total phosphorus (TP) concentrations. The series was used to validate SWAT simulations. The capability of the turbidity-TP regression and the SWAT simulations to predict the daily TP series has been verified by the cross-validation leave-one-out method, through the R package SMIR (Aitkin et al., 2009).

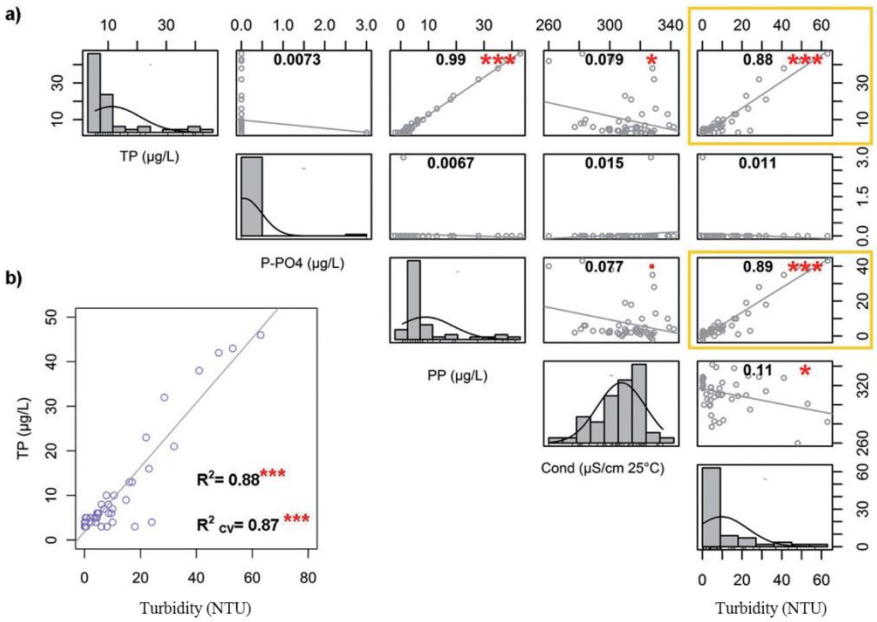

Figure 5. a) Correlation matrix for total phosphorus (TP), phosphorus orthophosphate ($P\text{-}PO_4$), particulate phosphorus (PP), conductivity (Cond) and turbidity values measured during high frequency monitoring in the Gajum sub-basin. The regression coefficient R^2 significance is indicated by stars ('***' 0.001; '**' 0.01; '*' 0.05). Yellow rings highlight the capacity of Turbidity parameter to predict the phosphorus (as PP and TP) concentrations. b) The turbidity-phosphorus regression model verified by R^2 and R^2_{CV} (cross-validated R).

Since SWAT is not able to model the point sources loading, the CSOs phosphorus load was estimated computing the exported amount by the specific unitary coefficients on the basis of the population census (Barbiero et al., 1991) and the management interventions (i.e., the construction of the sewage plant in 1986). The total annual load was finally computed for by the Vollenweider equation (OECD, 1982) and the TP time series measured during the winter lake overturn providing a long time input for the lake monodimensional model.

During the field measurements undertaken in 2010, the same high-frequency monitoring system previously described was settled into the Lambro River at the lake entering point. The water parameters and the samples were taken to determine nutrients (N, P) concentrations. A second multivariate analysis (see e.g. Horsburgh et al., 2010) was carried out to obtain linear models (Eq. 2-3) for the estimation of the nutrients input to the lake over a year.

TP=8.93TURB-35.16 [R^2=0.81*** p-value = 0.05711 n=25] Equation 2

TN=8.27+0.057TURB-6.42Q-0.017COND+0.018Q*COND [R^2=0.81***p-value=0.6063 n=25] Equation 3

The models were calibrated over during a rainfall event (15-16 February 2011) and validated (27-28 March 2011 and 1-8 June 2011. R^2=0.99 for TP; R^2=0.91 for TN; n=30. Figure 6-7).

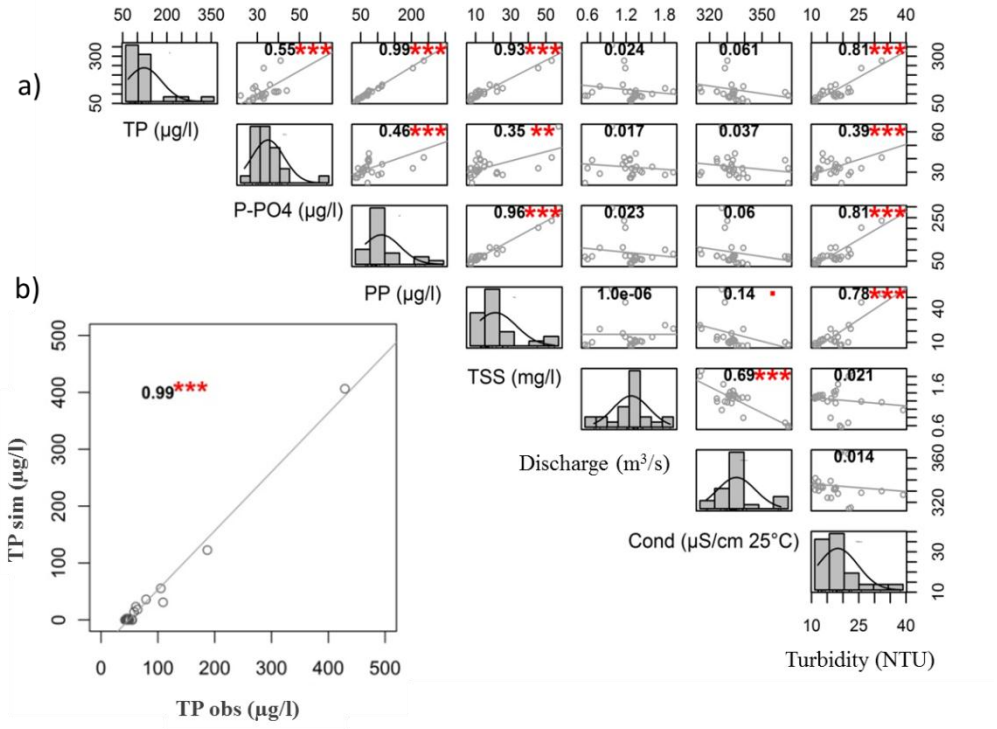

Figure 6. a) Correlation matrix for total phosphorus (TP), phosphorus orthophosphate (P-PO_4), particulate phosphorus (PP), total suspended solids (TSS), discharge, conductivity (Cond) and turbidity values measured during high frequency monitoring in Lambro river. The regression coefficient R^2 significance is indicated by stars ('***' 0.001; '**' 0.01; '*' 0.05). The turbidity was chosen as the only predictor for TP after the multiple regression analysis b) The capacity of prediction of the linear regression model for TP concentrations in Lambro river.

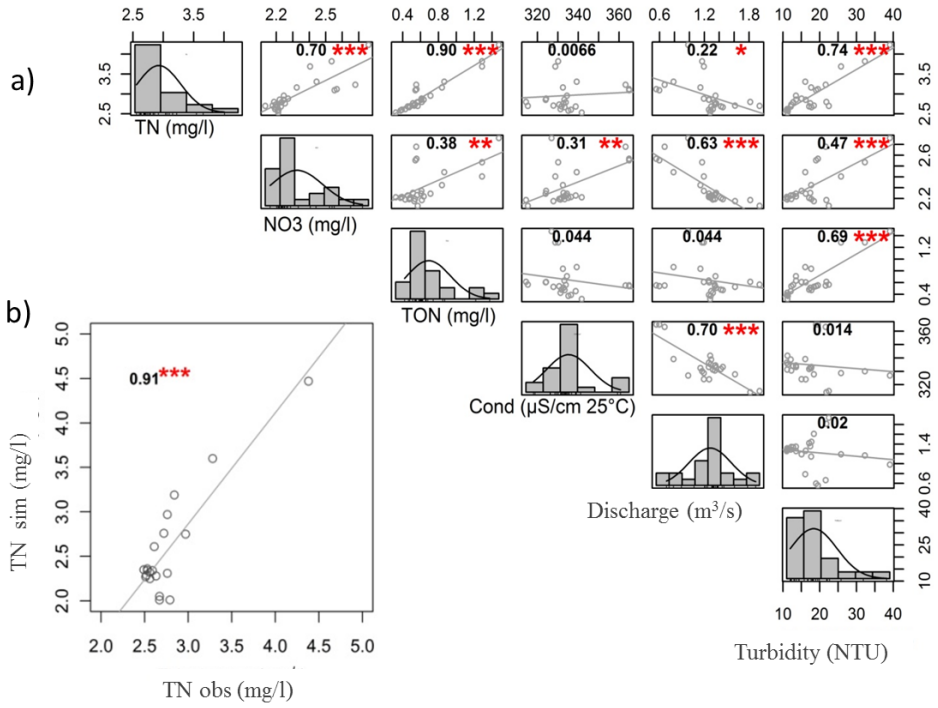

Figure 7. a) Correlation matrix for total nitrogen (TN), nitrates (N-NO_3), total organic nitrogen (TON), conductivity (Cond), discharge, and turbidity values measured during high frequency monitoring in Lambro river. The regression coefficient R^2 significance is indicated by stars ('***' 0.001; '**' 0.01; '*' 0.05). Turbidity, discharge and conductivity were chosen to predict TN (Horsburgh et al., 2010). b) The capacity of prediction of the multivariate model for TN concentrations in Lambro river.

The lake models

The Computational Aquatic Ecosystem Dynamics Model (CAEDYM) is a process-based ecological model, based on the 'N-P-Z' (nutrient-phytoplankton-zooplankton) type, but also includes algorithms for the resolution of the main biogeochemical state variables, e.g. oxygen, pH, dissolved nutrients, inorganic and organic particle and the underwater light extinction (Hamilton & Schladow 1997; Hipsey, 2008). A comprehensive presentation of all of the equations for phytoplankton and nutrient dynamics can be found in Robson & Hamilton (2004). The model is maintained by Centre for Water Research (CWR) of University of Western Australia. The model encompasses some compulsory and a large number of configurable variables, which allow the user to adapt the model to specific ecological cases. Its flexibility is enhanced by the opportunity to

choose among different algorithms in simulating such an ecological process and to simulate additional biological variables such us: fish, jellyfish, bacteria, macroalgae and invertebrates. The model also explicitly simulates the main gases exchanging at the air/water interface and the most important fluxes at the water/sediment boundary. The focus of the present study was narrowed on the phosphorus cycle (the limiting factor within the lake ecosystem) and to the equations governing the phytoplankton growth and dynamics.

The model distinguishes between inorganic and organic forms of the dominant macronutrients for phytoplankton: carbon, nitrogen and phosphorus and silicon (if Diatoms are simulated). CAEDYM also explicitly simulates the gas exchange between water surface and atmosphere (for nitrogen and carbon cycle). The phytoplankton light limitation can be simulated by using a saturating or a photo-inhibiting sub-model as well as the simulation of the uptake can be performed by a constant for the internal nutrient content or by a model which dynamically simulates the cells nutrient storage. In Table 3 the main general equations are reported.

Dissolved Sediment Flux:

$$f_g^{DSF}(T, DO, pH) = f_{SED}(T) S_g \left(\frac{K_{DOS-g}}{K_{DOS-g} + DO} + \frac{|pH - 7|}{K_{pHS-g} + |pH - 7|} \right) \frac{1}{\Delta z_{bot}}$$

Resuspension:

$$f_g^{RES}(g_{sed}) = \alpha_g (\tau - \tau_{cg}) \left(\frac{g_{sed}}{K_{sed-g} + g_{sed}} \right)$$

Settling:

$$f_g^{SET}(g) = \frac{v_g}{\Delta z} g$$

Decomposition:

$$f_g^{DEC}(T, DO, BAC^{\star}, g) = f_B(T) \mu_{g-DEC}\, g \min\left(f_B(DO), f_B(BAC)^{\star}\right)$$

Mineralization:

$$f_g^{MIN}(T, DO, BAC^{\star}, g) = f_B(T) \mu_{g-MIN}\, g \min\left(f_B(DO), f_B(BAC)^{\star}\right)$$

Adsorption/Desorption:

$$f_g^{ADD}(SS1, SS2, g, y) = \frac{SS1 + SS2}{\rho_{SS}} \left(g k_{ad-g} - E0C_g\right) - y$$

Biological Mortality & Excretion:

$$f_g^{BME}(A, M, Z) = \underbrace{\sum_i^{nphy} E_g(A_i)}_{\text{a-phytoplankton}} + \underbrace{\sum_j^{nmac} E_g(M_j)}_{\text{b-macroalgae}} + \underbrace{\sum_k^{nzoo} E_g(Z_k)}_{\text{c-zooplankton}}$$

Biological Uptake:

$$f_g^{BUP}(A, M, g) = \underbrace{\sum_i^{nphy} U_g(A_i)}_{\text{a-phytoplankton}} + \underbrace{\sum_j^{nmac} U_g(M_j)}_{\text{b-macroalgae}}$$

Biological Respiration:

$$f_{DIC}^{BRE}(A, M, Z, BAC) = \underbrace{\sum_i^{nphy} R_{DIC}(A_i)}_{\text{a-phytoplankton}} + \underbrace{\sum_j^{nmac} R_{DIC}(M_j)}_{\text{b-macroalgae}} + \underbrace{\sum_k^{nzoo} R_{DIC}(Z_k)}_{\text{c-zooplankton}} + \underbrace{R_{DIC}(BAC)}_{\text{d-bacteria}}$$

Table 3. A generic parameterization of the nutrients cycles (from Hipsey, 2008)

Total chlorophyll is the sums of the Chl-a content within all the groups; TP and TN concentration are the sum of the different chemical species (dissolved inorganic, particulate and dissolved organic and algal internal content). The list of the hydrodynamic and biogeochemical variables, simulated in this study, is reported in Table 4**.**

Simulated variable	**Code**	**Unit**
Temperature	T	°C
Salinity	S	Psu
Density	D	kg m^{-3}
Photosynthetic active radiation	PAR	µmol m^{-2} s^{-1}
Extinction coefficient	EXTC	m^{-1}

Dissolvd oxygen	DO	mg L^{-1}
Particulate organic carbon	POC	mg C L^{-1}
Dissolved organic carbon	DOC	mg C L^{-1}
Particulate organic phosphorus	POP	mg P L^{-1}
Dissolved organic phosphors	DOP	mg P L^{-1}
Reactive phosphorus	PO_4	mg P L^{-1}
Ammonium	NH_4	mg N L^{-1}
Nitrate	NO_3	mg N L^{-1}
Particulate organic nitrogen	PON	mg N L^{-1}
Dissolved organic nitrogen	DON	mg N L^{-1}
Cyanobacteria	P-rub	µg Chl a g L^{-1}
Cryptophyceae	Crypto	µg Chl a g L^{-1}
Diatoms	Diat	µg Chl a g L^{-1}
Other algae	G2	µg Chl a g L^{-1}
Zooplankton herbivores	ZOOP1	mg C L^{-1}
Total phosphorus	TP	mg P L^{-1}
Total nitrogen	TN	mg N L^{-1}
Total chlorophyll	TCHLA	µg Chl a L^{-1}

Table 4. List of the hydrodynamic and ecological variables simulated in this study

The main processes involving the phosphorus cycle are listed below:

1) Mineralization of DOP to PO4 (MIN)
2) Biological uptake of PO4 by phytoplankton into the IP (internal phosphorus) pool (BUP)
3) Dissolved sediment fluxes of PO4 and DOP (DSF)
4) Decomposition of POP to DOP (DEC);
5) Biological mortality and excretion into the DOP and POP pools (BME)
6) Settling of POP and IP (SET)
7) Resuspension of POP and IP (RES)

The main equations that have been involved in this study are reported below:

Reactive phosphorus

$$\frac{\partial PO_4}{\partial t} = f_{DOP}^{MIN}(T, DO, DOP) - f_{PO_4}^{BUP}(A, M, PO_4) + f_{PO_4}^{DSF}(T, DO) \quad \text{Equation 4}$$

Dissolved organic phosphorus

$$\frac{\partial DOP}{\partial t} = f_{POP}^{DEC}(T, DO, POP) - f_{DOP}^{MIN}(T, DO, DOP) + f_{DOP}^{DSF}(T, DO) + f_{DOP}^{BME}(A, M, Z) \quad \text{Equation 5}$$

Particulate organic phosphorus

$$\frac{\partial POP}{\partial t} = -f_{POP}^{DEC}(T, DO, POP) + f_{POP}^{SET}(POP) + f_{POP}^{RES}(POP_{SED}) + f_{POP}^{BME}(A, M, Z) \quad \text{Equation 6}$$

Internal (algal) phosphorus

$$\frac{\partial IP}{\partial t} = f_{PO_4}^{BUP}(A, M, PO_4) - f_{DOP,POP}^{BME}(A, M, Z) + f_{A_i}^{SET}(IP) + f_{A_i}^{RES}(IP_{SED}) \quad \text{Equation 7}$$

where *A* is for the algal uptake equations, *M* is for all biological lossess, *Z* is for grazing by zooplankton.

The model was setup to simulate the main labile forms while the optional model routines related to the refractory components were turned off. Thus the processes involving phosphorus transformations in the simulations were: a) the uptake of DRP by phytoplankton; b) the release of DRP from phytoplankton excretion; c) the excretion of DOP as faecal material by zooplankton; d) the sedimentation of POP; e) the mineralization of DOP and POP in the sediment; f) the release of DRP and DOP from sediments. The phosphorus mass balance can be roughly represented in terms of sources (positive terms) and loss (negative terms) as reported in Table 5.

P-Sources	P-Losses
$\Delta(DRP+DOP+POP)_{inflow\text{-}external\text{-}load}$ $\Delta(DRP+DOP+POP)_{initial\text{-}internal\text{-}load}$ $\Delta(Algal\text{-}IP)_{initial\text{-}biomass}$ $\Delta(DRP+DOP)_{sediment\text{-}release}$ $\Delta DRP_{DOP\text{-}mineralization}$ $\Delta DOP_{POP\text{-}decomposition}$ $\Delta(DOP+POP)_{biological\text{-}mortality/excretion}$ $\Delta(DOP+POP)_{settling} - \Delta DRP_{Algal\text{-}uptake}$	$\Delta DOP_{sediment\text{-}mineralization}$ $\Delta(DOP+POP)_{grazing}$ $\Delta POP_{mineralization}$ $\Delta(DRP+DOP+POP)_{loss\text{-}via\text{-}outflow}$

Table 5. List of sources and losses in the phosphorus mass balance ($\sum$P-Sources-$\sum$P-Losses=0) as simulated in this study.

A similar approach has been also applied to nitrogen where the total inorganic dissolved pool has been divided into ammonium and nitrate forms. The nitrogen cycle includes the additional processes of denitrification, nitrification and N_2 fixation as function of nitrogen and oxygen levels, temperature, interactions with bacteria and macrophytes (when the last two are simulated).

Algal groups have been simulated in terms of Chl-a concentration. CAEDYM potentially distinguishes between 7 groups of phytoplankton (Dinophytes, Cyanobacteria, Nodularia, Chlorophytes, Cryptophytes, fresh water and marine Diatoms). All the algal groups are simulated by the same algorithms, except for Diatoms for which the silica limitation is applied. For the long time study (DYCD) two algal groups has been simulated: Cyanobacteria group in opposition to all the other species aggregated in a single group called G2. Being *P. rubescens* the dominant species, Cyanobacteria dynamics has been parameterized by the *P. rubescens* eco-physiological parameters. In the 3D study (ELCD) a high-resolution spatial distributions of three keystone species (a Diatom, a Cryptophyta and *P. rubescens*) was obtained to investigate phytoplankton vertical distribution as a function of light, nutrient limitation, competition and governing hydrodynamics. The mechanism determining the metalimnetic growth and subsequent proliferation of *P. rubescens* was focused. The growth rate function μ_g (day^{-1}) for biomass has been represented by the following equation that determines the change in chlorophyll a of each phytoplankton group over the model time step:

$$\mu_g = \mu_{\max} \min\left[f(I), f(N), f(P), \right] f_{Ai}\, f(T) \qquad \text{Equation 8}$$

where $f(I)$ $f(N)$ $f(P)$ represent the limitation for light, nitrogen and phosphorus respectively, $f(T)$ is the temperature function and μ_{max} (day^{-1}) is the maximum growth rate at 20° C in the absence of significant limitation by light or nutrients.

The effect of light (PAR) limitation on the phytoplankton population has been simulated using a photo-inhibition model (Wallace *et al.*, 1999) for *P. rubescens* and Cryptophyta and using a simple (saturation) Webb model (Webb, 1974) for G2 and Diatoms.

The photo-inhibition model:

$$f(I) = \frac{I}{I_S} \exp\left(1 - \frac{I}{I_S}\right) \qquad \text{Equation 9}$$

And the simple saturation model:

$$f(I) = 1 - \exp\left(-\frac{I}{I_k}\right) \qquad \text{Equation 10}$$

In both equations *I* represents the incoming irradiance (µmol m^{-2} s^{-1}), in Eq. 9 *Is* (µmol m^{-2} s^{-1}) is the light saturation value at which production is maximal, whereas in Eq. 10 *Ik* is the light intensity at which the photosynthetic rate is numerically equivalent to P_{max}.

The kinetic up take of the nutrients has been modelled, for each group using a dynamic internal nutrient model. For phosphorus the limitation function take form:

$$f(P) = \frac{IP_{\max}}{IP_{\max} - IP_{\min}} \left[1 - \frac{IP_{\min}}{IP} \right] \qquad \text{Equation 11}$$

where IP_{max} and IP_{min} are the maximal and minimal internal phosphorus concentration respectively whereas IP is the current actual internal phosphorus concentration.

The internal phosphorus store for each phytoplankton group is modelled according to the following equation:

$$U_{PO_4}(A_i) = UP_{\max}\left[fA_i(T)\frac{IP_{\max} - IP}{IP_{\max} - IP_{\min}}\frac{PO_4}{PO_4 + K_P}\right]A_i \qquad \text{Equation 12}$$

where UP_{max} is the maximum rate for phosphorus uptake (mg P (mg Chl a)$^{-1}$ day^{-1}), A_i is the biomass of ith group (in terms of mg Chl-a m^{-3}). K_P represents the half saturation coefficient (mg P L^{-1}) for growth dependence from the external PO_4 concentration. The temperature function includes the limitation at high temperature and it is the same of the equation applied for the phytoplankton growth (see below).

A similar equation has been applied to simulate the nitrogen limitation. The nitrogen function simulates the internal nitrogen store as a function of the uptake of both ammonium and nitrate.

Within Eq. 8 f(T) represents the temperature limitation as a continuous function specifying the temperature as limit for the exponential increase in production (T_{sta}), an optimal temperature for production (T_{opt}) and the upper limit where production stops (T_{max}).

Metabolic losses (L) are simulated by a lamped term and take into account respiration, natural mortality and excretion:

$$L = k_{rA}\vartheta^{T-20} \qquad \text{Equation 13}$$

where k_{rA} is the respiration rate coefficient (although it also includes the effects of mortality end excretion). In addition, a constant f_{DOM} is also used to isolate the fraction of mortality and excretion that goes into the dissolved organic pool, and the fraction which enters the particulate organic matter.

For the effect of grazing on the phytoplankton biomass refer to the zooplankton model description (Copetti et al., 2006; Hipsey, 2008).

Phytoplankton settling has been parameterized for each group through a constant velocity settling. *P. rubescens* buoyancy control has been simulated, as simple as possible, assuming a constant slight positive settling velocity (upward the water column) to simulate the buoyancy changes during autumnal waterblooms (Walsby et al., 2006).

CAEDYM was coupled both with the mono-dimensional hydrodynamic driver DYnamic REServoir Simulation Model (DYRESM, Imerito 2007) for long term simulations

and with the three-dimensional hydrodynamic Estuary, Lake and Coastal Ocean Model (ELCOM) to simulate the hydrodynamic, nutrient cycles and food web dynamics in Lake Pusiano in 3D during 2010 (Hodges and Dallimore, 2006).

In DYRESM the lake is represented as a series of homogeneous horizontal layers of variable thickness (Yeates and Imberger, 2004; Imerito, 2007). The main modelled processes are surface heat, mass and momentum transfers, mixed layer dynamics, hypolimnetic mixing, benthic boundary layer mixing, inflows and outflows balance. It is based on the assumption of one-dimensionality, that is, variations in the lateral directions are small when compared with variations in the vertical. The assumption is based on observations that the density stratification usually found in lakes inhibits vertical motions, while horizontal variations in density are quickly relaxed by horizontal advection and convection. Horizontal exchanges generated by weak temperature gradients are communicated over several kilometers on time scales of less than a day, suggesting that a one-dimensional model such as DYRESM is applicable for simulations over daily time scales. For this lake or reservoir is represented as a series of horizontal layers. There is no lateral or longitudinal variation in the layers, and vertical profiles are obtained from proper values of each layer. The layers represented in DYRESM are of different thickness; as inflows and outflows enter or leave the lake, the affected layers expand or contract, and those above move up or down to accommodate the volume change. The vertical movement of the layers is accompanied by a corresponding change in layer thickness as the area occupied by each layer varies according to its vertical position. Mixing is modelled by an amalgamation of adjacent layers, with individual layer thickness dynamically set by the model to ensure an adequate resolution is obtained for each process. A criterion for assessing the validity of the one-dimensional assumption has been established by Patterson *et al.* (1984) who developed a set of criteria based on the Wedderburn number. The Wedderburn number represents the ratio of the buoyancy force acting on the surface layer to the shear stress due to the wind, and is defined as in Equation 14.

$$W = \frac{R_i}{L/h_1} = \frac{g' h^2}{u_*^2 L'} \qquad \text{Equation 14}$$

Where L is the fetch length, h is the thickness of the surface mixed layer, u_* is the surface wind shear velocity, and g' is the modified gravitational acceleration across the base of the surface mixed layer defined by the Equation 15:

$$g' = \frac{g\Delta\rho}{\rho_0} \qquad \text{Equation 15}$$

where is $\Delta\rho$ is the density difference between the bottom of the surface layer and the hypolimnion, and ρ_0 is the density of the hypolimnion. When the Wedderburn number is $W >> 1$ the buoyancy force is greater than applied wind stress, resulting in only a small tilting of the isopycnals and negligible horizontal variations. For this case the processes are essentially one-dimensional and the algorithms of DYRESM are valid. When $W \sim 1$, the forces due to the applied wind stress are similar to buoyancy forces. This is the critical condition and can be described physically as the point where the base of the surface layer tilts toward the surface at the upwind end, defined as upwelling. $W << 1$ results in broad upwelling at the upwind end of the lake with vertical motions occurring on smaller time scales than horizontal advection. For the two latter cases the assumption of one-dimensionality is not valid. The W number appears to impose the restriction that DYRESM only be applicable to 'small to medium size' lakes and reservoirs. As, if $L >> h$ then $W << 1$ unless the applied wind stress is always low. When the wind stress is large, small lakes may also violate $W >> 1$. However, when this occurs the resulting mixing is large and vertical density gradients are smoothed. Although the upwelling processes are not explicitly modelled by DYRESM the mixed layer algorithm will predict large vertical deepening for this case, resulting in DYRESM accurately predicting the same resulting density profile.

A calibration of the described parameters (Table 6) was necessary for the medium-sized Lake Pusiano to stabilize its thermal structure, by minimizing the sum of squares difference in measured and simulated water temperature (Copetti et al., 2006).

Parameters	Unit	Value (*calibrated)
Bulk aerodynamic momentum transport coefficient	-	$0.18\ 10^{-2}$
Albedo of water	-	0.08
Emissivity of water surface	-	0.96
Critical wind speed	$m\ s^{-1}$	3.00
Shear production efficiency	-	0.06
Potential energy mixing efficiency	-	0.20
Wind stirring efficiency	-	0.4*
Effective surface area coefficient	m^2	$1.07\ 10^{7}$*
Lake number mixing coefficient	-	50*
Light extinction coefficient	m^{-1}	0.3*
Min. layer thickness	m	2.00*
Max. layer thickness	M	4.00*
Non-neutral atmospheric stability	-	False
Buoyancy scaling parameter	-	0.083

Table 6. Parameters of the hydrodynamic model DYRESM

Mass balance of ecological variables is performed at each time step and at each layer via DYRESM as the layers expand, contract, merge or are affected by inflows and outflows (Bruce et al., 2006). DYRESM simulations are initialized through salinity and temperature profiles and require both meteorological and hydrological data input. Meteorological (daily average values) data include: air temperature, short and long wave radiation, vapour pressure wind speed and rainfall. Hydrological data encompass daily discharge, daily average water temperature and salinity for the main inflows and daily discharge for the main outflows to the lake. To run the coupled DYRESM-CAEDYM (DYCD), daily averaged data of all the biogeochemical simulated variables are also required.

The output for discharge and phosphorus loads from SWAT model were integrated as input to DYCD model that was run over a long period at daily time step. The format of inflow data input forcing DYCD simulations in this study is summarized in Table 7.

Model	Variable	Unit	Source
DYRESM	Discharge	$m^3 s^{-1}$	SWAT output
DYRESM	Water temperature	°C	Derived by a regression with measured air temperatures
DYRESM	Salinity	ppt	Constant value
CAEDYM	Dissolved oxygen	mg L^{-1}	Saturation value
CAEDYM	Particulate and dissolved organic carbon	mg C L^{-1}	Constant value
CAEDYM	Ammonia and nitrates	mg N L^{-1}	Derived by historical data, constant values in function of discharge.
CAEDYM	Particulate and dissolved organic nitrogen	mg N L^{-1}	As a constant percentage of TN
CAEDYM	Particulate and dissolved organic phosphorus and orthophosphate	mg P L^{-1}	SWAT output

Table 7. Data format for DYCD inflow forcing.

DYCD simulations were performed to study the long term evolution of lake temperature, biogeochemical variables and phytoplankton. The model calibration and validation for Lake Pusiano biogeochemical cycle had already been successfully gained in Copetti et al. (2006). The model was set up to account for the main cycling labile pools: Dissolved Reactive Phosphorus (DRP), Dissolved Organic Phosphorus (DOP), Particulate Organic Phosphorus (POP) and Algal Internal Phosphorus (Algal-IP) exchanging from sediment to water through biological processes as schematically represented in Figure 8. Total phosphorus (TP) is not explicitly simulated but rather estimated as the sum of the different simulated P-forms (i.e. DRP + DOP + POP + Algal-IP). One of the aims of the present modelling study was to get a fine representation of *P. rubescens* growth and evolution in Lake Pusiano.

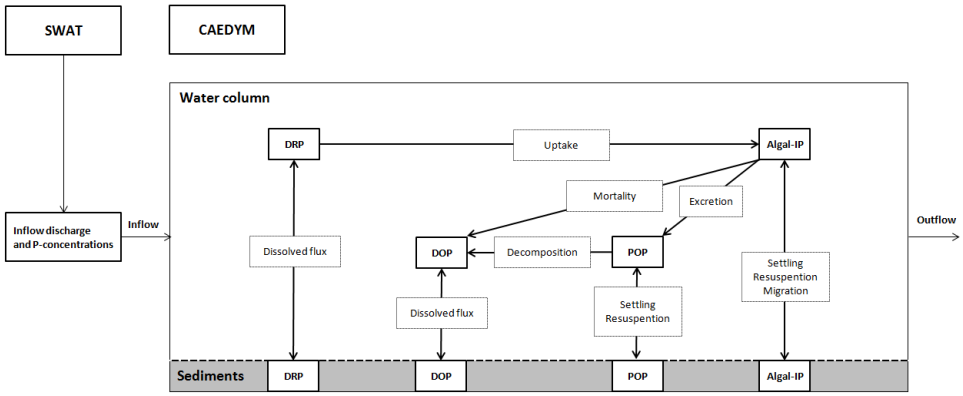

Figure 8. Simplified scheme of the phosphorus dynamics in the ecological model (CAEDYM), including the integration of output by the hydrological model (SWAT). DRP=Dissolved Reactive Phosphorus; DOP=Dissolved Organic Phosphorus; POP=Particulate Organic Phosphorus; Algal-IP= Algal Internal Phosphorus

ELCOM simulates velocity, temperature and salinity distributions in natural water bodies. It is based on the unsteady Reynolds-averaged, hydrostatic, Boussinesq, Navier-Stokes equations and uses a conservative ULTIMATE QUICKEST scheme for scalar transport, an Euler-Lagrange scheme for advection of momentum, and a semi-implicit method for free surface evolution (Hodges et al., 2000; Laval et al., 2003a). It includes external environmental forcing (e.g. from meteorology, inflows and outflows). Following Laval et al. (2003), a filter is applied to correct for vertical mixing due to numerical diffusion. ELCOM computes a model time step in a staged approach consisting of:

1) Introduction of surface heating/cooling in the surface layer
2) Mixing of scalar concentrations and momentum using a mixed-layer model
3) Introduction of wind energy as a momentum source in the wind-mixed layer
4) Solution of the free-surface evolution and velocity field
5) Horizontal diffusion of momentum
6) Advection of scalars
7) Horizontal diffusion of scalars

In this study, the filter was calibrated using field data. Table 8 shows a summary of the governing equations and fundamental models used for three-dimensional transport and surface thermodynamics in ELCOM.

Transport of Momentum:	$\frac{\partial U_\alpha}{\partial t} + U_j \frac{\partial U_\alpha}{\partial x_j} = -g \left\{ \frac{\partial \eta}{\partial x_\alpha} + \frac{1}{\rho_0} \frac{\partial}{\partial x_a} \int_z^\eta \rho' dz \right\} + \frac{\partial}{\partial x_1} \left\{ \nu_1 \frac{\partial U_\alpha}{\partial x_1} \right\} + \frac{\partial}{\partial x_2} \left\{ \nu_2 \frac{\partial U_\alpha}{\partial x_2} \right\} + \frac{\partial}{\partial x_3} \left\{ \nu_3 \frac{\partial U_\alpha}{\partial x_3} \right\} - .pdfilon_{\alpha\beta} f U_\beta$
Continuity:	$\frac{\partial U_j}{\partial x_j} = 0$
Momentum Boundary Conditions - Free Surface:	$\frac{\partial U_\alpha}{\partial x_3} = 0$
Momentum Boundary Conditions - Bottom and Sides:	$U_i = 0$
transport of Scalars:	$\frac{\partial C}{\partial t} + \frac{\partial}{\partial x_j}(CU_j) = \frac{\partial}{\partial x_1} \left\{ \kappa_1 \frac{\partial C}{\partial x_1} \right\} + \frac{\partial}{\partial x_2} \left\{ \kappa_2 \frac{\partial C}{\partial x_2} \right\} + \frac{\partial}{\partial x_3} \left\{ \kappa_3 \frac{\partial C}{\partial x_3} \right\} + S_c$
Scalar Boundary Conditions :	$\frac{\partial C_\alpha}{\partial x_j} = 0$
Free-Surface Evolution:	$\frac{\partial \eta}{\partial t} = -\frac{\partial}{\partial x_\alpha} \int_0^\eta u_\alpha dz$
Free-Surface wind shear:	$(u_*)_\alpha^2 = C_{10} \frac{\rho_{air}}{\rho_{water}} (W_\beta W_\beta)^{\frac{1}{2}} W_\alpha$
Momentum input by wind:	$\frac{\partial U_\alpha}{\partial t} = \frac{(U_*)_\alpha^2}{h}$

Table 8. Summary of Governing Hydrodynamic equations used in ELCOM (from the Science Manual by Hodges and Dallimore, 2006)

In the application of ELCOM–CAEDYM (ELCD) to Lake Pusiano inflows characterization was driven by inputs from three tributaries (Lambro river, Gallarana, Emissario del Segrino: see Figure 2). The multivariate model for TP (Equation 2) and TN (Equation 3) was used to obtain hourly estimation of water quality over a year for Lambro River. Dissolved and particulate forms of nitrogen and phosphorus were then derived from TN and TP (either from linear regressions or fixed ratios). Carbon (particulate and dissolved form) and silica were assumed to be constant in two ranges of discharge (0-10 m^3 s^{-1} and > 10 m^3 s^{-1}), according to an approximation based on historical measurements. Constant daily values, derived from averages on monthly data, were assumed for the other minor rivers. Carbon, silica and all organic forms were assumed in the same proportion as for the main river.

Meteorological data were entered as input to the model at hourly frequency. The lake initial condition was provided through lake hydrochemical and biological profiles taken

on 23 February 2010 and the simulation duration was 322 days, ending on 12 January 2011, at one-minute time step of computation. The applied grid size (100 x 100 x 1 m) was a compromise considering the spatial resolution for the monitoring multi-station grid, the thermal gradients, the computation time (CPU) and the numerical diffusion effects (Laval et al., 2003b).

1.7 Thesis overview

This thesis is based on three main research Chapters (Chapter 2–4) which have been published in peer–reviewed scientific journals or books.

Chapter 2 illustrates the assessment of a coupled three-dimensional hydrodynamic and ecological model of the lake ecosystemin order to analyze the increased prevalence of *P. rubescens* during the lake re-oligotrophication, using spectrally-specific fluorometric responses and validation with traditional cell enumeration microscopy in a new methodological purpose.

Chapter 3 proposes a long-term modelling study to differentiate the effects on the lake ecology by the global human disturbance (i.e. the temperature warming) from the local pollution caused by the external phosphorus loading.

In Chapter 4 the process-based basin and lake models were coupled with the aim to reconstruct a scenario with no human presence in the catchment. The hydrological model was calibrated and validated by data collected in the outflow of a fully and naturally forested sub-basin and then applied to the whole catchment. The lake dynamic response was compared to the most used methods for the estimation of reference conditions. Furthermore, the MEI index was re-assessed for subalpine lakes in this study. *P. rubescens* dynamics was simulated both in hypothetical undisturbed-reconstructed environment and in the current ecological conditions.

2 Coupling high-resolution measurements to a three-dimensional lake model to assess the spatial and temporal dynamics of the cyanobacterium *Planktothrix rubescens*

*__From:__ Carraro E., Guyennon N., Hamilton D.P, Viviano G., Manfredi E., Valsecchi L., Salerno F., Tartari G. and Copetti D. 2012. Coupling high-resolution measurements to a three-dimensional lake model to assess the spatial and temporal dynamics of the cyanobacterium *Planktothrix rubescens* in a medium-sized lake. Hydrobiologia 698:77–95.

2.1 Motivation

The intensive field campaign was conducted in the second year (February 2010 to January 2011) to provide highly spatially and temporally resolved phytoplankton population data suitable to calibrate and validate a coupled three-dimensional hydrodynamic and ecological model of the lake ecosystem in order to analyze the increased prevalence of *P. rubescens* during the lake re-oligotrophication. The parameterization of 'key-species' and the high-frequency simulated output were used to analyzed the role of physiological features of *P. rubescens* in observed vertical patterns of distribution, notably a deep chlorophyll maximum, the influence of lake hydrodynamic processes and the growth-limiting factors competing with other species. Most studies with ELCOM-CAEDYM model have used spatial field data for initialisation. For example Laval et al. (2003a) used a spatially varying wind field to improve the seiches amplitude and simulate mean surface circulation; León et al. (2005) used thermistor data at three stations in the eastern basin of Lake Erie to understand the flushing of the deep basin and circulation dynamics as drivers for future studies of fate and transport of nutrients. Hillmer et al. (2008) used 33 stations in Lake Kinneret to simulate phytoplankton patchiness in terms of concentration and composition. But none of these studies has used highly resolved spatial field data and an array of statistical measures of goodness–of–fit to compare model output and to assess the temporal and spatial complexity of both field data and model simulations. In this study we were able to use a three-dimensional hydrodynamic-ecological model to reproduce discrete measurements of hydro-chemical variables, including inferred behaviour of metalimnetic populations of *P. rubescens*, in a pre-

alpine lake. For the first time we obtained high-resolution spatial distributions of this keystone species to make direct comparisons with the corresponding state variable output from the model, using spectrally-specific fluorometric responses and validation with traditional cell enumeration microscopy. We compared measured lake profiles to the high temporal resolution model output and investigated phytoplankton vertical distribution as a function of light, nutrient limitation, competition and governing hydrodynamics. We finally focused on the mechanism determining the metalimnetic growth and subsequent proliferation of *P. rubescens*.

2.2 Results

2.2.1 Phytoplankton assemblage and field patterns

Cyanobacteria prevailed over the other taxonomic groups, representing the 64% of the total annual biovolume across all samples (Table 9). Concentrations were highest in May due to an isolated bloom of *Aphanizomenon flos-aquae*, and from October to January due to a bloom of *P. rubescens*. Other significant contributions to the phytoplankton assemblage were from Cryptophyceae (15% of total annual biovolume), Dinophyceae (7%) and Bacillariophyceae (3%) which together with Cyanobacteria amounted to 90% of the total annual biovolume. Phytoplankton biomass was concentrated in the epilimnion in autumn and in the metalimnion in summer. Phytoplankton sampling identified 109 different species in total, with greatest diversity in late summer, as observed in Legnani et al. (2005). The total annual biovolume can be represented for most of the year by the sum of just five species (*Aphanizomenon flos-aquae* (Aph-f-a), *Asterionella formosa* (Ast-f), *Cryptomonas erosa* (Cry-er), *Cryptomonas rostratiformis* (Cry-rostr), *Cryptomonas sp.* (Cry-sp), *Planktothrix rubescens* (P-rub)). Among these species P-rub exceeded the 90% of total biovolume in autumn-winter (Figure 2 a) and dominated the metalimnetic (> 8 m depth) species composition by the end of the summer: it was 70% of the biovolume on 02/09/2010; 40% on 29/09/2010 (*Chrysochromulina parva* was 18%; *Cryptomonas ovata* was 15%; *Ceratium hirundinella* was 10%) and 95% on 28/10/2010.

Date	n° spp.	Bacillariophyceae	Chlorophyceae	Chrysophyceae	Cyanobacteria	Coniugate	Cryptophyceae	Dinophyceae	Ultraplancton	Total by date	Epilimnion	Metalimnion	Hypolimnion
27/01/2010	**51**	0.0	0.0	0.2	3.8	0.0	0.1	0.2	0.0	**4.3**	100.0		
23/02/2010	**64**	0.1	0.1	0.1	4.6	0.0	1.4	0.1	0.2	**6.6**	100.0		
17/03/2010	**78**	0.6	0.1	0.3	3.5	0.0	2.7	0.5	0.1	**7.7**	100.0		
20/04/2010	**64**	0.1	0.0	0.4	0.4	0.0	0.5	0.1	0.1	**1.7**	46.5	28.0	25.6
26/05/2010	**56**	0.7	0.1	0.4	10.9	0.3	4.2	0.8	0.1	**17.5**	3.7	63.6	32.6
29/06/2010	**61**	0.3	0.1	1.0	1.4	0.1	1.2	1.6	0.1	**5.7**	12.4	69.7	17.9
20/07/2010	**87**	0.3	0.5	0.3	1.4	0.1	1.6	0.6	0.3	**5.2**	18.2	55.9	25.9
02/09/2010	**80**	0.2	0.6	0.2	1.2	0.0	0.8	0.8	0.3	**4.2**	26.4	23.1	50.5
30/09/2010	**83**	0.1	0.0	1.1	0.9	0.0	0.6	1.2	0.1	**4.0**	24.3	47.2	28.5
28/10/2010	**51**	0.2	0.0	0.3	5.9	0.0	0.4	0.6	0.2	**7.7**	49.2	50.8	
17/11/2010	**40**	0.1	0.1	0.3	9.9	0.0	0.8	0.3	0.2	**11.6**	72.8	27.2	
15/12/2010	**52**	0.1	0.0	1.3	10.5	0.0	0.5	0.1	0.3	**12.7**	43.5	56.7	
12/01/2011	**50**	0.4	0.0	0.0	9.7	0.0	0.7	0.1	0.2	**11.0**	100.0		
Total by group	**109** ***spp***	**3.2**	**1.7**	**5.8**	**64.2**	**0.7**	**15.3**	**6.9**	**2.2**	**100.0**	**53.6**	**32.5**	**13.9**

Table 9. Number of phytoplankton species and percentage of total annual biovolume, assembled into taxonomic groups for each sampling date and water column location (according to the thermal profile) in Lake Pusiano.

The total biovolume was compared to the total Chl-a based on the sum of all phyla contributions (Figure 9 b). Taxonomic-biovolume data have been combined into spectral groups and related to the FP-determined Chl-a, after a log-transformation (see 1.6.2) for P-rub (Figure 9 c), Cyano (Figure 9 d), Diat (Figure 9 e) and Crypto (Figure 9 f).

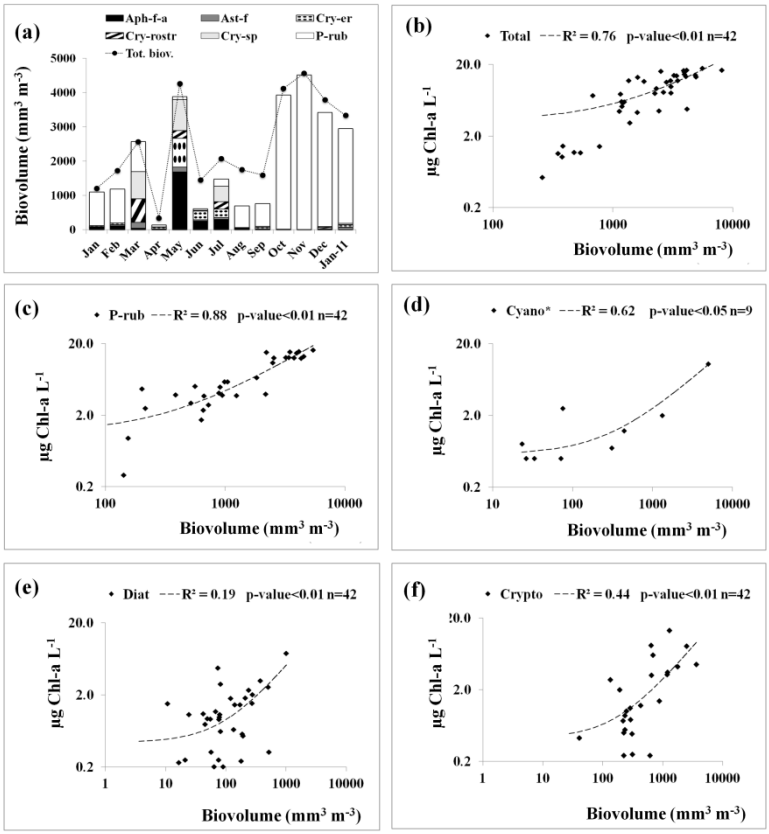

Figure 9 a Dominant species of the phytoplankton assemblage as mean biovolume ($mm^3 m^{-3}$) along water column by monthly identification. Mean total biovolume by all species is also reported as black dots. Log-regressions between biovolume ($mm^3 m^{-3}$) and chlorophyll concentration (µg Chl-a L^{-1}) determined fluorometrically at every depth and date for : **b** total biovolume and chlorophyll concentration; **c** P-rub fingerprint; **d** Cyanobacteria spectral group; **e** Diatoms spectral group; **f** Cryptophyta spectral group.

2.2.2 Phytoplankton modelling

CAEDYM can simulate up to seven groups which can be parameterized according to the assigned specific species, genre, classes or groups. In this study phytoplankton were characterized into three key algal groups (Crypto, Diat and P-rub) for the purpose of the model to represent the resultantdominant genera/species of *Cryptomonas sp*, *Asterionella formosa* and *Planktothrix rubescens* observed during 2010 (Figure 9 a). Functionally (Reynolds et al., 2002; Padisák et al., 2009), the first species represents those commonly found in mixed, eutrophic small-medium lakes, with physiology characterized by tolerance to light and sensitivity to stratification and silica depletion; the second genre of

species represents those found in mesotrophic small- and medium-sized lakes with sensitivity to stratification; the third represents a genre of phytoplankton common to the metalimnia of mesotrophic stratified lakes (usually deep lakes) with tolerance to low light and strong vertical segregation, and sensitivity to instability of water column.

The parameters for growth rate, temperature curve representation (as standard, optimum and maximum growth temperature), light limitation and vertical migration were obtained both from literature and previous modelling studies (Table 10). Carbon, nitrogen and silica (the last only for Diat) limitation were simulated with a simple Michaelis-Menten term while phosphorus limitation was simulated with the intracellular store option (for detailed explanation see Robson & Hamilton, 2004) since this is the limiting nutrient for phytoplankton growth in Lake Pusiano (Legnani et al., 2005; Copetti et al., 2006). The phosphorus limitation function was mathematically analyzed and calibrated to make P-rub less frequently limited by P than Diat and Crypto, (Feuillade, 1994; Dokulil & Teubner, 2000). Respiration rate and mortality were calibrated for all the groups. The coefficient for phosphorus sediment release has been measured in Lake Pusiano (Vuillermoz et al., 2006) while those for nitrogen and silica were calibrated. A general herbivore zooplankton group was configured in the model to prey on Crypto (preference at 60%) and Diat (preference at 40%) since measured zooplankton consisted mostly of small herbivores (rotifers and copepod nauplii) while the predatory taxa (adult copepods, predatory rotifers) co-dominated only in summer and early winter.

Phytoplankton parameters	Symbols	Units	Assigned Values		
			Diat	Crypt	P-rub
Maximum potential growth rate of phytoplankton	**Pmax**	day^{-1}	1.0	1.0 [c]	0.14 [a]
Average ratio of C to chlorophyll a	**Ycc**	mg C mg Chl-a^{-1}	40 [d]	40 [e]	90 [e]
Light half saturation constant for algal limitation	**IK**[§]	µmol m^{-2} s^{-1}	60 [d]		
Light saturation for maximum production	**Ist**[§]	µmol m^{-2} s^{-1}		80 [d]	10 [a]
Half saturation constant for phosphorus uptake	**KP**	mg L^{-1}	0.03	0.03 [c]	0.002 [c]
Half saturation constant for silica uptake	**KSi**	mg L^{-1}	0.24 [c]		

Maximum internal phosphorus concentration	**IPmax**	mg P mg Chl-a^{-1}	0.085 [b]	0.085	0.1
Minimum internal phophorus concentration	**IPmin**	mg P mg Chl-a^{-1}	0.02 [b]	0.02	0.0003
Maximum rate of phosphorus uptake	**UPmax**	mg P mg Chl-a^{-1} day^{-1}	0.11 [b]	0.04	0.1
Standard growth temperature	**Tsta**	°C	8	15	10 [a]
Phytoplankton optimum temperature	**Topt**	°C	12	18	13 [a]
Phytoplankton maximum temperature	**Tmax**	°C	33 [d]	25	20 [a]
Temperature multiplier function for phytoplankton	**vT**	-	1.01	1.08	1.06 [e]
Constant settling velocity	**ws**[*]	m d^{-1}	-0.086 [d]	-0.035 [d]	0.004
Phytoplankton mortality coefficient	**kr**	d^{-1}	0.3	0.18	0.005

[a] Bright & Walsby (2000)

[b] Bruce et al. (2006)

[c] Rigosi et al. (2011)

[d] Rinke et al. (2010)

[e] Copetti et al. (2006)

[§]Two options are available to model light limitation to growth (without photoinhibition *IK* or with photoinhibition *Ist*; refer to Robson & Hamilton, 2004).

[*]Negative values indicates downward velocity; the positive value for P-rub indicates an upward velocity to simulate the buoyancy changes during autumnal waterblooms (Walsby et al., 2006).

Table 10. List of selected parameters differentiating the phytoplankton dynamics for the three algal groups set in ELCOM–CAEDYM.

2.2.3 Model assessment

Simulation profiles for temperature (T), dissolved oxygen (DO), nutrients (SiO_2-Si, PO_4-P, NH_4-N and NO_3-N) and phytoplankton (Diat, Crypto and P-rub) were compared to the corresponding measured profiles at all the stations (note that nutrients were available only at ST6 station) for each sampling date, to estimate the model performance. The agreement was firstly tested computing E_{NS}, MB and RMSE over 6092 observations for T, DO and algal groups and over 488 observations for nutrients. The comparison is represented in scatterplots (simulated data are on Y axes; measured data are on X axes) using smoothed densities computed with the algorithm of Eilers & Goeman

(2004), to measure the spread of each data point from the 1:1 regression line (Figure 10).

A good agreement resulted for T (E_{NS}=0.78) and DO (E_{NS}=0.48): ELCOM reproduced observed profiles by the boundary conditions and CAEDYM modulated them, mainly through the phytoplankton dynamics, with a mean underestimation (MB) of 1.66° C and 0.66 mg L^{-1}, respectively. Nutrient simulations depended on external loading input and the internal biogeochemical cycle (sediment-water column-biomass): a good performance was obtained for SiO_2-Si and NH_4-N (E_{NS}=0.35 and E_{NS}=0.66, with an underestimation of 0.06 and 0.05 mg L^{-1} respectively) but deteriorated for PO_4-P and NO_3-N (E_{NS}= -0.02 and E_{NS}= -2.27, with an overestimation of 0.02 and 0.12 mg L^{-1}, respectively). For each algal group the chlorophyll concentration (µg Chl-a L^{-1}) was dynamic on the basis of assigned parameters for nutrient uptake, growth, grazing, mortality, settling and sediment mineralization. Considering the global model performance (without space and time distinction) a good prediction level was gained for Diat (E_{NS}=0.32, with a slight underestimation of 0.52 µg Chl-a L^{-1}) and deteriorated for Crypto and P-rub (E_{NS}= -0.08 and E_{NS}= -0.72, with an underestimation of 0.48 Chl-a L^{-1} and an overestimation of 4.86 µg Chl-a L^{-1}, respectively).

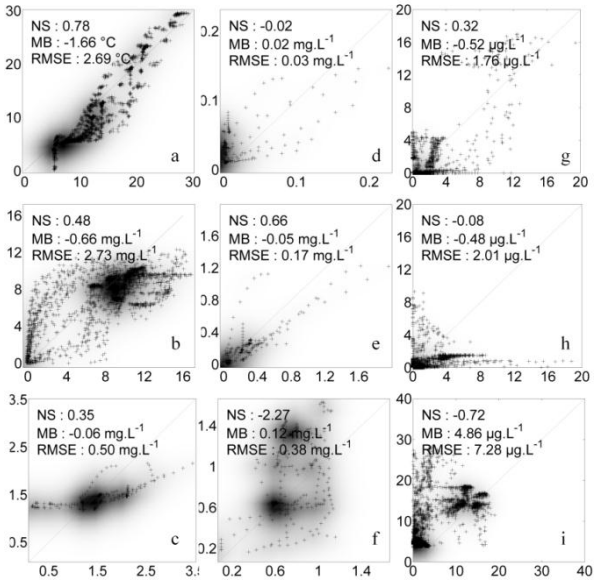

Figure 10. Scatterplots with smoothed densities by simulated (on Y axes) and field (on X axes) data; E_{NS} value (NS), Mean Bias (MB) and Root Mean Square Error (RMSE) are also reported as indices of model fit for **a** temperatures (° C), **b** dissolved oxygen (mg L^{-1}), **c** silica (mg L^{-1}), **d** orthophosphate (mg L^{-1}), **e** ammonium (mg L^{-1}), **f** nitrate

(mg L^{-1}), **g** Diat (µg Chl-a L^{-1}), **h** Crypto (µg Chl-a L^{-1}) and **i** P-rub (µg Chl-a L^{-1}). See in the text for more information.

The vertical and seasonal patterns were analyzed at the deepest station (ST6), where field data (at monthly scale) were overlapped with simulation data (at hourly scale) to describe the performance of the model to reproduce the seasonal evolution of each variable, in a qualitative and quantitative way. The RMSE and MB temporal evolution were thus computed by comparison between simulated and measured data at ST6 (Figure 11). The evolution of T was matched during the year: the associated error (RMSE) increased only during stratification due to colder simulated temperatures at the bottom probably because the model underestimated the heat exchange between upper and lower layers during the summer. The evolution of DO was well matched especially in relation to the bottom depletion during the summer; the error values increased in this period because of the peak measured in the surface layers during the occasional bloom of the cyanobacterium Aph-f-a (not considered in the model) during late spring. Sediment release of SiO_2-Si, NH_4-N and PO_4-P were well simulated during the summer as well as NO_3-N bottom depletion. Some problems arose in the upper layers: SiO_2-Si was underestimated during early spring and overestimated during the summer probably due to the simplicity of the flow-based model for silica; NO_3-N was generally overestimated from spring, possibly due to inability to properly represent external loading and perhaps insufficient nitrogen uptake by phytoplankton; PO_4-P was overestimated only during the lake overturn (Jan. 2011) probably due to an excess of sediment release in the model; the simulation of NH_4-N was the best matched among the nutrients. All the simulated algal groups resulted in correct reproduction of the timing and position in the water column based on qualitative comparisons with measured profiles of spectral groups: periods of rapid biomass increase of Diat were well matched with corresponding depletion of SiO_2-Si; Crypto growth was slightly underestimated during late winter while early–summer increases in biomass were simulated with the model but not so in spring. P-rub was well reproduced during the autumn bloom both in the spatial position and in the concentration values; the model correctly predicted the metalimnetic peak in summer but overestimated the productivity, probably because certain factors moderating the metalimnetic increase in the real world were not embraced.

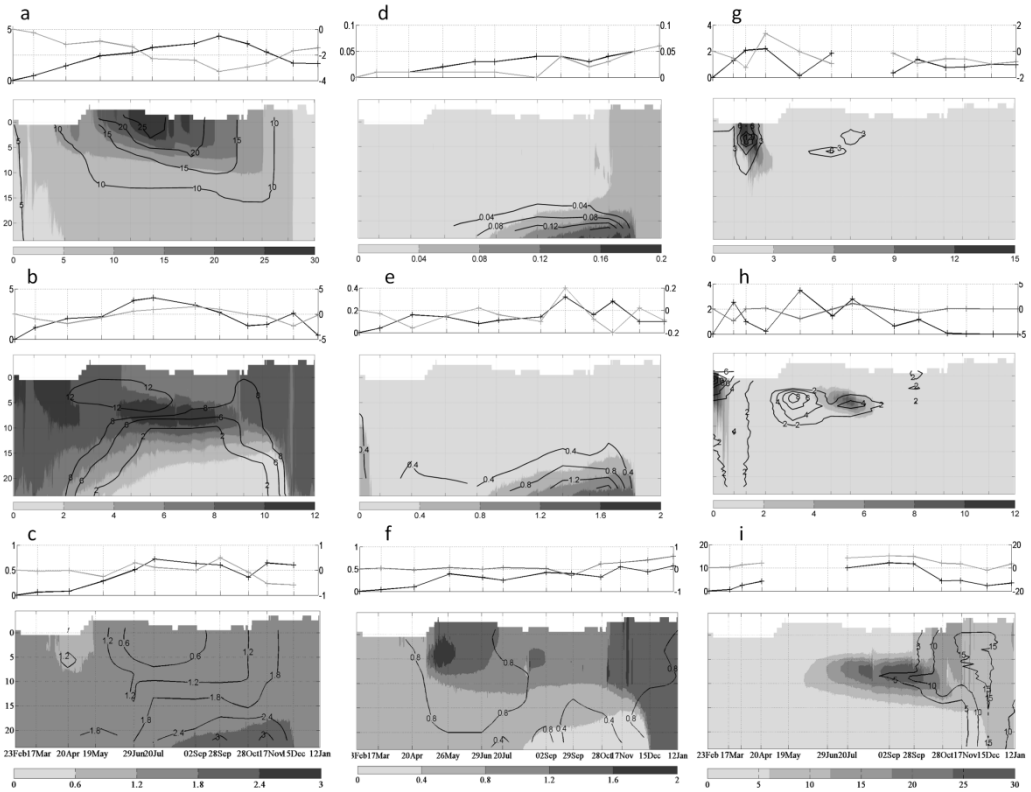

Figure 11 On each subplot: RMSE (black line, referred to the main Y axes) and MB (grey line, referred to the secondary Y axes) at ST6 station computed by simulated and field for each sampling date (above); field (black lines) versus model (contour plot in scale of gray) profiles at ST6 station (below) as **a** function of depth (as meters on Y axes) and time (sampling date on X axes) for a temperatures in °C, **b** dissolved oxygen in mg DO L^{-1}, **c** silica mg Si-SiO_4 L^{-1}, **d** orthophosphate mg P-PO_4 L^{-1}, **e** ammonium mg N-NH_4 L^{-1}, **f** nitrate mg N-NO_3 L^{-1}, **g** Diat, µg Chl-a L^{-1} **h** Crypto µg Chl-a L^{-1} and **i** P-rub µg Chl-a L^{-1}. The missing values among the RMSE and MB of Diat and P-rub depended on the absence of measured profiles.

The model performance in reproducing the spatial variability was shown through RMSE computed at each station, on the basis of the specific range of each variable (Figure 12). The model had an optimal performance in reproducing temperatures along the south side, near the entrance of Lambro River, as well as the north-east and the north-west shores near the entrance of a minor tributary at ST18 (see the map on Figure 2). Dissolved oxygen was generally well reproduced at all stations except ST16, where the main tributary enters. Phytoplankton simulations showed a good spatial performance for the Diat group, except ST16 where comparisons may have been affected by the major river. Crypto relative error was generally small, deteriorating only in a few stations. For

P-rub the error was slightly larger due to metalimnetic overproduction in the model, and there was a better performance in the shallower stations close to the shore.

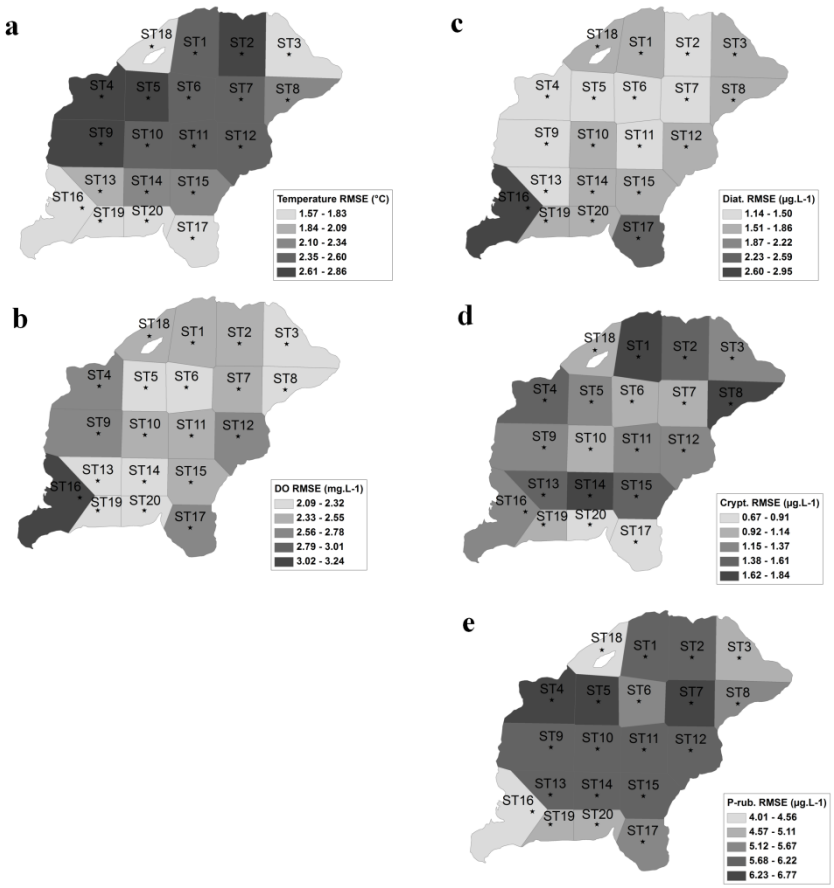

Figure 12. Spatial model performance description through RMSE computed by simulated and measured data residuals at each monitoring station for **a** temperatures, **b** dissolved oxygen, **c** Diat, **d** Crypto and **e** P-rub. For each variable RMSE is relative to the full scale. Light gray expresses a lower error.

Model outputs for phytoplankton growth and losses, which included gross production, mortality, changes due to hydrodynamics and settling, were graphically examined. Each group was analysed in a representative surface layer (2 m) and in a representative deep layer (8 m) and their 'capacity to grow' was represented with growth-polygons. The vertex of each polygon represented individual growth limitation functions, spanning from 0 to 1 while the temperature effect and mortality (i.e. grazing and respiration) were also normalized to values between 0 and 1, allowing evaluation of how the limitation factors and loss terms affected the growth potential. Phytoplankton production is

maximal when the value of limitation by nutrients and light and the temperature effect is close to 1 and when the value of grazing and respiration is close to zero. A bloom of Diat, from the end of winter to early-spring, was supported by near-optimal temperatures for growth (ca. 12° C; Table 10), high nutrient availability and very low grazing and competition in the upper layer (depth 2 m). Smaller peaks in Diat concentrations in the deeper layer (8 m) were due mostly to sedimentation of populations in surface waters, as irradiance was strongly limiting at this depth. This group was highly sensitive to increases in water temperature and declined rapidly with increases in spring temperatures. A further influence was the occurrence of stratification in spring when there was a conspicuous loss of Diat from the upper layer. The combination of relatively high temperature and strong stratification meant that conditions were generally unsuitable to support their growth again until autumn (Figure 13a).

Crypto at depth of 2 m attained highest concentrations in late-winter but quickly decreased in spring when there was strong limitation by temperature and light. In summer they had large losses because of mixing through the surface mixed layer as well as high mortality, and thus their growth rate remained close to zero. At a depth of 8 m they grew rapidly during mid-summer, mainly due to concomitant occurrence of favourable temperature, adequate nutrients and stronger density stratification in this deeper layer (Figure 13 b).

Specific physiological features of P-rub were included in the model, such as a relatively low growth and mortality rate, low light saturation of growth rate and buoyant properties (simulated by a low negative value for the sedimentation rate). The combination of low values of growth rate and settling velocity made it particularly sensitive to high turbulence occurring either throughout the water column during winter mixing or in the surface mixed layer during summer. In the late-autumn period concentrations gradually declined due to increasing turbulence and impending water column mixing. In the deeper (8 m) layer, concentrations increased during summer and were almost static even under strong wind forcing, while they suffered a flood event in mid-summer (15 Aug.) and finally decreased in winter when low irradiance and cold temperature did not support net growth (Figure 13 c).

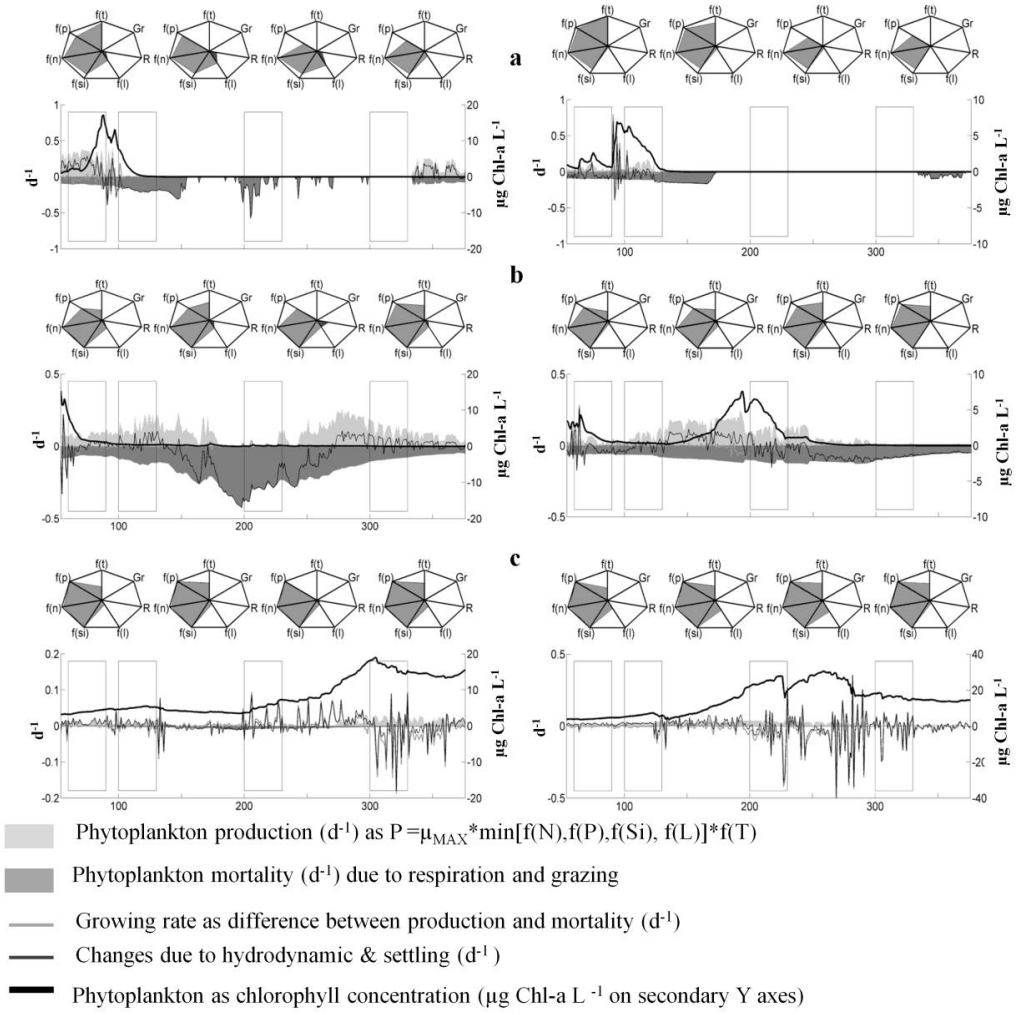

Figure 13 Simulation output at the depth of 2 meters (left) and of 8 meters (right) at ST6 station for the limitation terms to phytoplankton growth. For each algal group the time evolution (322 days from 23 Feb. 2010 to 12 Jan. 2011, expressed as day of year). Each window of 30 days in the sub-plots corresponds to the area in the polygons (above each sub-plot) representing determinant periods for the phytoplankton phenology: (from left to right) late-winter from 53 to 80 day of year, early-spring from 85 to 120 day of year, mid-summer from 200 to 230 day of year, late-autumn from 300 to 330 day of year. The algal growth is determined by the influence of temperature f(T), orthophosphate f(P), dissolved inorganic nitrogen f(N), silica f(Si), light f(L), respiration (R) and grazing (G) for: **a** Diat, **b** Crypto and **c** P-rub.

2.3 Discussion

2.3.1 Approach

A common problem in ecological modelling is the adequacy of representing changes in ecosystem dynamics without excessive complexity and over-parameterization of models

(Van Nes & Scheffer, 2005). Interactions of abiotic and biotic components shape the spatial distributions of organisms, thus appropriate mathematical relationships need to be developed to provide for spatial heterogeneity. In this study the physical variables (i.e., temperature) were first simulated satisfactorily at the deepest station (ST6) before calibration was undertaken of parameters relevant to the nutrient and algal dynamics.

Measurements of spectral signatures of phytoplankton based on functional groups proved to be a good strategy to parameterize different phytoplankton groups and allowed for direct calibration of the selected phytoplankton groups in the spatially-resolved (3D) model. *P. rubescens* emerged as keystone species, requiring assignment of its own group in the model, while two more generic phytoplankton groups were chosen, representing Diatoms and Cryptophytes. The model algal-group parameters represented specific physiological features of each group, collectively representing the dynamics of the entire phytoplankton community in Lake Pusiano. As has been noted in a number of other studies (Arhonditsis & Brett, 2004; Trolle et al., 2008; Rinke et al., 2010) the model performance, evaluated statistically, showed that temperature and oxygen profiles were simulated well, but there was a lower performance for nutrient and biological variables (three phytoplankton groups), attributable to the complexity governing these higher ecological levels (Robson & Hamilton, 2004; Missaghi & Hondzo, 2010; Vilhena et al., 2010). In our study the E_{NS} statistical index was positive for silica, ammonium and Diatoms and slightly negative for the other variables. A systematic further calibration (e.g. with a Bayesian approach) may be possible to parameterize mechanistic or process-based models (Arhonditsis et al., 2007) but it has been not yet completely extended to coupled physical-biogeochemical models (Zhang & Arhonditsis, 2009), thus here it has not been undertaken with a 3D approach in which the spatial comparison has been explicitly evaluated. A common 'trial and error' approach was used, supported by an expert modeler with an understanding of both the biophysics of the system and the structure of the model. Field data were compared to model output with goodness of fit evaluated using a'by eye' fit and with the aid of some measures of goodness of fit. In all cases parameter values were adjusted within literature or measured data ranges.

2.3.2 Vertical dynamics

The model provided good simulations of the seasonal patterns observed at the maximum depth for all of the variables. In particular, sediment nutrient releases (associated with increases in phosphate and ammonium concentrations) and depletion of nitrate (associated with denitrification) were inferred from the model simulations, whilst the timing and position of peaks in phytoplankton biomass in the water column were well-matched. The model had some problems in reproducing the temporal dynamics of nutrients within the upper layers, likely due to the coarseness of certain measurements of external loading, though we could not discount other possible effects resulting from inaccuracies in the timing and magnitude of phytoplankton biomass.

Complex ecosystem models are often examined only in terms of their ability to reproduce observed data against outputs of state variables from the model. As a result important physiological processes embedded within the model structure are often not elucidated and yet can yield important information. The analysis of growth polygons showed that *P. rubescens* is highly competitive in phosphorus-limiting conditions, especially compared with the other two phytoplankton groups. In spite of this, the physiological responses to nutrients were not the critical factor driving the algal growth in the model and other physiological properties (e.g. temperature range, growth rate, light and settling) determined ecological niches in which re-oligotrophication and increased duration and strength of stratification would favour such metalimnetic populations.

2.3.3 *Planktothrix rubescens* horizontal spatial patterns

Internal seiches derived from wind forcing are considered to drive the vertical and horizontal distributions of metalimnetic species such as *P. rubescens* (Pannard et al., 2011; Cuypers et al., 2011). In our study wind (maximum speed: 5.7 m s^{-1}) had a strong effect on its distributions at short-time scales, mainly affecting vertical distributions. A spectral analysis of thermocline oscillations in Lake Pusiano has previously allowed identification of the rapid degeneration of basin-scale internal wave activity that occurs within a few hours during maximum stratification (Boegman et al., 2005).

The effects due to the Lambro River entrance were more pronounced and long-lasting during high-discharge events, both in terms of vertical and horizontal patterns. A description was attempted in order to compare salinity mean values to the maximum P-rub concentrations of vertical profiles at each station before (14 Aug.), during (15 Aug.) and

after (16 Aug.) a flood event (maximum discharge: 263 m^3 s^{-1}). When the river entered the lake it was tracked by low-salinity water and was shown to have a circular anti-clockwise distribution along the shores. In summer maximum concentrations were in the metalimnion: before the flood, a stable condition was depicted by a horizontally-uniform distribution; during the flood, water movements pushed the population toward the lake centre, then to the west shores and progressively to the south side. After 48 hours, a horizontally-uniform, but more diluted, distribution formed again in the metalimnion (Figure 14).

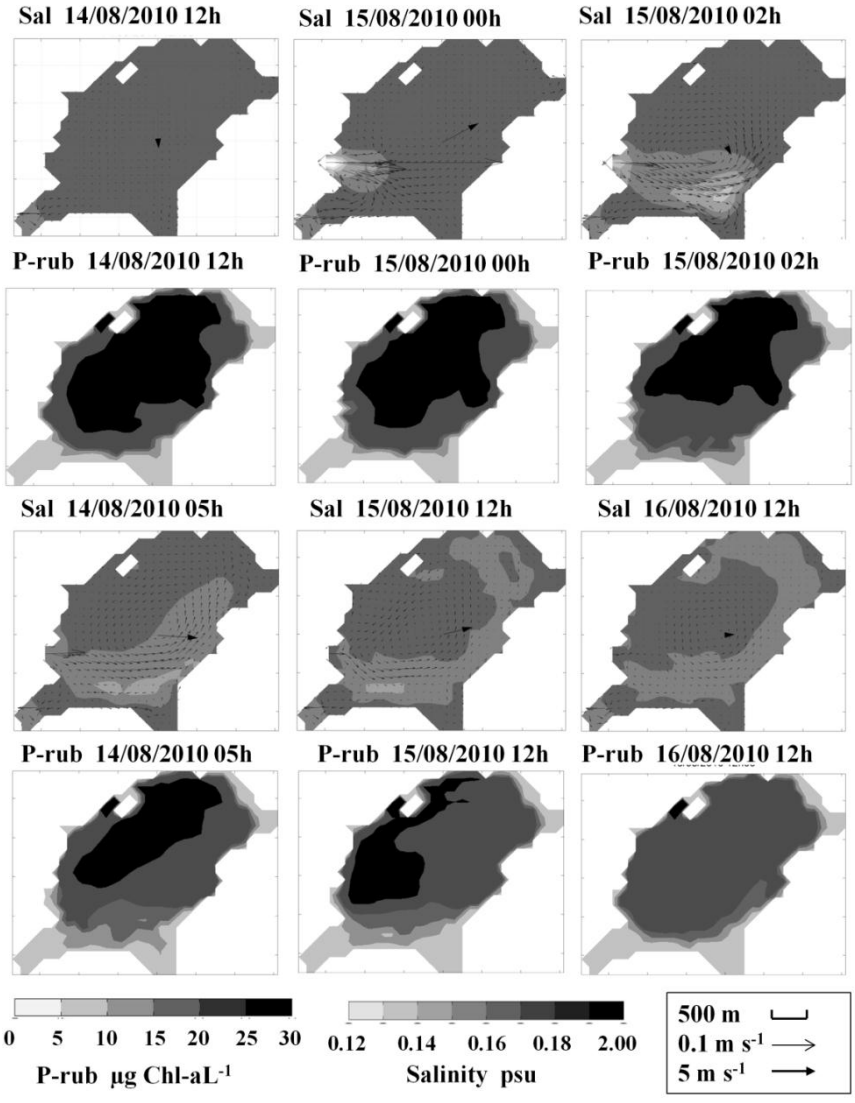

Figure 14 Representation of spatial horizontal patterns before, during and after a flood event as mean values of salinity (Sal) and P-rub maximum Chl-a concentrations on surface plots. X and Y are spatial axes (m); thin arrows represent velocity and direction of

the water currents in lake and the thick arrow on the lake center represents velocity and direction of the wind.

P. rubescens is the primary constituent of the DCMs in Lake Pusiano and its assigned physiological parameters led to simulations that replicated its presence in the metalimnion during the stratified period, as well as its horizontal variation. The other two algal groups that were simulated, representative of Diatoms and Cryptophytes, compete with it for resources over a typical annual phytoplankton succession sequence (Krivtsov et al., 2000). Vertical separation of resources, which is interrupted by storm events and inflow insertions, play a major role in alternating populations of these three groups through the annual cycle. Whilst the two competitors in the model had a higher potential growth rate, the growth-polygon for *P. rubescens* clearly showed how several of the key environmental variables (e.g. water temperature and light) were closer to its optimal at 8 m than for the other two phytoplankton groups. The model results offer support to the hypothesis that physiological features (D'Alelio et al., 2011) explain the widespread success of that species. The timing of the onset of stratification too, more than warmer water temperatures, should be considered amongst factors leading to increasing dominance of *P. rubescens* (Dokulil and Teubner, 2012). Variables relevant to a changing climate (e.g., air temperature) can be encompassed into model forcing terms and the length of simulation runs should be extended in future work in order to better understand, and potentially to isolate the effect of a changing climate on its distributions.

2.4 Conclusion

This study evaluated the use a three-dimensional hydrodynamic-ecological model to reproduce discrete measurements of hydro-chemical variables, including inferred behaviour of metalimnetic populations of *P. rubescens* in a pre-alpine lake. An innovative methodological approach was used to allocate classic taxonomic determinations into 'functional-groups' in order to validate a hydrodynamic-ecological model with three 'key' groups including the metalimnetic species *P. rubescens*. Spectrally-specific fluorometric responses and validation with traditional cell enumeration microscopy were used to provide highly temporally and spatially resolved distribution patterns of phytoplankton in Lake Pusiano, so that measured chlorophyll *a* concentrations assigned to the

three phytoplankton groups could be compared directly to the model output values of these groups.

Distributions of *P. rubescens* were strongly influenced by the lake hydrodynamics, particularly during high-discharge inflows in summer stratification. The river inflows shaped a circulation pattern in the lake, strongly altering its spatial distributions in the horizontal dimension. A vertically-resolved assessment, based on analyses of model output at depths of 2 and 8 m, revealed strong separation of environmental drivers between the two depths, indicating niche separation according to the two depths. A difference was noted in near-shore and pelagic profiles in the model output and may be attributed to a depth-specific calibration strategy, inflow dilution of cells or phytoplankton nutrient uptake variations associated with the stream-lake transition zone (Mackay et al., 2011). A further parameterization of phytoplankton and zooplankton and an improvement in tributary input characterization are identified as areas where model performance could be improved. The model used in this study may help in the refinement of field programs, allowing for measurements to be targeted more specifically to locations or times in Lake Pusiano when there are likely to be rapid changes in phytoplankton populations. The model also revealed how the physiological features of *P. rubescens*, specifically its ability to grow well in the metalimnion, may be well suited to a re-oligotrophication phase occurring concurrently with the strengthening stratification of a warming climate.

3 Impact of global and local pressures on Lake Pusiano ecology

***From:** Carraro E., Guyennon N., Viviano G., Manfredi E., Valsecchi L., Salerno F., Tartari G. and Copetti D. Impact of global and local pressures on the ecology of a medium-sized pre-alpine lake. In: Models of the Ecological Hierarchy: From Molecules to the Ecosphere. Elsevier B.V., pp. 259–274.

3.1 Motivation

Due to the scarcity of long time series of observations, there are only a limited number of publications which unequivocally measure the impact of climate change on nutrient loads or concentrations in water bodies (e.g., Parmesan and Yohe, 2003; Thackeray et al., 2008). Conversely, a vast number of physical and ecological modeling studies deal with the effects of increasing temperatures on lakes thermal stability, nutrients supply, and ecosystem responses (Peeters et al., 2002; Malmaeus et al., 2006; Trolle et al., 2011).

Recently, many different mathematical models have been implemented to investigate the lake responses to environmental pressures improving the cost-effective management options, but no profound scientific understanding on the ecosystem responses to multiple anthropogenic modifications has been achieved so far (Blenckner, 2008). Some authors (Malmaeus et al., 2006; Trolle et al., 2011) tried to link global or regional climate models to ecological lake models, simulating the impacts of meteorological alterations on lakes with different morphometry or trophic status. Nevertheless Global Climate Models (GCMs) and Regional Climate Models (RCMs) are still far from matching the real variability due to complex atmosphere-land processes at local scale, thus their outputs cannot be expected to exactly reproduce the observed local dynamics and may produce larger bias as higher the frequency of local simulations (Elliott et al., 2005; Portoghese et al., 2011).

An integrated lake-catchmentmodeling approach is presented here to differentiate the impacts of the atmospheric temperature increase (globally mediated) fromthe local im-

pact by external loads in a pre-alpine lake. The separation of the global and the local pressures is gained by analyzing four scenarios with different degrees of local and global weights. Pristine conditions were simulated coupling model outcomes with paleolimnological analysis, while a specific statistical technique (Spectral Singular Analysis) was performed to flatten the atmospheric temperature increasing trend detected on daily values between 1960 and 2010, thus isolating the human-induced global warming.

3.2 Integrated modelling tool

3.2.1 Meteoclimatic forcing

Both the lake and the catchment models required long-term and continuous time series of meteorological daily data. The Regional Earth System (RES) PROTHEUS hind cast simulation (Artale et al., 2010), forced by the ERA40 (1958–1999) reanalysis (Simmons and Gibson, 2000) was the long-term climate reference for the available local historical series. A statistical downscaling (S-DSC) was performed to correct the RES output for local bias (mainly due to the raw approximation of land use and topography in RES), thus obtaining a realistic meteorological forcing for local impacts analysis. The S-DSC technique is based on the estimation of the inverse of the Cumulative Distribution Function (CDF) or quantiles function. The quantiles of predictor and predictand was used to define a Quantile–Quantile (Q–Q) correction algorithm (Déqué, 2007), which was computed monthly and applied to the predictor.

Two meteorological stations (Erba and Merone), close to Lake Pusiano, were chosen as reference for cumulated daily rainfall, air temperature (minimum, maximum, and daily average values), short-wave solar radiation, vapor pressure, and wind speed (Figure 15 a). Data were supplied by the Lombardy Regional Agency for Environmental Protection (ARPA Lombardia http://ita.arpalombardia.it/meteo/dati/richiesta.asp) covering the period between 1991 and 2010. Cloud cover data were available at the National Oceanic and Atmospheric Administration website (http://cimss.ssec.wisc.edu/clavr/) for the entire period. A first S-DSC was applied to secondary stations distributed on the catchment area to fulfill missing data in the primary time series (Figure 15 a). The resulting dataset was then used to downscale the RES hind cast simulation, allowing to reconstruct a continuous daily dataset covering the 1960–2010 period with all the meteorological variables required for the integrated modeling approach (Figure 15 b).

A trend analysis was performed on the atmospheric temperatures with a statistical approach based on Singular Spectrum Analysis (SSA) proposed by Broomhead and King (1986). It was computed over a 20-year window, as a compromise between the maximum theoretical window of 25 years (half of the overall period) and the minimal time lag required to encompass the interannual and the interdecadal oscillations due to natural variability (4–10 years) in the temperatures trend (Ghil and Vautard, 1991), avoiding the effects of periodic climatic fluctuations, such as El Niño Southern Oscillation (ENSO) and the North Atlantic Oscillation (NAO). The resulting SSA trend was then removed from the time series using the mean value for the 1960–1980 time window, thus obtaining detrended atmospheric temperatures.

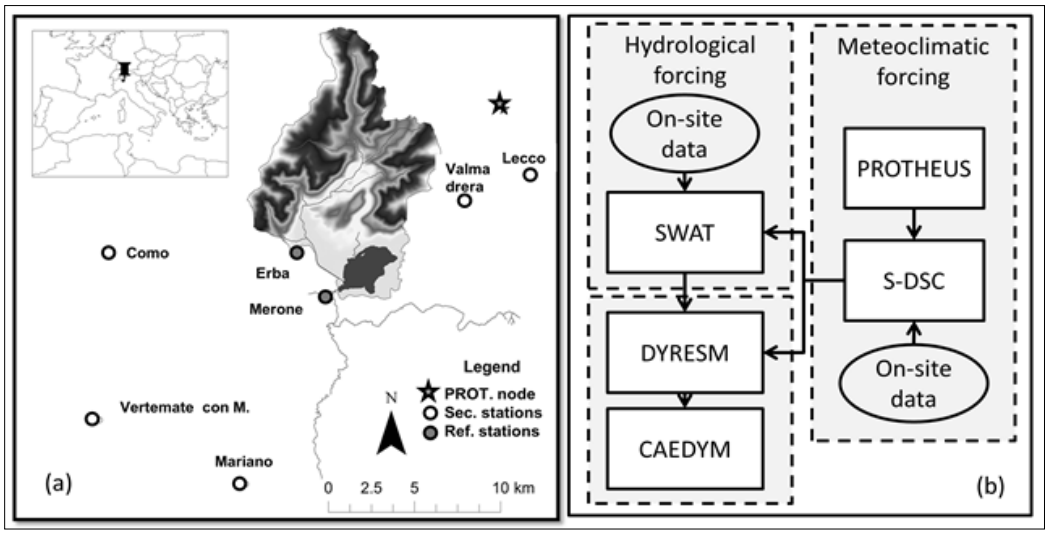

Figure 15. Panel (a) : Lake Pusiano with the catchment area, the reference and secondary meteorological stations and the closest PROTHEUS node. Panel (b): the method outline illustrating data flux to build the hydrological and meteorological forcing for the integrated modelling purpose.

3.2.2 Catchment modelling

The SWAT model was previously calibrated and validated (Salerno and Tartari, 2009) using available discharge data for different sections of Lambro River over several years (1974–1982; 1998–2004). In this study, a further validation was performed using new data collected in 2010; thus, the model was applied to the other smaller inlets, determining the direct drainage basin and the whole daily inflow to the lake.

The estimation of the pristine conditions (or reference conditions) is crucial in any ecological research, providing the baseline to determine human-induced changes and thus

drawing conclusions about the weight of the current or future human impact. Different proposed approaches have been summarized in the line-guide about reference conditions for the Water Framework Directive programs (Anonymous, 2003). Here the natural phosphorus load to Lake Pusiano was estimated comparing SWAT model and the use of the export coefficients approach (Johnes, 1996; Bennion et al., 2005), both calibrated using field data by a selected natural sub-basin (deciduous forests), representative of the catchment pristine condition.

Currently, the main source of phosphorus pollution originates by the point sources, consisting in a network of combined sewage overflows (CSOs), which release polluted water into the rivers during rainfall events (Boguniewicz et al., 2006). Since SWAT is not able to model the point sources loading, the CSOs phosphorus load was estimated computing the exported amount by the specific unitary coefficients on the basis of the population census (Barbiero et al., 1991) and the management interventions (i.e., the construction of the sewage plant in 1986). The actual annual load (Figure 16 a) was finally computed by the Vollenweider equation (OECD, 1982) and the lake TP concentration at overturn during 1973–2010, applying the reduction coefficients along the river axes (Tartari et al., 2002). Daily loads were estimated by the anthropic and natural annual ratio.

The nitrogen and carbon loads were computed in a simplified way. Nitrogen river concentration was marked as two discharges (0–5 $m^3 s^{-1}$ and $> 5 m^3 s^{-1}$) according to the historical data while carbon river concentration was considered to be a constant value according to the paleolimnological analysis. Nitrogen and carbon natural levels were referred to the analysis on sediment core in the pre-industrial age (ca. 1730).

3.2.3 Lake modelling

In this study the meteorological and hydrological forcing for the DYCD model were set from 1960 to 2010. The Lambro River discharges were supplied by SWAT simulations. The river temperature was computed through a regression with air temperature (Copetti et al., 2006), while salinity, oxygen (DO), and carbon (POC; DOC) and nitrogen (PON; DON; N-NH4; N-NO3) river concentrations (mg N L^{-1}) were set as constant values, according to the time series and paleolimnological data. The phosphorus river concentration (POP; DOP; P-PO4) was derived by the simulated or estimated loading. The input

was used to feed DYCD and to simulate both long-term nutrients and phytoplankton dynamics. The phytoplankton biomass was expressed as chlorophyll-a concentration (mg Chl-a L^{-1}) and the simple Michealis–Menten model was chosen to simulate the nutrient uptake. Phytoplankton biomass was divided into two groups. The first group (Cyanobacteria) was parameterized by the specific eco-physiological parameters of *P. rubescens* (Dokulil and Teubner, 2000; Omlin et al., 2001; Walsby and Schanz, 2002), while the second group was parameterized by the features of a general competitor similar to Chlorophyta, one of the largest taxonomic groups detected among the Lake Pusiano algal community in the last 50 years (Vuillermoz et al., 2006). The main parameters for algal groups are summarized in Table 11. The biological model was completed with a zooplankton herbivorous general group (mg C L^{-1}). A comprehensive description of DYCD setup and calibration for Lake Pusiano can be found in Copetti et al. (2006).

The lake was initialized in 1960 with mean values of carbon, nitrogen, phosphorus, and total Chl-a content from the paleolimnological survey. The phytoplankton and zooplankton groups were initialized according to data from the historical lake surveys. Model simulated with a 1 h time step and the outputs were assessed by available time series of measurements.

CYANO		**CHLOR**	
Cold stenotherm species	10-22.5 °C (Dukulil and Teubner, 2000)	Warm euryterm species	20-35 °C
Low growth rate	0.12 d^{-1} (Omlin et al. 2001b)	Higher growth rate	0.9 d^{-1}
Low respiration rate	0.0128 d^{-1} (Omlin et al. 2001b)	Higher respiration rate	0.1 d^{-1}
Low light threshold	10 µE m^{-2} s^{-1} (Walsby and Schanz, 2002)	Higher light threshold	90 µE m^{-2} s^{-1}
Low phosphorus threshold	kp=0.004 mg P-PO_4 L^{-1} (Dukulil and Teubner, 2000)	Higher phosphorus threshold	Kp=0.030 mg P-PO_4 L^{-1}
Vertical position regulation	0.1-0.8 m d^{-1} (Walsby et al., 2006)	No vertical position regulation	-
Grazing defence	(Dukulil and Teubner, 2000)	No grazing defence	-

Table 11. Two phytoplankton groups (CYANO and CHLOR are the identification names used in CAEDYM) have been parameterized to simulate the keystone species *P. rubescens* and a general competitor as representative of algal evolution (1960-2010) in Lake Pusiano.

3.2.4 Scenarios construction

To quantify the effects of temperature warming and phosphorus load on the ecology of Lake Pusiano, inputs for P-loads and air temperature driving the anthropic and natural pressure were combined into a set of four different scenarios, running over the same period (1960–2010). Table 12 summarizes the possible combinations of the drivers. The current scenario (CUR) represents the real world, used here for the model assessment, and included both the local and the global human impact. The global pressure scenario (GPS) was cleaned by the anthropogenic phosphorus load, representing only the effects of global impact. The local pressure scenario (LPS) was cleaned by the temperature warming, thus representing only the effects of local impact. The undisturbed scenario (UND) was cleaned by the global and the local impacts, implementing the model only with the natural loads and detrended air temperature. *P. rubescens* bloom was triggered to start around the end of 90s in all scenarios, in order to reproduce what really occurred (CUR) under different conditions (LPS, GPS and UND).

Scenario Code	Global Pressure	Local Pressure	Distance to reality
CUR	+	+	0
GPS	+	-	1
LPS	-	+	1
UND	-	-	2

Table 12. The possible combinations resulting by the inputs differentiation: CUR = current scenario (it corresponds to reality), GPS = global pressure scenario; LPS = local pressure scenario; UND = undisturbed scenario; 0 indicates no distance to reality (both the measured pressures are inside); 1 indicates a partial reality isolating both the global and the local (measured) pressures; 2 indicates maximum distance to reality (without human presence).

3.3 Results

3.3.1 Global and local pressures

Inflow discharges were calibrated and validated (R^2= 0.58; R^2=0.45) for a period of about 4 years, when all the measurements were available, to indirectly compute the weekly water balance of Lake Pusiano. The lake volume change was derived by the daily measured lake levels and compared to the simulated lake volume change, resulting by the water balance of the simulated inflow discharges, the measured rainfall and outflow discharges and the estimation of the other terms (i.e. evaporation or the groundwater contribution). The simulated pristine mean annual P-load was confirmed by the load estimation with the export coefficients methods, resulting respectively 2.4 and 2.6 t P y^{-1} and converted into lake TP concentrations (during winter overturn) through the Vollenweider equation (OECD, 1982), resulting respectively in around 12 and 14 µg P L^{-1}. The outcome was confirmed by data coming from the paleololimnological survey (Guilizzoni, 2011) and the application the Morphoedaphic Index (MEI) predicting the pristine lake conditions (Vighi and Chiaudani, 1985) which have pointed out similar concentrations (respectively in around 13 and 10 µg P L^{-1}). The actual or anthropic annual P-load estimation was converted into lake TP concentrations too and validated by the time series of TP concentrations taken in the lake from 1973 (Figure 16a).

The SSA was chosen to represent the air temperature trend dynamics which resulted in a mean annual increase 0.015 °C $year^{-1}$ (Figure 16 b), in line with the considerations issued in Ambrosetti and Barbanti (1999) for alpine and subalpine lakes in North Italy. The resulting detrended air temperature series showed no increasing trend but slightly higher mean annual values in the first 10 years, as the best compromise between the method requirement of long series to stabilize the outcomes, data availability for this study and the identification of a cold period in 60s (Ghil and Vautard, 1991). The temperature differentiation began in 80s and strongly separated in the last 15 years by almost 1° C in mean annual values.

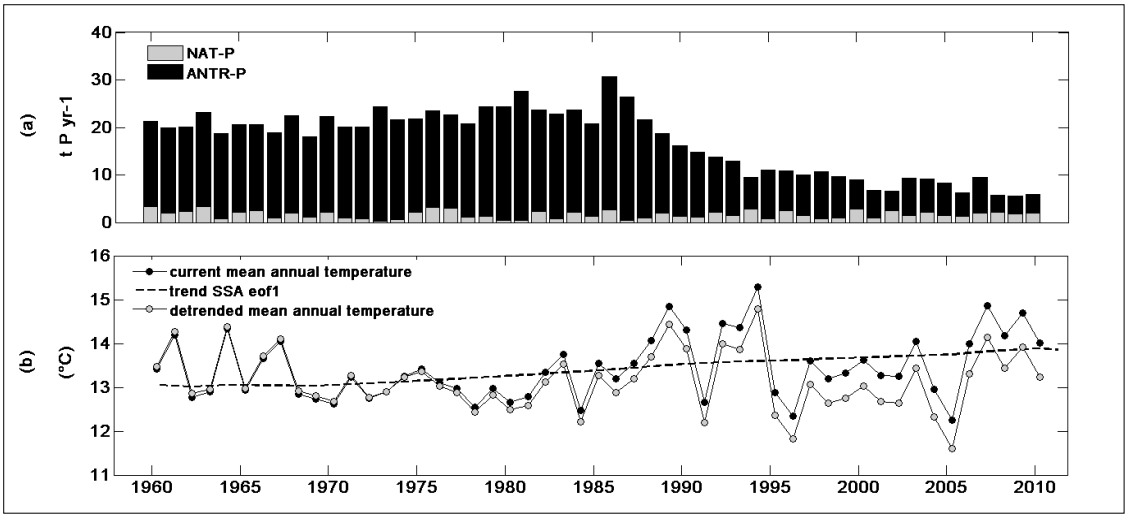

Figure 16. Panel a: natural (simulated by SWAT) and anthropogenic (estimated out of the model) annual P-load to Lake Pusiano. Panel b: mean annual atmospheric real temperature associated to the trend computed with SSA and annual series after a detrending computation on the real temperature.

3.3.2 Lake model assessment

After calibration DYCD was re-initialized and validated over 1960-2010 period for lake level, water temperature, TP, TN and total Chl-a (Figure 17). The lake level was the only daily series (except for the period 1973-1985 with no data). The simulated lake levels matched rather well the observed data, providing confidence of an accurately balance of water fluxes, showing a low mean bias of 0.16 m in relation to the vertical model resolution (1 m) while the Root Mean Square Error (RMSE) was of 0.46 m on 13674 observed data (Figure 17 a). Simulated temperatures as mean value by daily January values matched the observed temperature at winter overturn, though the model generally showed an underestimation (mean bias 0.98 °C and RMSE 1.24 °C on 28 observed data, Figure 17 b). Simulated TP lake concentration, showed as January monthly mean, followed the inter-annual trend of respective observed series as instantaneous recorded data at the lake overturn, with an increase from 70s to 90s and a decrease after the sewage plant construction and load reduction, (mean bias 0.0184 mg P L^{-1} and RMSE 0.0403 mg P L^{-1} on 30 observed data, Figure 17 c). Simulated TN lake concentration resulted within the range of the observed series, with a mean concentration of about 2 mg N L^{-1} , by January monthly mean values and also quite reproduced the interannual variability

though a general overestimation (mean bias -0.172 mg N L^{-1} and RMSE 0.308 mg N L^{-1} on 27 observed data, Figure 17 d). Despite too few available measurements of Chl-a lake concentration, the simulated biological response, as mean value of total Chl-a at early spring (April) in the upper layers, qualitatively caught higher productivity before 90s and an abrupt drop when the available phosphorus became limiting the algal growth. The model reproduced the peak due to P. rubescens first bloom at the end of 90s while it was firstly measured in April 2002 (Figure 17 e).

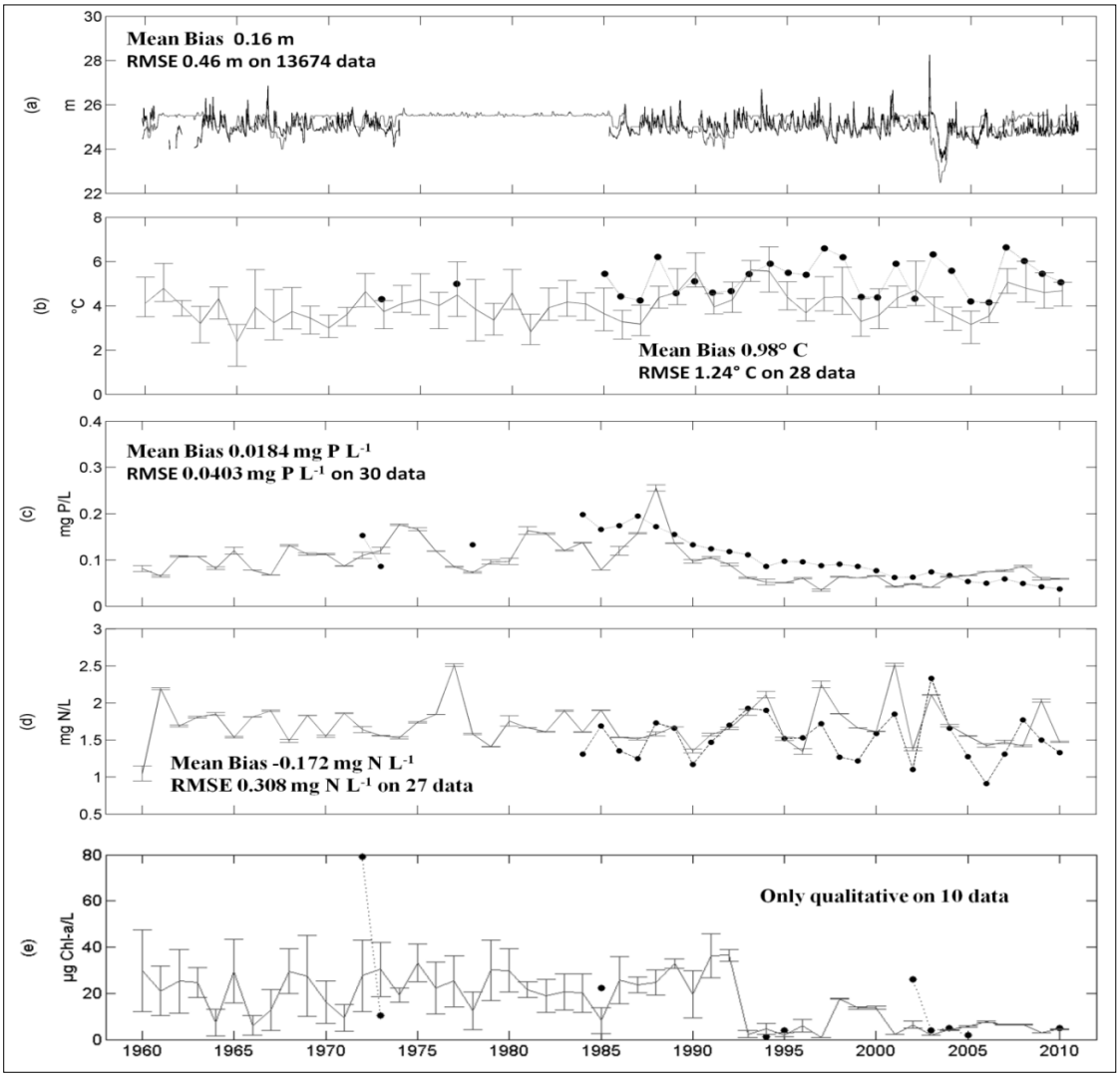

Figure 17. Measured (black line or circles) and simulated (grey solid line) daily values for the lake levels (a), the winter values for temperature (b), TP (c), TN (d) and the early spring values for total Chl-a (e). The error bars on simulated monthly mean values represent the daily maximum and minimum.

3.3.3 Scenarios comparison

Simulated scenarios have been compared for temperature, TP, TN and Chl-a as proxies tracking the lake changes. The evolution of the mean annual temperature, as lake volume-weighted, the winter mean concentration of TP and TN and the lake productivity as early spring Chl-a concentration are showed (Figure 18)

Generally the local pressures had more marked effects than the global pressure considering the scenarios comparison. On the whole the mean annual current water temperatures resulted lower than undisturbed ones (10.3 °C ± 13% and 9.8 °C ± 11% between UND and CUR p-value: < 0.001, Figure 18 a) but only the global impacted scenarios (CUR and GPS) produced a significant increasing trend by SSA. The SSA curve smoothed the annual series toward a first-order polynomial, thus it was linearized by a linear model. The analysis of covariance (ANCOVA) was used to test the different slopes for the scenarios considering the smoothed lake temperature as the covariate: the slope for the CUR scenario (0.012 °C y^{-1}, p-value: <0.001) significantly differed from GPS scenario (0.004 °C y^{-1}, p-value: <0.001).

The TP concentration had not a significant trend among GPS and UND scenarios: the mean value on 50 years of simulation was respectively of 0.0136 mg P L^{-1} (sd ± 25%) and 0.0127 mg P L^{-1} (sd ± 23%). The TP concentration in the CUR and LPS scenarios clearly reflected the dynamics of the anthropogenic P-load evolution: an increasing trend occurred until 1988 (slope: 0.0025 mg P L^{-1} p-value: <0.001) while a decrease started since 1989 (slope: -0.0015 mg P L^{-1} p-value = 0.005). No significantly differences was detected isolating the temperature warming among each coupled scenarios (Figure 18 b).

The TN concentration oscillated around a constant value both among the local impacted scenarios (CUR: mean value of 1.71 mg N L^{-1} sd ± 16%; LPS: mean value of 1.72 sd ± 17%) and the no-local impacted scenarios (mean value of 0.69 mg N L^{-1} sd ± 28% both for GPS and UND). No difference due to the temperature warming among each coupled scenarios was detected (Figure 18 c).

The Chl-a evolution partially reflected the trophic status due to TP concentration (directly linked to the available P-PO4 constituent) and confirmed the lake condition of

phosphorus limitation to the phytoplankton growth (Figure 18 d). However the biological pattern was not clear among the local impacted scenarios (CUR and LPS) and showed high variability due to interannual oscillations. A drop in spring lake total productivity abruptly occurred around 1993 changing from a high level (mean value of 27.4 µg Chl-a L^{-1} sd ± 49%) to a lower level (mean value of 5.8 µg Chl-a L^{-1} sd ± 56%) and resulting in a closer distance among local and no-local impacted scenarios. The GPS and UND scenarios presented a constant trend over the entire period and very low productivity values, except for the peak at the end of 90s quite similar to the other scenarios, due to the first appearance of *P. rubescens.*

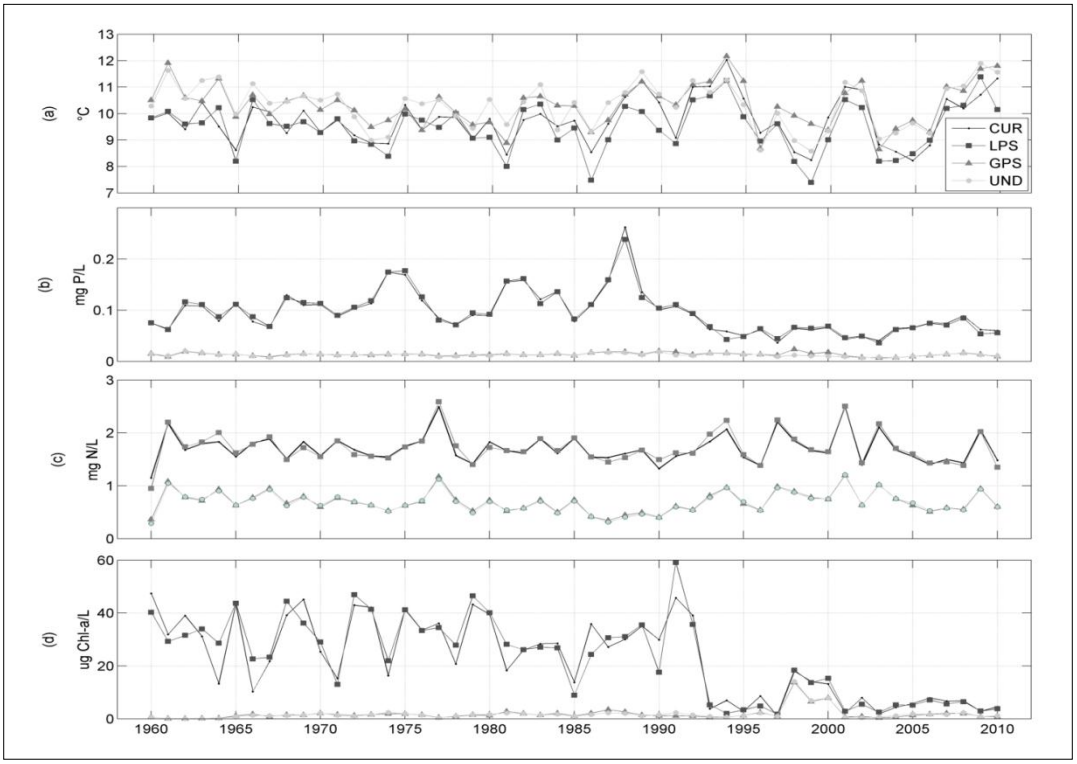

Figure 18. Scenarios comparisons: (a) simulated mean annual temperatures, representing the lake heat content; (b) simulated total phosphorus (TP) and (c) total nitrogen (TN) concentration at winter overturn; (d) simulated Chl-a concentration at early spring. CUR=Current scenario, GPS=Global Pressure Scenario; LPS=Local Pressure Scenario; UND=Undisturbed scenario.

Wavelet analysis (see Materials and methods) was used to extract periodic components from the simulated *P. rubescens* (as as µg Chl-a L^{-1}) daily time series. The wavelet power spectrum shows the decomposition of this series in time (along the x-axis) and period (along the y-axis) scale. The results of CUR and LPS scenarios identified the ab-

sence of a periodic pattern under the pression of nutrient enrichment from the catchment (Havens et al., 2009), confirming a year-round dominance since the blooms started (red spots) and additional components of variability at shorter periods (Winder and Cloern, 2011). The Global Wavelet Spectrum showed a tendancy to form an annual (between 300 and 400 days) periodicity in the GPS and UND scenarios, abruptly disturbed only by the arising of the first bloom, though characterized by a much lower intensity (mean Chl-a < 4 µg L^{-1}). Apparently the temperature warming had no effects regarding the natural two scenarios. Conversely, *P. rubesens* seems to be slightly when the temperature warming was turned off by the CUR scenario, as shown by the earlier arising in the LPS scenario (Figure 19).

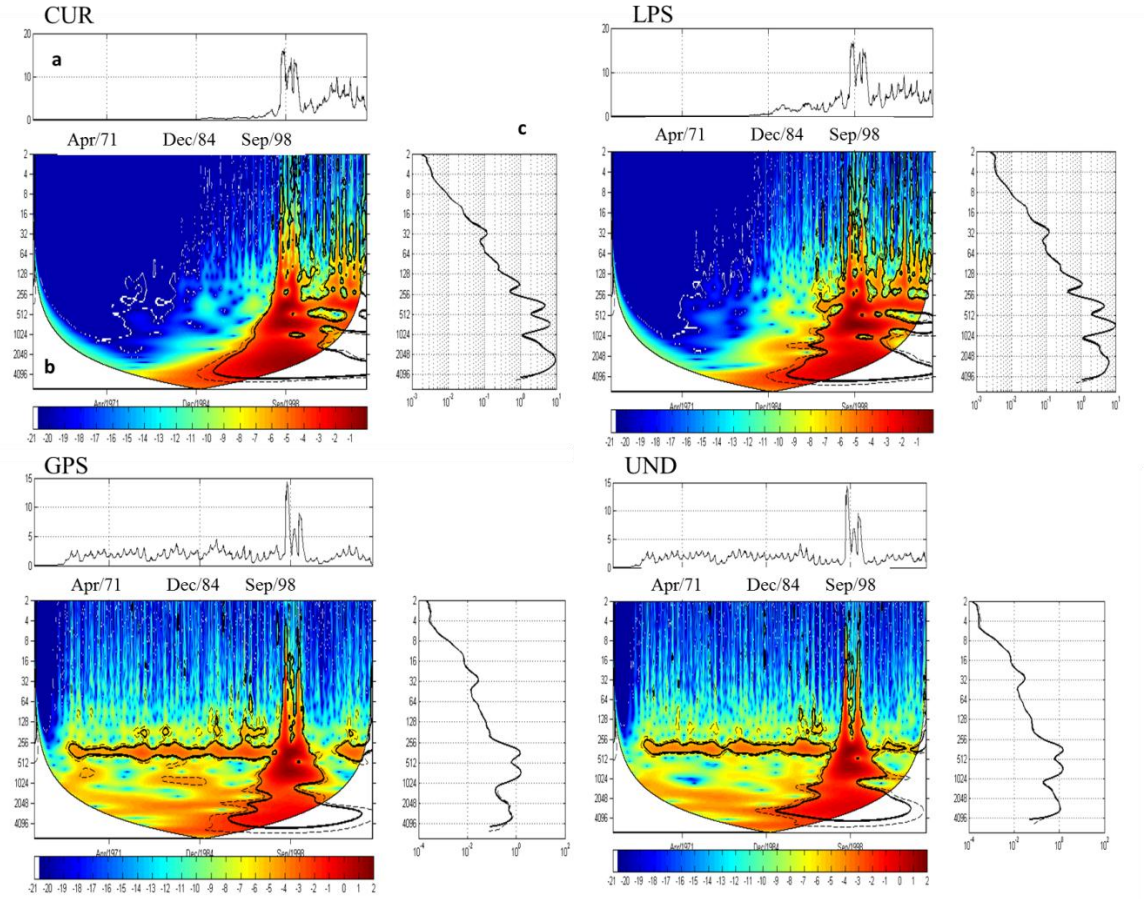

Figure 19. Continuous Wavelet Transform (CWT) spectrum of periodic frequencies of the simulated *P. rubescens* (as µg Chl-a L^{-1}) daily time series (from 1960 to 2010) for each scenarios (CUR=Current scenario, GPS=Global Pressure Scenario; LPS=Local Pressure Scenario; UND=Undisturbed scenario). (a) Daily simulated series of the Chl-a data, (b) continuous wavelet power spectrum showing the periodicity (the black curve

indicates the region without edge effects; solid lines are significant ($p < 0.05$) coherent time–frequency regions) and (c) the wavelet power for each period is normalized by the Global Wavelet Spectrum (GWS) and depicts the periods that explain a high proportion of the temporal variance of the series (y-axis) and the recurrence strength of the periods (x-axis). The continuous wavelet spectrum illustrates how the strength of the periodicities changed over time; colours indicate differing degrees of variance (dark red indicates high intensity; dark blue indicates low intensity).

The Mann-Kendall (MK) test statistic values and the trend slopes were used to analyse the annual evolution of *P. rubescens* (simulated values were monthly aggregated). The resulting slopes were splitted per month and per year in a colour plot (warm colours for positive slopes, cold colours for negative slopes). The significance of the annual trend was also shown per each month over 50 years. Finally the sequential version of the MK test was added to get global trend avoiding the autocorrelation and the seasonal effects in the series. The forward-trend (black line) and backward-trend (grey line) intersection is identified as the change point in the series.

The results (Figure 20) confirmed the increasing trend with a change point around 1975, in both the local impacted scenarios (CUR and LPS). The higher slopes corresponded to the metalimnetic initial growth (Carraro et al., 2012a) during the summer lake stratification (July to September). A more marked summer increasing resulted when the temperature warming was turned off (LPS) confirming an inverse relationship between the persistence of stratification and the *P. rubescens* biomass (Dokulil and Teubner, 2012). Conversely, both the local natural scenarios (GPS and UND) resulted in an overall slightly (not significant) decreasing trend with many change points until 1990 in the sequential test. Only the undisturbed scenarios had two decreasing monthly slopes (July and August) with a significant p-value. In this case the absence of the temperature warming did not favour the algal growth, meaning a potential effect of the global changes (GPS) to enhance the *P. rubescens* biomass, in a hypothetical undisturbed or in-natural-equilibrium ecosystem (UND).

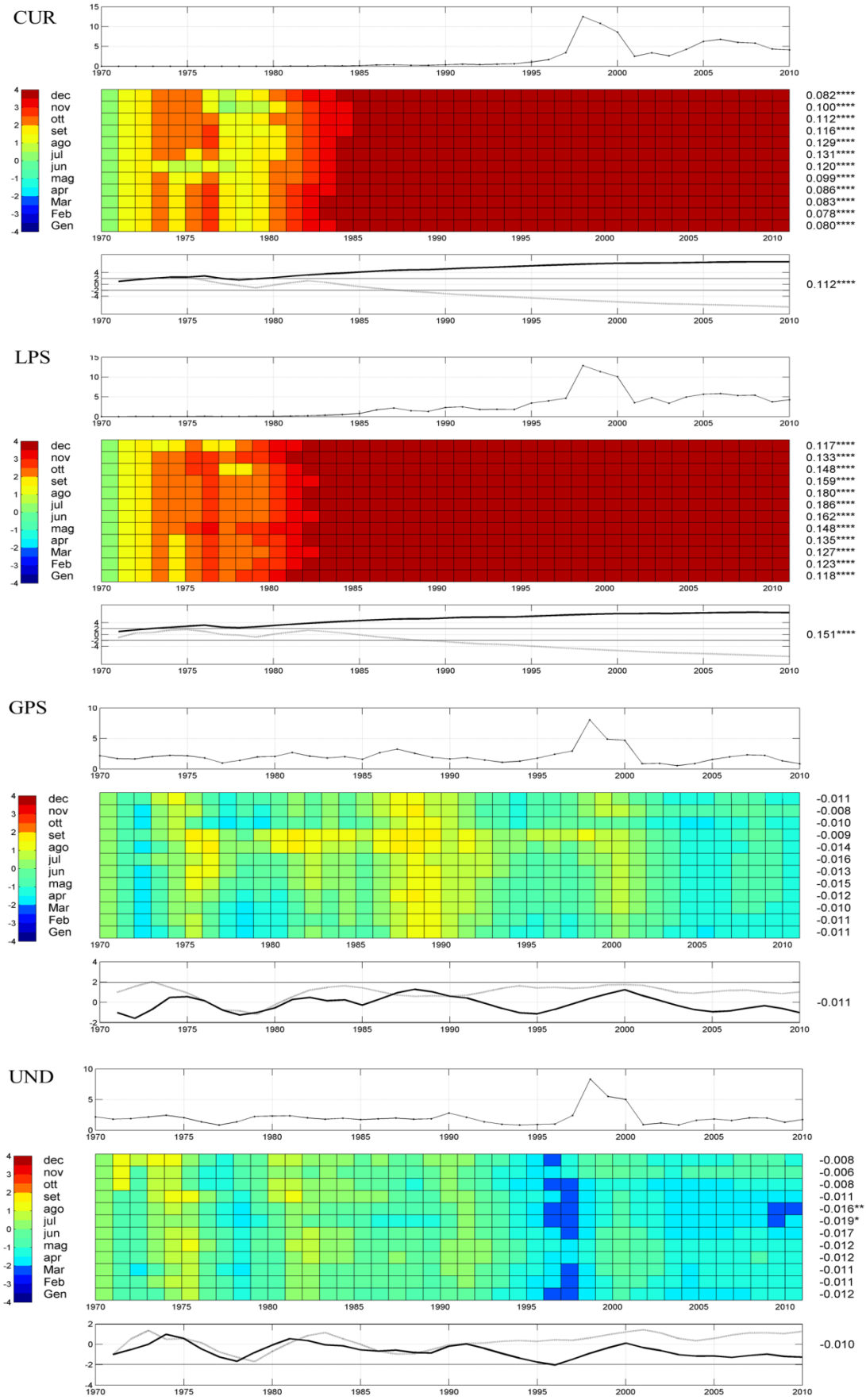
CUR
dec
nov
ott
set
ago
jul
jun
mag
apr
Mar
Feb
Gen
0.082****
0.100****
0.112****
0.116****
0.129****
0.131****
0.120****
0.099****
0.086****
0.083****
0.078****
0.080****
0.112****
LPS
0.117****
0.133****
0.148****
0.159****
0.180****
0.186****
0.162****
0.148****
0.135****
0.127****
0.123****
0.118****
0.151****
GPS
-0.011
-0.008
-0.010
-0.009
-0.014
-0.016
-0.013
-0.015
-0.012
-0.010
-0.011
-0.011
-0.011
UND
-0.008
-0.006
-0.008
-0.011
-0.016**
-0.019*
-0.017
-0.012
-0.012
-0.011
-0.011
-0.012
-0.010

Figure 20. *On the main sub-plots*: Mann–Kendall statistic for simulated *P. rubescens* (as µg Chl-a L^{-1}) monthly time series (from 1960 to 2010) for each scenarios (CUR=Current scenario, GPS=Global Pressure Scenario; LPS=Local Pressure Scenario; UND=Undisturbed scenario). *On the left:* the Sen slope values are associated to the colours-bar. *On the right*: the significance of annual trends (splitted for each month) *p-value=0.05;** p-value =0.01; *** p-value =0.005. *Above*: mean monthly simulated series for simulated *P. rubescens* (as µg Chl-a L^{-1}). *Below*: MKS test with forward-trend (black line) and backward-trend (grey line). Horizontal lines represent critical values [-2;2] corresponding to the 95% confidence interval. The intersection of the test statistic for the forward and the backward lines is identified as the change point in the series.

3.4 Discussion and concluding remarks

The modelling integrated purpose has been achieved through the use of paleolimnological information, a deterministic catchment model (SWAT), an empirical index (MEI) and a statistical method (temperature detrending) in order to produce the forcing for a process-based lake model (DYCD). The use of SWAT simulations allowed to realize a low P-load pressure extending a supposed natural sub-basin to the whole catchment, the so called 'no-human local impact' which mean values were confirmed by MEI and paleolimnological results for the pristine lake condition. However the model cannot reproduce the load from the point sources, thus the urban pollution have been computed out of the model and processed to equilibrate the lake trend concentrations by the Vollenweider equation. The global impact was represented by air temperatures trend computed by SSA and cleaned by the measured time series to obtain a sort of 'no-human global impact'. The different drivers were properly combined into the lake model (DYCD) simulating four different scenarios characterizing a gradient in both locally and globally mediated pressures. This model is adequate to investigate both the daily or seasonally lake fluctuations for a long time and the annual aggregated mean values or a particular monthly mean values. In this preliminary study only the last option was considered to analyse the assessment with available time series and establish an integrated methodology for the study of reference conditions.

Considering the lake after the winter overturn the first macroscale-analysis confirmed the local pressures provided more marked lake responses over long time changes, determining significant differences on the water quality and phytoplankton biomass.

Nitrogen lake concentrations remained relatively constant as the catchment nitrogen loads were inferred by rivers quality data and hardly influenced by wet and dry deposition amount (Balestrini et al., 2000). The phosphorus pattern showed a clear response to the load reduction occurred after sewage plant building leading to a decline of the phytoplankton production in spring, as shown by the abrupt drop in the Chl-a concentrations after the 1990s. No effects on annual phosphorus content were detected isolating the warming temperature driver, but a variability on primary production was revealed and thus a possible response on biogeochemical seasonal behavior could emerge by daily investigation. The lake temperatures underwent a low differentiation. Warmer temperatures occurred removing the local impact (anthropogenic P-load); a possible explanation should refer to a lower lake productivity, a greater light transmission, a weaker thermal stratification during the summer, and thus an anticipated overturn or warmer hypolimnetic waters. The current scenario showed a significant increase in water warming, while the respective scenario with no-global-change (without air temperature warming) resulted generally colder with a flat trend.

Further analysis were performed to investigate *P. rubescens* dynamics under different conditions; a common injection was triggered in 1998, such as the first bloom occurred for all scenarios around 2000 (Legnani et al., 2005). All the analysis confirmed that this species well established finding a favorable condition (Brookes & Carey, 2011) after decades of pollution and ecological shifts (Scheffer et al., 2001). The Wavelet Analysis revealed a chaotic behaviour (no seasonal patterns) since the late 90s when blooms started occurring, in a high trophic state. A regular annual cycle emerged, instead, in a low trophic state. In other words, *P. rubescens* can grow even in a natural environment which is strongly phosphorus limited, meaning that the blooming dynamic is controlled by the lake trophic evolution.

From a methodological point of view, *P. rubescens* was modelled as a cold-stenotherm species and a shade-requiring organism which not tolerates the higher temperatures and irradiances in the epilimnion (Walsby and Schanz, 2002; Dokulil and Teubner, 2000). Thus, the climate warming did not result to favour it directly. On the other hand, it is a slow growth-rate species and longer periods of summer stratification, due to temperature warming, potentially enhance its biovolume in the metalimnetic niche (Dokulil and Teubner, 2012). The Mann-Kendall statistics pointed out a negative relation between *P.*

rubescens biomass and the increasing temperature in a high trophic level and a positive one the undisturbed conditions. The eco-physiological traits which dynamically respond to the equilibrium between the temperature, the length of stratification period and the trophic conditions may explain a different behaviour: the global change effect on *P. rubescens* growth is clear only when the local pressure is absent.

This outcome did not solve the debate about the paradoxical behaviour of *P. rubescens* but certainly progressed a further step in the methodological temptative to separate and weight the causes acting at different spatial scales.

4 Total phosphorus reference conditions for subalpine lakes: a comparison between traditional methods and a process-based lake-basin approach

Submitted to: Environmental Science & Technology.

List of authors: Salerno F., Viviano G., Carraro E., Manfredi E., Lami A., Guyennon N., Copetti D. and Tartari G.

4.1 Motivation

Phosphorus accumulation in aquatic systems often causes a delay in response to reduction of external loading (Søndergaard et al., 2003; Jeppesen et al., 2005). Therefore, the control of nutrient enrichment is crucial to achieve a good ecological status, as mandated by the Water Framework Directive 2000/60/UE (WFD for lake restoration plans).

Lake restoration plans should aim at restoring a set of conditions which are as close as possible to a 'natural' or reference condition, taking into account anthropic modifications that occurred over time. Without this information, it would be difficult to draw any conclusions on the degree of human impact on the current status of the lake or the potential for future changes (Cardoso et al., 2007). However, the definition of an accurate methodology to identify this set of conditions remains a challenge (Kirilova et al., 2010; Battarbee and Bennion, 2011)

Parameters such as nutrient concentration (e.g., phosphorus and nitrogen), chemical and physical properties (e.g., transparency, dissolved oxygen) and biological features (e.g., chlorophyll and other algae pigments) have been utilized for this purpose. However, phosphorus concentration remains the crucial issue in lakes eutrophication. (OECD, 1982; Schindler et al., 2008). This creates a need for accurate targets to guide decisions on remediation strategies (Bennion et al., 2005).

A number of approaches can be used to define phosphorus reference conditions, including time series analysis, inferential models and watershed models (WFD, 2003; Solheim, 2005).

In the absence of long-term monitoring data sets, inferential models as well as watershed models are currently used (http://www.rbm-toolbox.net/rebecca/ index.php). Among the first ones, the most used are: a) the paleolimnological reconstruction of past conditions using established relationships between Diatoms, Chlorophyll and Total Phosphorus (TP); b) the morphoedaphic model exploiting the positive correlation between indicators of total ionic concentration (e.g., conductivity and total alkalinity) and the phosphorus concentration found in water bodies with relatively undisturbed catchments (Battarbee et al., 2005; Cardoso et al., 2007; Bennion and Simpson, 2011).

A wide range of watershed models, also known as land-use models, are currently available. The export coefficient approach is likely to have wider practical applications, particularly in the context of the WFD (European Union, 2000), because it is simple to apply and requires limited amounts of data. On the other hand, the most complex approach is based on dynamics and physical models at basin scale, requiring specific information on weather, soil properties, topography and vegetation as inputs to simulate water movement, nutrient transport, vegetation growth and sediment movement processes (Solheim, 2005). An additional model is required to convert the the phosphorus loading into the mean TP in-lake concentration. The simplest of them is the stochastic model of Vollenweider (OECD, 1982), which is able to predict the mean TP concentration at lake overturn on the basis of the water volume, the hydraulic residence time in the lake, the mean lake depth, combined with phosphorus loading (OECD, 1982; Reynolds, 2006). Another approach could be the implementation of a process-based hydrodynamic and ecological coupled lake model. Differently from a stochastic approach, this kind of models requires more data input, including nutrients loading, meteorological and hydrological forcing (Carraro et al., 2012a).

Coupled basin-lake deterministic models potentially provide dynamic scenarios tracing the loading evolution and the relative lake response (Jørgensen et al., 2010; Mooij et al., 2010; Trolle et al., 2008; Thackeray et al., 2008; Trolle et al., 2011; Carraro et al., 2012a).

In this paper the most used traditional methods were applied to a sample of Italian South-Alpine lakes in order to define the mean phosphorus concentrations in a pristine condition. The same methods are then applied to Lake Pusiano (North Italy) together

with a calibrated deterministic basin-lake modelling tool, aiming to evaluate their performance in the predictive capacity and accuracy of predictions. Moreover the deterministic models are here presented to simulate the lake ecological status under the current and natural phosphorus loads, showing an innovative methodology for the reconstruction of past ecological conditions.

4.2 Data and methods

4.2.1 Inferential models

Palelimnology (Chlorophyll and Diatom inferred TP)

One of the most commonly used paleolimnological methods to determine the past trophic state in lakes one of the most rapid and which requires less expertise is based on the analysis of sedimentary algal pigments through spectrophotometry (Guilizzoni and Lami, 2002; Guilizzoni et al., 2011). This is based on evidence that sedimentary total carotenoid and total chlorophyll derivative concentrations are highly correlated with primary productivity estimates made during the period of sediment deposition (Adams et al. 1978). From these studies, Guilizzoni et al., 2011 developed a model for 28 Italian lakes which has as its endpoint the TP concentration. We applied this model to Lake Pusiano with data collected during a field campaign carried out in spring 2010. Six sediment cores of about 80 cm each were collected at two stations, the first at the main tributary entrance and the second at the lake deepest station. The cores were cut at 1 cm layers and dated by radiometric techniques through to the pre-industrial period (1730 AC). The sedimentation rate was determined using the Constant Rate of Supply (CRS) model for the ^{210}Pb profiles (Appleby, 2001). Geochemical analysis, i.e. water content, organic matter, carbonates, carbon, nitrogen, sulphur, algal pigments, fossil diatom and metals, were carried out on core layers to reconstruct the time series (1730-2010). Spectrophotometrically-measured total chlorophyll derivatives and total carotenoids relative to the content of organic matter in the sediment samples were analyzed according to standard methodologies (Guilizzoni and Lami, 2002).

The error associated to the chlorophyll inferred TP model (hereafter this model is named TP Chloro), was computed over a selected population of 15 subalpine lakes (Figure 21a) from the datataset used by Guilizzoni et al. (2011) to assess their model.

Furthermore, we estimated the TP reference condition for Lake Pusiano inferred by the compostion of the diatomic frustules (hereafter this model is named TP Diato) revealed along the core. A numerical technique, based on the method of weighted averages and corrected by an inverse regression (Anderson, 1993), was chosen to calibrate the values on the pan-European training set EDDI-TP (Battarbee et al. 2001). This method assumes that the species respond to an environmental gradient (e.g. the concentration of TP) according to a Gaussian distribution. Hence a specific taxa require their optimal phosphorus concentration, to be found in the lake with a greater abundance.

Morpho-Edaphic model

Phosphorus export from a catchment in an undisturbed area depends on the natural fertility and solubility of local rocks and soils. Greater solubility of the geological South-stratum also affects the concentrations of the major ions leaching out of the catchment. Measures of total ionic concentrations (e.g. alkalinity or conductivity) are thus often positively correlated with phosphorus concentrations in water bodies with relatively undisturbed catchments (Ryder et al., 1974). Because both alkalinity and conductivity are generally less modified by anthropogenic activity in the catchment and by biological activity in the lake, either one are considered useful as a potential predictor of reference TP concentrations (Ryder et al., 1974; Cardoso et al., 2007). We applied here the Morpho-Edaphic Index (MEI) model (Vighi and Chiaudani, 1985) that predicts reference TP concentrations from the ratio of alkalinity and conductivity in lake water on the lake mean depth (MEI alk = alkalinity meq L^{-1}/mean depth; MEI cond = conductivity μS crn^{-1} 20°C/mean depth). Furthermore we apply the correction proposed by Cardoso observing a correlation between the TP concentration and the altitudes from the sea level (TP MEI alk ; Cardoso et al., 2007).

In order to get information about the error associated with the inferred TP using the MEI, we used data from the LIMNO Database (Tartari et al., 2004) that collects morphometric, physical, chemical, biological and anthropogenic pressures data of 241 natural and artificial lakes with a surface area > 0.2 km^2 distributed over the whole Italian territory. We selected 35 subalpine lakes and reservoirs (Figure 21a) with negligible phosphorus load due to human influence (< 200 inhabitants per square kilometer for lakes and an elevation > 800 m a.s.l. for reservoirs). However, according to Vighi and

Chiaudani 1985, we considered only the water bodies with TP < 20 μg L^{-1}. Water bodies presenting a strongly modified hydrology or a complex catchement hydrmorphology were excluded. Water quality data were available since middle 80s. If for a lake more samples were available, we used the median value. The final selected lakes represent different characteristics in the subalpine Region (Figure 21a) as reported in Table 13 showing a wide range of values both for morphometric and chemical features. The spectrum of trophic conditions ranges from ultraoligotrophic (2 μg L^{-1}) to natural mesotrophic (20 μg L^{-1}).

4.2.2 Watershed models

Export coefficient model

Of the wide range of models available, the export coefficient modelling approach is likely to have wide practical application for the evaluation of the actual TP loads, in particular in the context of the EU WFD, because it is simple to apply and requires little existing data. This kind of approach is used to estimate the historical TP concentrations in the streams by information about the catchment, including land cover and specific export coefficients. It applies a *space for time substitution* (Pickett, 1989). Indeed the assumption is that the current uncontaminated environments export the same quantitative of TP exported in the past pristine conditions. Thus it is heavily based on the accurate determination of TP export coefficients, even if these values are very difficult to estimate as they are affected by land cover type or land use, climate, soil type, topography, local agricultural practices and erosion patterns (Johnes et al., 2007). As such, the coefficients are validated by locally measured data and rarely transferable to other catchments (Solheim, 2005; Ostrofsky and Bradley, 2006). Most of the coefficients were derived by studies sites in North America and Great Britain (Johnes, 1996; Ferrier et al., 1996; Lin, 2004). For subalpine area (North-Italy), only a generic TP export coefficient was calibrated (0.10 kg ha^{-1} y^{-1}) on uncultivated soils, including forested and naked soils, without any geographic and topographic differentiation (Camusso and Tartari, 1988; Barbiero et al., 1991; Marchetti and Verna, 1992). The generic coefficient for Italy may represent an average condition for non-anthropic land cover, as it is within the range reported for different studies worldwide, spanning from 0.05 to 0.30 kg ha^{-1} y^{-1} (Lin, 2004).

The TP load was computed using the generic export coefficient and the watershed surface area, including the potential connected basin for the reservoirs (LOAD TP = TP export coefficient * total watershed area). Finally the loading was converted into the mean lake TP concentration at the lake overturn using the Vollenweider's equation (described below). Hereafter the model was named TP EXP coeff. and the error associated with the TP estimation was computed over the sample of water bodies selected for the MEI index (Figure 21a).

Code	Lake name	Type[a]	Elevation	Lake surface	Total basin surface area[b]	Precipitation	Total inflow	Water renewal time	Volume	Mean Depth	Conductivity	Alkalinity	calcium	pH	TP MEI conductivity*	TP MEI alkalinity *	TP MEI alkalinity **	TP MEI conductivity***	TP MEI alkalinity ***	TP export doefficient model	TP observd
			(m a.s.l.)	(km^2)	(km^2)	(mm)	$m^3 s^{-1}$	(y)	($10^6 m^3$)	(m)	($\mu S\ cm^{-1}$)	($meq\ l^{-1}$)	($mg\ l^{-1}$)		($\mu g\ l^{-1}$)	($\mu g\ l^{-1}$)	($\mu g\ l^{-1}$)	($\mu g\ l^{-1}$)	($\mu g\ l^{-1}$)	($\mu g\ l^{-1}$)	($\mu g\ l^{-1}$)
1	**Agnel**	R	2284	0.2	11	750	0.2	0.4	2	10	117	1.000	18	8.2	15	16	14	13	12	13	**20**
2	**Alpe Gera**	R	2125	1.3	63	880	1.1	2.1	68	54	54	0.470	8	7.4	7	8	9	7	8	11	**9**
3	**Anterselva**	L	1642	0.4	19	900	0.3	0.8	9	21	85	0.590	15		11	11	11	10	10	13	**6**
4	**Arno**	R	1817	0.9	38	1400	1.0	0.7	23	27	17	0.110	3	7.6	7	6	7	6	7	9	**12**
5	**Baitone**	R	2282	0.4	8	1100	0.2	2.1	11	30	15	0.060	4	6.6	6	5	6	6	6	9	**4**
6	**Barbellino II**	R	1869	0.6	22	1650	0.7	0.9	19	34	37	0.010	5	7.5	8	3	4	7	4	8	**5**
7	**Benedetto**	R	1929	0.4	41	1360	1.1	0.2	7	18	14	0.300	4	6.8	7	9	10	7	9	11	**7**
8	**Camplicciolì**	R	1360	0.3	35	1460	1.0	0.3	9	27	13	0.020	2	6.4	6	4	5	6	5	10	**5**
9	**Camposecco**	R	2331	0.4	4	1300	0.1	1.8	6	13	12	0.050	2	6.3	7	6	6	7	7	6	**10**
10	**Chiotas**	R	1978	0.6	257	1350	6.6	0.1	27	47	43	0.290	7	7.6	7	7	8	7	8	12	**8**
11	**Dosazzo**	R	2083	0.4	12	1100	0.2	0.2	2	4	11	0.060	2	7.6	10	9	8	9	9	10	**16**
12	**Gemelli**	R	1953	0.3	7	1730	0.2	1.0	7	21	30	0.250	4	7.9	8	8	9	8	8	7	**4**
13	**Gran Lago**	R	2492	0.2	3	1100	0.1	0.2	0	2	27	0.150	4	7.3	15	14	10	13	12	10	**10**
14	**Malga Bissina**	R	1788	1.4	74	950	1.3	1.4	61	43	14	0.072	2	6.9	5	5	6	5	6	11	**6**
15	**Mergozzo**	L	194	1.8	10	1900	0.4	7.1	83	46	52	0.223	6	6.8	8	6	9	7	7	3	**5**
16	**Mezzola**	L	199	4.9	723	1200	16.5	0.3	149	31	151	0.690	21	7.7	12	10	13	10	10	12	**13**
17	**Molveno**	L	823	3.3	74	1000	1.4	3.6	161	50	79	0.710	12	7.3	8	9	11	8	9	8	**10**
18	**Monte Spluga**	R	1902	1.7	27	1200	0.6	1.7	33	19	29	0.230	4	6.9	8	8	9	8	9	8	**8**
19	**Orta**	L	290	17.8	119	1900	4.3	9.6	1300	73	120	0.018	12	5.5	9	3	5	8	4	3	**5**
20	**Palu**	L	1925	0.2	3	1000	0.1	0.9	2	9	36	0.254	5	7.4	11	11	10	10	10	9	**5**
21	**Piastra**	R	957	0.4	88	1350	2.2	0.2	12	32	50	0.350	8	7.9	8	8	10	8	8	11	**8**
22	**Resia**	L	1498	6.5	311	900	5.3	0.7	112	17	97	0.400	11	7.1	12	10	10	11	10	14	**12**
23	**Salarno**	R	2070	0.4	33	1170	0.7	0.5	11	27	12	0.030	2	6.7	6	4	5	6	6	11	**10**
24	**San Giacomo di Fraele**	R	1949	2.2	275	850	4.4	0.5	64	29	125	0.550	18	7.6	11	10	10	10	9	15	**18**
25	**Scais**	R	1495	0.2	53	2000	2.0	0.1	9	41	47	0.590	4	7.9	8	9	10	7	9	8	**12**
26	**Vacca**	R	2359	0.2	2	950	0.0	2.7	2	11	10	0.001	1	5.5	7	2	3	7	4	6	**3**
27	**Val di Lei**	R	1930	4.2	48	700	0.6	9.9	197	47	54	0.430	14	7.6	8	8	9	7	8	7	**8**
28	**Venina**	R	1824	0.4	20	1600	0.6	0.6	11	31	36	0.230	4	7.2	8	7	8	7	8	9	**3**
	Median		**1914**	**0**	**34**	**1185**	**0.7**	**0.8**	**12**	**28**	**37**	**0.24**	**4**	**7.3**	**8**	**8**	**9**	**7**	**8**	**9**	**8**
	Max		**2492**	**18**	**723**	**2000**	**17**	**10**	**1300**	**73**	**151**	**1.00**	**21**	**8.2**	**15**	**16**	**14**	**13**	**12**	**15**	**20**
	Min		**194**	**0.2**	**2**	**700**	**0.03**	**0.1**	**0.5**	**2**	**10**	**0.001**	**1**	**5.5**	**5**	**2**	**3**	**5**	**4**	**3**	**3**
29	**Braies**	L	1489	0.3	29.7	770	0.6	0.3	5	17	204	2.430	25	7.8	15	17	16	13	13	14	**3**
30	**Brasimone**	R	1496	0.5	13.4	1130	0.2	1.0	6	12	200	1.810	33	7.8	17	17	16	14	13	11	**13**
31	**Caldaro**	L	214	1.2	49.1	740	0.9	0.2	6	5	443	5.200	64		28	31	27	22	19	11	**10**
32	**Cavazzo**	L	195	1.3	20.1	2250	0.4	1.8	21	17	735	2.500	131	8.1	22	17	19	18	13	10	**4**
33	**Morasco**	R	1816	0.6	49.2	1290	0.9	0.6	18	31	149	1.130	26	7.7	12	12	12	10	10	13	**2**
34	**Sauris**	R	980	1.6	140.9	1630	2.7	0.9	79	49	502	2.200	86	7.9	15	12	14	12	11	12	**5**
35	**Tovel**	L	1178	0.4	40.7	1050	0.8	0.4	9	24	199	2.300	32	8.0	14	15	16	12	12	14	**5**
	Median		**1178**	**1**	**40.7**	**1130**	**0.8**	**0.6**	**9**	**17**	**204**	**2.30**	**33**	**7.9**	**15**	**17**	**16**	**13**	**13**	**12**	**5**
	Max		**1816**	**2**	**141**	**2250**	**3**	**2**	**79**	**49**	**735**	**5.20**	**131**	**8.1**	**28**	**31**	**27**	**22**	**19**	**14**	**13**
	Min		**195**	**0.3**	**13**	**740**	**0.19**	**0.2**	**5.3**	**5**	**149**	**1.13**	**25**	**7.7**	**12**	**12**	**12**	**10**	**10**	**10**	**2**

[a] R = Reservoir, L = Lake [b] including connected basin for the reservoirs * Vighi and Chiaudani, 1985 **Cardoso et al., 2007 *** This study

Table 13. Limnological database (LIMNO) was used to estimate the TP reference conditions for a selection of lakes using the Morpho-Edaphic and the Export Coefficient model. Lakes were divided into two groups based on alkalinity (refer to Figure 22).

Hydrological transport models

Hydrological transport models, simulating the TP reference conditions, add to the *space for time substitution,* already applied in the export coefficient modelling, a *space for space substitution.* The presence of current uncontaminated or less contaminated area inside or close to the watershed can be used to train the model. Subsequently, the parameters calibrated in this condition are applied to the whole watershed area, thus simulating a sort of pristine scenario. This kind of parameters 'spreading' is allowed if the general climatic, topographic and soil conditions are similar in the watershed and the land cover ot the reference site is verified to be the one that hypothetically characterized the watershed in natural or pristine conditions.

The SWAT model (see Materials and Methods) was choose to implement the metodology described. It enables to quantify the impact of alternative input data such as changes in land use on water quality and quantity (Tong and Chen, 2002; Mango et al., 2011), thus allowing the *space for space substitution* to simulate a pristine scenario for Pusiano watershed.

SWAT calibration and validation was performed in the sub-basin of reference (the Gajum sub-basin, see Fig. 21 b) and then for the entire watershed (refer to Materials and Methods).

TP was trained through the use of a continuous high-frequency (sub-hourly) monitoring system, thus ensuring an accurate characterization of transport processes (Jordan et al., 2007; Horsburgh et al., 2010). The turbidity was chosen as predictor to measure indirectly the presence of suspended solids and thereby of phosphorus that is strictly associated at the particulate form (Grayson et al., 1996; Stubblefield et al., 2007). In the sub-basin of reference a turbidity probe (April 2010- June 2011) was previously calibrated in laboratory with a reference formazin suspension (APAT e IRSA-CNR, 2003) and then installed at the sub-basin closing point. An hourly sampling was simultaneously conducted during three precipitation events characterized by a different intensity (31 May, 1 June, 8-9 June, 17-18 September 2011) to evaluate the turbidity-TP regression model (Table 2 and Figure 5 in Materials and Methods). The regression was used to convert the turbidity data into the corresponding TP river concentrations. Finally data were aggregated at daily scale to be validate SWAT phosphorus transport simulated output.

4.2.3 Input-output phosphorus lake models

Vollenweider's model

Model predictions of annual mean TP concentrations in rivers can be converted into the mean TP concentration at overturn in-lake estimation using the Vollenweider empirical equation (OECD, 1982) and adopting the correction proposed for Alpine lakes. The model (Table 14) predicts the mean phosphorus concentration in-lake (TP_{lake}) based on the lake volume (VOL), surface (SUR), mean depth (Z), hydraulicresidence time (T) and the phosphorus total loading (LOAD TP). The hydraulic residence time is the most difficult parameter to compute, as the estimation of the inflow volume is often too inacurate. For this reason, the inflow discharges (Q) were estimated for all the lakes on the basis on the cumulated mean annual precipitation (PREC), the total watershed area (BASIN), including potential connected basins for the reservoirs, and the precipitation-discharge rate (K=0.6) that was calibrated for Pusiano watershed (Salerno and Tartari, 2009).

Parameter	**Equation**
Discharge (Q)	$\mathrm{Q} = \mathrm{PREC} * \mathrm{BASIN} * \mathrm{K}$
Hydraulic residence time (T)	$T = \frac{\mathrm{VOL}}{\mathrm{Q}}$
Mean depth (Z)	$Z = \frac{\mathrm{VOL}}{\mathrm{SUR}}$
Phosphorus concentration prediction (TP_{lake})	$If\ Z \geq 15\ TP_{lake} = 1.58 * \left[\left(\frac{\mathrm{LOAD\_TP}}{\mathrm{Q}}\right) * \left(\frac{1}{1+\sqrt{T}}\right)\right]^{0.83}$
	$If\ Z < 15\ TP_{lake} = 1.02 * \left[\left(\frac{\mathrm{LOAD\_TP}}{\mathrm{Q}}\right) * \left(\frac{1}{1+\sqrt{T}}\right)\right]^{0.88}$

Table 14. Vollenweider's model

Hydrodynamic-ecological coupled model

The DYCD model (see Materials and Methods), hereafter named DYNAMIC-LAKE, was implemented for Lake Pusiano to simulate both pristine and current conditions. The model set up was from Carraro et al. (2012b), where the human global and local impacts (as temperature warming and phosphorus pollution, respectively) were differentiated over 50 years of daily simulated scenarios (1960-2010). Four scenarios characterized by a different degree of human impact were compared (refer to Chapter 3). The most impacted scenarios (CUR, current) included both the trend of air temperature and phos-

phorus catchment loading (as real forcing), the less impacted scenarios (UND, undisturbed) was turn off by them, while the other two intermediate scenarios were setup to include the impact of only the nutrient load (LPS, local pressure) and of the temperature increase (GPS, global pressure).

In this study Lake Pusiano ecological processes were simulated in pristine and current external loading, using the CUR (hereafter named CURRRENT-sim) and the GPS (hereafter named REFERENCE-sim) set up, respectively. Simulations were run between 1998 and 2010.

The P-load used to force the REFERENCE-sim was the SWAT simulated output for the pristine phosphorus transport. The release of phosphorus was explicitly simulated (Table 3, Materials and Methods). The critical values for S_g were set equal to 0.004 and 0.01 g m^{-2} day^{-1} for the REFERENCE-sim CURRRENT-sim respectively, to account for a mesotrophic and eutrophic condition, while K_{DOS} was set equal to 0.1 mgO_2 L^{-1} in both of them (Trolle et al., 2009). The phytoplankton succession was simulated dividing the total chlorophyll (TChl-a) between *P. rubescens* and another competitor group (Carraro et al., 2012b), focusing on the recent *P. rubescens* dominance on the phytoplankton assemblage (Vuillermoz et al., 2006). This set allowed to get insights on the potential evolution of the cyanobacterial species in response to a hypothetical lake restoration to pristione phosphorus loading (Posch et al., 2012).

4.2.4 Statistical analysis

The predictive capability of the models has been tested by the coefficient of correlation (r) after the analysis of the distribution of residuals by Q-Q plot model. The cross-validation (r_{cv}) of the models was performed by means of the leave-one-out resampling technique with the package SMIR of the R Project (Aitkin et al., 2009).

The Root Mean Squared Error (RMSE) is one of the commonly used error index statistics. It represents the square root of the Mean Squared Error (MSE) and quantifies the model performance of each variable (refer to Materials and Methods). The Coefficient of Variation of the RMSE CV(RMSE) was obtained mormalizing the RMSE to the average of the observed values, thus it is similar to the standard deviation (sd).

When the population of data came from an unique case study, the Percent BIAS (PBIAS) was chosen to compare each simulated (sim) to the relative observed value (obs), by their difference (sim-obs/obs). In case of a multi-errors estimation, the total error was computed as the root mean squared of all the errors (Salerno et al., 2012).

The Principal Components Analysis (PCA) was performed to define different classes (Wold et al., 1987) of lakes, based on the alkalinity level. The test was performed using 'prcomp' function in R Project and plotting the results by the 'biplot' function.

4.3 Study area

A population of 35 subalpine lakes (Figure 21a) was selected by the LIMNO database and the datased used in Guilizzoni et al. (2011) among more than 200 Italian lakes of glacial origin, including large, deep and small, shallow water bodies or reservoirs, mostly located between the Po River Plain and the Alps.

The methodological purpose was assessed on Lake Pusiano watershed (Figure 21b). The climate here is defined as humid mesothermic without dry season (Class Cf, Köppen, 1936). The precipitation is concentrated in the spring and autumn months and tends to progressively increase, in a range from 1500 mm to 2000 mm per year, from south to north along the watershed. The soils of Pusiano basin belong to the following 4 groups in accordance to the WRB1998 classification (FAO, ISRIC and ISSS, 1998): *Leptosols*, *Regosols*, *Cambisols*, *Phaeozems.* All these soils are characterized by a temperate climate and by a geological Southstrate composed of different calcareous forms, associated with glacial formations and that have developed on mountainsides of varying slope gradients. The soil erodibility (*K*) factor, for the USLE equation, was computed following the criteria established by Wischmeier and Smith (1978). The area chosen as the reference for the natural TP concentrations is a sub-basin of 5.5 km^2 called hereafter Gajum sub-basin.

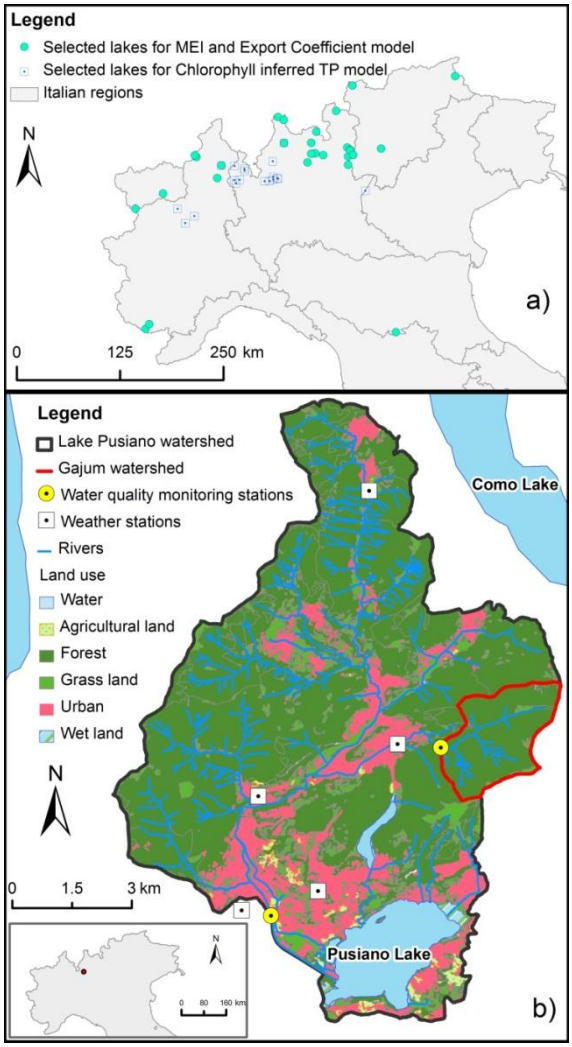

Figure 21. a) Map showing the location of the selected lakes used for MEI, Export Coefficient model and chlorophyll inferred TP model (Guilizzoni et al., 2011); b) Map of Lake Pusiano watershed for land use, meteorological and water quality monitoring stations. The sub-basin of reference (Gajum) used to calibrate the natural P-loading is marked (red line).

4.4 Results

4.4.1 Traditional methods for subalpine lakes

The correlation between MEI index and the observed TP values was tested, considering the monitored data by the 35 selected lakes. Since the correlation was not significant, lakes typology were analysed by a PCA exploring TP, alkalinity, calcium and pH measurements. Two distinct groups of data emerged: the first (lake codes 1-28) was called Low-Medium Alkalinity (LM-A) and based on alkalinity ≤ 1 (median = 0.25 meq L^{-1}), lower pH (median= 7.3), Ca ≤ 21 mg L^{-1} (median = 4 mg L^{-1}) and 3<TP < 20 µg L^{-1}

(median = 8 g L^{-1}); the second (lake codes 29-35) was called High Alkalinity (H-A) and based on alkalinity > 1 (median = 2.3 meq L^{-1}), higher pH (median= 7.9), Ca ≥ 25 mg L^{-1} (median = 33 mg L^{-1}) and 10<TP < 13 µg L^{-1} (median = 5 g L^{-1}).

The LM-A group was associated to a general TP<20 µg L^{-1} condition while the HA group was associated to high alkalinity, calcium and pH, but ultra-oligotrophy and the oligotrophy (median=5 g L^{-1}) lakes in opposition to the relation found in Vighi and Chiaudani (1985). A similar distinction was found using conductivity instead alkalinity values (not show here). The PCA explained the 85% of the variance by the first two components. In Figure 22 the features of lakes in functio of the two principal components (the labels represent the lake codes) are shown. Based on the results obtained from the PCA, the correlation MEI/TP was separately tested for the two groups finding a significant regression only for the LM-A.

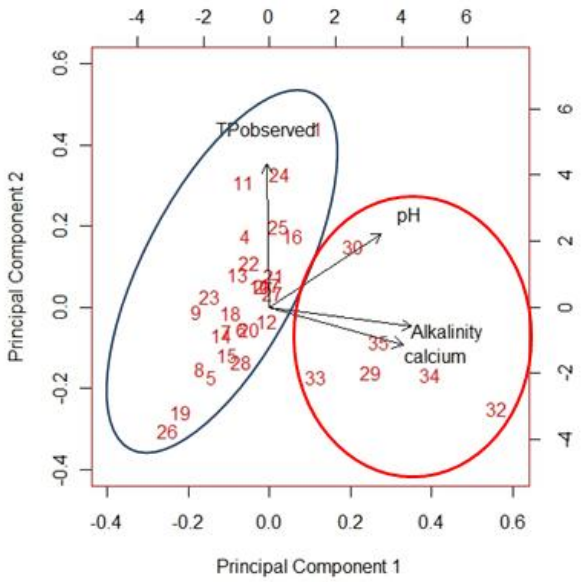

Figure 22. PCA Biplot for 35 selected lakes considering the TP, alkalinity, calcium and pH measured values. The red line includes the High Alkalinity (H-A) and the blue line includes the Low-Medium Alkalinity (LM-A) group.

The relationships between TP observed concentrations and the estimates gained with traditional prediction models are reported in Figure 23 for TP MEI cond., TP MEI alk., TP EXP coeff. and TP Chloro. Both the MEI models (Figure 23 a,b) explain about 50% of the variance in TP (r = 0.58 p-value<0.01; r = 0.55 p-value<0.01, respectively). The cross-validation confirms the statistical significance of the performance (r_{cv} = 0.49

p<0.05 and r_{cv} = 0.45 p-value<0.05, respectively). The RMSE shows a mean error associated to each prediction for both model of about ±4 µg L^{-1} that corresponds to CV-RMSE of about ±40%. The regression equations found for subalpine lakes are:

$$\text{Log [P]} = 1.23 + 0.16 \text{ Log MEI alk} \qquad \text{(Equation 16)}$$

$$\text{Log[P]} = 0.83 + 0.27 \text{ Log MEI cond} \qquad \text{(Equation 17)}$$

The TP MEI alk. corrected for lake altitudes (results are not shown here) by Cardoso et al. (2007) did not enhance the performance of the normal TP MEI alk., we used here (r = 0.51, r_{cv} = 0.33, RMSE = ±4 µg L^{-1},CV-RMSE)= ±44%).

The TP EXP coeff. model (Figure 23 c) shows a slightly higher predictivity (r = 0.65 and r_{cv} = 0.52), but with high error (RMSE = ±4 µg L^{-1}, CV-RMSE = ±41%). Lastly, the TP Chloro model (Figure 23 d) presents a more significant correlation (r = 0.84 and r_{cv} = 0.75) due to a wider range of TP values, but the highest error (RMSE = ±8 µg L^{-1}, CV-RMSE = ±42%).

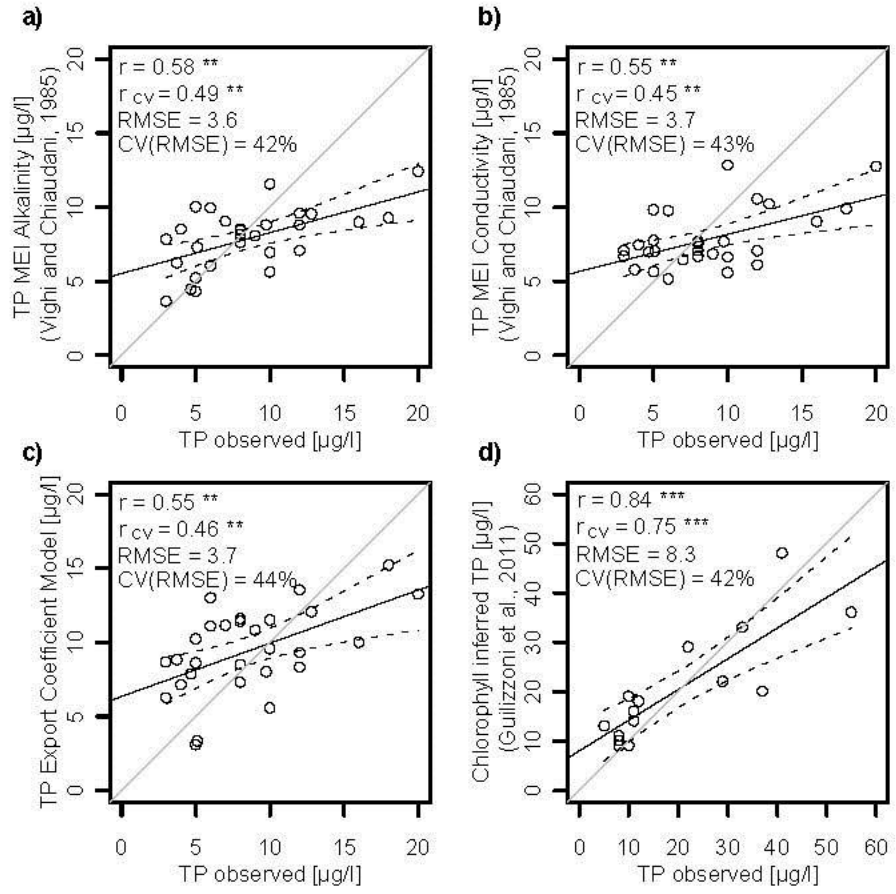

Figure 23. Analysis of the correlation coefficient, the significance and the associated error for the traditional models used to predict the phosphorus (as mean TP concentration) reference condition for subalpine lakes. Morpho-Edaphic model using as predictor a) alkalinity (TP MEI alk) and b) conductivity (TP MEI cond); c) Export coefficient model (TP EXP coeff) d) Chlorophyll inferred TP model (TP Chloro) tested over 15 subalpine selected lakes from Guilizzoni et al. (2011) dataset. For each correlation, the coefficient (r) is significant at p-value<0.001 '***'; p-value <0.01 '**'; p-value<0.05 '*'; p-value <0.1 '.' (2-tailed). Confidence level is at 95%.

4.4.2 Traditional methods for Lake Pusiano

The phosphorus reference conditions (as mean TP concentration during winter overturn) for Lake Pusiano was estimated by: a) TP Chloro (TP = 10 µg P L^{-1} RMSE= ± 2 µg P L^{-1}); b) TP Diato (TP = 10 µg P L^{-1} RMSE= 2 µg P L^{-1}); c) TP MEI alk (TP = 14 µg L^{-1} RMSE = 4 µg P L^{-1}); d) TP MEI cond (TP = 15 µg L^{-1} RMSE = 4 µg P L^{-1}); f) TP EXP coeff (TP = 6 µg L^{-1} RMSE = 3 µg P L^{-1}).

The TP Chloro and Diato inferred by the paleolimnological analysis of Lake Pusiano sediment core, resulted quite constant over 250 years (1730-1968) before the increasing in the 70s, due to the demographic growth.

Both the TP MEI models were compared to the results by equations proposed in Vighi and Chiaudani (1985): TP=19 µg L^{-1} (±3 µg P L^{-1}) for TP MEI alk and TP=18 µg P L^{-1} (±3 µg P L^{-1}) for TP MEI cond. Also the model proposed by Cardoso et al. (2007) was tested for Lake Pusiano: TP= 20 µg P L^{-1} (±4 µg P L^{-1}) for TP MEI alk.

TP EXP coeff model was estimated over 1578 mm of precipitation (as cumulated annual average from 1998 to 2010) confirming the hydraulic residence time (0.8 y^{-1}) evaluated for Lake Pusiano (Vuillermoz et al., 2006).

4.4.3 Hydrological transport and input-output TP lake models for Lake Pusiano

The coefficient (Figure 24) for the regression between hourly concentrations of TP and turbidity values, measured at the outlet of Gajum sub-basin, was significant (r=0.94 p-value <0.001; r_{cv} = 0.93; RMSE= ± 4 µg P L^{-1}; CV-RMSE=±40%)

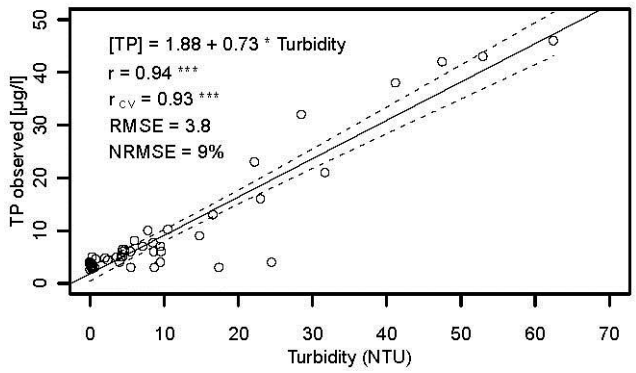

Figure 24. a) Regression analysis between the turbidity and the corresponding hourly TP concentration, measured at the outlet of Gajum sub-basin ('***'p-value<0.001).

The TP-turbidity linear model was applied to the continuous series of turbidity measured by the probe, for the estimation of a continuous series of TP concentrations. The series was used to compute the TP load by measured data of discharge (PBIAS = 24%) and, after an aggregation into daily data, to calibrate the SWAT simulation of TP load (PBIAS= 6%). The overall error was computed as root mean square of the two PBIASs (RMSE=25%). The SWAT calibrated parameters were spread to the whole watershed for the period 1998-2010 when continuous series of daily meteorological data were available. The annual mean P-load to Lake Pusiano resulted 1.1 t P y^{-1} (Figure 25a), corresponding to, after applying both the Vollenweider's model and the DYCD model, a mean in-lake concentration (as µg TP L^{-1} during winter overturn) of 8 and 11 µg P L^{-1} respectively (Figure 25 b).

The cumulated annual precipitation and the simulated P-load were compared over the period of study (1998-2010). The P-load was likely dependent on rainfall as the correspondence of peaks revealed (Figure 5a). The maximum load (2.5 tP y^{-1}) indeed, corresponded to the greater cumulated precipitation (2310 mm) and thus higher soil erosion in 2002. The lower load (0.2 tP y^{-1}) corresponded to the minimum rainfall (994 mm).

The TP lake concentrations were converted by the P-load, through Vollenweider's model and the DYCD model (Figure 25b). The daily outputs of TP from the REFERENCE-Sim were aggregated into monthly mean values and February was chosen as representative of the lake winter overturn. The results underlined a certain variability for the TP in-lake concentrations, values ranging from 8 to 17 µg P L^{-1} (sd=2 µg L^{-1}, CV-sd=21%).

The estimation by the Vollenweider model was characterized by a narrower range of values ranging from 5 to 13 µg P L^{-1} but higher variability (sd=4 µg L^{-1}, CV-sd=43%).

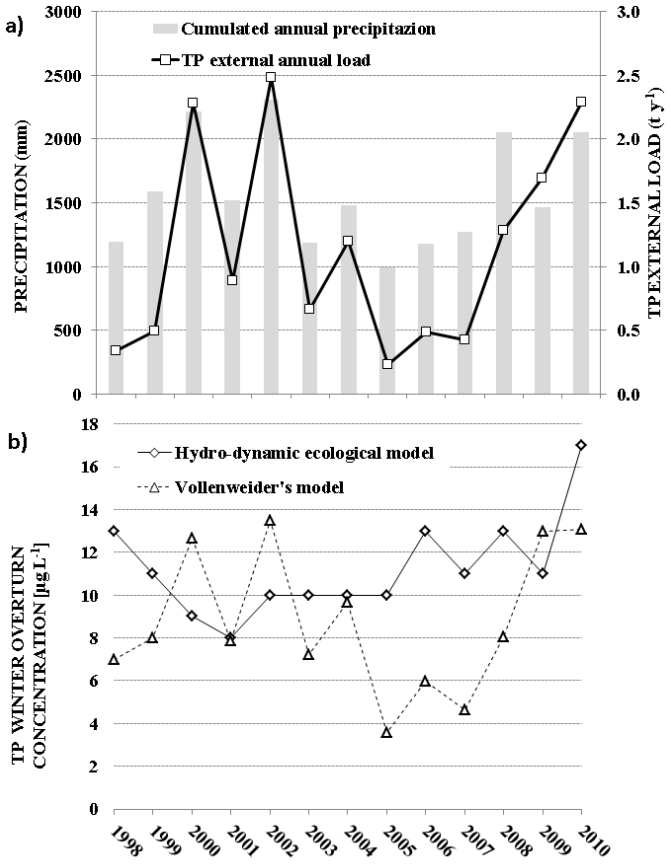

Figure 25. Process-based and dynamic lake-basin modelling (1998-2010) results, as annual aggregated values. a) Cumulated annual rainfall (measured data) and TP external loading (SWAT simulation); b) TP lake concentrations at winter overturn estimated with the Vollenweider's model and simulated by DYCD (REFERENCE-Sim).

4.5 Discussion

4.5.1 Comparison of traditional methods

The TP MEI models evaluated for subalpine lakes (Eq. 16 and 17) overestimated the lakes with TP < 10 µg P L^{-1} and underestimate the oligo-mesotrophic lakes. Also the equations developed by Vighi and Chiaudani (1985) for European lakes (not shown here) had a similar bias. In general the TP MEI alk was more robust, but it has to be considered statistically valid only for the low-alkalinity (LM-A) group of lakes. Also the correction proposed by Cardoso for the altitude was tested without gaining any improvement in performance.

The predictive capability of TP EXP coeff model was assessed applying the same export coefficient to all the selected lakes, resulting that the hydro-morphological features are more determinant than external loading in evaluating a reference condition for phosphorus in-lake. In general, the statistical performances of TP EXP coeff. and TP MEI were similar.

The development of a comprehensive model based on all the hydro-morpho-edaphic features could result in an increased predictive capability. Indeed, TP MEI model cannot take into account the global P-load reaching a lake, inferring the TP lake concentration by conductivity and alkalinity proxy values. The TP amount from the inflows is represented in the TP EXP coeff model as a morphometric relation (catchment surface and water renewal time). Some authors (e.g. Reavie et al., 2002; Bennion et al., 2005) have already demonstrated that watershed models provided accurate predictions.

The TP Chloro model was based on the inference by the paleolimnology surveys, thus comprising also currently anthropic environments and a wider range of TP concentrations. However, the error associated to estimations of TP reference conditions was high (twice than the other methods), making it inapplicable at the moment.

4.5.2 Uncertainty and accuracy of predictions

The phosphorus reference conditions for Lake Pusiano was evaluated applying traditional methods and a coupled lake-basin modelling approach (Figure 26). The error bars represent the RMSE associated at each method. The hydrological transport, the input-output phosphorus lake and the TP Diato models showed an acceptable performance (Batterbee et al. 2000). TP EXP coeff and TP MEI models resulted not adequate for Lake Pusiano (±4 µg P L^{-1}). The paleolimnological methodology resulted a reliable tool for defining lakes reference conditions (Guilizzoni et al. 1992; Battarbee et al. 2005), even though it strongly depends on the kind of inferential relation. The TP-Diatoms relation showed an acceptable performance comparing to the others.

The process-based and dynamic lake-basin approach here proposed, showed a low error too. The hydrological transport model was coupled both to Vollenweider's and the DYNAMIC-LAKE models, to compare the resultant phosphorus reference conditions in-lake, as mean TP concentration in winter overturn (8 µg P L^{-1} and 11 µg P L^{-1}, respectively). The outcome by the paleolimnological analysis was 11 µg P L^{-1}.

Moreover, the integrated modelling approach offered the opportunity to investigate the in-lake ecological response in a reconstructed natural condition, at daily scale.

In general, Lake Pusiano resulted in a oligo-mesotrophic state; only the TP EXP coeff model ascribed the lake in a full oligotrophy, while the TP MEI models, Vighi and Chiaudani (1985) and Cardoso et al. (2007) versions, placed the lake in a full mesotrophy.

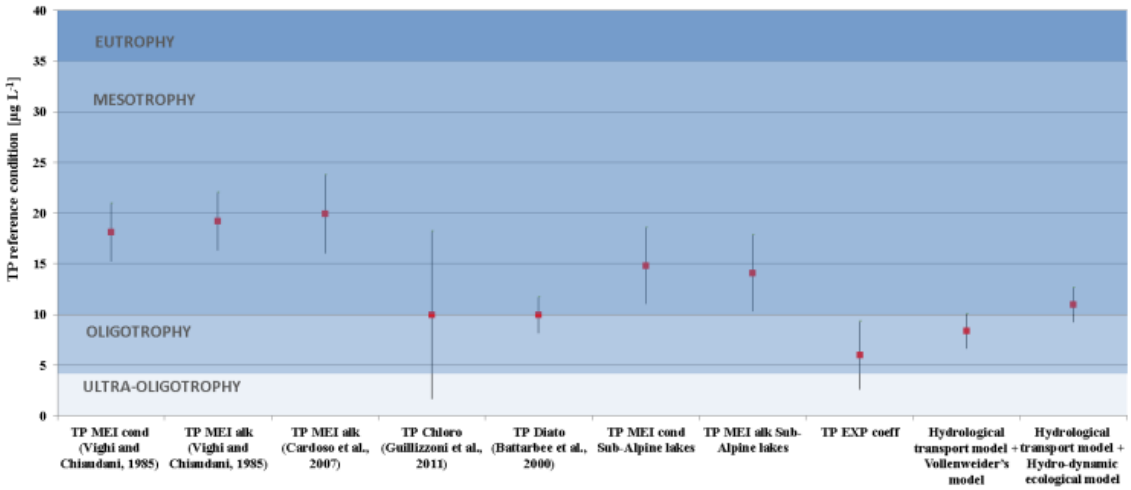

Figure 26. Phosphorus reference conditions for Lake Pusiano as evaluated by traditional methods and the process-based and dynamic lake-basin approach. The error bars represents the RMSE associated at each predictive model. The trophic classification was based only on phosphorus concentration (OECD, 1982).

4.5.3 Potential of the process-based and dynamic lake-basin approach

The lake TP dropped (TP<6 µg P L^{-1}) concurrently with low (TP < 500 kg y^{-1}) external loads (Figure 25), suggesting a strong dependency of Vollenweider equation on the external P-loading. It is reasonable considering that the Vollenweider model does not include an explicit representation of the lake cycling (OECD, 1982). The REFERENCE-Sim output has a lower variability, because less dependent from the external loading due to the modulator action of the lake biogeochemical cycle, as simulated in the CAEDYM model (Trolle et al., 2008).

One of the advantages in using complex ecological models is the opportunity to investigate the outcome as a balance of the physical, chemical and biological processes. Daily simulated output for 12 years (1998-2010) of transparency (as Secchi Disk), total phosphorus (as weighted average of TP concentrations in the first 20 m) and total chlorophyll (as weighted average of TChl-a concentrations in the first 10 m) were chosen as

the most relevant indicator of trophic state. Also *P. rubescens* concentrations (as weighted average of Chl-a concentrations in the first 10 m) were drawn to complete the trend of the lake ecological status. The pristine REFERENCE-sim (grey line) and the CURRENT-sim (black line) scenarios were compared to evaluate the difference in the ecological status, at a macro-scale (Figure 27). Transparency (as Secchi Disk, SD) was derived from the light extinction coefficient (η) simulated by DYCD using the empirical relationship: $SD=1.7/\eta$ (Wetzel, 2001). The oxygen content as well as the release of orthophosphate from the sediments were analysed as monthly mean dissolved concentrations (mg DO L^{-1} and mg $P\text{-}PO_4$ L^{-1}, respectively) at the lake bottom (25 m). The difference of concentrations for DO and $P\text{-}PO_4$ (computed a REFERENCE-sim – CURRENT-sim) is also put on the figure. The Trophic State Index (TSI, Carlson, 1977) was used to provide a numerical indicator of the trophic status for Lake Pusiano, including all the daily values of TP (as weighted average in the first 20 m), TChl-a (as weighted average in the first 10 m) and the transparency (as Secchi Disk), then aggregated in mean annual values. The index was modified (TSI*) to be adapted to Italian lakes and ranked by trophic thresholds (De Bernardi et al., 1985). Bars on the plots are for standard deviation (sd) referring to the mean average over daily values for each year from 1998 to 2010. Furthermore the monthly average for TP concentrations during the lake overturn (February) was reported, according to the OECD (1982) trophic thresholds for phosphorus (Figure 28).

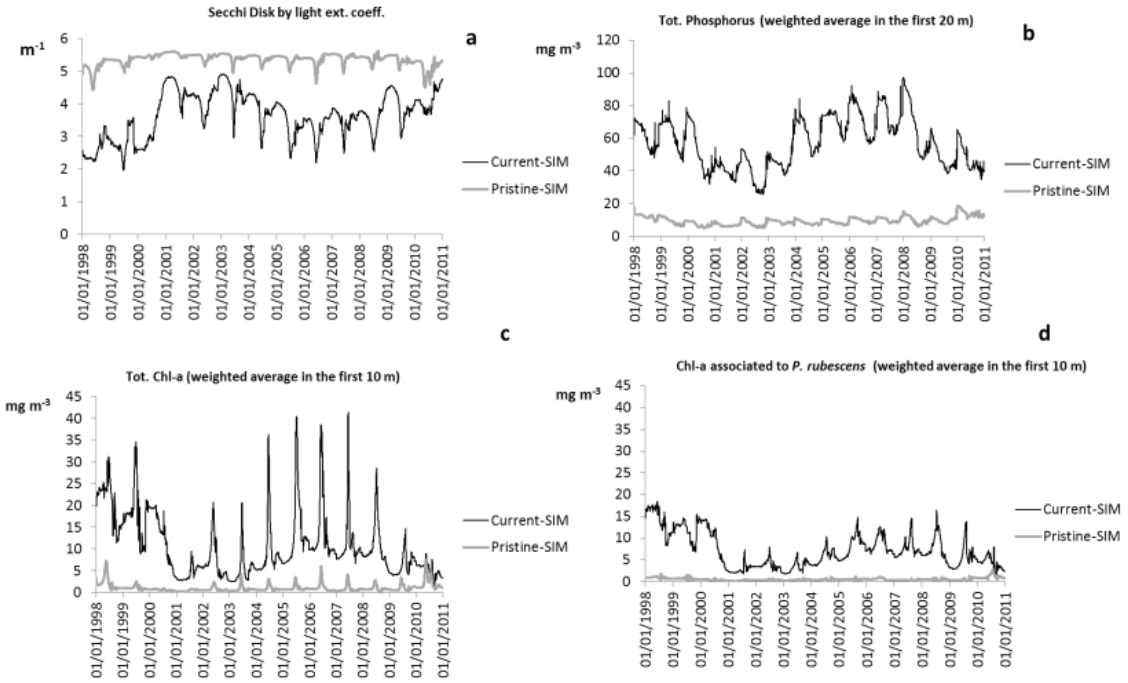

Figure 27. Daily time series of transparency (SD), TP, TChl-a and *P. rubescens* Chl-a as simulated in the pristine (REFERENCE-sim) and current (CURRENT-sim) scenarios.

The lake trasparency increased from an average of 3.6 m in the CURRENT-sim to an average of 5.3 in the REFERENCE-sim, mainly due to a lower primary production. Indeed the lake productivity was lower under the pristine loading: TChl-a concentrations annual average passed from 11 µg Chl-a L^{-1} (CURRENT-sim) to 1.1 Chl-a µg L^{-1} (REFERENCE-sim). The pristine simulation also showed a lower variability, depending on the equilibrium with the natural constant P-load. Indeed the human-induced phosphorus external loads produced a mean annual TP in-lake concentration in the CURRENT-sim (57 µg P L^{-1}) sixfold higher than the REFERENCE-sim (9 µg P L^{-1}). *P. rubescens* simulted concentrations (as µg Chl-a L^{-1}) contributed with 60% of total production in the REFERENCE-sim and 70% in the CURRENT-sim. Although still in the lake, the cyanobacterial species growth was much more limited under the pristine conditions, without significant peaks during the growing season nor increasing trend over the entire period.

This result suggested that a hypothetical strong reduction of phosphorus external load would lead to an evident improvement of the lake trophic state, being the lake phosphorus concentrations reduced of about 85% and resulting in a reduction of about

90% of lake productivity. Also a pristine condition potential limits the *P. rubescens* growth and an increase of around 50% is expected for the lake transparency.

The seasonal trend of oxygen concentrations (Figure 28) suggested the lake strongly lays to anoxic conditions, also in a supposed natural condition, slightly higher than the current status only during the winter overturn and in the early summer. This result reinforced the outcome of the paleolimnological survey that proved the presence of anoxic layers in the lake sediment core back to XVIII century (not shown). However the phosphorus release from the sediments resulted strongly lower, due to a different rate characterizing an oligotrophic-mesotrophic initial condition. Moreover, the sediment storage mirrored the lower external loading and the higher exchange rate during the lake annual cycle (especially during the stratification), as highlighted by the increasing trend by the scenarios difference (CURRENT-sim – REFERENCE-sim).

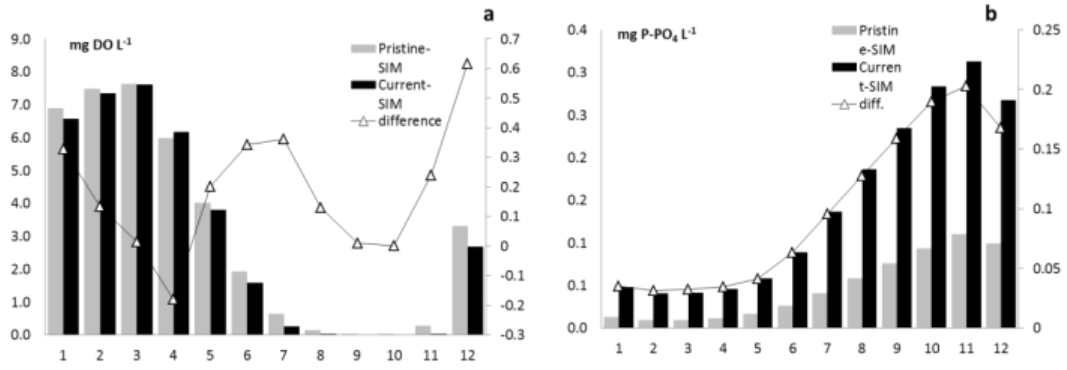

Figure 28. Monthly evolution (as monthly mean over the 1998-2010 period) of a) dissolved oxygen (DO) and b) orthophosphate ($P\text{-}PO_4$) at lake bottom (25 m depth) as simulated in the pristine (REFERENCE-sim) and current (CURRENT-sim) scenarios. The difference between scenarios (as REFERENCE-sim – CURRENT-sim) is also shown.

The analysis of the trophic index (as annual mean) confirmed the lake is between the eutrophic and the mesotrophic threshold at the present, while it could not reach a full oligothrophy under natural boundaries but only a oligo-mesotrophic condition. Considering only the phosphorus concentrations at the winter overturn the lake is still in an eutrophic condition at the present while it is confirmed an oligo-mesotrophic threshold as the maximum-achieved under a pristine loading (Figure 29).

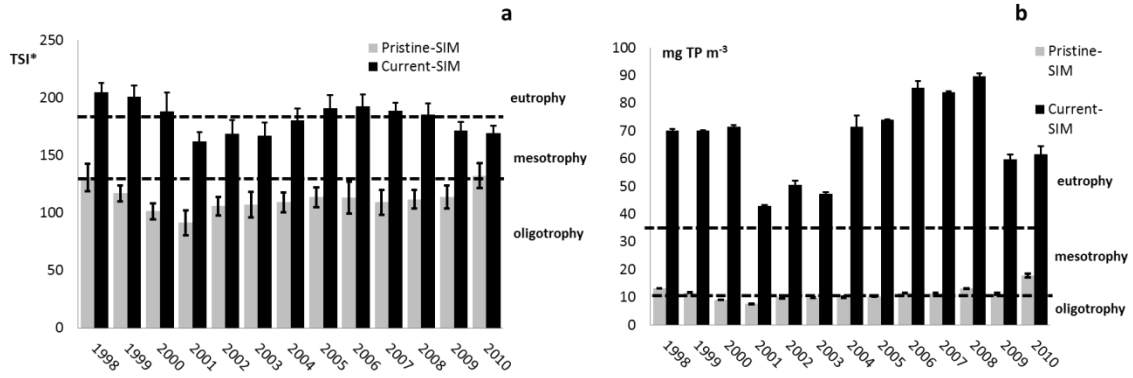

Figure 29. a) The Trophic State Index (Carlson, 1977) modified (TSI*), adapted to Italian lakes and ranked by trophic thresholds (De Bernardi et al., 1985), aggregated in mean annual values. Bar errors indicates the sd over all the daily data for each year. b) The TP at lake winter overturn, as mean monthly value in February for each year. Bar errors indicates the sd over the daily data of February for each year. The trophic thresholds refer to OECD (1982).

4.6 Conclusion

The proposed lake-basin dynamic approach advanced a further step in the definition of an alternative methodology to evaluate the phosphorus reference conditions in lakes. The static mean values by the traditional methods were used to validate the integrated modelling tool, used to dynamically simulate the lake ecological processes in a reconstructed pristine environment. The final mean phosphorus lake concentration, used as reference condition, resulted after more than 100000 hourly steps of simulation of all biogeochemical variables, across the exchanging pools. The paleolimnological survey supported the model requirement for the initial conditions. The reduction of current phosphorus load to a pristine level projected the lake into a higher transparency due to lower phosphorus levels and, consequently, a lower productivity. *P. rubescens* potentiality persisted at low phosphorus concentrations (Carey et al., 2012) but strongly limited in the biomass. Nevertheless, the oxygen content in the bottom waters did not increase and the lake sediments remained anoxic during the summer stratification. The phosphorus release was instead remarkably lower in the pristine simulations due both to a lower release rate in the sediment parameters and a reduced external loading contribution and organic matter sedimentation. At the equilibrium with the external phosphorus loading,

the simulation of biogeochemical cycle and the resultant trophic index confirmed a low eutrophy for the current state and a oligo-mesotrophy for the pristine state, associated to phosphorus reference conditions. The general improvement of the trophic index, after a strong reduction of external loading, has a potential implication for the lake water uses, e.g. an increase of water trasparency and a reduction of *P. rubescens* blooming should result in a positive outcome for bathing or irrigation uses.

5 Final remarks

5.1 Simulation of *P. rubescens* dynamics

The results addressed some of the knowledge gaps regarding the factors that govern its bloom in medium-sized and meso-eutrophic lake. The particular physiological traits, such as a cold-stenotherm, low growth rate, shade-requiring, low irradiances, buoyant and P-limiting adapted species (Walsby and Schanz, 2002; Dokulil and Teubner, 2000), gave it the ability to occupy and grow in the metalimnetic niche during summer, entrain into the surface mixed layer during autumn, survive during the winter turbulence and form the inoculum for the following growing season. The implementation of the three-dimensional ecological model revealed a clear vertical distribution of environmental drivers evidencing a niche separation between two depths and *P. rubescens* resulted to be influenced by lake hydrodynamics, particularly during high-discharge inflows. A simple seasonal succession was identified based on two more phytoplankton functional-groups which are in competition with *P. rubescens* for light and nutrients, each one in its optimal temperature range. The model lost performance in near-shore and pelagic areas, due to depth-specific calibration, the dilution processes by inflowing waters and the spatial interactions due to a different phytoplankton nutrient uptake associated with the stream-lake transition zone (Mackay et al., 2011).

The expected trophic status was assessed with a trophic index, evidencing that oligo-mesotrophy is the natural condition for Lake Pusiano, simulated under a natural external loading. The reference condition for the phosphorus loads and lake concentrations was confirmed through other available methods (paleolimnology, MEI indices, empirical equations). Even in its reference condition, the lake deep/hypolimnetic waters were simulated to remain anoxic during the thermal stratification, although the total anoxic volume and period are lower compared to the eutrophic simulated condition. This suggests the lake morphometry and physiographic features determine the oxygen depletion on the bottom and the lake monomictic pattern, more than the productivity. The general improvement of the trophic index has a potential implication for the lake water uses, i.e. an increase of water trasparency and a reduction of *P. rubescens* blooming should result in a positive outcome for bathing or irrigation uses.

The interactions between *P. rubescens* eco-physiological traits and the lake ecological state are crucial factors in determining the effects of the climate forcing (e.g. temperature warming) on its growth and may cause a different behaviour, depending on the lake trophic evolution. The Wavelet Analysis of 50-years daily output by simulated scenarios highlighted a chaotic behaviour (no seasonal patterns) since the late 90s, when *P. rubescens* blooms started to occur after decades of phosphorus pollution from the catchment. A regular 12-month period (an autumn peak) was instead extracted during the simulation of a pristine condition, characterized by a low productivity.

After decades of lake eutrophication, the global warming did not increase the blooming events. In fact, its growth rate took benefit from a colder climate rather than the increasing temperatures, under the same eutrophic condition. Apparently, this outcome counteracts the recent findings about the positive relation between the establishment of *P. rubescens*, a warmer climate and the longer-lasting stratification periods (i.e. more stable conditions for its growth), especially in deep subalpine lakes (Carey et al., 2012; Posch et al., 2012). Yet, there are evidences that benefits from climate warming are restricted to the winter signal leading the on-set of thermal stratification, or even they are not directly demonstrated, while longer periods of summer stratification showed no advantage for population development (Salmaso 2010, Dokulil and Teubner, 2012). Conversely, a positive relation between *P. rubescens* and the increasing temperatures arose when the pressure from the catchment (e.g. phosphorus pollution) was switched off, as emerged by the Mann-Kendall statistics on daily output data. In other words, these outcomes suggest that the warming temperatures may have a different effect on *P. rubescens* dynamics, depending on the trophic evolution of a lake.

The present study did not solve, but could only confirm, the paradoxical behaviour of *P. rubescens* (Padisák et al., 2010). Although the present study is based only on one case, the output gained separating the causal factors and comparing the effects support the formulation of some important hypothesis, to be tested in a further study on other lakes:

1. the large diffusion of the filamentous cyanobacterium was caused by the common politics of lakes restorations, based on an unidirectional reduction of phosphorus loads;

2. decades of pollution, catastrophic shifts, loss of biodiversity etc. weakened the natural fender of ecosystems, offering the gap for the instauration of invasive species;

3. the eco-physiological traits of *P. rubescens* became a key factor matching the first two conditions and determining its ubiquitous success;

4. climate change did not cause a direct effect on blooming mechanism in lakes that were already locally impacted;

5. lake ecosystems, that are in their original (or natural) condition, are stronger in contrasting *P. rubescens* instauration, being the ecological niches already occupied by several species, but they may be more vulnerable to global warming, favouring the population growth.

5.2 Future perspectives

This study assessed an innovative methodological approach to allocate classic taxonomic determinations into 'functional-groups' in order to validate a three-dimensional model with three 'key' groups based on cell enumerating. The use of a spectrally-specific submergible fluorimeter coupled to continuous simulations of a calibrated model can potentially supply a high-frequency monitoring for Lake Pusiano, in a next future. This device can also be employed for a real-time warning of the risk of *P. rubescens* blooms, or be used to manage the population growth predicting the effects of the regulation of the existing dam and extraordinary hydrologic events. The methodological approach was developed to integrate high-frequency measurement and models of the lake and its catchment is an exportable tool, regardless of the model options. The innovative use of an integrated lake-basin modelling tool enabled to separately simulate the effects on lake ecology of human pressures at acting at different spatial scales. Thanks to its architecture, it can be used to predict the future effect of climate change and land use on lake thermal structure (as circulation, stratification or oscillation patterns), trophic evolution, sediment fluxes, cyanobacterial blooming etc. The Intergovernmental Panel on Climate Change scenarios (IPCC, 2007) can be integrated into the model as a meteorological forcing after they have been processed by a statistical downscaling.

In general, after the first effort to implement deterministic models for lakes, these tools are useful to predict changes within any quantitative variable, thus variation in biogeochemical cycles, consequences of a regime shift, the effects of different restoration plans or human pressure, physical processes and nutrients storage (e.g. carbon lake budget). A predictive study is already in progress by the author, based on scenarios simulating different practices to reduce the current phosphorus loading in Lake Pusiano, regarding the goals of the European Water Framework Directive (2000/60/EU). The evolution of lake ecological processes are distinguished under different management plan and the efficiency is compared evaluating the simulated output by a cost/benefit analysis.

6 References

Adams MS, Guilizzoni P and Adams S, 1978. Sedimentary pigments and recent primary productivity in northern Italian lakes. Mem Ist Ital Idrobiol 36:267–285.

Aitkin M. A., Francis B. and Hinde J., 2009. Statistical Modelling in R, New York: Oxford University Press, Oxford xii, 576 pp.

Anderson, N.J. 1993. Natural versus anthropogenic change in lakes: The role of the sediment record. Trends in Ecology and Evolution, 8: 356-361.

Anonymous, 2003. River and lakes–typology, reference conditions and classification systems. Guidance No 10. CIS Working Group 2.3 REFCOND, European Communities, Luxembourg, 87p.

Ambrosetti, W. and Barbanti L., 1999. Deep water warming in lakes: an indicator of climatic change. Journal of Limnology 58: 1–9.

American Public Health Association (APHA), 1992. Standard methods for examination of water and wastewater. 18th edition, American Public Health Association, Washington, DC.

APAT and IRSA-CNR. 2003. Manuali analitici per le acque. Manuali e Linee Guida 29/2003. Vol.I, 177-182.

Appleby, P.G., 2001. Chronostratigraphic techniques in recent sediments. In: Last W.M. and Smol J.P. (eds) Tracking Environmental Change using Lake Sediments. Volume 1: Basin Analysis, Coring, and Chronological Techniques. Kluwer, Dordrecht, pp. 171–203.

Arhonditsis, G.B. and Brett M.T., 2004. Evaluation of the current state of mechanistic aquatic biogeochemical modelling. Marine Ecology Progress Series 271: 13–26.

Arnold J.G., Allen P.M. and Bernhardt G., 1993. A comprehensive surface–groundwater flow model. Journal of Hydrology 142:47–69.

Artale, V., Calmanti, S., Carillo, A., Dell'Aquila, A., Herrmann, M., Pisacane, G., Ruti, P.M., Sannino, G., Struglia, M.V., Giorgi, F., Bi, X., Pal and J.S., Rauscher, S., 2009. An atmosphere–ocean regional climate model for the Mediterranean area: assessment of a present climate simulation. Climate Dynamics 35: 721–740.

Balestrini, R., Galli L. and Tartari G., 2000. Wet and dry atmospheric deposition at prealpine and alpine site in Northern Italy. Atmospheric Environment 4: 1455–1470.

Barbiero, G., Carone, G., Cicioni, G., Puddu, A. and E Spaziani, F.M., 1991. Valutazione dei carichi inquinanti potenziali per i principali bacini idrografici italiani: Adige, Arno, Po e Tevere. Quaderni Istituto di Ricerca sulle Acque, 90. 233 pp.

Bargu, S., White J. R., Li C., Czubakowski J. and Fulweiler R.W., 2011. Effects of freshwater input on nutrient loading, phytoplankton biomass, and cyanotoxin production in an

oligohaline estuarine lake. Hydrobiologia 661: 377–389.

Battarbee RW, Juggins S, Gasse F, Anderson NJ, Bennion H, Cameron NG, Ryves DB, Pailles C, Chalie F and Telford R., 2001. European diatom database (EDDI). An information system for palaeoenvironmental reconstruction. ECRC Research Report No 81, University College London, 94 pp.

Battarbee R.W., Anderson N.J., Jeppesen E. and Leavitt P.R., 2005. Combining palaeolimnological and limnological approaches in assessing lake ecosystem response to nutrient reduction. Freshwater Biology 50:1772–1780.

Battarbee, R.W. and Bennion, H., 2011. Palaeolimnology and its developing role in assessing the history and extent of human impact on lake ecosystems. Journal of Paleolimnology 45:399–404.

Bennion, H., Johnes, P., Ferrier, R., Phillips, G. and Haworth, E.Y., 2005. A comparison of diatom phosphorus transfer functions and export coefficient models as tools for reconstructing lake nutrient histories. Freshwater Biology 50: 1651–1670.

Bennion H. and Simpson, G.L., 2011. The use of diatom records to establish reference conditions for UK lakes Southject to eutrophication. Journal of Paleolimnology. 45(4):469–488.

Beutler, M, Wiltshire K.H., Meyer B., Moldaenke C., Lüring C., Meyerhöfer M., Hansen U.P. and Dau H., 2002. A fluorometric method for the differentiation of algal populations in vivo and in situ. Photosynthesis Research 72: 39–53.

Blenckner, T., 2008. Models as tools for understanding past, recent and future changes in large lakes. Hydrobiologia 599:177 – 182.

Boguniewicz, J., Capodaglio, A., Salerno and F., Tartari, G., 2006. Approach to Support Water Quality catchment Project. WSEAS Transactions on Environment and Development. 2: 1079–1084.

Boegman, L., Imberger J., Ivey G. N. and Antenucci J. P., 2003. High-frequency internal waves in large stratified lakes. Limnology and Oceanography 48: 895– 919.

Bright, D.I. and Walsby A. E., 2000. The daily integral of growth by Planktothrix rubescens calculated from growth rate in culture and irradiance in Lake Zürich. New Phytologist 146: 301–316.

Broomhead, D.S. and King, G.P., 1986. Extracting qualitative dynamics from experimental data. Physica D20: 217–236.

Brookes, J. D. and Carey C. C., 2011. Resilience to Bloom. Science 334: 46–47.

Bruce, L.C., Hamilton D., Imberger J., Gal G., Gophen M., Zohary T. and Hambright K. D., 2006. A numerical simulation of the role of zooplankton in C, N and P cycling in Lake

Kinneret, Israel. Ecological Modelling 193: 412–436.

Bruce, L. C., Jellison, R., Imberger, J. and Melack, J. M., 2008. Effect of benthic boundary layer transport on the productivity of Mono Lake, California. Saline System 4: 1–21.

Bürgi, H. and Stadelmann P., 2002. Change of phytoplankton composition and biodiversity in Lake Sempach before and during restoration. Hydrobiologia 469: 33–48.

Camusso M. and Tartari G., 1988. An avaluation of point and non point source loads of nutrients to a highly eutrophic lake. In A. Marani (Ed.). Advanced in environmental modelling. Elsevier, Amsterdam. 105-120 pp.

Cardoso A.C., Solimini A., Premazzi G., Carvalho L., Lyche A. and Rekolainen S., 2007. Phosphorus reference concentrations in European lakes. Hydrobiol 584:3–12.

Carey, C.C., Ibelings, B.B., Hoffmann, E.P., Hamilton, D.P. and Brookes, J.D., 2012.Eco-physiological adaptations that favour freshwater cyanobacteria in a changing climate. Water Research 46: 1394 – 1407.

Carmichael, W.W., 2001. Health effects of toxin producing cyanobacteria: the 'CyanoHABS'. Human and Ecological Risk Assessment 7: 1393–1407.

Carlson RE. 1977. A trophic state index for lakes. Limnology and Oceanography 22:361–9.

Carraro E., Guyennon N., Hamilton D., Valsecchi L., Manfredi E.C., Viviano G., Salerno F., Tartari G., Copetti D., 2012 a. Coupling high-resolution measurements to a three-dimensional lake model to assess the spatial and temporal dynamics of the cyanobacterium Planktothrix rubescens in a medium-sized lake. Hydrobiologia 698:77–95.

Carraro, E., Guyennon, N., Viviano, G., Manfredi, E.C., Valsecchi, L., Salerno, F., Tartari, G., Copetti, D., 2012 b. Impact of Global and Local Pressures on the Ecology of a Medium-Sized Pre-Alpine Lake. In: Models of the Ecological Hierarchy: From Molecules to the Ecosphere. Elsevier B.V., pp. 259–274.

Chiaudani, G. and Premazzi, G., 1992. I laghi briantei. Situazione trofica e soluzioni scientifiche per il risanamento. Report EUR 14548 IT (In Italian).

Copetti, D., Tartari G., Morabito G., Oggioni A., Legnani E. and Imberger J., 2006. A biogeochemical model of the Lake Pusiano (North Italy) and its use in the predictability of phytoplankton blooms: first preliminary results. Journal of Limnology 65: 59–64.

Copetti, D., Carniato, L., Crise, A., Guyennon, N., Palmeri, L., Pisacane, G., Struglia, M.V., and Tartari, G., Accepted. Chapter 3: Impacts of climate change on water quality. In Regional Assessment on Climate Change in the Mediterranean (Part 2: Water). Springer.

Cuypers, Y., Vinçon-Leite B., Groleau A., Tassin B. and Humbert J. F., 2011. Impact of internal waves on the spatial distribution of *Planktothrix rubescens* (cyanobacteria) in an alpine

lake. The Isme Journal 5: 580 - 589.

D'Alelio, D., Gandolfi A., Boscaini A., Flaim G., Tolotti M. and Salmaso N., 2011. *Planktothrix* populations in subalpine lakes: selection for strains with strong gas vesicles as a function of lake depth, morphometry and circulation. Freshwater Biology. 56: 1365–2427.

Daubechies, I., 1992. In: Ten Lectures on Wavelets. Society for Industrial and Applied Mathematics. p. 357.

Davis, P. A., Dent M., Parker J., Reynolds C. S. and Walsby A. E., 2003. The annual cycle of growth rate and biomass change in *Planktothrix spp*. in Blelham Tarn, English Lake District. Freshwater Biology 48: 852–867.

De Bernardi R., Giussani G., Mosello., Origgi I.,1985. Indagine conoscitiva per una caratterizzazione limnoloogica dei "Piccoli Laghi Lombardi". Doc. Ist. Ital. Idrob., n ° 8. Pallanza.

Déqué, M., 2007. Frequency of precipitation and temperature extremes over France in a anthropogenic scenario: model results and statistical correction according to observed values. Global Planetary Change 54: 16–26 .

Directive 2000/60/EC of the European Parliament and the Council of 23.10.2000 establishing a framework for Community action in the field of water policy. Official Journal of the EC L 327: 1–72.

Directive 2008/105/EC of the European Parliament and the Council of 16.12.2008 on environmental quality standards in the field of water policy, amending and subsequently repealing Council Directives 82/176/EEC, 83/513/EEC, 84/156/EEC, 84/491/EEC, 86/280/EEC and amending Directive 2000/60/EC. Official Journal of the EC L 348: 84–97.

Dokulil, M. T. and Teubner K., 2000. Cyanobacterial dominance in lakes. Hydrobiologia 438: 1–12.

Dokulil M. T. and Teubner K., 2012. Deep living *Planktothrix rubescens* modulated by environmental constraints and climate forcing. Hydrobiologia DOI 10.1007/s10750-012-1020-5.

Eilers, P.H. and Goeman J.J., 2004. Enhancing scatterplots with smoothed densities. Bioinformatics 20: 623–628.

Elliott, J.A., Thackeray, S.J., Huntingford, C. and Jones, R.G., 2005. Combining a Regional Climate Model with a phytoplankton community model to predict future changes in phytoplankton in lakes. Freshwater Biology 50: 1404–1411.

Elliot, J.A., 2010. The seasonal sensitivity of Cyanobacteria and other phytoplankton to changes

in flushing rate and water temperature. Global Change Biology 16: 864–876.

Ernst, B., Hoeger S. J., O'Brien E. and. Dietrich D. R, 2009. Abundance and toxicity of Planktothrix rubescens in the pre-alpine Lake Ammersee, Germany. Harmful Algae 8: 329–342.

EU-Intercalibration Technical Report, 2006. European environmental NGO technical review of the water framework directive intercalibration process. http://www.eeb.org/activities/water/200609_NGO-review-WFD-Intercalibration

FAO, ISRIC, ISSS, 1998. World Reference Base for Soil Resources. World Soil Resources Report, vol. 84, Food and Agriculture Organization of the United Nations, Rome. p. 90 pp.

Ferrier R.C., Malcolm A., McAlister E., Edwards T., Morrice J. and Owen R., 1996. Hindcasting of in-loch phosphorus concentrations based on land cover classification. Report for the Scotland and Northern Ireland Forum for Environmental Research.

Feuillade, J., 1994. The cyanobacterium (blue-green algae) Oscillatoria rubescens D.C. Archiv für Hydrobiologie – Beiheft Ergebnisse der Limnologie 41: 77–93.

Gal G.,. Hipsey M. R, Parparov A., Wagner U., Makler V. and Zohary T., 2009. Implementation of ecological modelling as an effective management and investigation tool: Lake Kinneret as a case study. Ecological Modelling 220: 1697–1718.

Gassman PW, Reyes MR, Green CH, Arnold JG. 2007. The soil and water assessment tool: historical development, applications, and future research directions. Transactions of the ASABE 50: 1211–1250.

Gerletti, M. and Marchetti., R., 1977. Indagini sui laghi della Brianza. Water Research Institute (CNR Italy) Books n. 19 (In Italian).

Ghil, M. and Vautard, R., 1991. Interdecadal oscillations and the warming trend in global time series. Nature 350: 324–327.

Grayson R.B., Finlayson B.L., Gippel C.J., Hart B.T., 1996. The potential of field turbidity measurements for the computation of total phosphorus and suspended solids loads. Journal of Environmental Management 47: 257–267.

Grayson, R.B., Blöschl G., Western A.W. and McMahon T.A., 2002. Advances in the use of observed spatial patterns of catchment hydrological response. Advances in Water Resources 25: 1313 – 1334.

Grinsted, A., Moore, J., Jevrejeva, S., 2004. Application of the cross wavelet transform and wavelet coherence to geophysical time series. Nonlinear Processes in Geophysics 11: 561–566.

Guilizzoni P., and Lami, A. 2002. Paleolimnology: use of algal pigments as indicators. In:

Bitton G (ed) The encyclopedia of environmental microbiology. Wiley, New York, pp 2306–2317.

Guilizzoni, P., Marchetto, A., Lami, A., Gerli, S. and Musazzi, S., 2011. Use of sedimentary pigments to infer past phosphorus concentration in lakes. Journal of Paleolimnology 45: 433–445.

Gupta, H. V., Sorooshian S., and Yapo P. O., 1999. Status of automatic calibration for hydrologic models: Comparison with multilevel expert calibration. Journal of Hydrologic Engineering. 4: 135–143.

Guiry, M. D. & G. M. Guiry, 2011. AlgaeBase. World-wide electronic publication, National University of Ireland, Galway. Accessed 13 September 2012, http://www.algaebase.org.

Hamilton, D.P. and S.G. Schladow, 1997. Prediction of water quality in lakes and reservoirs. Part I – Model description. Ecological Modelling 96: 91–110.

Hamilton D. P., O'Brien, K. R. Burford M. A., Brookes J. D. and McBride C. G., 2010. Vertical distributions of chlorophyll in deep, warm monomictic lakes. Aquatic Sciences 72: 295–307.

Havens, K. E., Elia, A. C., Taticchi, M. I. and Fulton, R. S., 2009. Zooplankton-phytoplankton relationships in shallow subtropical versus temperate lakes Apopka (Florida, USA) and Trasimeno (Umbria, Italy). Hydrobiologia 628: 165–175.

Hillmer, I., Van Reenen P., Imberger J., and Zohary T., 2008. Phytoplankton patchiness and their role in the modeled productivity of a large, seasonally stratified lake. Ecological Modelling 218: 49–59.

Hipsey, M.R., 2008. The CWR Computational Aquatic Ecosystem Dynamics Model CAEDYM. User Manual. Centre for Water Research, The University of Western Australia.

Hodges, B.R., Imberger J., Saggio A. and Winters K.B., 2000. Modelling basin scale waves in a stratified lake. Limnology and Oceanography 45: 1603–1620.

Hodges, B.R. and Dallimore, C. 2006. Estuary Lake and Coastal Ocean Model: ELCOM V2.2 Science Manual, Centre for Water Research, Perth. 54 pp.

Horsburgh, J. S., Spackman Jones A., Stevens D. K.,. Tarboton D. G and Mesner N. O., 2010. A sensor network for high frequency estimation of water quality constituent fluxes using surrogates. Environmental Modelling & Software 25: 1031–1044.

Howarth, R.J. and Earle S. A. M., 1979. Application of a generalized power transformation to geochemical data. Mathematical Geology 11: 45–62.

Huisman, J.M., Matthijs H.C.P. and Visser P.M., 2005. Harmful Cyanobacteria. Springer Aquatic Ecology Series 3. Dordrecht, the Netherlands.

Hupfer, M., Rübe, B., and Schmieder, P., 2004. Origin and diagenesis of polyphosphate in lake

sediments: a ^{31}P NMR study. Limnology and Oceanography 49:1-10.

Ibelings B. W., Vonk M., Los F. J., Van Der Molen D. T. and Mooij W. M., 2003. Fuzzy modeling of cyanobacterial surface water-blooms, validation with NOAA-AVHRR satellite images. Ecological Applications 13: 1456–1472.

Imerito, A., 2007. Dynamic Reservoir Simulation Model v4.0 Science Manual. Centre for Water Research, the University of Western Australia (online). http://www.cwr.uwa.edu.au/services/models/legacy/model/dyresmcaedym/dyresmcaedymdocumentation.html

IPCC, 2007. Climate change 2007 Synthesis report. In: Core Writing Team, Pachauri, R.K., Reisinger, A. (Eds.), Contribution of Working Groups I, II and III to the Fourth Assessment Report of the Intergovernmental Panel on Climate Change. IPCC, Geneva, Switzerland, p. 104.

Jeppesen, E., Søndergaard, M., Jensen, J.P., Havens, K., et al., 2005. Lake responses to reduced nutrient loading–an analysis of contemporary long-term data from 35 case studies. Freshwater Biology 50: 1747–1771.

Jeppesen, E., Kronvang, B., Meerhoff, M., Søndergaard, M., et al., 2009. Climate change effects on runoff, catchment phosphorus loading and lake ecological state, and potential adaptations. Journal of Environmental Quality 38: 1930–1941 .

Johnes, P.J., 1996. Evaluation and management of the impact of land use change on the nitrogen and phosphorus load delivered to surface waters: the export coefficient modelling approach. Journal of Hydrology 183: 323–349.

Jordan P., Arnscheidt A., McGrogan H., McCormick S., 2007. Characterizing phosphorus transfers in rural catchments using a continuous bank-side analyser. Hydrology and Earth System Sciences. 11:372-381.

Jørgensen S.E., 2010. A review of recent developments in lake modelling. Ecological Modelling 221: 689–692.

Kirilova, E.P., Cremer, H., Heiri, O. and Lotter A.F., 2010. Eutrophication of moderately deep Dutch lakes during the past century: flaws in the expectations of water management? Hydrobiologia 637: 157–171.

Krivtsov, V., Corliss J., Bellinger E. and Sigee D., 2000. Indirect regulation rule for consecutive stages of ecological succession. Ecological Modelling 133: 73–82.

Lami, A., Guilizzoni, P. and Marchetto, A., 2000. High resolution analysis of fossil pigments, carbon, nitrogen and sulphur in the sediment of eight European Alpine lakes: the MOLAR project. Journal of Limnology 59: 15–28.

Larson, D. R., 2007. Unitary systems and wavelet sets. Wavelet Analysis and Applications.

Appl. Numer. Harmon. Anal.. Birkhäuser. pp. 143–171.

Laval, B., Imberger J., Hodges B.R. and Stocker R., 2003a. Modeling circulation in lakes: spatial and temporal variations. Limnology and Oceanography 48: 983–994.

Laval, B., Hodges B.R., and Imberger J., 2003b. Reducing numerical diffusion effects with pycnocline filter. Journal of Hydraulic Engineering 129: 215–224.

Le Vu B., Vinçon-Leite B., Lemaire B.J., Bensoussan N., Calzas M., Drezen C. et al., 2011. High-frequency monitoring of phytoplankton dynamics within the European water framework directive: application to metalimnetic cyanobacteria. Biogeochemistry 106: 229–242.

Leboulanger, C., Dorigo U., Jacquet S., Leberre B., Paolini G. and Humbert J.-F., 2002. Application of a submersible spectrofluorometer for rapid monitoring of freshwater cyanobacterial blooms: a case study. Aquatic Microbial Ecology 30: 83–89.

León, L. F., Imberger, J. Smith, R. E. H., Hecky, R. E., Lam,, D. C. L. and Schertzer, W. M., 2005. Modeling as a tool for nutrient management in Lake Erie: a hydrodynamic study. Journal Great Lakes Research 31: 309–318.

Legnani, E., Copetti D., Oggioni A., Tartari G., Palumbo M.T. and Morabito G., 2005. *Planktothrix rubescens* seasonal and vertical distribution in Lake Pusiano (North Italy). Journal of Limnology 64: 6 –73.

Lileikytė D. and Belous O., 2011. Water quality evaluation: toxic cyanobacteria in surface water. Environmental Research, Engineering and Management 1: 43-48.

Lin J.P., 2004. Review of published export coefficient and event mean concentration (EMC) data ERDC TN-WRAP-04-3, U.S. Army Engineer Research and Development Center, Vicksburg, MS. 15 pp.

Livingstone, D.M., 2003. Impact of secular climate change on the thermal structure of a large temperate central European lake. Climatic Change 57: 205–225.

Mackay, E.,. Ian D.J, Folkard A.M. and Thackeray S.J., 2011. Transition zones in small lakes: the importance of dilution and biological uptake on lake-wide heterogeneity. Hydrobiologia 678: 85-97.

Malmaeus, J. M., Blenckner, T., Markensten, H. and Persson, I., 2006. Lake phosphorus dynamics and climate warming: A mechanistic model approach. Ecological Modelling 190: 1 – 14.

Mango L.M., Melesse A.M., McClain M.E., Gann D. and Setegn S.G., 2011. Land use and climate change impacts on the hydrology of the upper Mara River Basin, Kenya: results of a modeling study to support better resource management. Hydrology and Earth Systems Science. 15: 2245–2258.

Marchetti, R., Verna, N., 1992. Quantification of the phosphorus and nitrogen loads in the minor rivers of the Emilia-Romagna coast (Italy). A methodological study on the use of theoretical coefficients in calculating the loads. In: Vollenweider, R.A., Marchetti, R., Viviani, R. (Eds.), Marine Coastal Eutrophication. Elsevier Science, Amsterdam. 315-335 pp.

Mellard, J.P., Yoshiyama K., Litchman E. and Klausmeier C. A., 2011. The vertical distribution of phytoplankton in stratified water columns. Journal of Theoretical Biology 269: 16 – 30.

Mieleitner, J. and Reichert P., 2008.Modelling functional groups of phytoplankton in three lakes of different trophic state. Ecological Modelling 211: 279–291.

Missaghi S. and Hondzo M., 2010. Evaluation and application of a three–dimensional water quality model in a shallow lake with complex morphometry. Ecological Modelling 221: 1512–1525.

Mooij W. M., Trolle D., Jeppesen E., Arhonditsis G. et al., 2010. Challenges and opportunities for integrating lake ecosystem modelling approaches. Aquatic Ecology 44: 633–667.

Moriasi D. N., Arnold J. G., Van Liew M. W., Bingner R. L., Harmel R. D., and Veith T. L., 2007. Model evaluation guidelines for systematic quantification of accurancy in watershed simulations. Transactions of the ASABE 50(3):885-900.

Nash, J.E. and Sutcliffe J.V., 1970. River flow forecasting through conceptual models. Part I. A discussion of principles. Journal of Hydrology 10: 282–290.

Neitsch, S.L., Arnold, J.G., Kiniry, J.R. and Williams, J.R, 2005. Soil and Water Assessment Tool Theoretical Documentation and User's Manual, Version 2005, GSWR Agricultural Research Service & Texas Agricultural Experiment Station, Temple Texas.

Organisation for Economic Co-operation and Development (OECD), 1982. Eutrophication of waters. Monitoring, Assessment and Control. OECD, Paris, 154 pp.

Oberhaus L, Briand J-F, Leboulanger C, Jacquet S and Humbert J-F., 2007. Comparative effects of the quality and the quantity of light and of the temperature on the growth of *Planktothrix agardhii* and *P.rubescens.* Journal of Phycology 43: 1191–1199.

Olberg M, and Rakoczi, F. 1984. Informationstheorie in Meteorologie und Geophysik. Akademie-Verlag, Berlin.

Omlin M., Brun, P. and Reichert P., 2001a. Biogeochemical model of Lake Zürich: sensitivity, identifiability and uncertainty analysis. Ecological Modelling 141: 105–123.

Omlin, M., Reichert, P. and Foster, R., 2001b. Biogeochemical model of Lake Zürich: model equations and results. Ecological Modelling 141: 77 – 103.

Ostrofsky M.L. and Bradley C.P., 2006. Reconstructing the historical trophic status of

northwestern Pennsylvania lakes using GIS. Hydrobiologia 571:273–281.

Padisák, J., Crossetti L. O. and Naselli-Flores L., 2009. Use and misuse in the application of the phytoplankton functional classification: a critical review with updates. Hydrobiologia 621: 1–19.

Padisák J., Hajnal É., Krienitz L., Lakner J. and Üveges V., 2010. Rarity, ecological memory, rate of floral change in phytoplankton and the mystery of the Red Cock. Hydrobiologia 653: 45–64.

Paerl H.W. and Huisman J., 2008. Blooms like it hot. Science 320: 57–58.

Pannard A., Beisner B. E., Bird D.F., Braun J., Planas D. and Bormans M., 2011. Recurrent internal waves in a small lake: Potential ecological consequences for metalimnetic phytoplankton populations. Limnology & Oceanography: Fluids & Environments 1: 91-109.

Parmesan, C. and Yohe, G., 2003. A globally coherent fingerprint of climate change impacts across natural systems. Nature 421: 37–42.

Patterson, J. C., Hamblin, P. F. and Imberger J.,1984. Classification and dynamics simulation of vertical density structure of lakes. Limnology and Oceanography 29: 845-861.

Peeters, F., Livingstone, D. M., Goudsmit, G. H., Kipfer, R. and Forster, R., 2002. modelling 50 years of historical temperature profiles in a large central European lake. Limnology and Oceanography 47: 186 – 197.

Pickett, T.A., 1989. Space-for-time substitution as an alternative to long-term studies. In Long-Term Studies in Ecology: approaches and alternatives, ed. Likens E (Springer, New York), pp 110–135.

Pomati F., Jokela J., Simona M., Veronesi M. and Ibelings B. W., 2011. An Automated Platform for Phytoplankton Ecology and Aquatic Ecosystem Monitoring. Environmental Science & Technology 45: 9658-9665.

Portoghese, I., Bruno, E., Guyennon, N. and Iacobellis V., 2011. Stochastic bias-correction of daily rainfall scenarios for hydrological applications. Natural Hazards and Earth System Sciences 11: 2497 – 2509.

Posch, T., Koster O., Salcher M. M. and Pernthaler J., 2012. Harmful filamentous cyanobacteria favoured by reduced water turnover with lake warming. Nature Climate Change. 2: 809–813.

Psenner, R., Puesko, R. and Sager, M., 1984. Die Fractionierung Organischer and Anorganischer Phosphorverbindungen von Sedimenten Versuch einer Definition Okologisch Wichtiger Fractionen. Archiv für Hydrobiologie 10: 115–155.

Redfield, A.C. 1934. On the proportions of organic derivatives in seawater and their relation to

the composition of plankton. In: R.J. Daniel (Ed.), James Johnston Memorial Volume. University Press of Liverpool, Liverpool: 176-192.

Reichert P. and Mieleitner J., 2008. Lake Models. In: Jørgensen S.E., Fath BD (eds) Ecological models, vol 3 of Encyclopedia of ecology. Elsevier, Oxford, pp 2068–2080.

Reynolds, C. S., Huszar V., Kruk C., Naselli-Flores L. and Melo S., 2002. Towards a functional classification of the freshwater phytoplankton. Journal of Plankton Research 24: 417–428.

Reynolds, C.S. 2006. The Ecology of Phytoplankton. Cambridge University Press, Cambridge.

Rigosi, A., Marcé R., Escot C. and Rueda F. J., 2011. A calibration strategy for dynamic succession models including several phytoplankton groups. Environmental Modelling & Software 26: 697–710.

Rinke, K., Yeates P. and Rothhaupt K. O., 2010. A simulation study of the feedback of phytoplankton on thermal structure via light extinction. Freshwater Biology 55: 1674–1693.

Robson, B.J. and Hamilton D.P., 2004. Three-dimensional modelling of a Microcystis bloom event in the Swan River estuary, Western Australia. Ecological Modelling 174: 203 – 222.

Robson B.J., Hamilton D.P., Webster I.T. and Chan T., 2008. Ten steps applied to development and evaluation of process-based biogeochemical models of estuaries. Environmental Modelling & Software 23:369–384.

Ryder R A, Kerr S R, Loftus K H and Regier H A, 1974 The morphoedaphic index as a fish yield estimator: review and evaluation. Journal of the Fisheries Research Board of Canada. 31: 663-688.

Salerno, F. and Tartari G., 2009. A coupled approach of surface hydrological modelling and Wavelet Analysis for understanding the baseflow components of river discharge in karst environments. Journal of Hydrology 376: 295–306.

Salerno F., Thakuri S., D'Agata C., Smiraglia C., Manfredi E.C., Viviano G. and Tartari G. 2012. Glacial lake distribution in the Mount Everest region: Uncertainty of measurement and conditions of formation. Global and Planetary Change. 92–93: 30–39.

Salmaso, N., 2005. Effects of climatic fluctuations and vertical mixing on the interannual trophic variability of Lake Garda, Italy. Limnology and Oceanography 50: 553–565.

Salmaso, N., 2010. Long-term phytoplankton community changes in a deep subalpine lake: responses to nutrient availability and climatic fluctuations. Freshwater Biology 55: 825–846.

Salmaso, N., and Cerasino L., 2012. Long-term trends and fine year-to-year tuning of

phytoplankton in large lakes are ruled by eutrophication and atmospheric modes of variability. Hydrobiologia 698:17–28.

Scheffer, M., Rinaldi S., Gragnani A., Mur L. R. and. Van Nes E. H, 1997. On the dominance of filamentous cyanobacteria in shallow turbid lakes. Ecology 78: 272–282.

Scheffer, M., Carpenter S., Foley J.A., Folke C. and Walker B., 2001. Catastrophic shifts in ecosystems. Nature. 413: 591-596.

Schindler, D.W., 2001. The cumulative effects of climate warming and other human stresses on Canadian fresh-waters in the new millennium. Canadian Journal of Fisheries and Aquatic Sciences 58: 18–29.

Serra T., Vidal J., Colomer J., Casamitjana X. and Soler M., 2007. The role of surface vertical mixing in phytoplankton distribution in a stratified reservoir. Limnology and Oceanography 52: 620–634.

Simmons, A.J. and Gibson, J.K., 2000. The ERA-40 Project Plan. ERA- 40 project report series no.1 ECMWF pp 62.

Solheim A.L., 2005. Reference conditions of European lakes. Indicators and methods for the Water Framework Directive Assessment of Reference conditions. Version 5. REBECCA Working Group, 105 pp.

Søndergaard, M., Jensen, J.P. and Jeppesen, E., 2003. Role of sediment and internal loading of phosphorus in shallow lakes. Hydrobiologia 506/509, 135–145.

Søndergaard M., Larsen S.E., Jørgensen T.B. and Jeppesena E., 2011. Using chlorophyll a and cyanobacteria in the ecological classification of lakes. Ecological Indicators 11: 1403–1412.

Sneyers, R., 1990: On the statistical analysis of series of observation. WMO, Technical Note N. 143, Geneve, 192pp.

Srinivasan, R. and Arnold, J.G., 1994. Integration of a Basin-Scale Water Quality Model with GIS. Water Resources Bulletin 30: 45 –462.

Stubblefield A.P., Reuter J.E., Dahlgren R.A., Goldman C.R., 2007. Use of Turbidometry to Characterize Suspended Sediment and Phosphorus Fluxes in the Lake Tahoe Basin, California, USA. Hydrological Processes 21:281-291.

Tartari G., Copetti D., Barbiero G., Tatti S. and Pagnotta R., 2002. Contribute of GIS technique in the evaluation of anthropic impact change in a sub-alpine shallow lake. Proc. Int. Congr. iEMSs 2002, Integrated Assessment and Decision Support. Lugano, June 24-27 2002, 610.

Tartari G., Buraschi E, Monguzzi C, Marchetto A, Copetti D, Salerno F, Previtali L, Tatti S, Barbero G and Pagnotta R, 2004. Progetto LIMNO: Qualità delle acque lacustri italiane,

vol 1: Sintesi dei risultati. Quaderni IRSA 120:339 pp

Thackeray, S.J., Jones, D. and Maberly, C., 2008. Long-term change in the phenology of spring phytoplankton: species-specific responses to nutrient enrichment and climatic change. Journal of Ecology 96: 523–535.

Tong S.T.Y. and Chen W. 2002. Modeling the relationship between land use and surface water quality. Journal of Environmental Management. 66: 377–393.

Torrence, C. and Compo, G.P., 1998. A practical guide to wavelet analysis. Bulletin of the American Meteorological Society 79: 61–78.

Trolle, D., Skovgaard H. and Jeppesen E., 2008. The Water Framework Directive: setting the phosphorus loading target for a deep lake in Denmark using the 1D lake ecosystem model DYRESM–CAEDYM. Ecological Modelling 219: 138–152.

Trolle, D., Hamilton, D. P., Pilditch, C. A. and Duggan, I. C., 2011. Predicting the effects of climate change on trophic status of three morphologically varying lakes: implications for lake restoration and management. Environmental Modelling and Software 26: 354–370.

Trolle D., Hamilton D. P., Hipsey M. R. et al., 2012. A community-based framework for aquatic ecosystem models. Hydrobiologia 683: 25–34.

Van den Wyngaert, S., Salcher, M.M., Pernthaler, J., Zeder, M., and Posch, T., 2011. Quantitative dominance of seasonally persistent filamentous cyanobacteria (*Planktothrix rubescens*) in the microbial assemblages of a temperate lake. Limnology and Oceanography 56: 97–109.

Van Nes, E. H. and Scheffer M., 2005. A strategy to improve the contribution of complex simulation models to ecological theory. Ecological Modelling 185: 153–164.

Venables, W.N. and B.D. Ripley. 2002. Modern applied statistics with S-Plus. Fourth edition. New York, Springer-Verlag.

Verburg, P., Hecky, R.E. and Kling, H., 2003. Ecological consequences of a century of warming in Lake Tanganyika. Science 301: 505–507.

Vighi, M. and Chiaudani, G., 1985. A simple method to estimate lake phosphorus concentrations resulting from natural, background, loadings. Water Research 19: 987–991.

Vilhena L. C., Hillmer I. and Imberger J., 2010. The role of climate change in the occurrence of algal blooms: Lake Burragorang, Australia. Limnology and Oceanography 55: 1188–1200.

Vollenweider, R. A. 1975. Input-output model with special reference to phosphorus loading concept in limnology. Schweizerische Zeitschrift für Hydrologie 37: 53-84.

Vuillermoz, E., Legnani E., Copetti D. and Tartari G., 2006. Limnological evolution of Pusiano

Lake (1972-2004). Verhandlungen des Internationalen Verein Limnologie 29: 2009–2014.

Yeates, P.S. and Imberger, J., 2004. Pseudo two-dimensional simulations of internal and boundary fluxes in stratified lakes and reservoirs. International Journal of River Basin Management 1: 1–23.

Wallace, B. B. and Hamilton, D. P. 1999. The effect of variation in irradiance on buoyancy regulation in Microcystis aeruginosa. Limnology and Oceanography 44 : 273-281.

Walsby, A. E. and Booker M. J., 1980. Changes in buoyancy of a planktonic blue-green alga in response to light intensity. European Journal of Phycology 15: 311–319.

Walsby, A.E., Hayes P.K., Boje R. and Stal L.J., 1997. The selective advantage of buoyancy provided by gas vesicles for planktonic cyanobacteria in the Baltic Sea. New Phytologist 136: 407–417.

Walsby, A.E, Z. Dubinsky, J.C. Kromkamp, C. Lehmann & F. Schanz. 2001. The effects of diel changes in photosynthetic coefficients and depth of Planktothrix rubescens on the daily integral of photosynthesis in Lake Zürich. Aquatic Science 63: 326 - 349.

Walsby, A.E. and Schanz F., 2002. Light-dependent growth rate determines changes in the population of *Planktothrix rubescens* over the annual cycle in Lake Zurich, Switzerland. New Phytologist 154: 671–687.

Walsby, A.E., Schanz F., and Schmid M., 2006. The Burgundy-blood phenomenon: a model of buoyancy change explains autumnal waterblooms of Planktothrix rubescens in Lake Zurich. New Phytologist 169: 109–122.

Webb, W. L., W. Newton and Starr, D. 1974. Carbon dioxide exchange of Alnus rubra: a mathematical model. Oecologia. 17: 281-291.

Wetzel, R.G. 2001 Limnology: Lake and River Ecosystems. 3rd edition. Academic Press, San Diego, CA. 1006 pp.

Winder, M. and Cloern, J. E., 2010. The annual cycles of phytoplankton biomass. Philosophical Transactions of the Royal Society-Biological Science 365: 3215–3226.

Wold S., Esbensen K. and Geladi P., 1987. Principal component analysis. Chemometrics and Intelligent Laboratory Systems 2: 37–52.

Wurtsbaugh W.A., Gross H.P., Budy P. and Luecke C., 2001. Effects of epilimnetic versus metalimnetic fertilization on the phytoplankton and periphyton of a mountain lake with a deep chlorophyll maxima. Canadian Journal of Fisheries and Aquatic Sciences 58: 2156–2166.

Zhang, M., Duan H., Shi X., Yu Y. and Kong F., 2011. Contributions of meteorology to the phenology of cyanobacterial blooms: implications for future climate change. Water

Research, 46: 442–452

Zhao, J., Ramin M., Cheng V., Arhonditsis B., 2008. Competition patterns among phytoplankton functional groups: how useful are the complex mathematical models? Acta Oecologica 33: 324–344.

7 Appendix

7.1 Lake Pusiano limnological survey (2010)

The following elaborations belong to data supplied by the Water Research Institute of the National Council of Research (IRSA-CNR, Brugerio) and owned by CARIPLO and Parco Valle del Lambro (PVDL) which funded the PIROGA Project (2009-2011).

7.1.1 Hydrochemical analysis

Variable	n	Max	Min	Mean	Median	25%	75%
Alkalinity meq/L	68	3.52	2.29	2.93	3.01	2.80	3.08
Conductivity µs/cm (20°C)	84	322.00	222.00	278.83	286.50	264.35	292.60
$N\text{-}NH_4$ mg/L	83	1.70	0.02	0.28	0.22	0.04	0.37
$N\text{-}NO_3$mg/L	61	1.14	0.03	0.69	0.66	0.57	0.93
pH	84	9.26	7.42	8.07	8.09	7.92	8.21
$P\text{-}PO_4$ mg/L	84	0.23	0.00	0.02	0.00	0.00	0.01
$Si\text{-}SiO_2$ mg/L	79	3.45	0.16	1.43	1.49	1.13	1.76
SO_4^{2-} mg/L	59	10.37	4.21	9.05	9.38	8.85	9.91
TDN mg/L	71	2.31	0.88	1.35	1.30	1.12	1.49
TDP mg/L	71	0.22	0.00	0.02	0.01	0.01	0.02
TN mg/L	71	2.47	0.99	1.43	1.38	1.24	1.53
TP mg/L	71	0.40	0.01	0.05	0.03	0.02	0.04
Na mg/L	61	7.63	4.82	5.38	5.30	5.03	5.52
Cl mg/L	61	8.44	4.85	7.02	7.27	6.60	7.65
Mg mg/L	61	9.50	8.26	8.73	8.70	8.56	8.90
K mg/L	61	1.02	0.77	0.94	0.94	0.90	0.98
Ca mg/L	61	52.78	33.34	45.54	47.20	42.32	49.22
DOC mg/L	43	6.94	2.04	3.45	3.26	2.61	3.85
POC mg/L	6	1.8	0.6	1.1	1.03	-	-

Table A1. Statistical indexes for the hydrochemical analysis in water samples of Lake Pusiano taken during 2010.

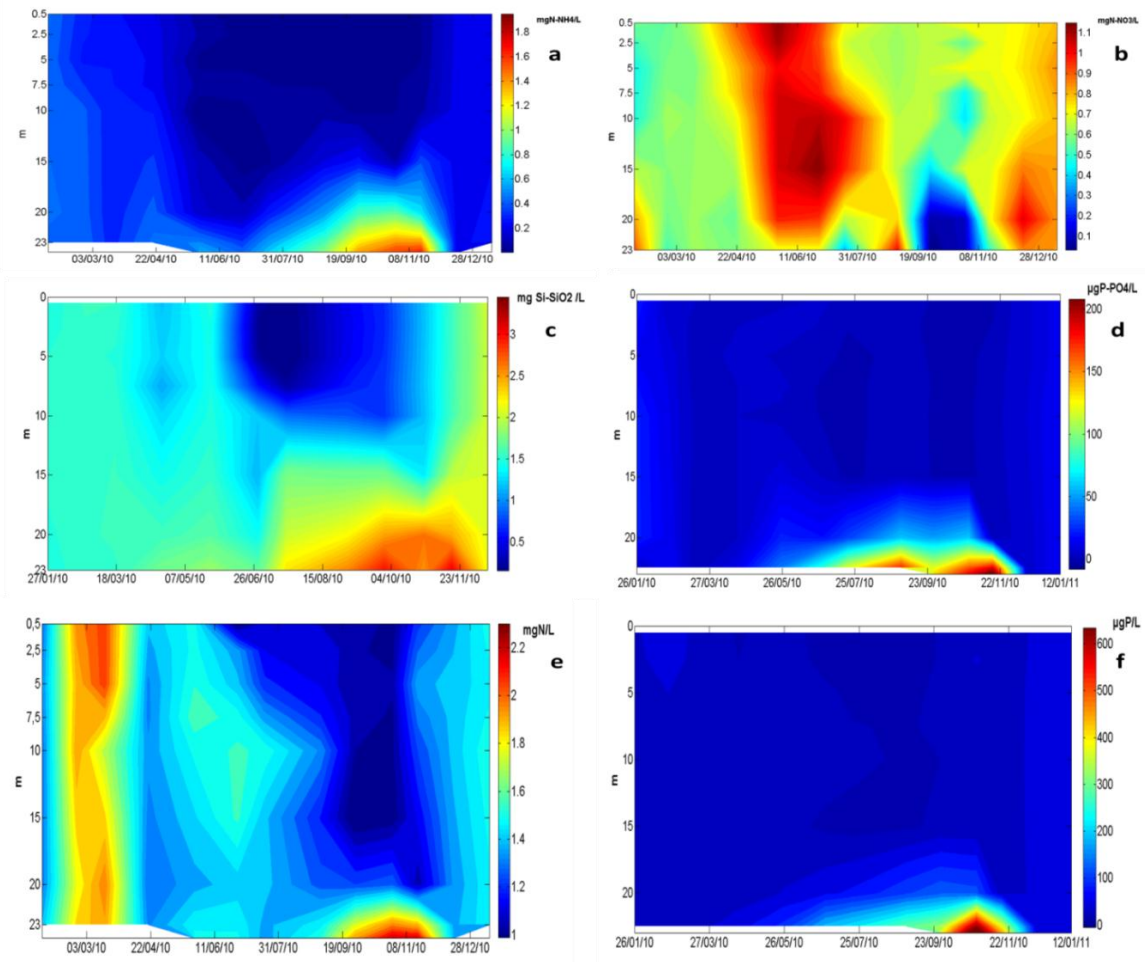

Figure 1A. Lake Pusiano seasonal evolution of nutrients (as linear interpolation of monthly values measured at the maximum depth ST6 during 2010) for: a) ammonium (mg N-NH_4 L^{-1}); b) nitrate (mg N-NO_3 L^{-1}); c) silica (mg Si-SiO_2 L^{-1}); d) orthophosphate (µg P-PO_4 L^{-1}); e) total nitrogen (mg N L^{-1}); f) total phosphorus (µg P L^{-1}). It was used to initialize the nutrient levels in CAEDYM model and to assess them along the simulations.

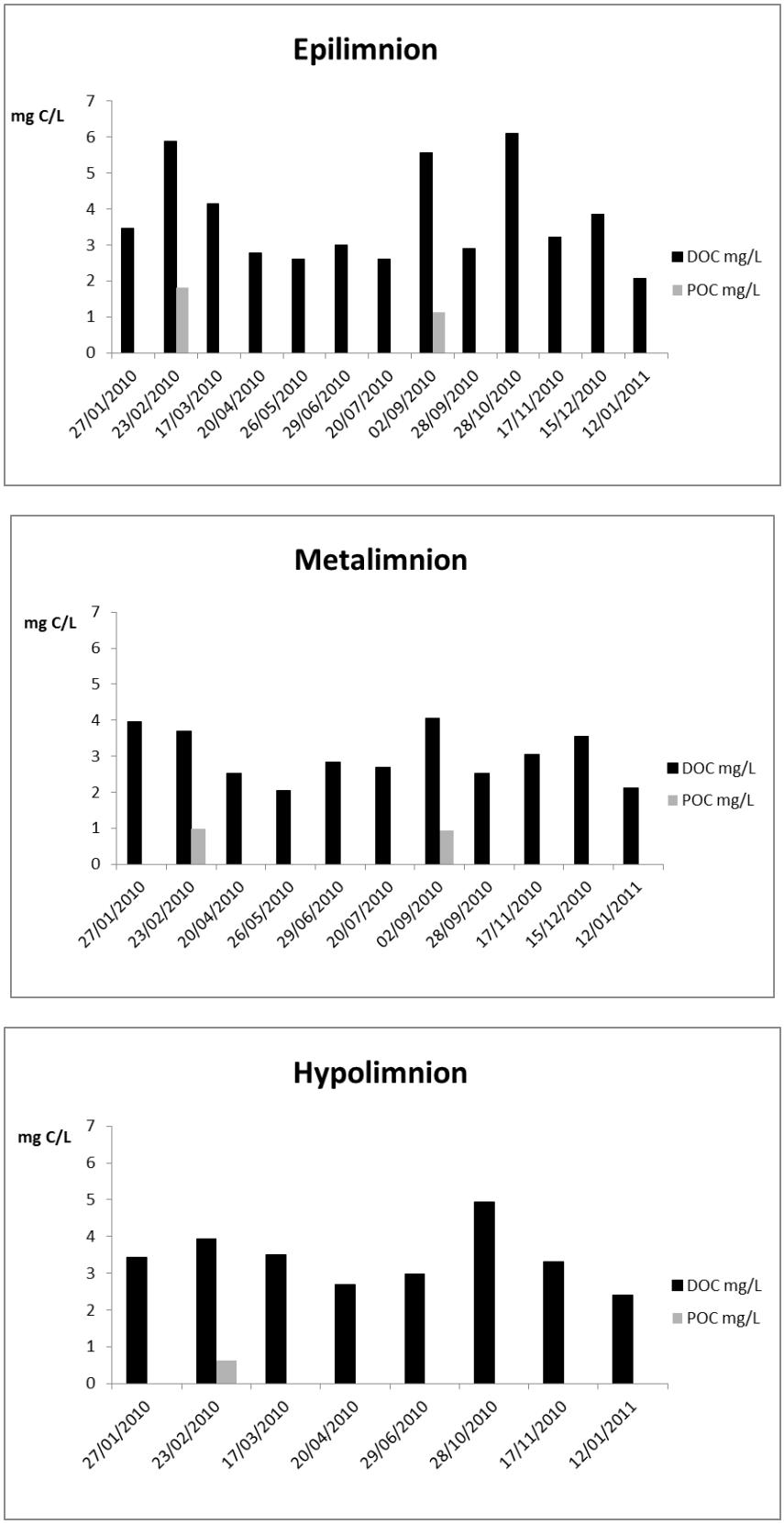

Figure 2A. Lake Pusiano seasonal evolution of carbon, as monthly concentrations of Dissolved Organic Carbon (DOC) and Particulate Organic Carbon (POC) measured at

the maximum depth (ST6) during the water sampling in 2010 for: epilimnion, metalimnion and hypolimnion. POC content was determined only for lake circulation (23rd February) and maximum stratification (2nd September). It was used to initialize the carbon level in CAEDYM model and to assess it along the simulation.

7.1.2 Phytoplankton

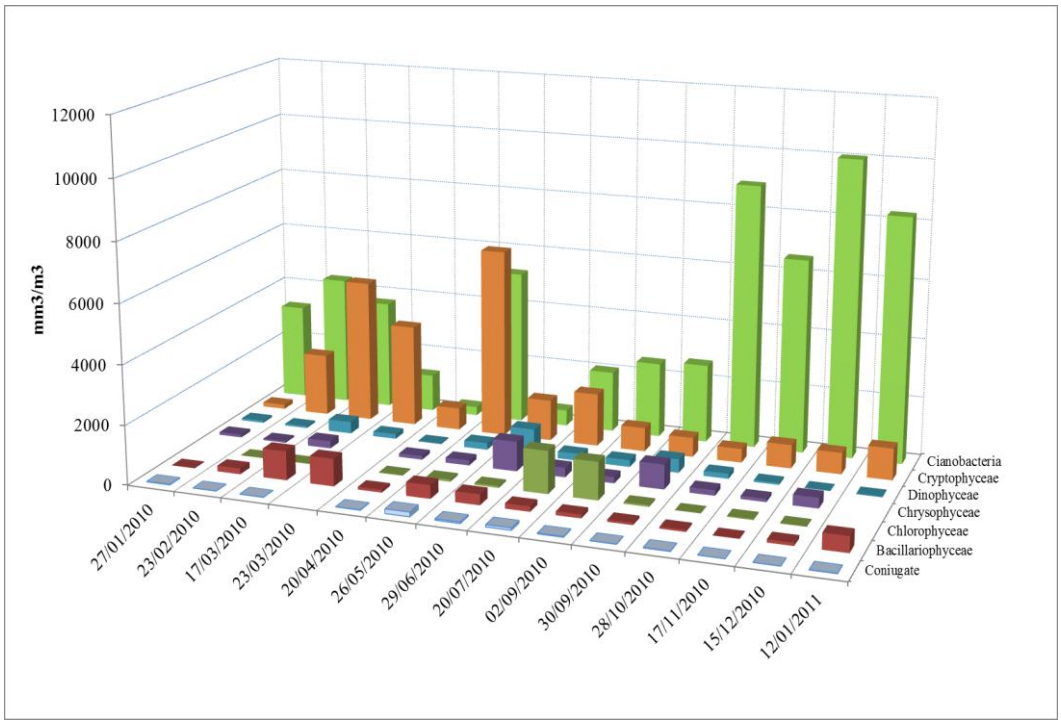

Figure 3A. Lake Pusiano monthly evolution of phytoplankton, as the biovolume (mm^3/m^3) of the main taxonomic groups in the water column, by cell enumeration microscopy of the samples taken at the maximum depth (ST6).

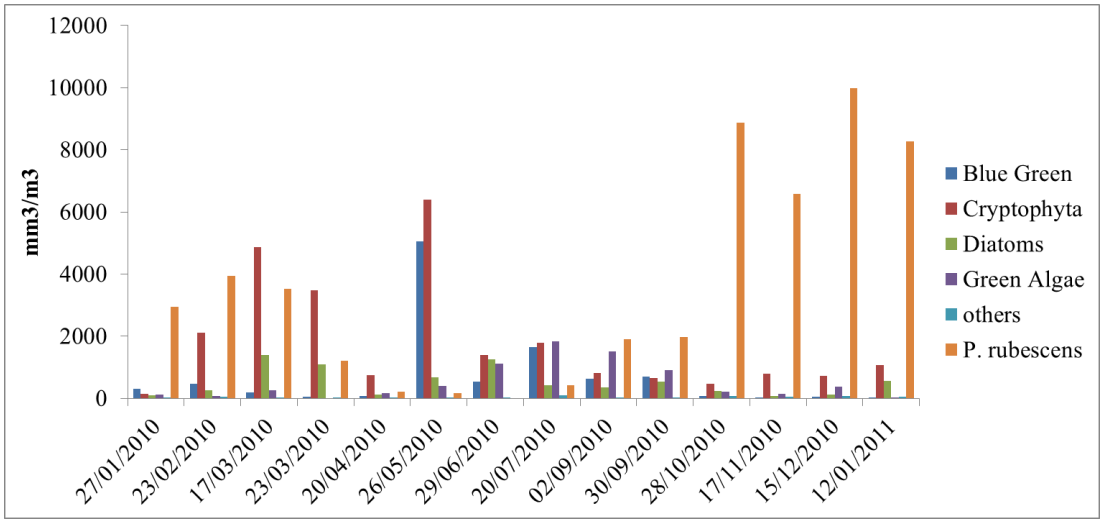

Figure 4A. Lake Pusiano monthly evolution of phytoplankton, as the biovolume (mm^3/m^3) of the main spectral groups in the water column, evaluated by cell enumeration of the samples taken at the maximum depth (ST6). It was used to calibrate the spectral groups of the FluoroProbe for four the dominant taxonomic groups.

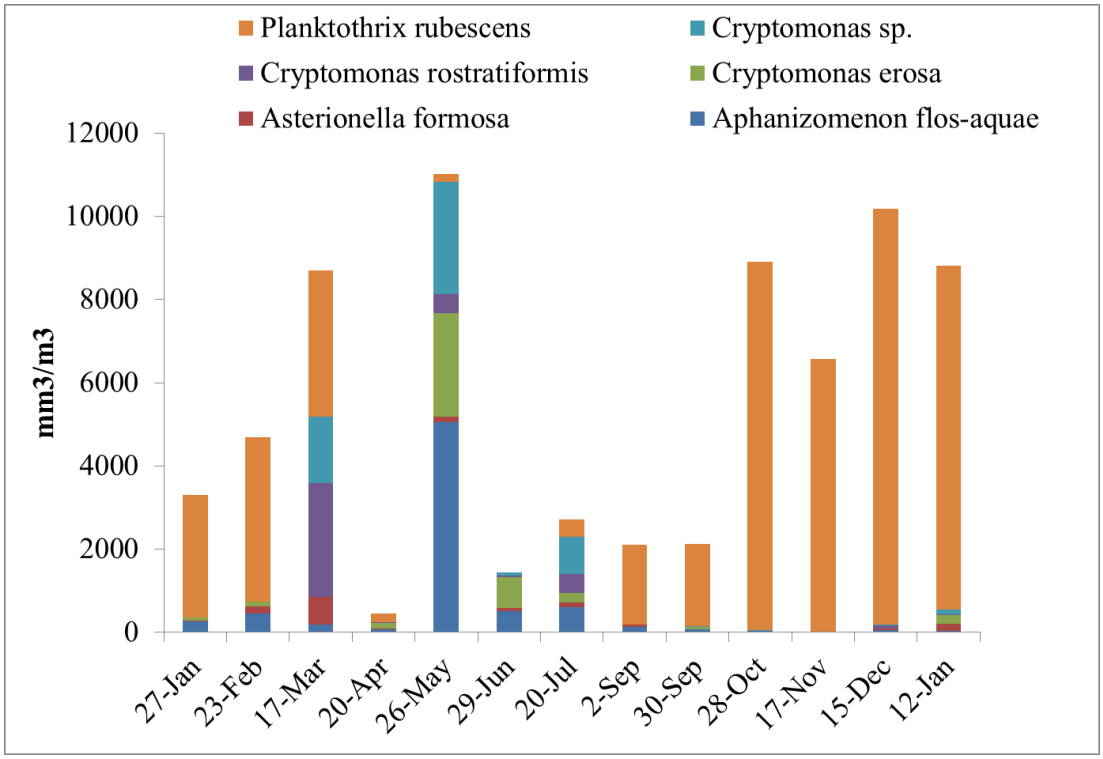

Figure 5A. Lake Pusiano monthly evolution of phytoplankton, as the biovolume (mm^3/m^3) of the key-species in the water column, by cell enumeration of the samples taken at the maximum depth (ST6). It was used to determine the key-species and parameterize the three algae groups in the CAEDYM model.

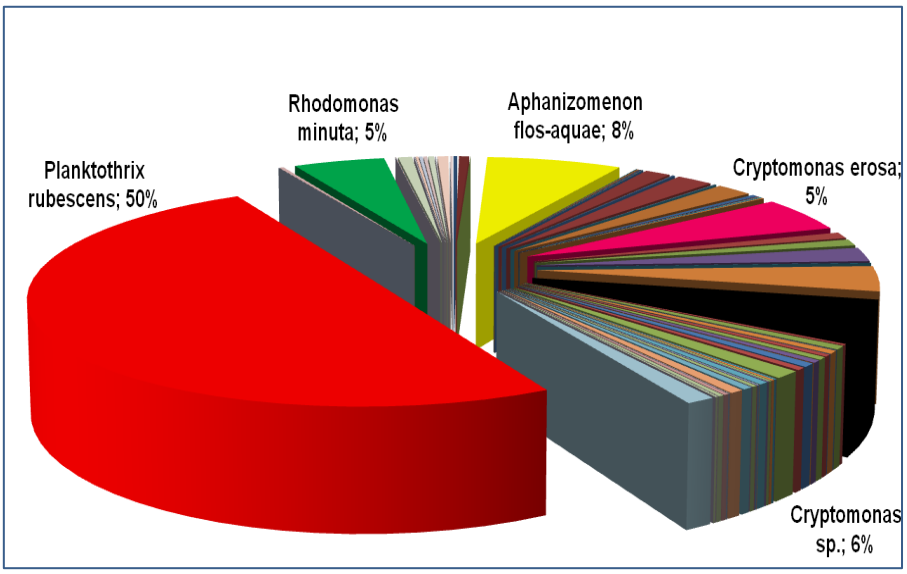

Figure 6A. Lake Pusiano total annual biomass of phytoplankton, as percentage of the species by cell enumeration of the samples taken at the maximum depth (ST6).

7.1.3 Determination of *P. rubescens* potential toxicity

Date	Lake depth	Microcystin (type)	µg/L
27/01/2010	0.5	Dm-MC-RR	0.70
	10	Dm-MC-RR	0.80
23/02/2010	0.5	Dm-MC-RR	0.20
	10	Dm-MC-RR	0.40
17/03/2010	0.5	Dm-MC-RR	0.27
		MC-LR	0.13
	2	Dm-MC-RR	0.24
		MC-LR	0.13
28/10/2010	2.5	Dm-MC-RR	2.59
		Dm-MC-LR	0.31
	5	Dm-MC-RR	2.37
		Dm-MC-LR	0.23
	10	Dm-MC-RR	2.35
		Dm-MC-LR	0.31
17/11/2010	0.5	Dm-MC-RR	3.99
		Dm-MC-LR	0.74
	5	Dm-MC-RR	4.08
		Dm-MC-LR	0.76
	10	Dm-MC-RR	4.23
		Dm-MC-LR	0.90
15/12/2010	5	Dm-MC-RR	1.27
		Dm-MC-LR	0.34
	10	Dm-MC-RR	1.04
		Dm-MC-LR	0.29
	20	Dm-MC-RR	1.54
		Dm-MC-LR	0.43
12/01/2011	0.5	Dm-MC-RR	1.50
		Dm-MC-LR	0.27
	5	Dm-MC-RR	1.30
		Dm-MC-LR	0.24
	10	Dm-MC-RR	1.38
		Dm-MC-LR	0.24

Table A2. The microcystin concentration detected at different depth in Lake Pusiano, during crucial peak of chlorophyll in 2010. The Dimethyl-Microcystin-RR (Dm-MC-RR) and Dimethyl-Microcystin-LR (Dm-MC-LR) are the main kind of endocellular microcystin revealed in laboratory by the HPLC-DAD.

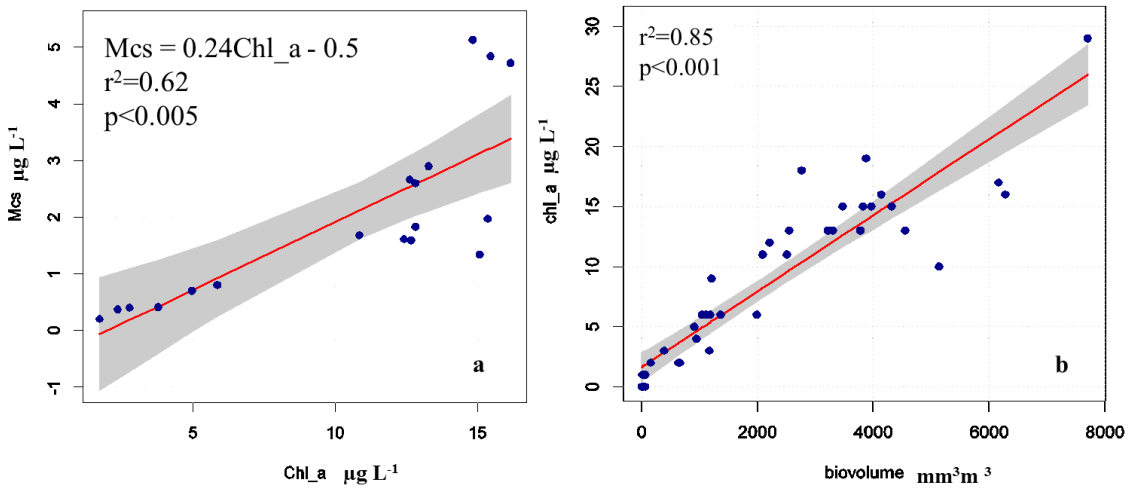

Figure 7A. Linear regression between **a)** total microcystins and *P. rubescens* as Chl-*a* concentrations measured by FP **b)** *P. rubescens* as Chl-*a* concentrations measured by FP and the relative biovolume by cell counting, taken at different depths in 2010. Confidence interval (95%) corresponds to grey area. These data provided the fingerprint for *P. rubescens.*

7.1.4 Zooplankton

Rotifers	Cladocerans
Asplanchna priodonta Gosse, 1850	*Daphnia hyalina* Leydig, 1860
Keratella cochlearis (Gosse, 1851)	*Ceriodaphnia quadrangula-hamata* (O.F.M. 1890)
K. quadrata (O.F.M. 1786)	*Eubosmina longispina* (Leydig, 1860)
Kellicottia longispina (Kellicott, 1879)	*Bosmina longirostris* (O.F.M., 1785)
Polyarthra vulgaris-dolichoptera Ruttner-Kolisko, 1974	*Chydorus sphaericus* (O.F.M., 1785)
Synchaeta pectinata Ehrenberg , 1832	*Leptodora kindtii* (Focke, 1844)
Filinia terminalis (Plate, 1886)	*Diaphanosoma brachyurum* (Lievin, 1848)
F. longiseta (Ehrb. 1834)	*Alona affinis* (Leydig, 1860)
Conochilus unicornis (Rousselet, 1892)	*Pleuroxus truncatus* (O.F.M., 1785)
Brachionus sp.	
Lecane sp.	**Copepods**
Platyias quadricornis (Ehrenberg, 1832)	*Mesocyclops leuckarti* (Klaus, 1857)
Ascomorpha saltans Bartsch, 1870	*Thermocyclops crassus* (Fischer, 1853)
Trichocerca chattoni (de Beauchamp, 1907)	*Cyclops abyssorum* Sars, 1863
	Eudiaptomus gracilis (Kiefer, 1978)

Table A3. List of zooplanktonic taxa detected in Lake Pusiano during the four seasonal surveys (30th March, 16th June, 10th September, 14th December 2010). It was used to parameterize the dominant herbivore species in the CAEDYM model.

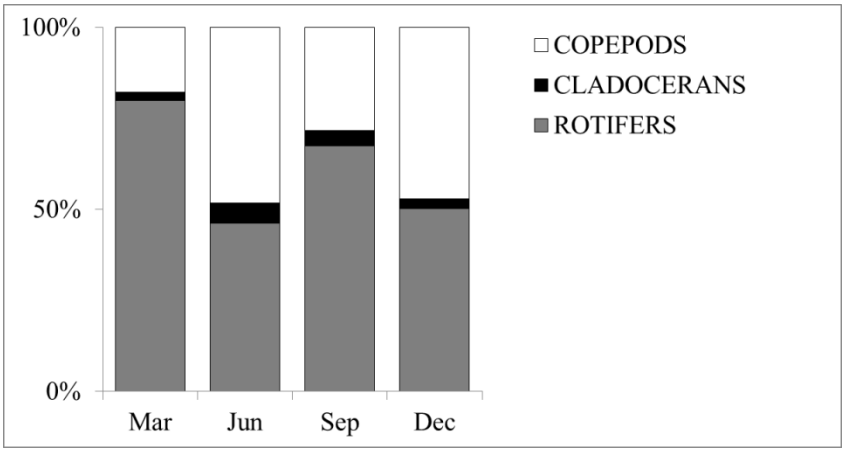

Figure 8A. Percentages of the three main zooplanktonic groups by the annual (2010) survey in Lake Pusiano. It was used to initialize the zooplankton model (CAEDYM).

7.1.5 Lake profiling with multiparametric and fluorometric probes

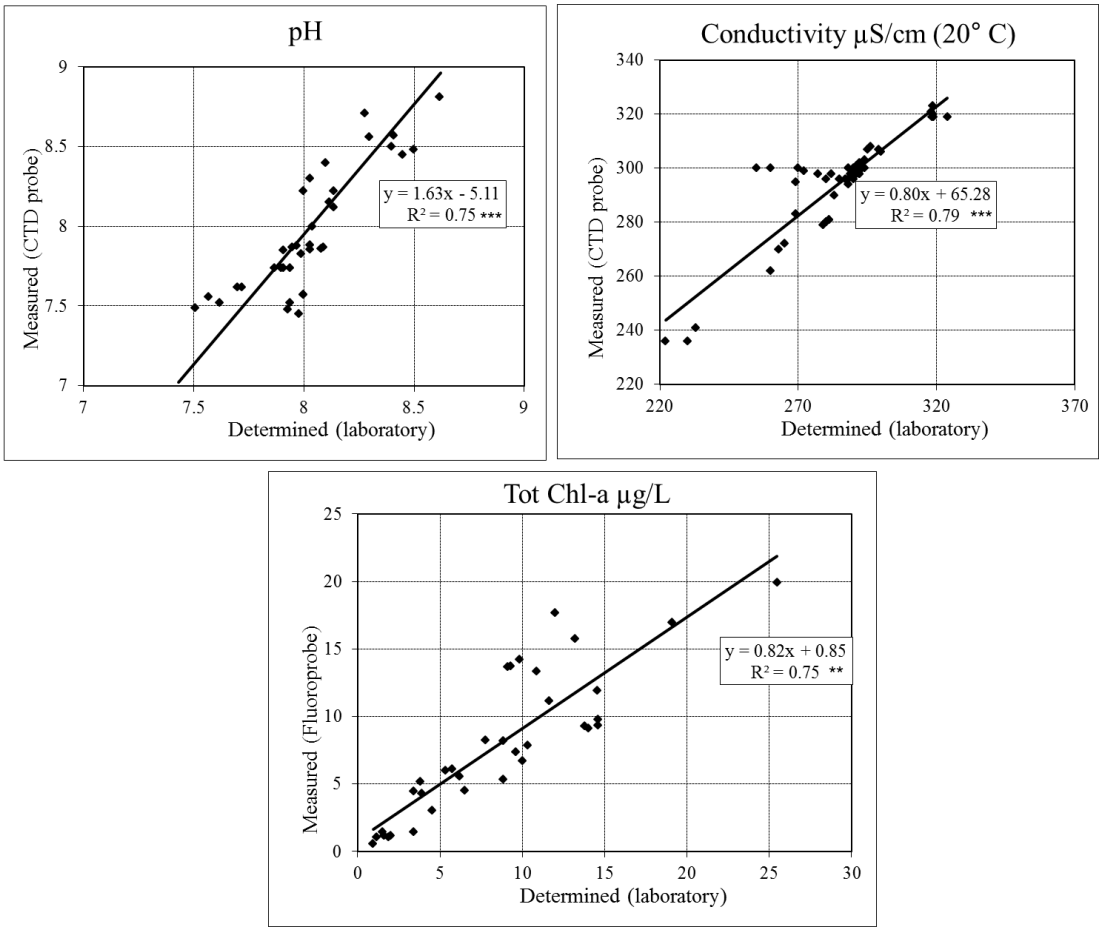

Figure 9A. Linear regressions between measured values (by CTD or fluorimetric probe) and the relative analytic determinations for pH, conductivity and total chlorophyll-a. (***) is for p-value < 0.005 and (**) for p-value < 0.01. It was used to calibrate both

the probes profiling all the lake stations and to get a three-dimensional description of variability along the time and the space axes.

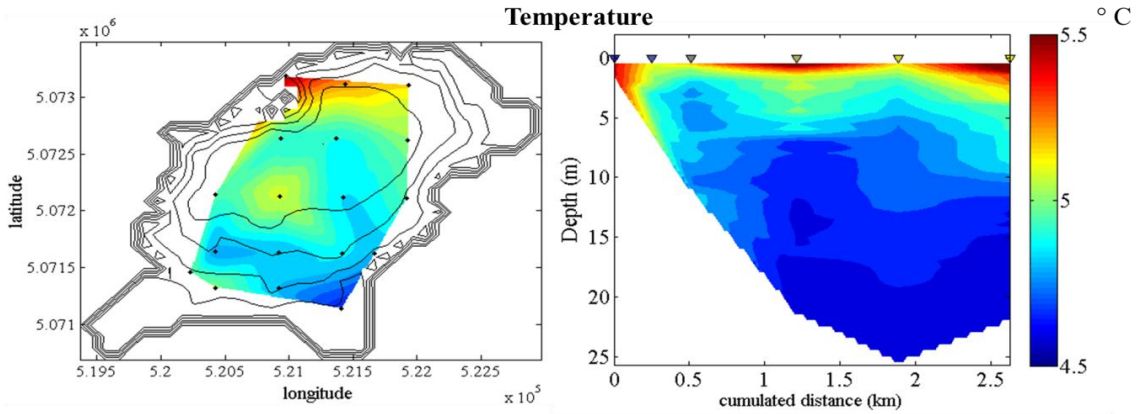
Temperature
° C
x 10^6
5.073
5.0725
5.072
5.0715
5.071
latitude
5.195
5.2
5.205
5.21
5.215
5.22
5.225
longitude
x 10^5
Depth (m)
0
5
10
15
20
25
0
0.5
1
1.5
2
2.5
cumulated distance (km)
5.5
5
4.5

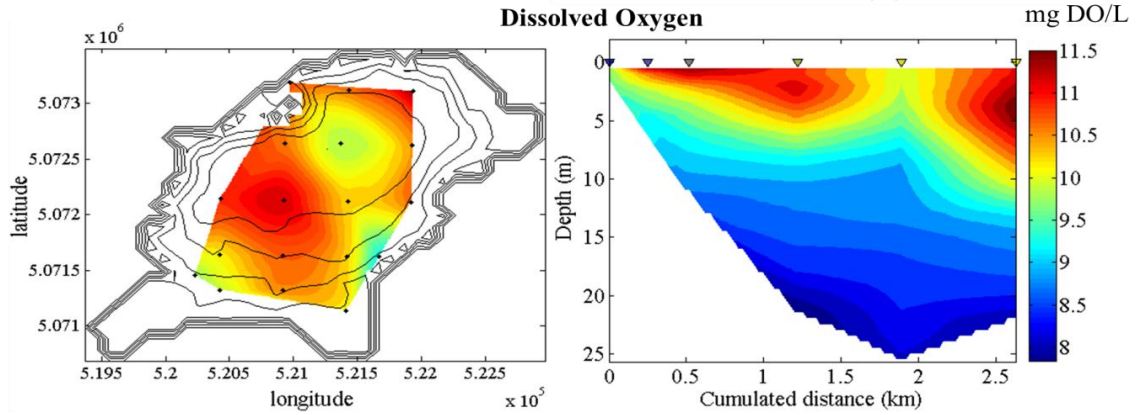
Dissolved Oxygen
mg DO/L
x 10^6
5.073
5.0725
5.072
5.0715
5.071
latitude
5.195
5.2
5.205
5.21
5.215
5.22
5.225
longitude
x 10^5
Depth (m)
0
5
10
15
20
25
0
0.5
1
1.5
2
2.5
Cumulated distance (km)
11.5
11
10.5
10
9.5
9
8.5
8

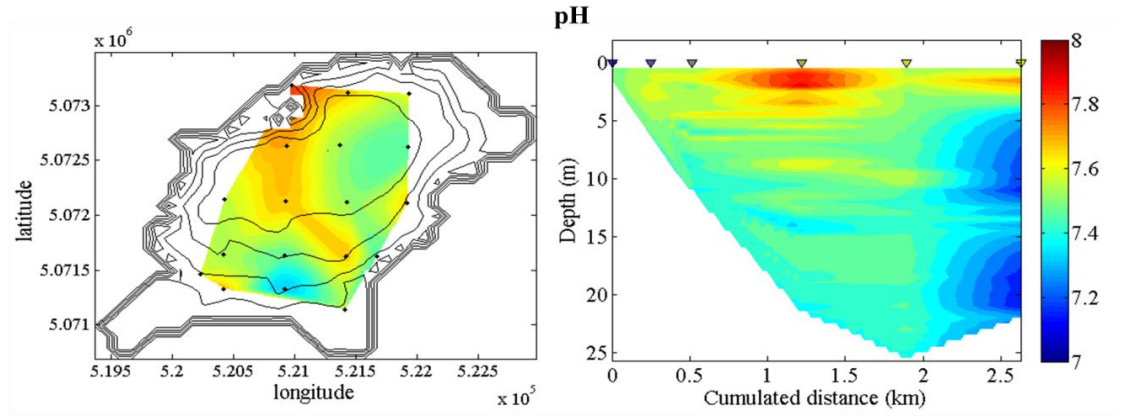
pH
x 10^6
5.073
5.0725
5.072
5.0715
5.071
latitude
5.195
5.2
5.205
5.21
5.215
5.22
5.225
longitude
x 10^5
Depth (m)
0
5
10
15
20
25
0
0.5
1
1.5
2
2.5
Cumulated distance (km)
8
7.8
7.6
7.4
7.2
7

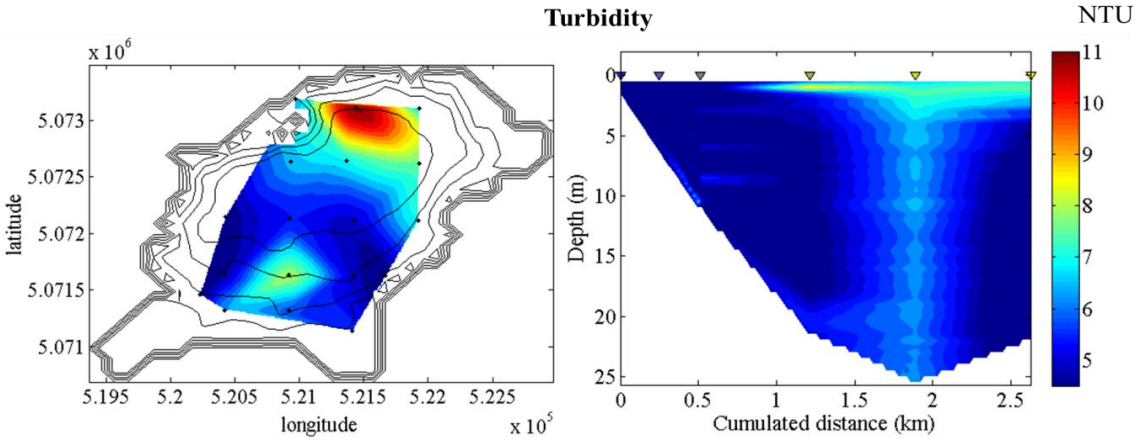
Turbidity
NTU
x 10^6
5.073
5.0725
5.072
5.0715
5.071
latitude
5.195
5.2
5.205
5.21
5.215
5.22
5.225
longitude
x 10^5
Depth (m)
0
5
10
15
20
25
0
0.5
1
1.5
2
2.5
Cumulated distance (km)
11
10
9
8
7
6
5

Figure 10A. Surface (the section cut is at 2 meters depth) and vertical (the section cut is on SW-NE axis: ST16c; ST13; ST10; ST6; ST2; refer to the map in Figure 2) profiles of temperature, dissolved oxygen, pH and turbidity, measured by the CTD probe on the 23rd February for each station and depth of the lake and used to initialize the three-dimensional model (ELCD).

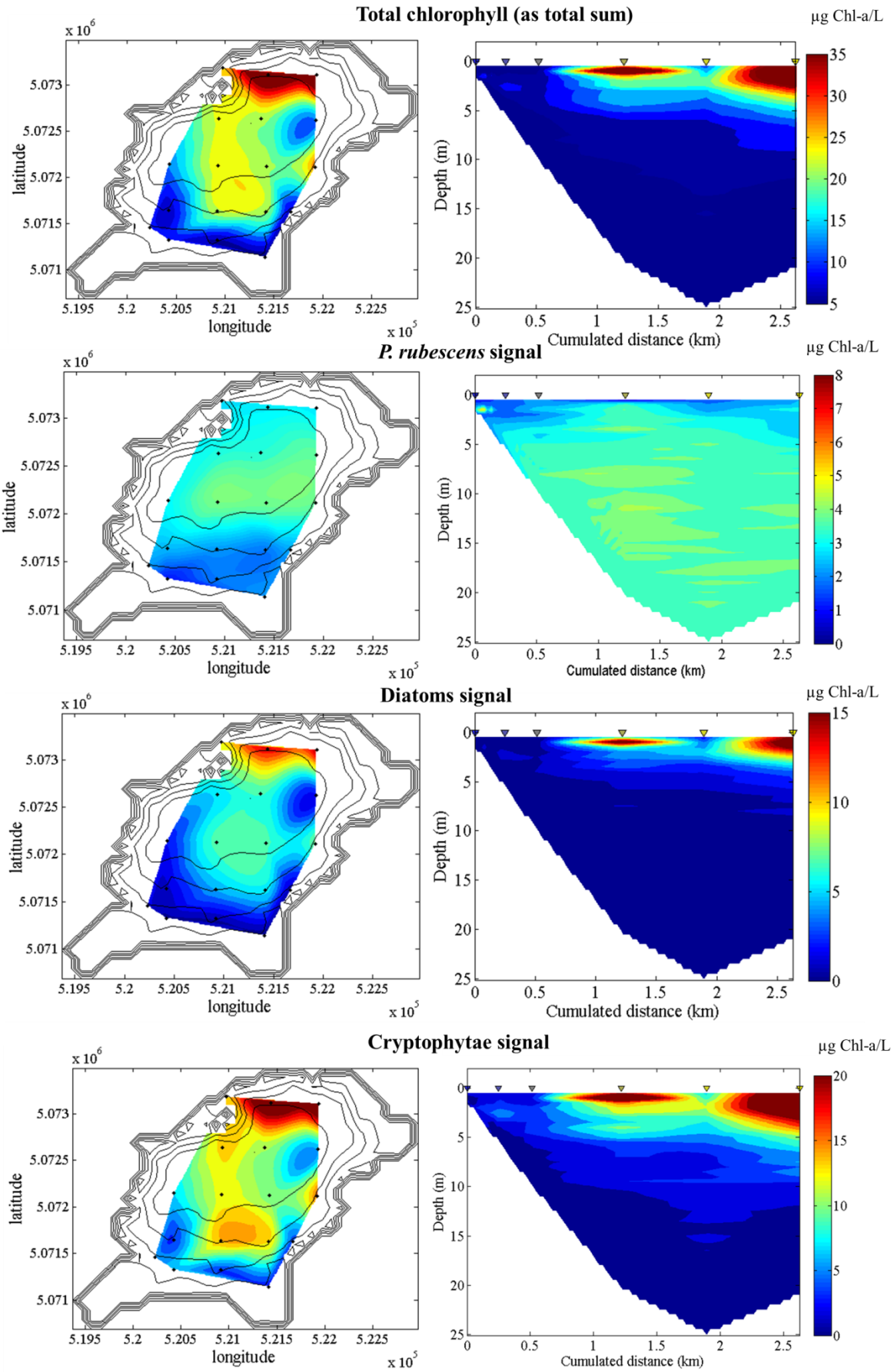
Total chlorophyll (as total sum)
µg Chl-a/L
x 10^6
latitude
longitude
x 10^5
Depth (m)
Cumulated distance (km)
P. rubescens signal
µg Chl-a/L
Diatoms signal
µg Chl-a/L
Cryptophytae signal
µg Chl-a/L

Figure 11A. Surface (the section cut is at 2 meters depth) and vertical (the section cut is on SW-NE axis: ST16c; ST13; ST10; ST6; ST2; refer to the map in Figure 2) profiles of the chlorophyll-a concentration measured by the FluoroProbe on the 23rd February for each station and depth of the lake and used to initialize the three-dimensional model (ELCD). The spectral response (or signal) is associated to the total concentration (as sum of all), *P. rubescens*, Diatoms and Cryptophytae.

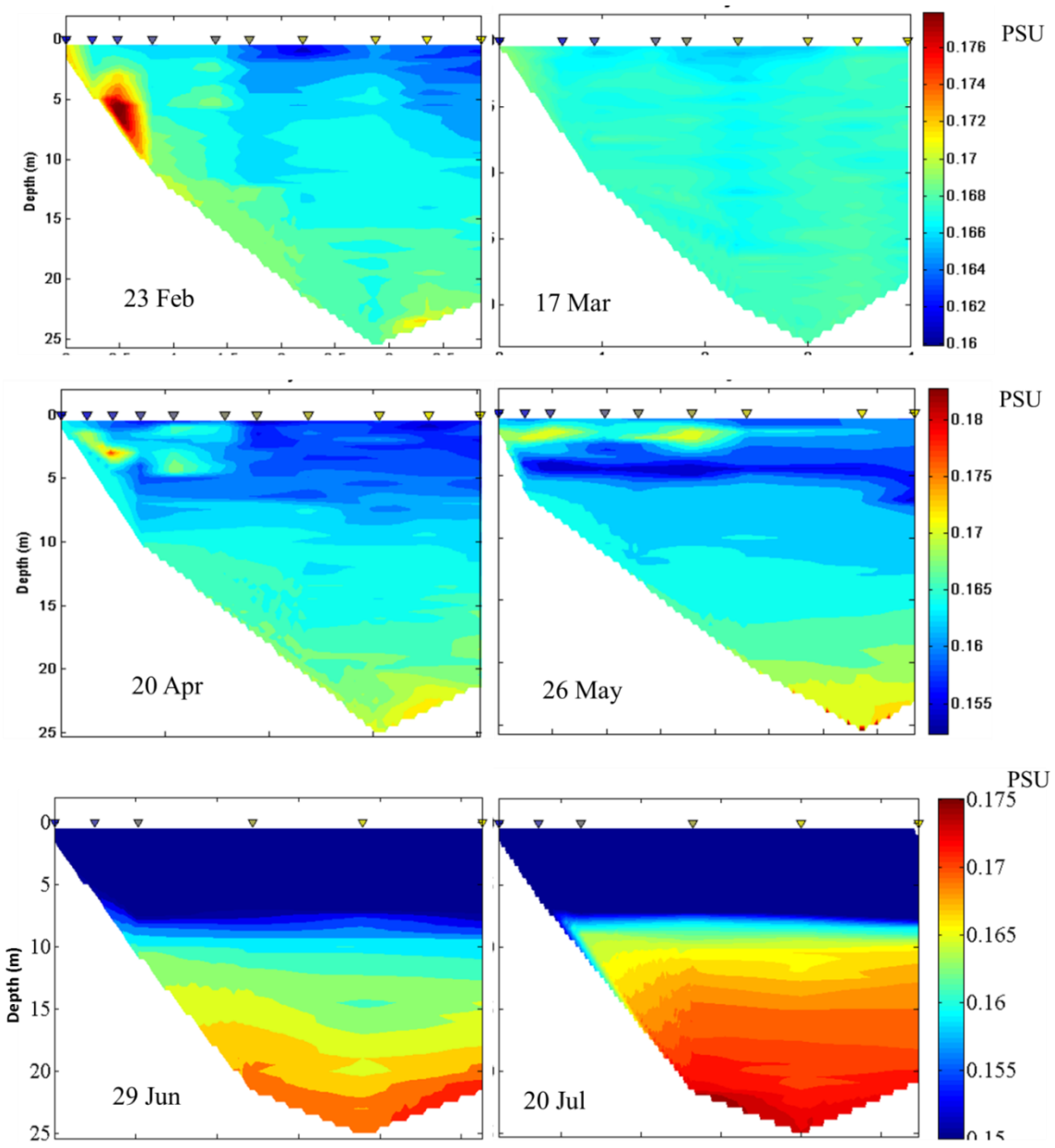

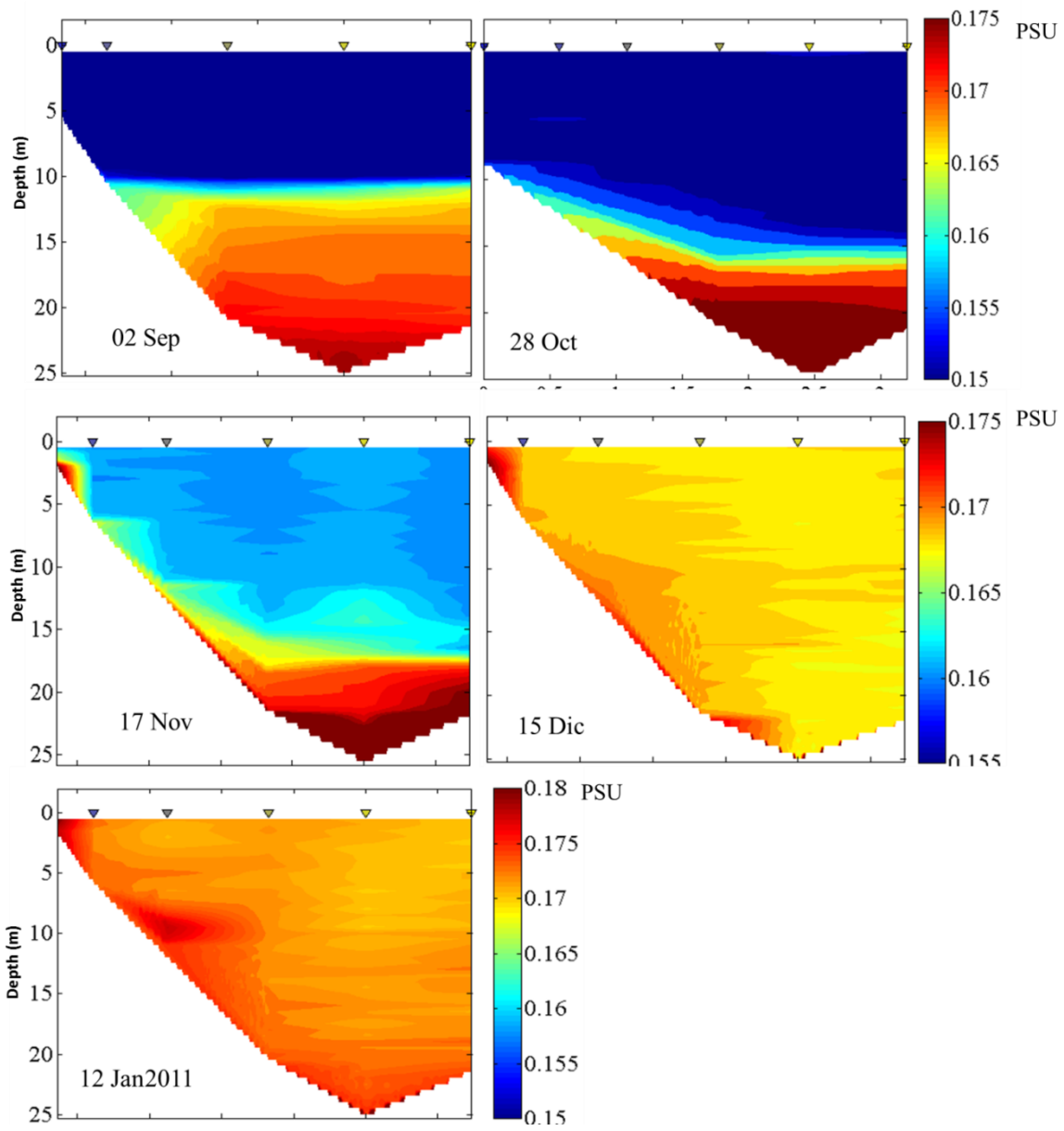

Figure 12A. Vertical (section cut is on SW-NE axis: ST16c; ST13; ST10; ST6; ST2; refer to the map in Figure 2) profiles of salinity measured on each sampling date and used to check the river entrance plume and the lake patterns during the simulation of the three-dimensional model (ELCD).

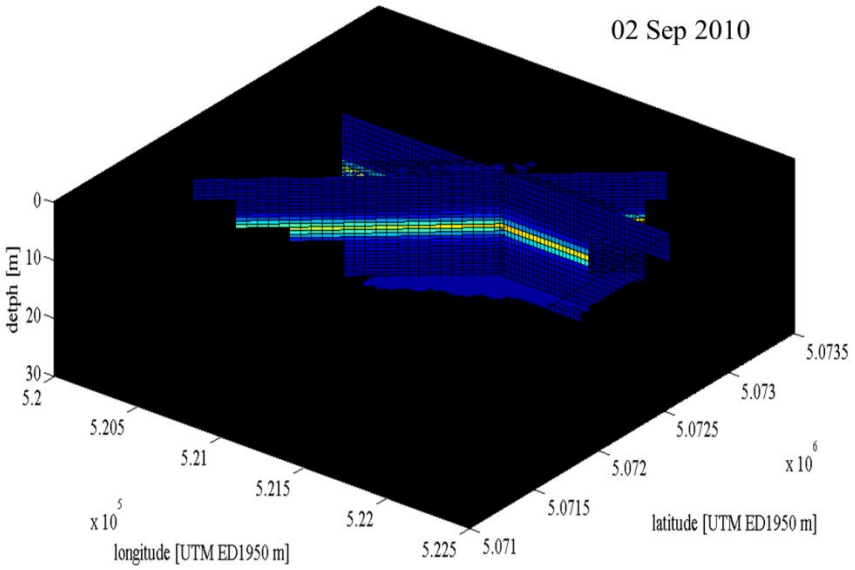
02 Sep 2010
detph [m]
0
10
20
30
5.2
5.205
5.21
5.215
5.22
5.225
x 10^5
longitude [UTM ED1950 m]
5.071
5.0715
5.072
5.0725
5.073
5.0735
x 10^6
latitude [UTM ED1950 m]

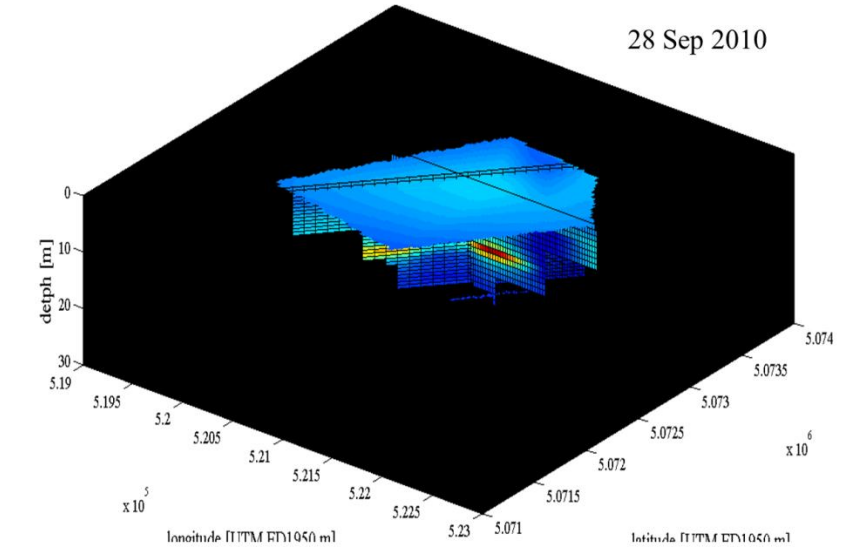
28 Sep 2010
detph [m]
0
10
20
30
5.19
5.195
5.2
5.205
5.21
5.215
5.22
5.225
5.23
x 10^5
5.071
5.0715
5.072
5.0725
5.073
5.0735
5.074
x 10^6

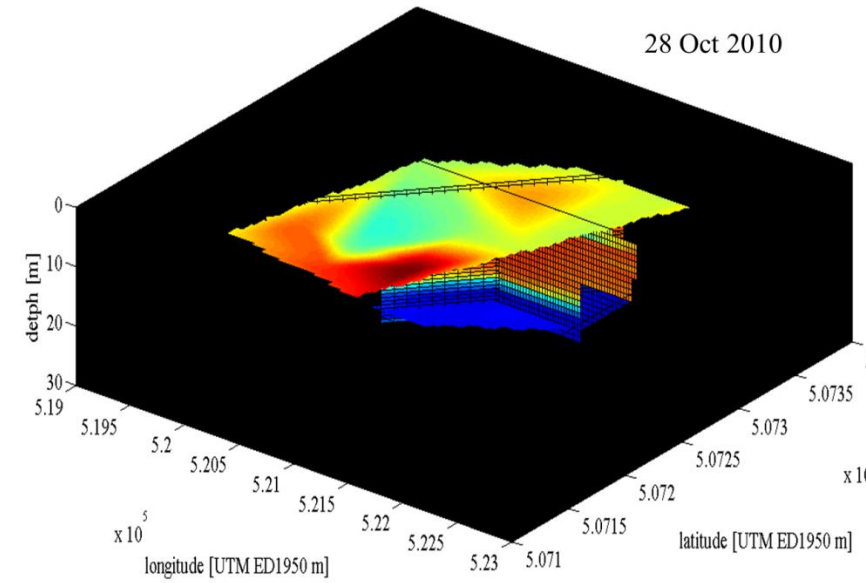
28 Oct 2010
detph [m]
0
10
20
30
5.19
5.195
5.2
5.205
5.21
5.215
5.22
5.225
5.23
x 10^5
longitude [UTM ED1950 m]
5.071
5.0715
5.072
5.0725
5.073
5.0735
5.074
x 10^6
latitude [UTM ED1950 m]

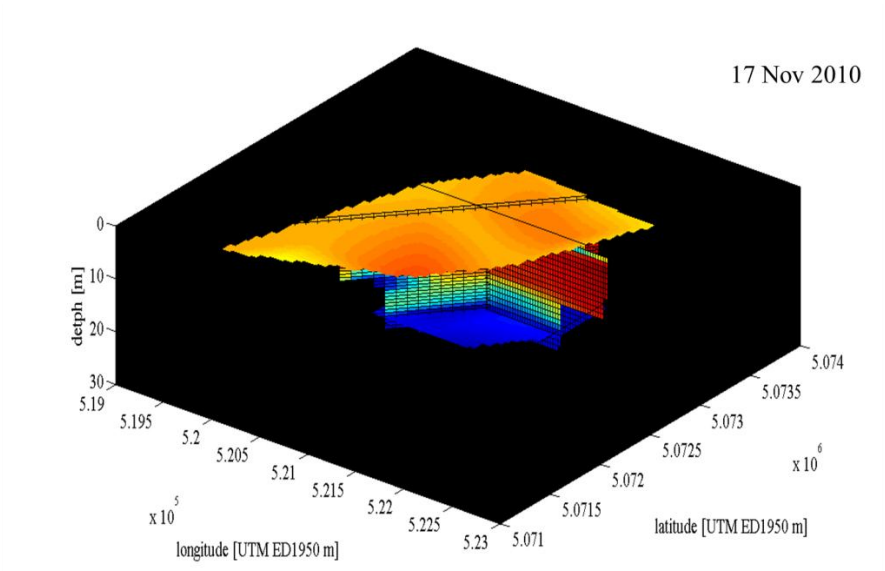
17 Nov 2010
detph [m]
0
10
20
30
5.19
5.195
5.2
5.205
5.21
5.215
5.22
5.225
5.23
x 10^5
longitude [UTM ED1950 m]
5.071
5.0715
5.072
5.0725
5.073
5.0735
5.074
x 10^6
latitude [UTM ED1950 m]

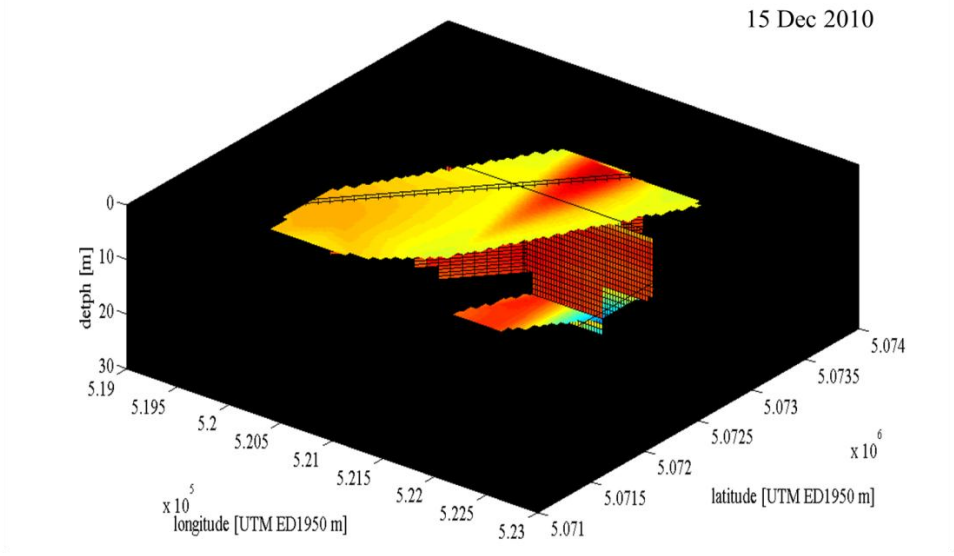
15 Dec 2010
detph [m]
0
10
20
30
5.19
5.195
5.2
5.205
5.21
5.215
5.22
5.225
5.23
x 10^5
longitude [UTM ED1950 m]
5.071
5.0715
5.072
5.0725
5.073
5.0735
5.074
x 10^6
latitude [UTM ED1950 m]

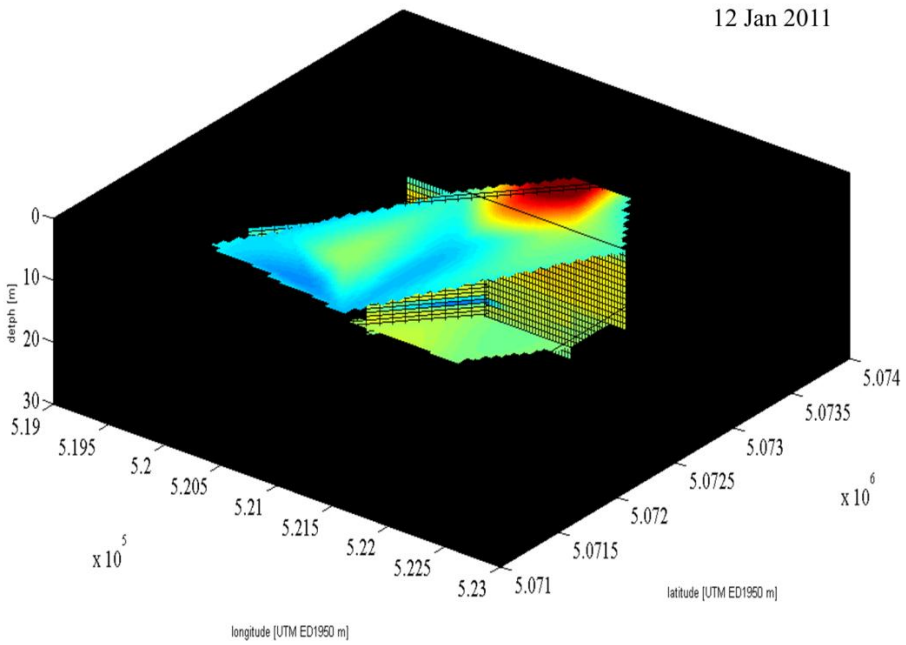
12 Jan 2011
detph [m]
0
10
20
30
5.19
5.195
5.2
5.205
5.21
5.215
5.22
5.225
5.23
x 10^5
longitude [UTM ED1950 m]
5.071
5.0715
5.072
5.0725
5.073
5.0735
5.074
x 10^6
latitude [UTM ED1950 m]

Figure 13A. Three-dimensional interpolations (Matlab® software) of all the measured profiles, here only to show *P. rubescens* spatial and temporal evolution during the seasonal growth, from the metalimnetic niche formation at the end of the summer, through the bloom in autumn up to the cells deterioration in late winter. This was used to check and calibrate the *P. rubescens* behaviour during high-frequency simulation of the three-dimensional model (ELCD).

7.1.6 Sediment composition

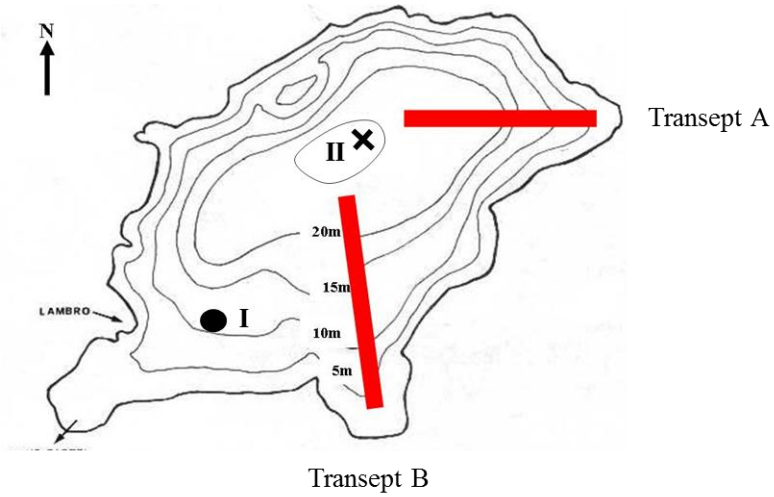

Figure 14A. Lake Pusiano map showing the two transept for the sediment sampling, the maximum depth station (II) and the middle-depth (Lambro River closest) station (I). Sediment transepts were characterized at the beginning and at the maximum of the thermal stratification (30th March and 7th September, respectively). Furthermore sediment cores were taken on 28th September in the I and II stations to determine the phosphorus content by Psenner Fractionation.

Date	Position	Depth	H_2O	Dry wt.	LOI	CaCO3	CO3
		m	%ww	%dw	%dw	%dw	%dw
30/03/10	Trans A	4.0	78.11	21.89	13.09	59.33	35.55
30/03/10	Trans A	15.0	72.49	27.51	9.63	56.41	33.80
30/03/10	Trans A	22.0	69.32	30.68	9.68	56.89	34.08
30/03/10	Trans B	4.0	46.49	53.51	4.12	33.31	19.96
30/03/10	Trans B	12.0	85.37	14.63	10.29	50.65	30.34
30/03/10	Trans B	20.0	74.73	25.27	9.40	56.52	33.86
30/03/10	**Max. depth X**	24.0	70.09	29.91	9.87	57.70	34.57
07/09/10	Trans A	2.5	72.56	27.44	7.72	74.60	44.69
07/09/10	Trans A	11.0	69.82	30.18	9.09	62.38	37.37
07/09/10	Trans A	23.0	71.68	28.32	9.49	57.25	34.30
07/09/10	Trans B	3.0	47.76	52.24	3.93	31.19	18.69
07/09/10	Trans B	12.0	68.10	31.90	9.81	50.07	30.00
07/09/10	Trans B	20.0	75.55	24.45	9.50	56.19	33.66
07/09/10	**Max. depth X**	24.0	71.87	28.13	9.35	57.52	34.46

Figure 15A. Results for the sediment transepts characterization by water content (as % of wet weight), dry sediment weight (as %), organic matter (Loss On Ignition, as % of dry weight), calcium carbonate (as % of dry weight) and carbonate (as % of dry weight). This was used to calibrate the sediment parameters in the CAEDYM model.

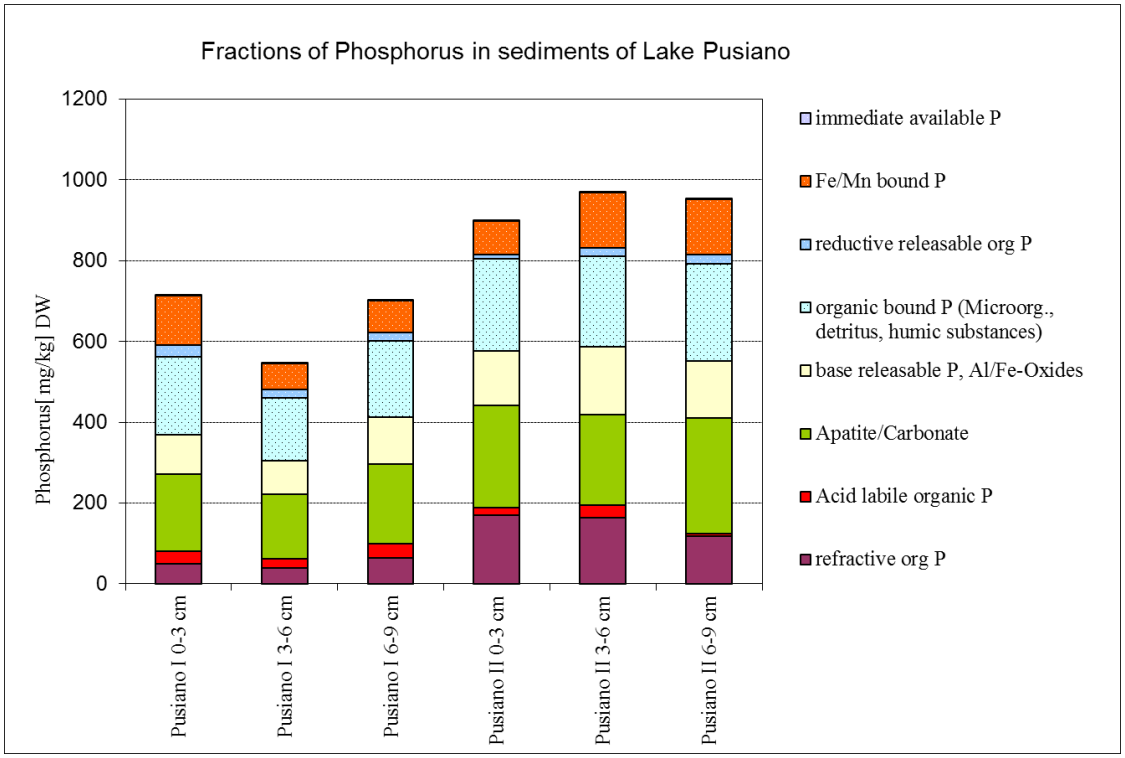

Figure 16A. Phosphorus fractionation (Psenner et al. 1984, modified by Hupfer et al., 2004) of Lake Pusiano sediment. This was used to calibrate the sediment P-content and release rate in the CAEDYM model.

7.2 Metereology

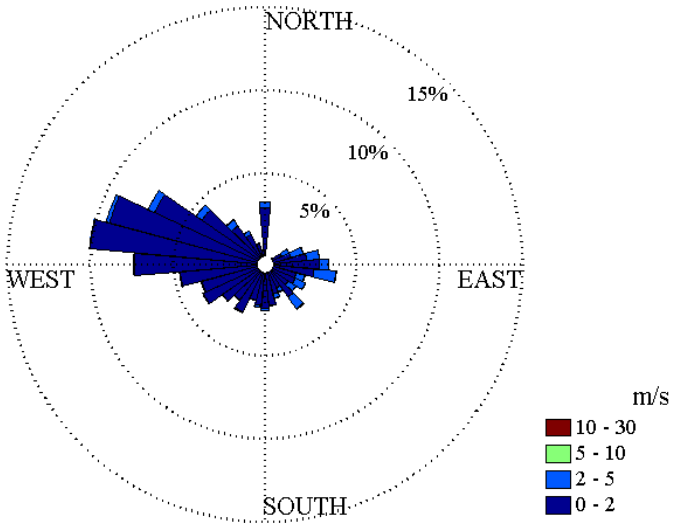

Figure 17A. The wind rose was plotted with the wind speed and direction hourly data collected at the lake meteoreological station (Geretta, refer to map in Figure 2). This was used as metereological input for the simulation with the three-dimensional model (ELCD).

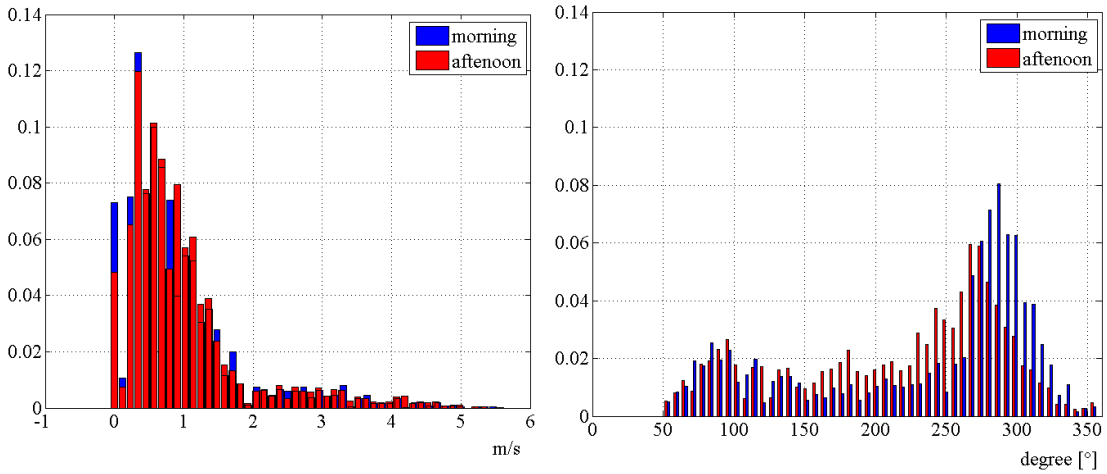

Figure 18A. The wind speed (on the left) and direction (on the right) hourly data are shown as histograms of distribution classes (frequency), aggregated for the morning and the afternoon events.

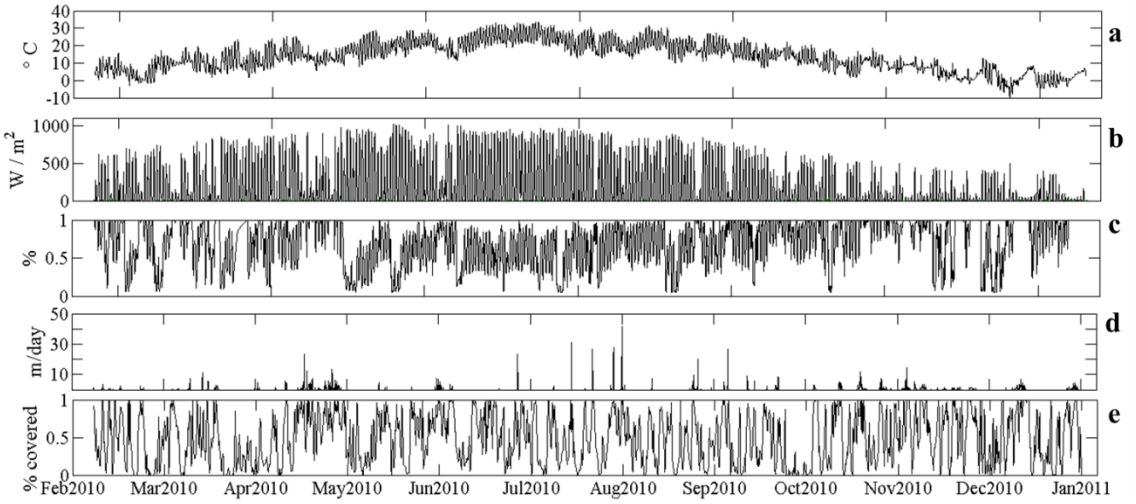

Figure 19A. All the other meteoreological hourly series: a) temperature: b) global solar radiation; c) percentage of humidity; d) rainfall; e) percentage of cloud cover. This was used to force the metereology of the three-dimensional model (ELCD).

7.2.1 Lake physics

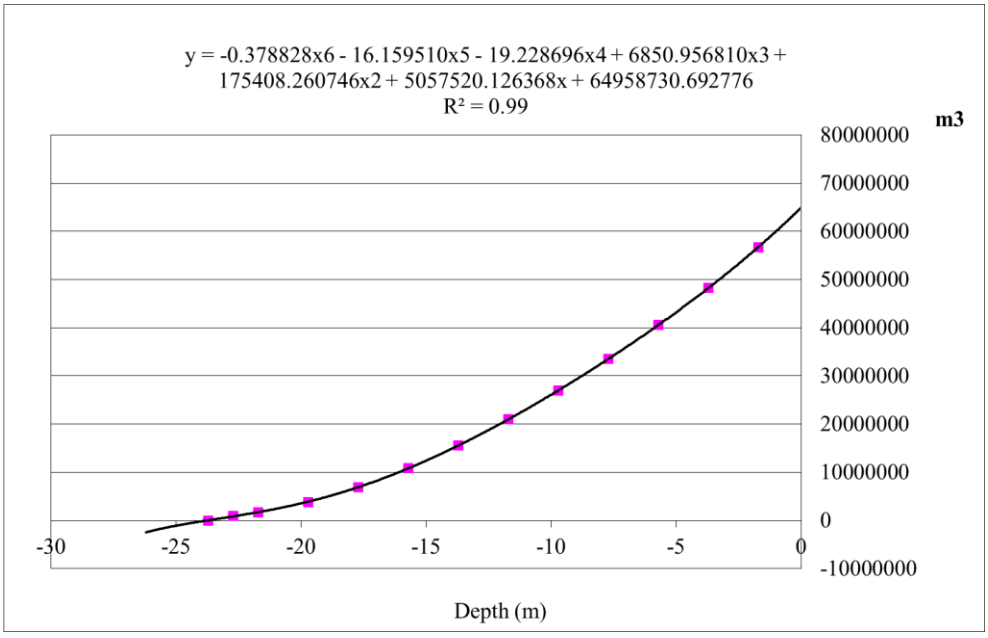

Figure 20A. Lake Pusiano Hypsographic curve of the lake volume by the depth, used to compute the weight averages of such a variables.

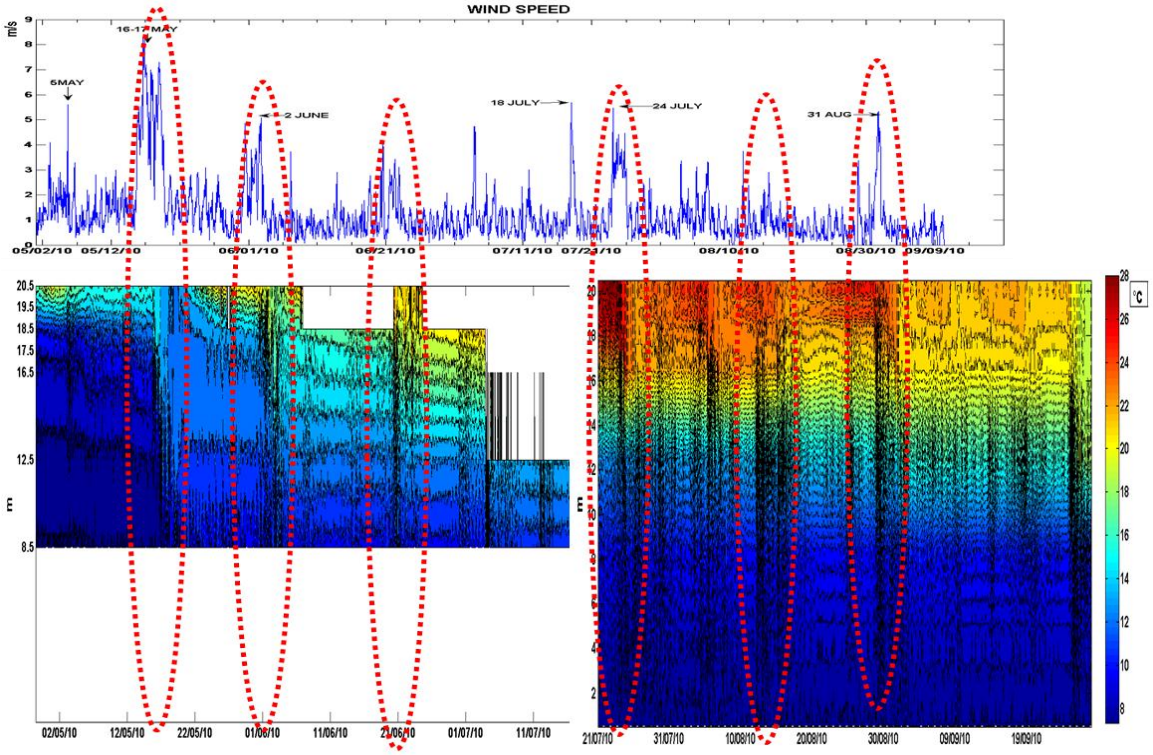

Figure 21A. A visualization of the internal wave activity by the interpolation of the lake temperature measured every 15 minutes by the thermistors chain at each meters of depth from 30th April to 20th September 2010. The wind speed plot is also shown to compare the intensity peaks to the microcirculation patterns occurring in the lake. White in the plot is for lost data. This was compared to the internal wave activity simulated by the three-dimensional model (ELCD).

7.3 Rivers hydrology and water quality

7.3.1 High frequency data analysis

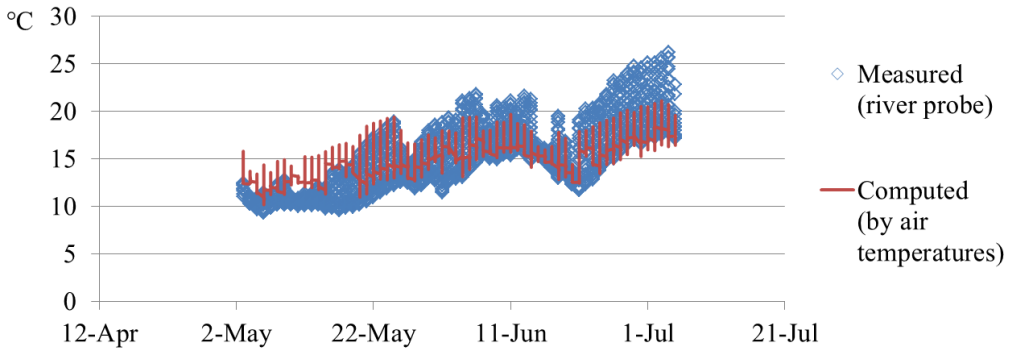

Figure 22A. Lambro River high-frequency (15 minutes) measured temperature (blue dot) by the multiparametric probe sensor that was fixed near the lake entrance, compared to the same series computed by the measured air temperature (red line). This was used both to force the hydrology of the 3D model (ELCD) and to reconstruct the river water temperature for the long term series.

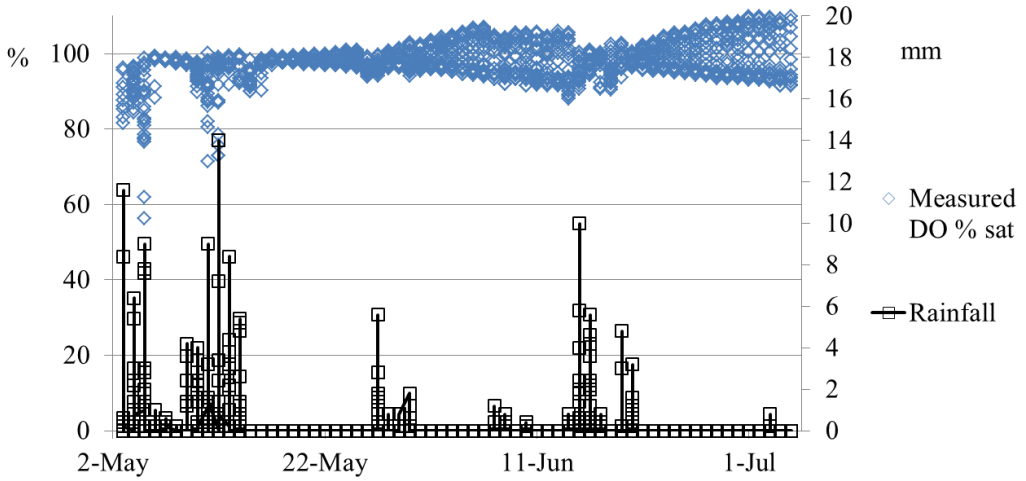

Figure 23A. Lambro River high-frequency (15 minutes) measurements for dissolved oxygen (DO), as % of saturation (blue dot) by the multiparametric probe sensor that was fixed near the lake entrance, compared the measured rainfall (black lines and rings). This was used as input of river water quality forcing the 3D model (ELCD).

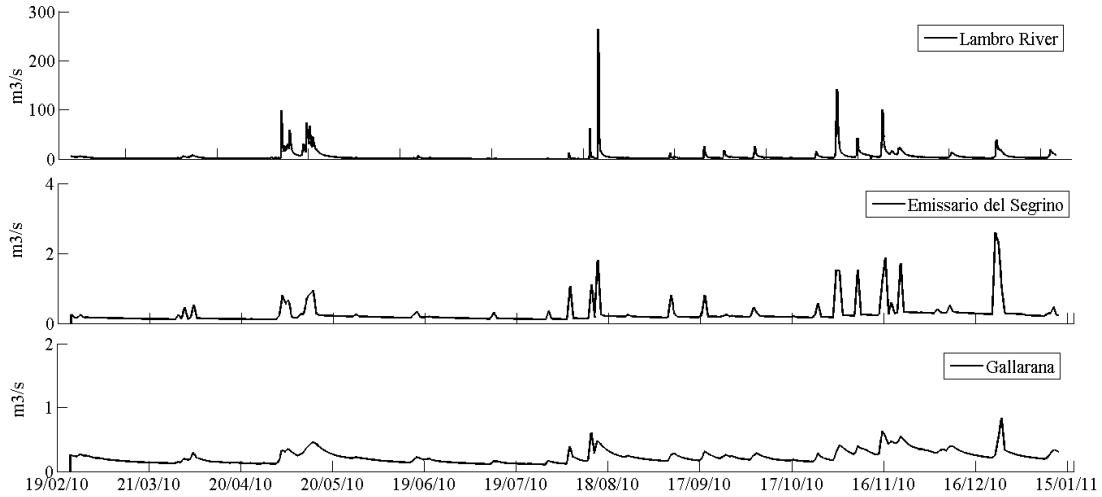

Figure 24A. High-frequency (15 minutes) measured discharge of the three main tributaries to Lake Pusiano, used to prepare the hydrological forcing for the 3D model (ELCD).

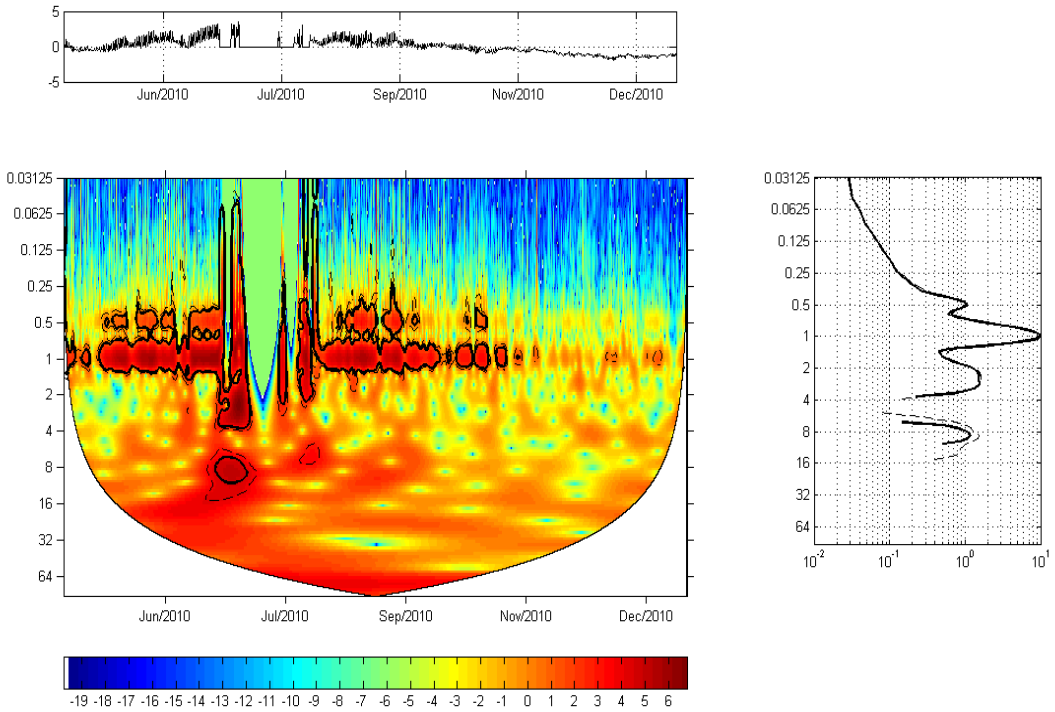

Figure 25A. Continuous Wavelet Transform (CWT) spectrum for Lambro River temperature, measured at high frequency (15 minutes) in 2010. The sub-plot above shows the average centered and normalized by the standard deviation series. The wavelet power for each period is normalized by the Global Wavelet Spectrum (dimensionless, on the right) and highlights the dominant recurrent cycles. Here the daily and the half-daily are the dominant cycles, but some patterns were found also for 2,4,8 days in June. The power of the wavelet spectrum decreased considerably in autumn and winter ow-

ing to a low temperature excursion and resulting in low resolution in that period. The cone of influence (black curve) indicates the region without edge effects. The power values are coded from dark blue for low power to dark red for high power, as shown in the bar of classes below (refer to Materials and Methods for further information). This was performed to find a synchronicity between lake and river ocillations.

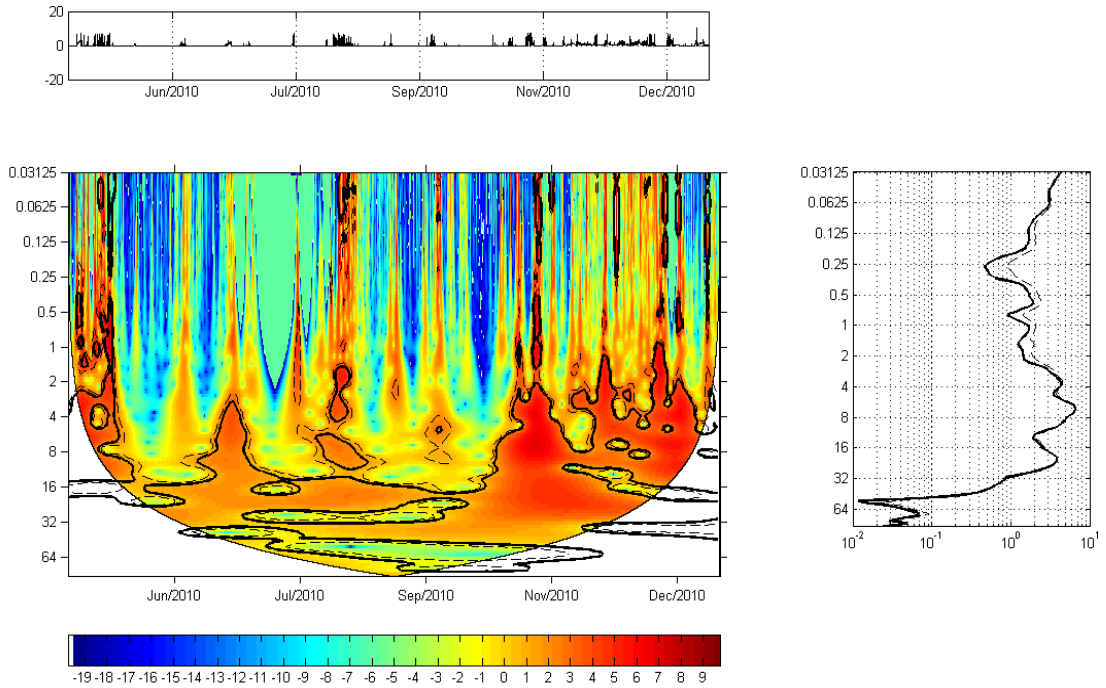

Figure 26A. Continuous Wavelet Transform (CWT) spectrum for Lambro River turbidity, measured at high frequency (15 minutes) in 2010. The sub-plot above shows the average centered and normalized by the standard deviation series. The wavelet power for each period is normalized by the Global Wavelet Spectrum (dimensionless, on the right) and highlights the dominant recurrent cycles. Here the dominant recurrent patterns are between 4 and 16 days, but some pulses were found also at hourly scale during rainfall. The power of the wavelet spectrum increase in autumn and winter owing to higher rainfall and runoff from the catchment. The cone of influence (black curve) indicates the region without edge effects. The power values are coded from dark blue for low power to dark red for high power, as shown in the bar of classes below (refer to Materials and Methods for further information). This was performed to find the period of pulses due to the catcment runoff during the rainfall.

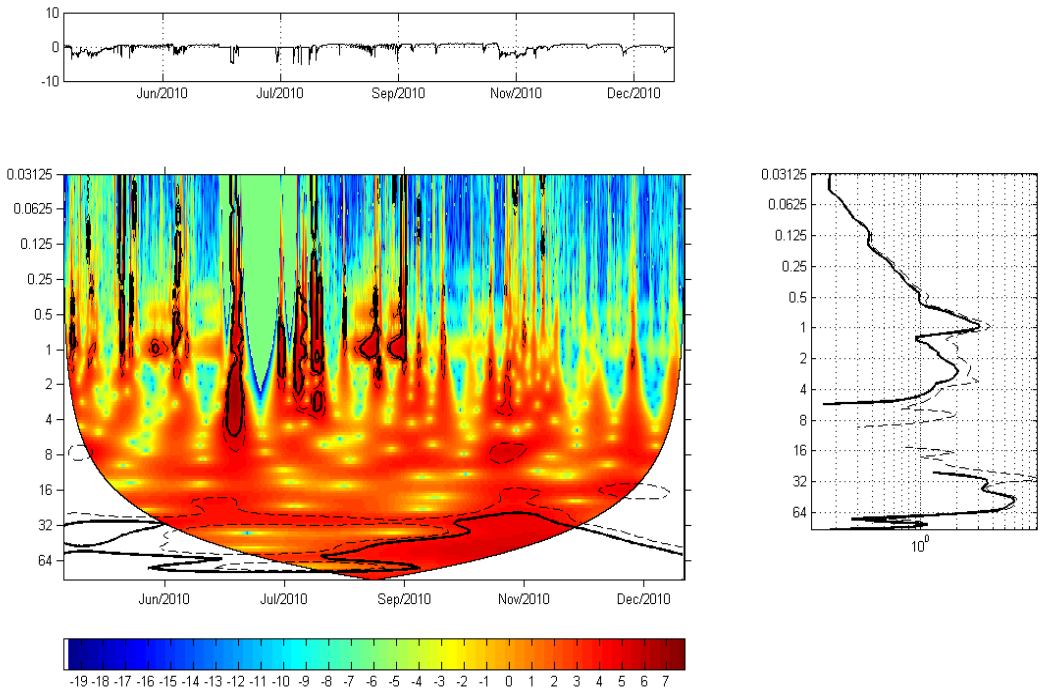

Figure 27A. Continuous Wavelet Transform (CWT) spectrum for Lambro River conductivity, measured at high frequency (15 minutes) in 2010. The sub-plot above shows the average centered and normalized by the standard deviation series. The wavelet power for each period is normalized by the Global Wavelet Spectrum (dimensionless, on the right) and highlights the dominant recurrent cycles. Here the dominant period is between 1 and 4 days, thus meaning a daily periodic chage in the river water composition. The power of the wavelet spectrum decrease in autumn and winter owing to higher rainfall and water diluition. The cone of influence (black curve) indicates the region without edge effects. The power values are coded from dark blue for low power to dark red for high power, as shown in the bar of classes below (refer to Materials and Methods for further information). This was performed to find the periodicity of Lambro River chemical variation.

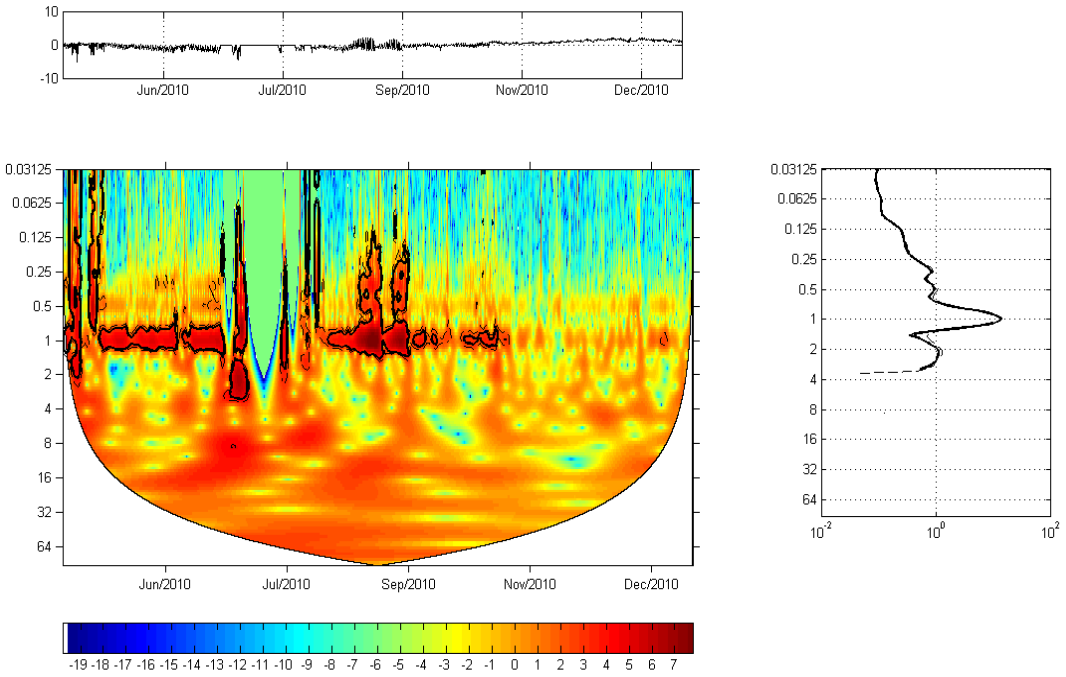

Figure 28A. Continuous Wavelet Transform (CWT) spectrum for Lambro River dissolved oxygen, measured at high frequency (15 minutes) in 2010. The sub-plot above shows the average centered and normalized by the standard deviation series. The wavelet power for each period is normalized by the Global Wavelet Spectrum (dimensionless, on the right) and highlights the dominant recurrent cycles. Here the daily and the half-daily are the dominant cycles, thus resulting linked to the temperature patterns. The power of the wavelet spectrum decreased considerably in autumn and winter owing to higher discharges and low variability thus resulting in low resolution in that period. The cone of influence (black curve) indicates the region without edge effects. The power values are coded from dark blue for low power to dark red for high power, as shown in the bar of classes below (refer to Materials and Methods for further information). This was performed to characterize the river water quality.

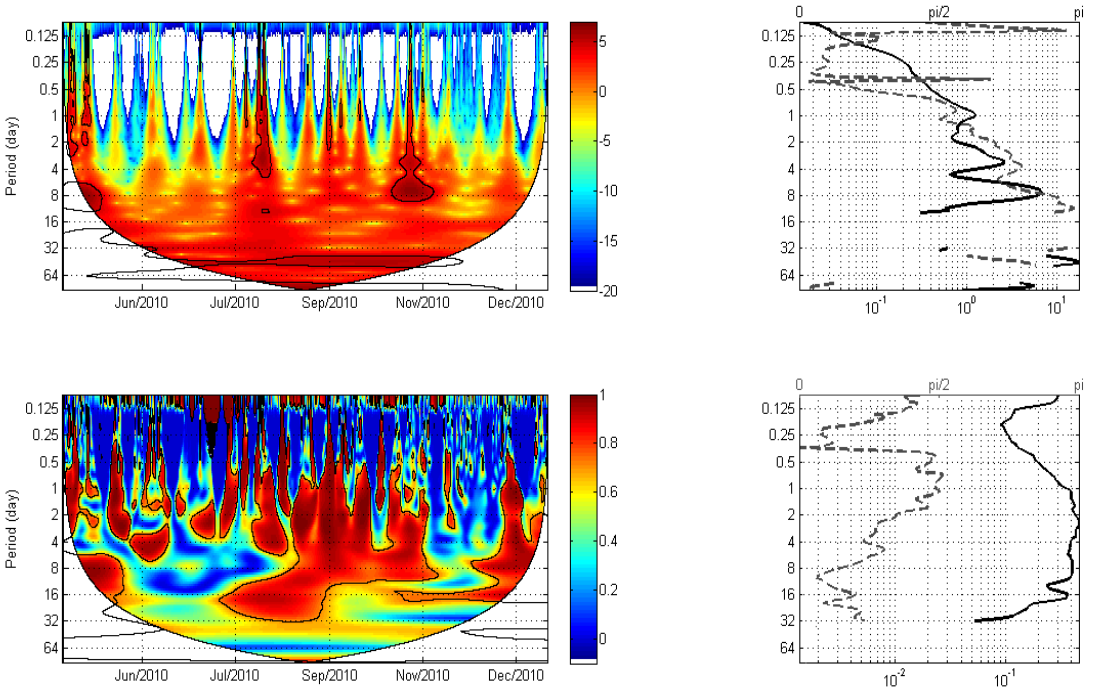

Figure 29A. Cross Wavelet Transform (XWT, above) and Wavelet Coherence (WTC, below) spectra for rainfall and Lambro River discharge comparison. The Global Wavelet Spectrum (dimensionless, on the right) of both the variables were compared to analyze their covariance. The river discharge strongly responded to high rainfall events, with a time lag of few hours (the corrivation time of Pusiano watershed is 4-6 hours) only at high frequency (1-8 days). This was helpful to isolate the events during the multiregression analysis used to build the catchment loading.

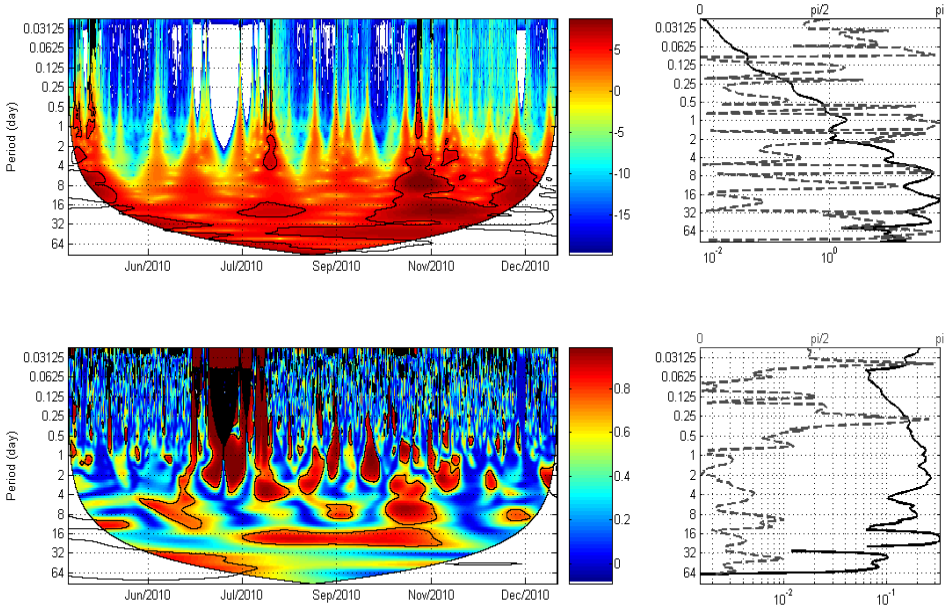

Figure 30A. Cross Wavelet Transform (XWT, above) and Wavelet Coherence (WTC, below) spectra for turbidity and Lambro River discharge comparison. The Global Wavelet Spectrum (dimensionless, on the right) of both the variables were compared to analyze their covariance. A covariance was hard to detect; apparently a tendency to form a common pattern is identified around a period of recurrence of 1, 2, 4 and 16 days probably owing to a strong change of turbidity depending on the rainfall span and the river discharge. This supported the outcome by the 3D simulation (ELCD): during an important rainfall event the river enters to the lake with higher concentrations of substances at the beginning and with a more diluite water after 1-2 or more days.

7.3.2 Rivers water quality

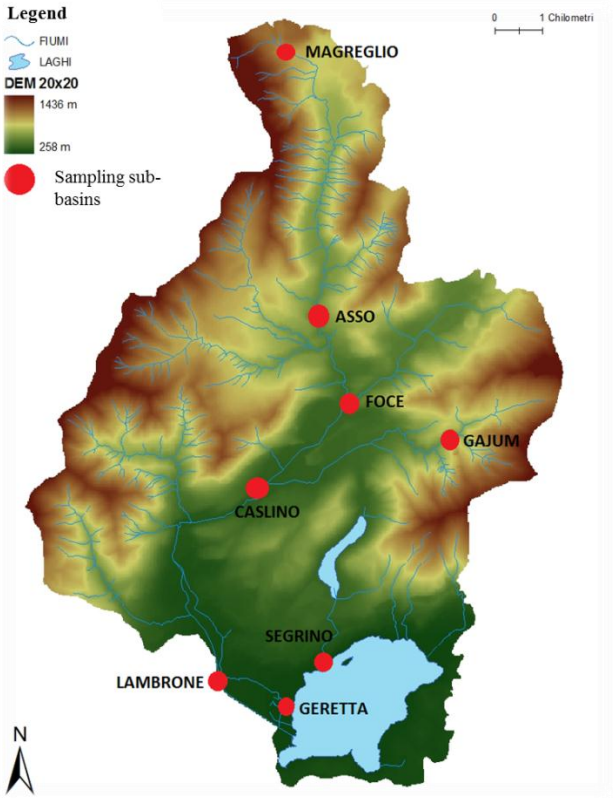

Figure 31A. Map of Pusiano watershed with the rivers monitoring points.

MAGREGLIO		**TN**	**N-NO_3**	**TON**	**N-NH_4**	**TIN**
	Mean (mg/l)	2.64	2.15	0.44	0.05	2.20
	Standard dev. (mg/l)	0.52	0.50	0.24	0.05	0.50
	Mean (as TN %)	100	81	17	2	83
	Standard dev. (%)	19.6	23.0	55.5	92.2	22.6
ASSO		**TN**	**N-NO_3**	**TON**	**N-NH_4**	**TIN**
	Mean (mg/l)	2.91	2.50	0.38	0.02	2.53
	Standard dev. (mg/l)	0.42	0.52	0.28	0.03	0.51
	Mean (as TN %)	100	86	13	1	87
	Standard dev. (%)	14.6	20.8	72.5	122.9	20.3
FOCE		**TN**	**N-NO_3**	**TON**	**N-NH_4**	**TIN**
	Mean (mg/l)	2.98	2.43	0.50	0.05	2.47
	Standard dev. (mg/l)	0.57	0.60	0.32	0.09	0.59
	Mean (as TN %)	100	81	17	2	83
	Standard dev. (%)	19.0	24.5	64.7	189.4	23.9
GAJUM		**TN**	**N-NO_3**	**TON**	**N-NH_4**	**TIN**
	Mean (mg/l)	2.83	2.68	0.18	0.01	2.69
	Standard dev. (mg/l)	0.33	0.24	0.27	0.01	0.24

	Mean (as TN %)	100	95	5	0	95
	Standard dev. (%)	11.5	9.1	146.9	68.6	9.0
CASLINO		**TN**	**N-NO_3**	**TON**	**N-NH_4**	**TIN**
	Mean (mg/l)	3.42	2.96	0.43	0.03	2.99
	Standard dev. (mg/l)	0.43	0.49	0.44	0.05	0.48
	Mean (as TN %)	100	86	13	1	87
	Standard dev. (%)	12.6	16.6	101.5	165.2	15.9
LAMBRONE		**TN**	**N-NO_3**	**TON**	**N-NH_4**	**TIN**
	Mean (mg/l)	3.55	2.95	0.61	0.11	3.07
	Standard dev. (mg/l)	0.85	0.84	0.62	0.31	0.83
	Mean (as TN %)	100	83	14	3	86
	Standard dev. (%)	24.1	28.6	106.1	291.5	44.3
GERETTA		**TN**	**N-NO_3**	**TON**	**N-NH_4**	**TIN**
	Mean (mg/l)	4.73	3.95	0.64	0.14	4.09
	Standard dev. (mg/l)	1.20	1.33	0.89	0.27	1.24
	Mean (as TN %)	100	83	14	3	86
	Standard dev. (%)	25.4	33.8	138.5	193.0	30.4
SEGRINO		**TN**	**N-NO_3**	**TON**	**N-NH_4**	**TIN**
	Mean (mg/l)	3.13	2.35	0.52	0.09	2.40
	Standard dev. (mg/l)	0.98	0.83	0.36	0.22	0.87
	Mean (as TN %)	100	75	22	3	78
	Standard dev. (%)	31.3	35.2	68.0	234.8	36.2

Table 4A. Statistics of the nitrogen species detected by the water samples collected at each station to characterize the nutrients transport in the Pusiano catchment during 2010. This was used to prepare the nutrients input to the 3D model (ELCD).

MAGREGLIO	**TP**	**P-PO_4**	**TDP**	**PP**
Mean (µg/l)	34	21	24	10
Standard Dev. (µg/l)	28	22	26	17
Mean (as TP %)	100	61	69	31
Standard Dev. (%)	82	109	109	165

ASSO	**TP**	**P-PO_4**	**TDP**	**PP**
Mean (µg/l)	35	23	25	10
Standard Dev. (µg/l)	26	9	10	23
Mean (as TP %)	100	66	71	29
Standard Dev. (%)	75	40	42	233

FOCE	TP	$P\text{-}PO_4$	TDP	PP	TSS
Mean (µg/l)	80	50	58	22	19.7
Standard Dev. (µg/l)	47	17	19	43	39.1
Mean (as TP %)	100	63	73	28	
Standard Dev. (%)	59	34	32	196	

GAJUM	TP	$P\text{-}PO_4$	TDP	PP	TSS
Mean (µg/l)	11	2	3	8	12.1
Standard Dev. (µg/l)	21	2	2	19	32.4
Mean (as TP %)	100	18	27	73	
Standard Dev. (%)	190	105	77	238	

CASLINO	TP	$P\text{-}PO_4$	TDP	PP	TSS
Mean (µg/l)	56	18	20	37	41.4
Standard Dev. (µg/l)	98	9	10	94	85.9
Mean (as TP %)	100	32	36	66	
Standard Dev. (%)	176	49	51	255	

LAMBRONE	TP	$P\text{-}PO_4$	TDP	PP	TSS
Mean (µg/l)	75	26	31	45	48.8
Standard Dev. (µg/l)	107	21	23	99	172.3
Mean (as TP %)	100	35	40	60	
Standard Dev. (%)	143	80	76	220	

GERETTA	TP	$P\text{-}PO_4$	TDP	PP	TSS
Mean (µg/l)	172	63	73	99	26.8
Standard Dev. (µg/l)	202	49	54	192	36.6
Mean (as TP %)	100	37	42	58	
Standard Dev. (%)	117	78	74	194	

SEGRINO	TP	$P\text{-}PO_4$	TDP	PP
Mean (µg/l)	78	35	41	29
Standard Dev. (µg/l)	84	32	37	65
Mean (as TP %)	100	45	53	37
Standard Dev. (%)	108	92	90	224

Table 5A. Statistics of the phosphorus species and the total suspended solids (TSS) detected by the water samples collected at each station to characterize the nutrients

transport in the Pusiano catchment during 2010. This was used to prepare the nutrients input to the 3D model (ELCD).

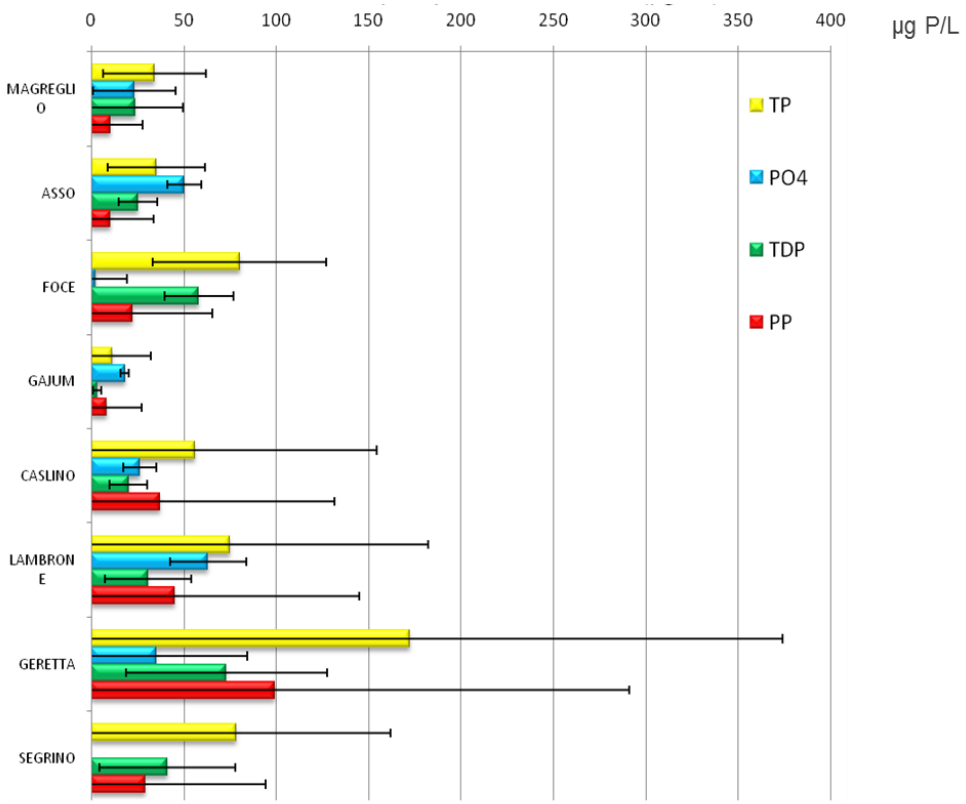

Figure 32A. Characterization of different sub-basins by annual average and variability (via standard deviation) of phosphorus species during the field campaign in 2010, used to calibrate and validate the SWAT model for natural P-load (Gajum sub-basin).

7.4 Long-term data

7.4.1 Paleolimnological survey

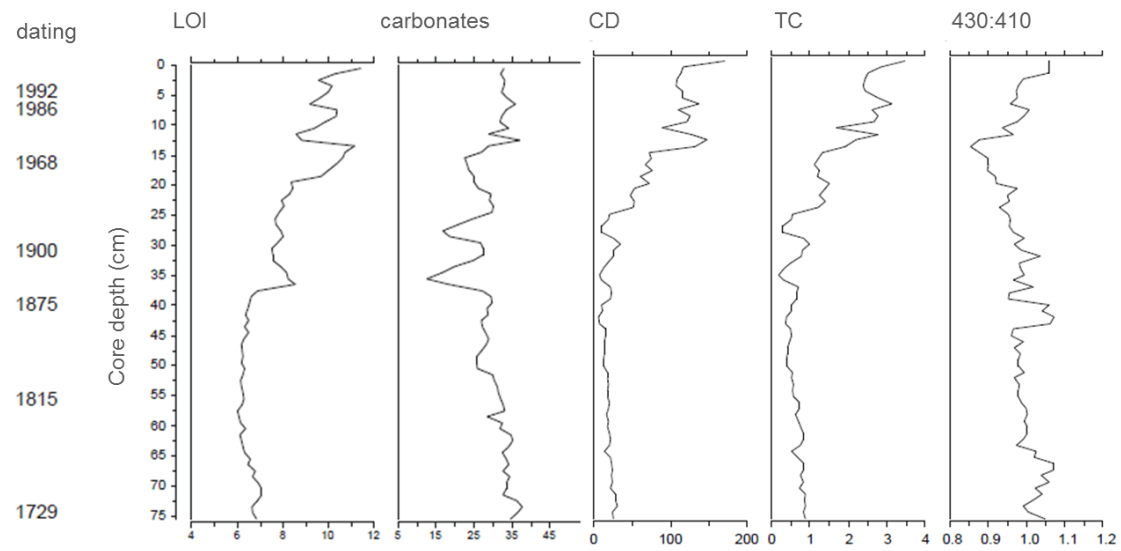

Figure 33A. Percentage of organic matter (% LOI d.w.), carbon (% CO_3 d.w.), total sedimentary chlorophyll derivatives (as unit CD g LOI^{-1}), sedimentary total carotenoids (as mg TC g LOI^{-1}) and 430 nm : 410 nm pigments ratio detected in the core cut sections. The estimated chlorophyll water concentrations was used to initialize the unidimensional model for long term simulations (DYCD).

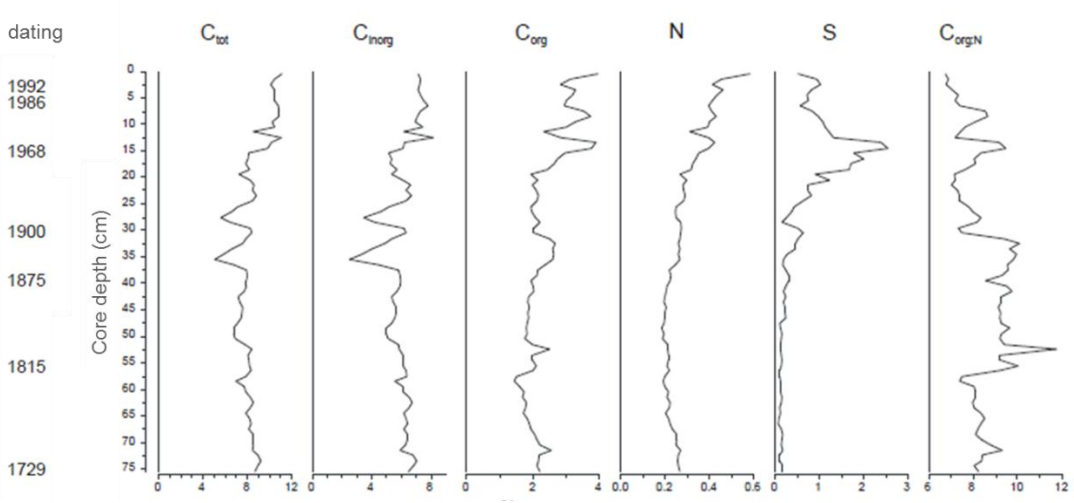

Figure 34A. Percentage (% d.w.) of total carbon (C_{tot}), inorganic carbon (C_{inorg}), organic carbon (C_{org}), total nitrogen (N) and sulphur (S) and the C_{org} : N ratio. The estimated nitrogen and carbon water concentrations were used to initialize the unidimensional model for long term simulations (DYCD).

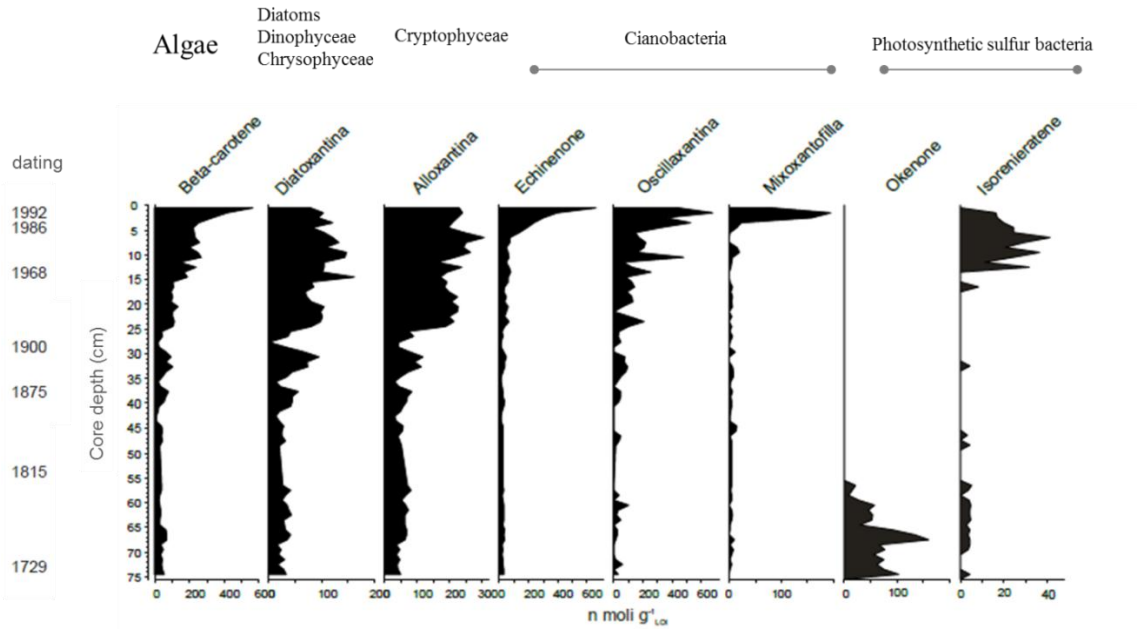

Figure 35A. Distribution of pigment concentrations in Lake Pusiano sediment dated core and the relative association to algal groups. This information was used to characterize the algal community in the unidimensional model for long term simulations (DYCD) and for the assessment of phosphorus reference conditions by inferential models.

7.4.2 Time series

Data were supplied by the Lombardy Regional Agency for Environmental Protection (ARPA Lombardia) and the Water Research Institute of the National Council of Research (IRSA-CNR, Brugerio) by which the authors could carry out the present research.

	Cond	pH	TALK	N_NH4	N_N03	TN	TP	P_PO4	SiO2	SO4	Cl	Ca	Mg	Na	K	Chl_a	Phaeo	O2	O2_sat	DOC	TIN	TON
Cond	**1**																					
pH	-0.76	**1**																				
TALK	0.89	-0.73	**1**																			
N_NH4	0.49	-0.45	0.56	**1**																		
N_N03	0.12			-0.17	**1**																	
TN					0.44	**1**																
TP	0.50	-0.43	0.51	0.78	-0.12		**1**															
P_PO4	0.47	-0.40	0.50	0.72	-0.11		0.87	**1**														
SiO2								0.08	**1**													
SO4	0.11			-0.36	0.10					**1**												
Cl	0.11	-0.27	0.16	0.14	-0.11		0.24	0.28		0.27	**1**											
Ca	0.80	-0.69	0.81	0.42			0.36	0.29	0.48		0.17	**1**										
Mg	0.13	-0.13	0.14	-0.17						0.70	0.12	0.30	**1**									
Na							0.18	0.12	0.11	0.22	0.22			**1**								
K									0.18		-0.09				**1**							
Chl_a	-0.17	0.23	-0.19	-0.21		-0.37		-0.21	-0.16	0.23			0.19		-0.18	**1**						
Phaeo			-0.16	-0.24			-0.15	-0.22	-0.20	0.45			0.24		-0.30	0.59	**1**					
O2	-0.29	0.47	-0.30	-0.31			-0.31	-0.31				-0.21			-0.13	0.44	0.28	**1**				
O2_sat	-0.63	0.77	-0.66	-0.52			-0.47	-0.46	-0.16	0.20	-0.22	-0.43	0.14		-0.40	0.39	0.25	0.52	**1**			
DOC	-0.78	0.55	-0.86	-0.74	-0.76	-0.83			-0.49			-0.89	-0.64						0.66	**1**		
TIN	0.60	-0.44	0.65	0.82			0.65	0.71	0.57	-0.30		0.51	-0.13		0.25			-0.19	-0.37	-0.84	**1**	
TON					0.47	1.00					0.13			0.14								**1**

Table 6A. Pearson correlation matrix for all the variables measured in Lake Pusiano during the limnological campaigns from 1972 to 2005 (performed to assess the experimental plan of the last campaigns in 2010). Correlation coefficients are significant at the 0.05 level (2-tailed).

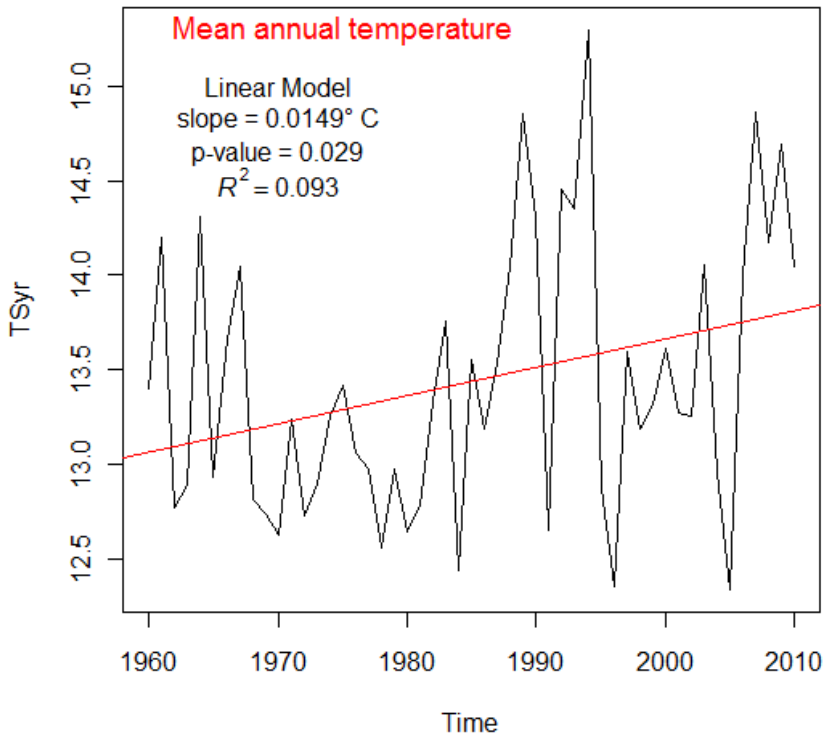

Figure 36A. Increasing trend over the annual averages of daily air temperature since 1960 to 2010, collected at the metereological stations within Pusiano catchment area. The slope (0.015° C yr^{-1}) confirmed those found for Italian lakes (Ambrosetti and Barbanti, 1999).

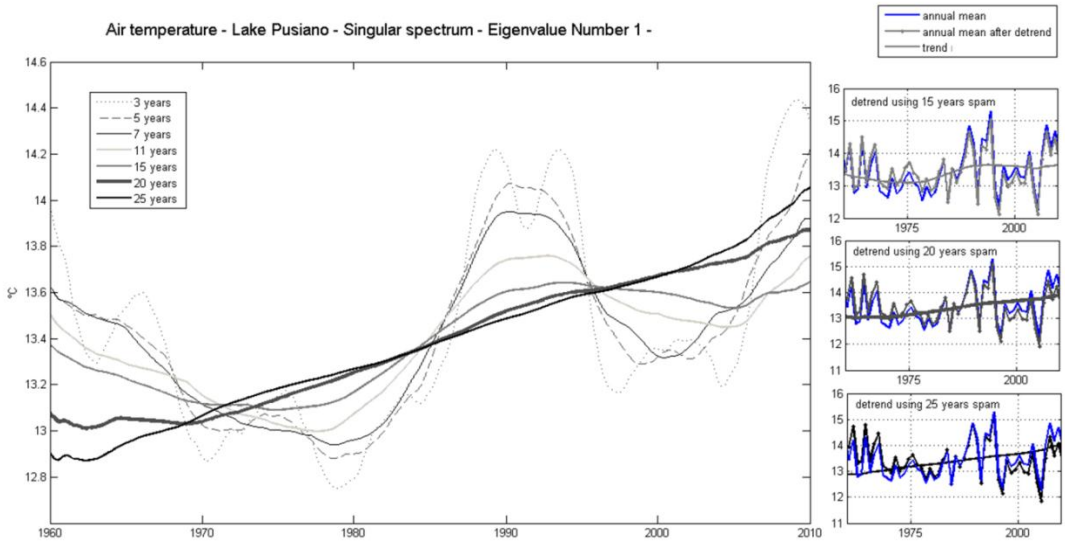

Figure 37A. Air temperature daily series was processed by the Singular Spectrum Anlysis (Ghil and Vautard, 1991) to detect the best running average (thick lines are for 3 to 25 years span). The closest to the linear trend (15, 20 and 25 years span) were compared to choose the slope for the best detrended series (i.e. the 20 years span), which the onset was the closest to the original series (refer to Chapter 3 for a further explanation).

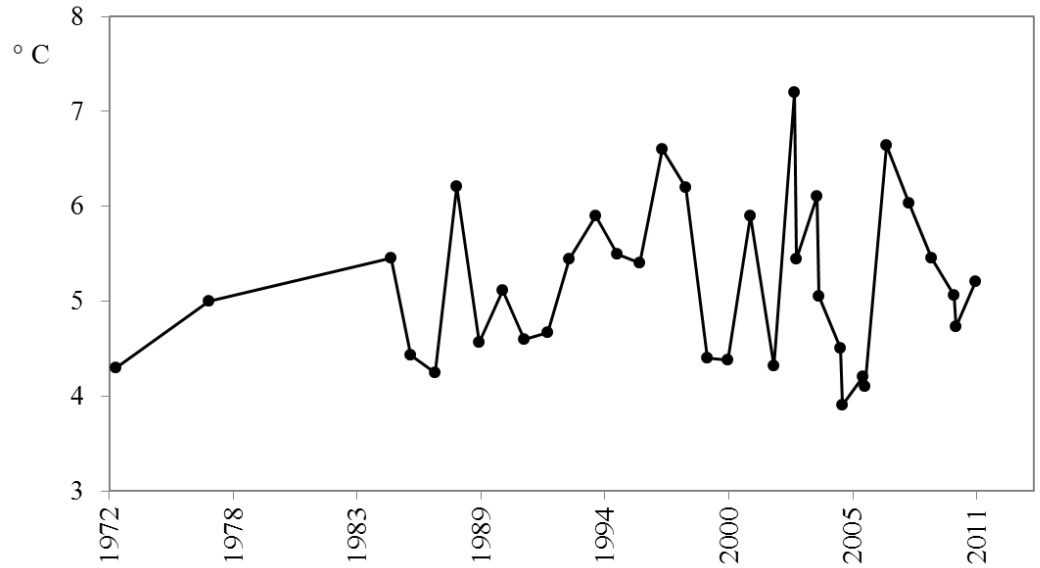

Figure 38A. Water temperature measured in Lake Pusiano during the winter overturn (end of January) since 1972.

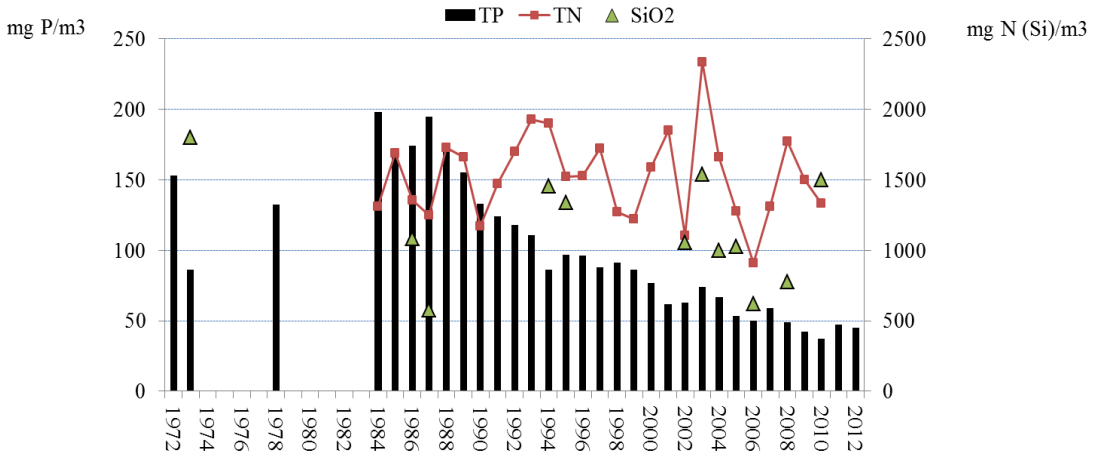

Figure 39A. Total phosphorus (TP), nitrogen (TN) and silica (Si-SiO_2) detected in Lake Pusiano during the winter overturn (end of January) since 1972.

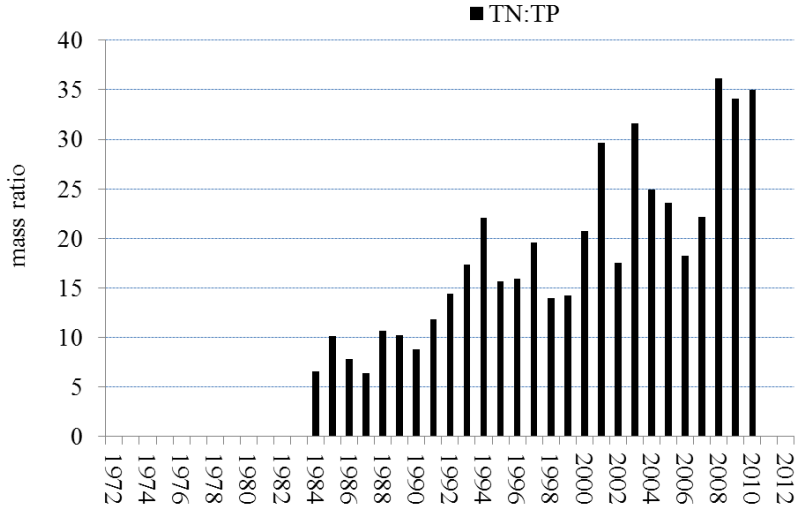

Figure 40A. Phosphorus and nitrogen ratio evolution, as TN:TP mass ratio, computed by the winter overturn series since 1984 to 2010.

7.4.3 Seasonal trends (2002-2010)

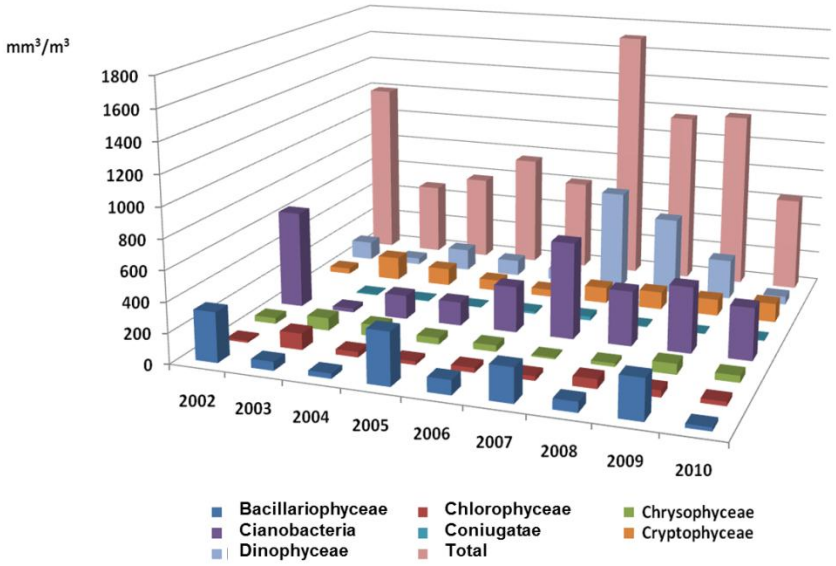

Figure 41A. Mean annual biomass (mm^3 m^{-3}) of the main phytoplankton groups in Lake Pusiano by monthly surveyes from 2002 to 2010.

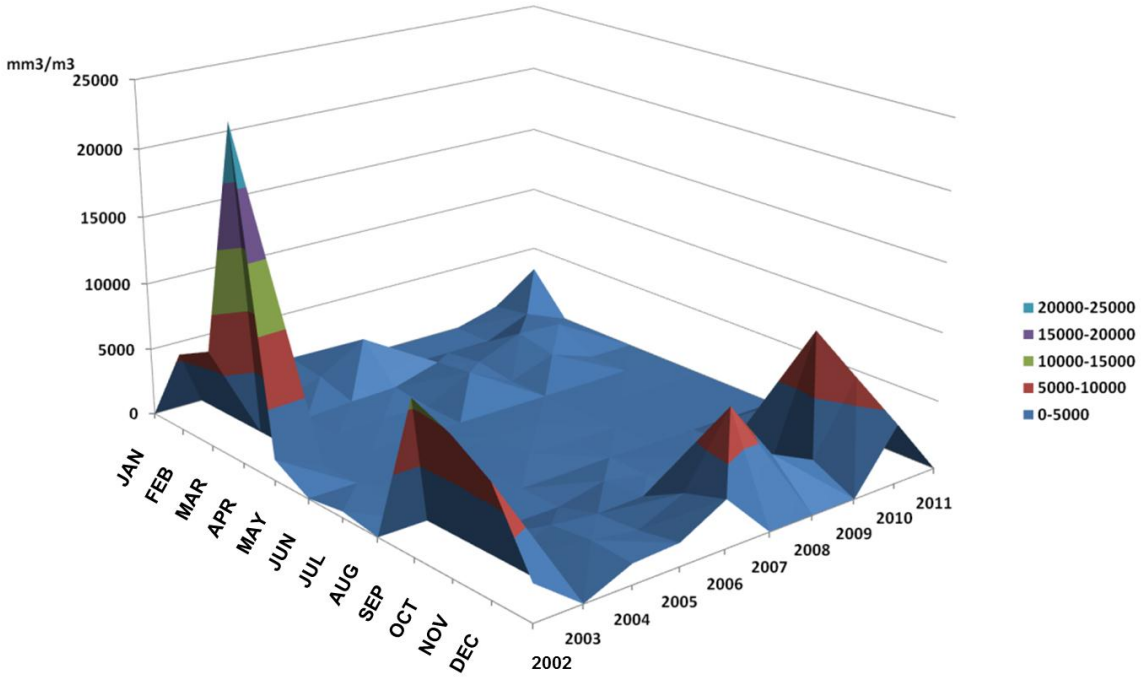

Figure 42A. Seasonal evolution of *P. rubescens* biomass (mm^3 m^{-3}) by cell enumeration in water samples taken at different depths from 2002 to 2010, in Lake Pusiano. The series was used to assess the last 9 years of the long term simultions with the 1D model (DYCD).

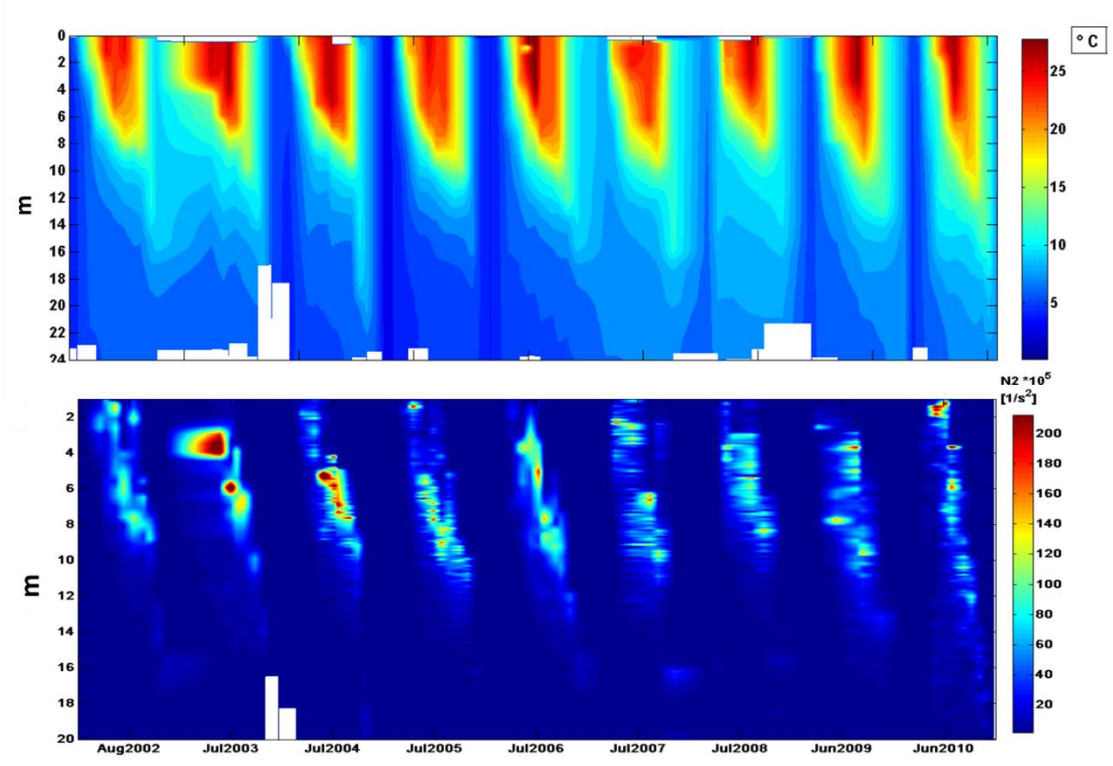

Figure 43A. Seasonal evolution of: *above*) thermal profile measured by CTD probe at the maximum depth station (ST6, refer to the map in Figure 2) from 2002 to 2010, in Lake Pusiano; *below)* thermal stability computed by temperature and salinity profiles to get the Brunt-Väisälä frequency, or buoyancy frequency (Mortimer, 1974) at the maximum depth station (ST6, refer to the map in Figure 2) from 2002 to 2010, in Lake Pusiano. The series was used to assess the last 9 years of the long term simultions with the 1D model (DYCD).

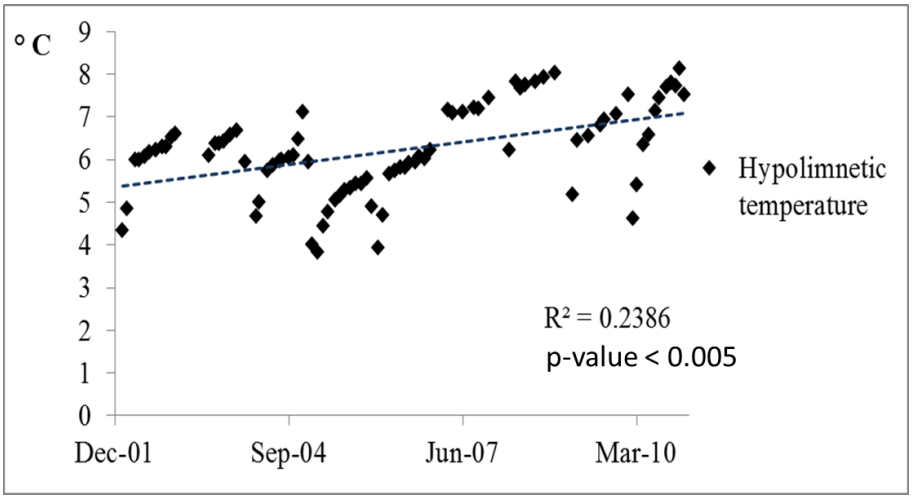

Figure 44A. Increasing trend over the monthly temperature series, measured by the CTD probe at Lake Pusiano bottom (22-25 meters depth) from 2002 to 2010.

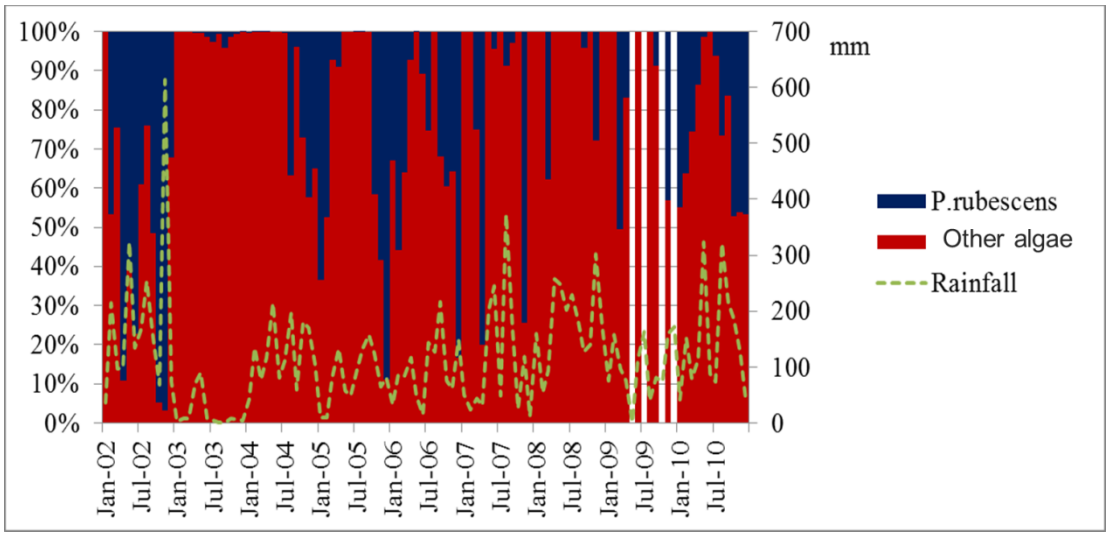

Figure 45A. Seasonal evolution of *P. rubescens* compared to the remaining biomass (as % of total), by cell enumeration in water samples taken at different depths in Lake Pusiano and the cumulated monthly rainfall measured from 2002 to 2010 in Pusiano catchment. This elaboration was used to parameterized the two algal groups (*P. rubescens* and a general competitor G2) in long term simultions with the 1D model (DYCD).